Preparation, stability testing and *in vitro* antiproliferative determination of ester and amide derivatives of Temozolomide

by

Oliver Ingham

A thesis submitted in partial fulfilment for the requirements for the degree of Doctor of Philosophy at the University of Central Lancashire

April 2020

STUDENT DECLARATION FORM

Concurrent registration for two or more academic awards

*I declare that while registered as a candidate for the research degree, I have not been a registered candidate or enrolled student for another award of the University or other academic or professional institution

Material submitted for another award

***I** declare that no material contained in the thesis has been used in any other submission for an academic award and is solely my own work

Collaboration

Where a candidate's research programme is part of a collaborative project, the thesis must indicate in addition clearly the candidate's individual contribution and the extent of the collaboration. Please state below:

Signature of Candidate _____

Type of Award _____

School _____

PREFACE

ABSTRACT

Temozolomide (TMZ) is the standard of care treatment for patients diagnosed with glioblastoma multiforme. However, median survival of patients diagnosed with glioblastoma is only increased by 2.5 months when treated with TMZ and radiotherapy, compared with radiotherapy alone. Furthermore, current literature suggests that 60-75% of patients experience no clinical benefit from TMZ and a further 15-20% of these patients develop clinically significant toxicity, which can make further treatment unsafe. Therefore, there is an inherent need for a chemotherapeutic agent that is safer and more effective for patients with high-grade glioma.

A comprehensive review of the literature indicated that position 8 on the imidazole ring of TMZ, held significant promise in terms of improving the activity of the molecule. Numerous studies have demonstrated a degree of success investigating both ester and amide analogues of TMZ. However, to date, modifications at position 8 of the imidazole ring of TMZ have not been fully explored. Consequently, the aim of the current study was to synthesise a series of novel ester and amide analogues of TMZ, with the aim of improving our understanding of structure activity relationships at this position, thus, improving activity of the molecule.

Novel ester and amide analogues of TMZ, were synthesised using two routes. One utilising reactions between TMZ acyl chloride and various alcohols and amines, the other utilising dehydrating agents, dicyclohexylcarbodiimide and 1-ethyl-3-(3-dimethylaminopropyl)carbodiimide, to achieve direct coupling of TMZ acid to various alcohols and amines. Novel analogues were characterised using ^{1}H and ^{13}C nuclear magnetic resonance (NMR) spectroscopy, infrared spectroscopy, high resolution mass spectrometry (HMRS) and melting point analysis. Upon characterisation, the novel analogues were assessed for their cytotoxic potency against the high-grade glioma cell lines, U87-MG, 1321-N1 and GOS-3. Additionally, the human glial cell line, SVGp12 was included as a control. Cells were incubated

for 144 hours with various concentrations of drug before assessing viability with CellTitreGlo©, to obtain the IC_{50}.

Antiproliferative determination of novel esters and amides analogues of TMZ revealed that phenolic ester analogues of TMZ displayed increased potency, up to 5-fold, against specified HGG cell lines. The promising activity displayed by phenolic TMZ esters prompted further investigations against patient-derived primary glioblastoma cultures, obtained from The Royal Preston Hospital. Primary cultures, BTNW914 and BTNW374, were revealed to be MGMT positive and MGMT negative by pathology staff at the hospital, using Immunohistochemical analysis. Lead phenolic TMZ esters were found to decrease viability in primary cells at clinically obtainable concentrations, irrespective of *O6*-alkylguanine DNA alkyltransferase (MGMT) expression. Furthermore, TMZ was found to be ineffective against the same primary cells at clinically relevant concentrations, suggesting that the novel phenyl ester analogues of TMZ have potential as chemotherapeutics agents for the treatment of glioblastoma.

Porcine liver esterase was used to assess the stability of the ester linkage of lead analogues, using HPLC as a means of analysis. Results from this work suggest a potential marked fragility of the ester bond in lead analogues with half-lives ranging from 3.2 – 13.7 minutes.

In conclusion, the lead phenolic TMZ esters described in the present study have been shown to exhibit improved *in-vitro* activity against HGG cells, compared with TMZ. It is hoped that this improvement can be translated to *in-vivo* models, and that the lead analogues can display a positive outcome.

Acknowledgements

I would like to express the deepest appreciation to my supervisors, Leroy and Amal Shervington. Without their guidance, I would surely not find myself in position I find myself in today. Their immense knowledge, patience and enthusiasm have helped me immeasurably throughout both the practical and written aspects of my PhD. I could not have hoped for two better mentors.

I would also like to express gratitude towards the following: to Pat Cookson for his assistance with NMR training; to Tamar Garcia-Sorribes and Sameera Mahroof for their assistance and knowledge of repairing various pieces of analytical equipment, throughout my studies; and to Sarah Dennison, Julie Burrows, Murassa Shaikh and Roshini Mathews for their advice and training during Tissue Culture studies. Additionally I would like to express thanks to Fiaz Shah for assisting with esterase mediated stability studies.

A big thank you to Kate Ashton and Tim Dawson at The Brain Tumour North West Tissue Bank, for supplying primary cells and for their guidance and protocols.

I also extend my thanks to the University for financially supporting this project and again to Leroy Shervington for selecting me to undertake this research.

Finally, I would like to thank my parents, Lance and Judith Ingham, for their emotional and financial support throughout the past 3 years.

Abbreviations

AIC	5-Aminoimidazole-4-carboxamide
AMP	Adenosine Monophosphate
APNG	Alkylpurine-DNA-N-glycolase
ATCC	American Type Culture Collection
ATP	Adenosine Triphosphate
BBB	Blood Brain Barrier
BER	Base Excision Repair
BTNW	Brain Tumour North West
CNS	Central Nervous System
DCC	N,N'-Dicyclohexylcarbodiimide
DCM	Dichloromethane
DCU	Dicyclohexyl Urea
DMAP	4-Dimethylaminopyridine
DMEM	Dulbecco's Modified Eagle Medium
DMF	Dimethylformamide
DMSO	Dimethyl Sulfoxide
DMSZ	Deutsche Sammlung von Mikroorganismen und Zellkulturen
DTIC	Dacarbazine
ECCAC	European Collection of Cell Cultures
EDC.HCl	1-(3-Dimethylaminopropyl)-3-ethylcarbodiimide hydrochloride
EDU	1-Ethyl-3-(3-dimethylaminopropyl) Urea
EGFR	Epidermal Growth Factor Receptor
EMEM	Eagle's Minimum Essential Medium

FBS	Fetal Bovine Serum
GBM	Glioblastoma Multiforme
GI	Gastro-Intestinal Tract
HBA	Hydrogen Bond Acceptor
HBD	Hydrogen Bond Donator
HBSS	Hank's Balanced Salt Solution
hCE	Human Carboxylesterase
HCMV	Human Cytomegalovirus
HEPES	4-(2-Hydroxyethyl)-1-piperazineethanesulfonic acid
HGG	High Grade Glioma
HRMS	High Resolution Mass Spectrometry
ICH	Immunohistochemistry
ICH	International Council for Harmonization of Technical Requirements for Pharmaceuticals for Human Use
IS	Intensity Score
LLOD	Lower Limit of Detection
LLOQ	Lower Limit of Quantification
MeCN	Acetonitrile
MGMT	*O*6-Methylguanine-DNA Methyltransferase
MMR	DNA Mismatch Repair
MTIC	5(3-Methyl-1-triazeno) imidazole-4-carboxamide

MTS	3-(4,5-Dimethylthiazol-2-yl)-5-(3-carboxymethoxyphenyl)-2-(4-sulfophenyl)-2H-tetrazolium
MTT	3-(4,5-Dimethylthiazol-2-yl)-2,5-diphenyltetrazolium bromide
NEAA	Non-Essential Amino Acids
NICE	The National Institute of Health and Care Excellence
NMR	Nuclear Magnetic Resonance
***O6*-MeG**	*O*6-methyl guanine
PA	Peak Area
Petroleum Ether	Note: Refers to the fraction that boils at 40-60 ^{o}C
PLE	Porcine Liver Esterase
PS	Proportional Score
QALY	Quality Assured Life Year
RSD	Relative Standard Deviation
R^2	Coefficient of Determination
SAR	Structure Activity Relationship
THF	Tetrahydrofuran
TMZ	Temozolomide (3-methyl-4-oxo-imidazo[5,1-d][1,2,3,5]tetrazine-8-carboxamide)
TMZ Acid	Temozolomide Acid (3-methyl-4-oxo-imidazo[5,1-d][1,2,3,5]tetrazine-8-carboxylic acid)

TMZ Acyl Chloride	Temozolomide Acyl Chloride (3-methyl-4-oxo-imidazo[5,1-d][1,2,3,5]tetrazine-8-carbonyl chloride)
TS	Total Score
U87-MG	Uppsala 87 Malignant Glioma
UHPLC-ToF-MS	Ultra-High Performance Liquid Chromatography-Quadrupole Time-of-Flight Mass Spectrometry
WHO	The World Health Organisation

Contents

List of Figures

Chapter 1 Figures

Chapter 2

Chapter 3

Chapter 4

Chapter 5

List of Tables

Chapter 1

Chapter 2

Chapter 3

Chapter 4

List of Schemes

Chapter 1

Chapter 2

Chapter 3

Chapter 4

CHAPTER 1:

INTRODUCTION

1.1. Neuroglia

Neuroglial cells, more commonly referred to as glial cells, account for the majority of cells in the central nervous system (CNS), outnumbering nerve cells by a ratio of approximately 3:1. Glial cells were named in the early 19th century from the belief that these cells acted as the "glue" that held the nervous system together. The presumption that glial cells acted as glue was born from early visualisation of brain tissue, where these cells appeared to cover all the space between neurons in the brain. This appearance led early scientists to believe that glial cells provided a scaffold for the neurons. However, it is now widely recognised that glial cells have a variety of different functions Purves *et al.* (2001). Glial cells differ from nerve cells since they are not directly involved in synaptic interactions, instead they work to support neuron signalling (Kettenmann and Ransom, 2013).

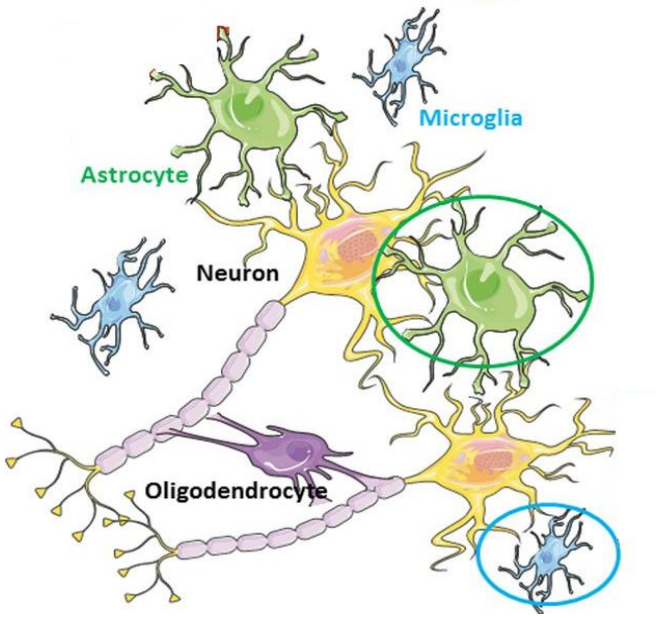

Figure 1.1: A graphical illustration summarising the cells of the CNS. Green – astrocytes; Blue – microglia; Purple – oligodendrocyte. Adapted from (Argente-Arizon et al., 2017).

Glial cells of the mature CNS are classified as microglial cells or macroglial cells. As the name suggests, microglial cells are the smallest of these subtypes and function as the brain's immune cells of the brain. In the resting healthy brain tissue these cells are highly mobile and work to actively detect brain insults and to monitor synaptic integrity (Purves *et al.*, 2001). In early postnatal development, microglial cells interact with neurons to help develop neuronal pathways influencing maturation of the brain. Macroglial cells include a number of specialised cells each with different functions. Such examples of macroglial cells found in the CNS are oligodendrocytes whose function is to myelinate axons; astrocytes whose function is to support neuron signalling; and ependymal cells which maintain homeostasis in the brain (Figure 1.1) (Kettenmann and Ransom, 2013; Wolburg *et al.*, 2015). Cancers originating from glial cells, more commonly referred to as gliomas, are the most common primary brain tumour diagnosed in the adult cohort.

1.2. Glioma and Glioblastoma Multiforme

Glioma is a general term used to describe primary brain tumours originating from glial cells including oligodendrocytes, astrocytes and ependymal cells (Wolburg *et al.*, 2015). While the global incidence of glioma is relatively low, the prognosis of the malignancy is extremely poor, with only half of patients responding positively to treatment (Ernest and Sontheimer, 2009). Although gliomas account for a very small proportion of cancers diagnosed in adults, the poor prognosis of the condition means that gliomas are the second largest cause of cancer-related deaths in children and the single largest cause of cancer related deaths in adult men (aged 20-39) (Liu *et al.*, 2018). Gliomas are also most prevalent in individuals over 55 years of age, a group that tends to have the poorest prognosis (Figure 1.2) (Ernest and Sontheimer, 2009).

A summary of survival rates for glioma, grades I-IV, is shown in Table 1.1. The most common and aggressive type of glioma is glioblastoma multiforme (GBM), a tumour of astrocytic lineage and classified as grade IV by the World Health Organisation (WHO) (Louis *et al.*, 2016).

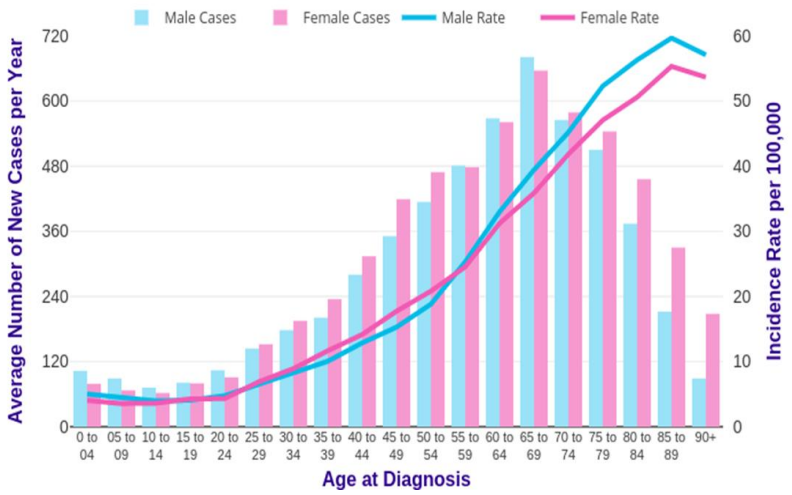

Figure 1.2: Average Number of New Brain Tumour Cases per Year and Age-Specific Incidence Rates per 100,000 Population, UK, 2013-2015. (Cancer Research UK).

GBM accounts for 54% of all gliomas and remains an incurable disease with very poor prognosis (Ostrom *et al.*, 2013). In 2016 the classification of GBMs was updated by the WHO. Currently GBMs are assessed for mutations in the IDH1 gene, coding for cytosolic $NADP^+$ dependent isocitrate dehydrogenase (Louis *et al.*, 2016). The IDH status of GBMs is used to distinguish between primary and secondary tumours as well as being a useful predictor for treatment response (Combs *et al.*, 2011; Choi and Curry, 2017). GBMs are classified into three main sub types by the WHO; glioblastoma IDH wild type (primary); glioblastoma IDH mutant (secondary); and glioblastoma NOS (Glioblastoma NOS refer to a glioblastoma where full IDH evaluation cannot be performed (Louis *et al.*, 2016)). Primary IDH wild type GBMs occur predominantly in older patients (mean age 62 years). Whereas secondary IDH mutant GBMs are much more common in the younger cohorts (mean age 46 years), these tumours are usually a result of the development of lower-grade astrocytomas or oligodendrogliomas (Ohgaki *et al.*, 2004; Ohgaki and Kleihues, 2007; Ohgaki and Kleihues, 2009).

Table 1.1: Survival rates and grading of diffuse astrocytic and oligodendroglial tumours. (Liu et al., 2012).

WHO Grade	Glioma	Median Survival
I	Pilocytic astrocytoma	10 years +
II	Diffuse astrocytoma; Oligodendroglioma	5-10 years
III	Anaplastic astrocytoma; Anaplastic oligodendroglioma	2-5 years
IV	Glioblastoma	9-12 months

Age-adjusted incidence rates of GBM range from 0.59 to 3.69 persons per 100,000 persons, across different countries (Arora *et al.*, 2009; Gausia *et al.*, 2009; Dobes *et al.*, 2011; Liu *et al.*, 2012; Thakkar *et al.*, 2014). Thakkar *et al.,* 2014 indicated that the incidence of GBMs is significantly higher in developed countries. This phenomenon is likely accounted for by poor access to health care and different diagnostic practices resulting in under reporting of GBMs in developing countries (Fisher *et al.*, 2007). It is well documented that GBM predominantly occurs in males compared to females (Thakkar *et al.*, 2014). However, although primary GBMs are 3 times more common in men; secondary GBMs are actually 1.5 times more common in women (Sturm *et al.*, 2014). Age also plays an important factor in the incidence rates of GBM with the majority of diagnoses occurring in elderly patients. The median age of diagnosis is 64 years, with peak incidence between the ages of 75-84 years (Ostrom *et al.*, 2013). As the incidence rate in children under the age of 19 years is much less common, epidemiological studies traditionally combine diffuse intrinsic pontine glioma, anaplastic astrocytomas with GBMs, under the umbrella of high grade gliomas (HGG) (Sturm *et al.*, 2014). HGGs affect 0.8 per 100,000 children per year, representing the most common group of CNS neoplasms in this age group (Thakkar *et al.*, 2014).

Limited information is available for the etiology of brain tumours, including GBM (Hanif *et al.*, 2017). Hochberg et al*.,* 1990, failed to show a significant increase in GBM incidence as a result of various lifestyle behaviours, such as smoking, drugs, excessive alcohol consumption or high N-nitroso exposure through diet (Hochberg *et al.*, 1990). There is, however, evidence that supports that intracranial radiation exposure significantly increases the incidence of GBM (Hanif *et al.*, 2017). Following 116 cases of GBM that were directly caused by radiation exposure it was estimated/calculated that the overall risk of developing GBM as a direct result of radiotherapy was 2.6% (Salvati *et al.*, 2003; Hanif *et al.*, 2017). This represents a significant increase in incidence when compared with the <0.01% global incidence of GBMs. Within the paediatric cohort, it has been shown that there is an increased risk of glioma after therapeutic intracranial radiation exposure, which is both dose and age dependent (Hanif *et al.*, 2017). Exposure to

atomic bomb radiation in Nagasaki and Hiroshima also increased the incidence of gliomas (Prasad and Haas-Kogan, 2009). However, no direct evidence has been presented that shows an increase in the risk of developing GBM through exposure to routine diagnostic radiation exposure in both the adult and paediatric cohorts (Prasad and Haas-Kogan, 2009). Therefore there is an assumption that the manifestation of GBM is usually a result of sporadic genetic mutation within the astrocytes of the brain leading to tumour development. It should also be noted that in approximately 10% of cases, patients have been found to have a genetic predisposition to developing GBM, but the gene/genes responsible are yet to be identified (Fisher *et al.*, 2007; Backes *et al.*, 2014). A meta-analysis conducted by Linos et al., 2007 found a significant decrease in the risk of developing glioma in patients suffering from allergies (Linos *et al.*, 2007). This has been hypothesised to be as a result of stimulation of immune surveillance mechanisms helping prevent gliomas, such as GBMs from developing (Bondy *et al.*, 2008).

Human cytomegalovirus (HCMV) has also been associated with a significant increase in the risk of GBM development. HCMV is known to exhibit tropism for glial cells, inducing upregulation of specific proteins; intermediate-early proteins IE1 and IE2, chemokine receptor homologue US28 and glycoprotein gB (Cobbs *et al.*, 2014). These proteins have the ability to activate mitogenesis, angiogenesis, inflammation, apoptosis and mutagenesis. Activation of these pathways results in gene products that work to deregulate key signalling pathways STAT3 and Akt, compromising glial cells and increasing their susceptibility to malignant transformation (Soroceanu *et al.*, 2015).

The current standard treatment of care for GBM involves surgical resection followed by postoperative radiotherapy and adjuvant chemotherapy (Stupp *et al.*, 2005). Despite the intensive treatment regimen the prognosis for patients with GBM is still very poor. Surgical resection plays a pivotal role in the treatment of GBM (Manrique-Guzman *et al.*, 2017). The resection of malignant glial tissue has historically been the initial approach for the treatment of brain tumours, reducing tumour mass and harvesting tissue used for diagnosis (Sanai and

Berger, 2009). The first multivariate analysis investigating survival benefit of surgical resection with radiotherapy in GBM, found that at least 89% of the tumour must be resected for the patient to gain a significant survival benefit (Lacroix *et al.*, 2001). Furthermore, resection of >98% of the tumour resulted in 13 months median survival of the patient. In contrast resection of <98% of the tumour only resulted in 8.8 months median survival (Lacroix *et al.*, 2001). Although it is clear that maximal resection of GBM increases median survival, it is often difficult to achieve due to the diffuse nature of GBMs and the tendency for tumours to develop close to important anatomical features (Manrique-Guzman *et al.*, 2017). In practise, some studies show treatment of GBM by surgical resection without radiotherapy to exhibit median survival as low as 1.9 months. Consequently, other treatment strategies are employed in order to further increase patient survival (Lanzetta and Minniti, 2010).

Following maximal surgical resection, dependant on the size and location of the tumour, patients begin postoperative radiotherapy. Typically radiotherapy commences once craniotomy wounds heal, usually 4 weeks after surgery (Davis, 2016). Historically, whole-brain radiotherapy was the standard in radiotherapy for GBM treatment, however clinically significant toxicities caused by whole-brain irradiation resulted in the need for a more sophisticated approach (Shih *et al.*, 2015). Currently, three-dimensional conformal beam or intensity-modulated radiotherapy is the standard of care method. This strategy allows radiation to be delivered specifically to the tumour reducing side-effects associated with whole brain radiotherapy. GBM reoccurrence often takes place within 2 cm of the original tumour and consequently tumours are irradiated with an additional 2-3 cm margin (Shih *et al.*, 2015). The typical total dose administered to a patient diagnosed with GBM is 60 Gy, which is delivered 5 days per week over a period of 6 weeks in 1.8 – 2 Gy fractions (Barani and Larson, 2015). Doses of 60 Gy are well established to deliver maximal benefit to patients. Doses above 60 Gy have resulted in increased toxicity without any increase to patient survival rates (Barani and Larson, 2015). Prior to 2005, the standard treatment of GBM included surgical resection followed by radiotherapy, resulting in median survival of 12.1 months (Stupp *et al.*, 2005). However, the inclusion of temozolomide

(TMZ; 3-methyl-4-oxo-imidazo[5,1-d][1,2,3,5]tetrazine-8-carboxamide, **1**), an imidazotetrazine prodrug, into the treatment regimen alongside surgical resection and RT, increases median survival by 2.5 months (Stupp *et al.*, 2005). The relative effectiveness of TMZ is attributed in-part to its excellent bioavailability and ability to cross the blood-brain barrier (BBB).

1.3. Imidazotetrazine Prodrug Discovery and Temozolomide

TMZ **1** is part of a family of drugs known as imidazotetrazines. Shown in Figure 1.3, this class of drug contains several nitrogen atoms throughout their core which give rise to a number of unique properties. Imidazotetrazines have often been described in the literature as being derived from dacarbazine (DTIC) **3** (Newlands *et al.*, 1997). DTIC itself was introduced in the 1970s to treat melanoma, following successful *in vivo* investigations (Mizuno and Decker, 1976). However, the drug displayed limited effectiveness during clinical trials due to poor distribution of the active metabolite 5(3-methyl-1-triazeno) imidazole-4-carboxamide (MTIC), (discussed in section 1.4), proven by *in-vivo* micro dialysis (Newlands *et al.*, 1997). This effect was later known to a result of liver enzymes being required to convert the DTIC prodrug into its active metabolite (Sankar *et al.*, 1999).

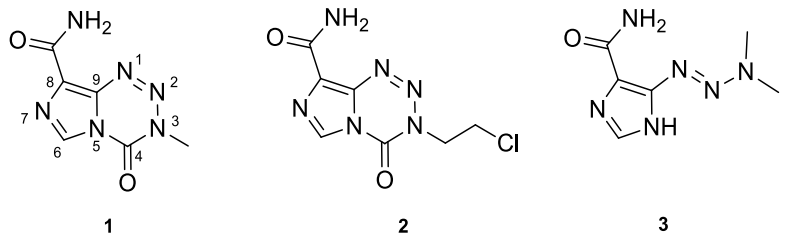

*Figure 1.3: Chemical structures of: Temozolomide **1**; Mitozolomide **2**; DTIC **3**.*

The first imidazotetrazine prodrugs were synthesised at Aston University by the Malcom F. G. Stevens research group. The original publication, "Antitumor imidazotetrazines 1", sought to utilise the versatile reactivity observed in cyclic and acyclic N-N-N linkages to give rise to small molecules with selective antitumor effects, using the chemical structure of DTIC as a starting point (Stevens *et al.*, 1984). Similar to DTIC **3**, imidazotetrazines also degrade *in vivo* to the corresponding MTIC analogue **12**. However, degradation of imidazotetrazines to MTIC occurs spontaneously at physiological pH and does not require liver enzymes, resulting in an improved

bio-distribution of the active MTIC (Newlands *et al.*, 1997). Imidazotetrazines **1**, **2** were found to have a number of advantageous properties such as excellent bioavailability, stability at acidic pH, oral administration suitability, as well as being able to clear the BBB due to the lipophilic nature of the imidazotetrazine core, making them excellent candidates for potential brain tumour chemotherapeutics (Newlands *et al.*, 1997). The first imidazotetrazine to enter clinical trials was mitozolomide **2** (Stevens *et al.*, 1984). However, the drug induced life-threatening myelosuppression in patients and was quickly removed from testing (McKeage *et al.*, 1992). The adverse side effects observed were attributed to DNA crosslinking properties of the chloroethyl diazonium ion (Neijt *et al.*, 1989; Smyth *et al.*, 1989). As a result, attention focused on the 3-methyl derivative, TMZ **1**. TMZ was obtained through substitution of the chloroethyl group on the tetrazinone ring by a methyl group (Stevens *et al.*, 1984; Lunt *et al.*, 1987). TMZ differed from mitozolomide since its cytotoxic effect was generated through methylation of DNA rather than DNA cross-linking (Denny *et al.*, 1994). Clinical trials using TMZ, showed the drug was able to generate similar antitumor effects without eliciting the life-threatening side-effects associated with mitozolomide (Hegi *et al.*, 2005; Stupp *et al.*, 2005).

Summarised in Scheme 1.1, the initial synthesis of imidazotetrazines the involved conversion of commercially available 5-aminoimidazole-4-carboxamide **4** (AIC) to the corresponding diazoimidazole **5** using sodium nitrite. The diazoimidazole **5** was then carefully treated in the absence of light with an isocyanate to yield the desired imidazotetrazine **1** (Stevens *et al.*, 1984). Although Scheme 1.1 yielded the desired imidazotetrazines in favourable yields, attempts were made to produce a scheme that obviated the need for isocyanates, due shortages of this compound as a result of the 1984 Bhopal disaster (Wang *et al.*, 1998; Varma and Varma, 2005). During the disaster, methyl isocyanate, needed for the synthesis of TMZ (Scheme 1.1), was accidently released to an estimated 200,000 inhabitants living near the manufacturing plant, killing approximately 20,000 people. Consequently, the TMZ precursor was all but removed from the market prompting a need for an alternative route of synthesis.

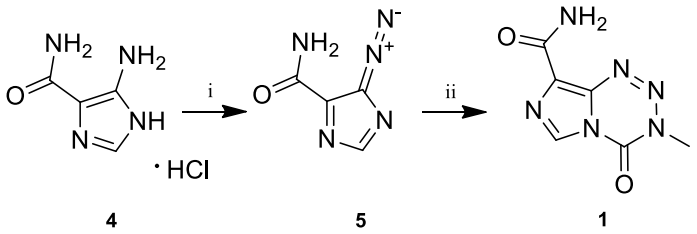

4 **5** **1**

Scheme 1.1: Original synthesis of imidazotetrazines described by Stevens et al., 1984, (TMZ example). Reagents: (i) Sodium nitrite, aq. hydrochloric acid; (ii) methyl isocyanate, dichloromethane, 25 °C, 20 days.

Due to the difficulties of sourcing and shipping industrial quantities of methyl isocyanate, isolation of the potentially dangerous and unstable 5-diazo-1H-imidazole-4-carboxamide **5** and the 20 day synthesis time (Scheme 1.1), a new synthesis, more suited to industry was developed (Stevens *et al.*, 1984). Schering-Plough Corporation, now merged with Merck, initially licensed TMZ and currently have two patented procedures for its industrial scale synthesis, which obviate the use of isocyanates (Moody and Wheelhouse, 2014; Schering-Plough, 2005). The first of these routes, Scheme 1.2, utilises the commercially available AIC **4** as the starting material, consistent with the original route described in scheme 1.1. AIC **4** is treated with 4-nitrophenyl chloroformate to yield the corresponding carbamate **6**. Substitution of the 4-nitrophenyl ester group of carbamate **6** is achieved through treatment with methyl hydrazine, resulting in the formation of a semicarbazide **7**. Cyclisation is achieved through oxidation of intermediate **7** by treating it with tetrabutyl ammonium iodide and periodic acid, yielding TMZ **1** (Kuo, 2005). Although this route avoids the use of methyl isocyanate, the use the highly toxic reagent methyl hydrazine is suboptimal in industry, generating the need for a safer alternative (Zelnick *et al.*, 2003).

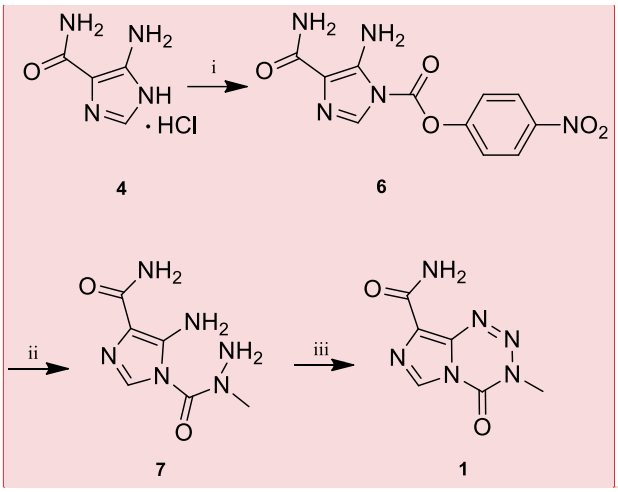

Commented [OI1]: Add yields

Scheme 1.2: Industrial synthetic route to TMZ, patented by Schering-Plough. Reagents: (i) 4-nitrophenyl chloroformate, triethylamine, dichloromethane; (ii) methylhydrazine, dimethylformamide; (iii) tetrabutyl ammonium iodide / periodic acid, tetrahydrofuran / acetonitrile.

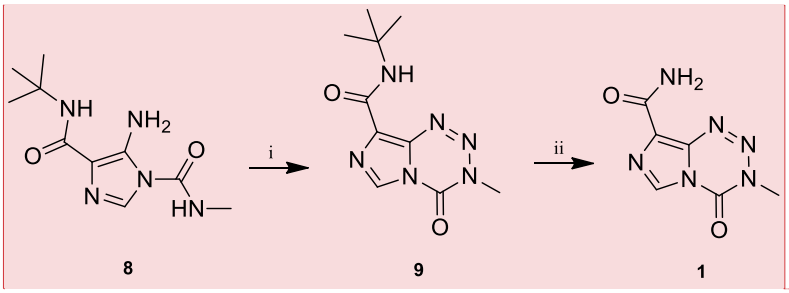

Commented [OI2]: Add yields

Scheme 1.3: Alternate industrial synthetic route to TMZ, patented by Schering-Plough. Reagents: (i) sodium nitrite, acetic acid, lithium chloride, water; (ii) conc. sulphuric acid.

Schering-Plough's second patented route to TMZ, outlined in scheme 1.3, involves a multi-step synthesis to yield a tert-butyl protected imidazole urea **8** (Kuo *et al.*, 2006). Treatment of compound **8** with sodium nitrite and acetic acid causes cyclisation forming the tetrazine ring **9**. The tert-butyl group is then removed by either conc. sulphuric acid or hydrochloric acid /

dioxone (Han *et al.*, 2001; Kuo *et al.*, 2006). Although ultimately more cumbersome, Scheme 1.3 yields TMZ while avoiding the use of methyl isocyanate and methyl hydrazine incorporating improved safety procedures (Moody and Wheelhouse, 2014). However, despite the two schemes patented by Schering-Plough, the method of choice for small-scale research remains coupling diazoimidazoles **5** with isocyanates to form the imidazotetrazine core **1** (Stevens *et al.*, 1984; Wang *et al.*, 1998).

1.4. Mechanism of Action of Temozolomide

TMZ requires an aqueous environment to become biologically active (Agarwala and Kirkwood, 2000). To elicit cytotoxicity the molecule must first be hydrolysed to 5-(3-dimethyl-1-triazenyl) imidazole-4-carboxamide **12** (MTIC). MTIC **12** undergoes further degradation to produce a methyl diazonium ion **13** which is responsible for methylation of the DNA (Scheme 1.4) (Newlands *et al.*, 1997). The first step in the mechanism involves a base catalysed addition of water to the C4 terminus on the tetrazinone ring **1**, forming an unstable tetrahedral intermediate **2** (Scheme 1.4). Mechanistic studies conducted by Mirzaei *et al.,* 2015 confirm a preference for the C4-N5 bond to break over the C4-N3 bond during ring opening (scheme 1.4) (Mirzaei *et al.*, 2015). This is followed by spontaneous decarboxylation at N5, (**11 -** Scheme 1.4). MTIC **12** further degrades through acid catalysed fragmentation of the triazene to afford AIC **4** and the methyl diazonium ion **13** (Scheme 1.4). Although the methyl diazonium **13** ion exists in equilibrium with diazomethane **14**, it is the methyl diazonium ion that methylates DNA, generating cytotoxicity (Newlands *et al.*, 1997).

Figure 1.4 shows the fate of each of the atoms that make up TMZ. The imidazole containing AIC is excreted in the urine following degradation (red), the carbonyl at position 4 on the tetrazinone ring is lost as CO_2 during biological activation under physiological conditions (blue) and N2 and N3 are lost as N_2 (green) during methylation of DNA (Figure 1.4) (Newlands *et al.*, 1997; Nuthalapati *et al.*, 2018). Due to the mechanism of action, TMZ is considered as a carrier designed to deliver the methyl diazonium ion to DNA (Newlands *et al.,* 1997).

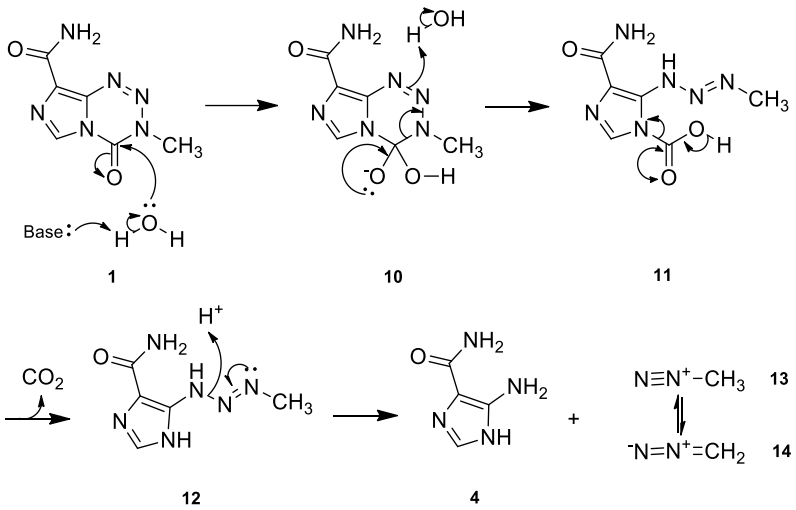

Scheme 1.4: Activation of temozolomide under physiological conditions.

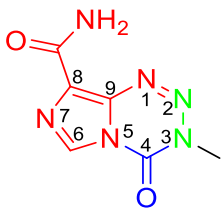

Figure 1.4: Structure of temozolomide showing the biological fate of each atom. Atoms excreted in the urine following degradation are shown in red. N2 and N3 are lost as N2 following methylation of DNA, shown in green and the carbonyl at position 4 is lost as CO_2 following tetrazine ring opening, shown in blue.

As previously stated, TMZ undergoes hydrolytic degradation in order to become biologically active. The cytotoxic methyl diazonium ion **13** (scheme 1.4) is responsible for methylation of DNA, inducing a cytotoxic response (Denny *et al.*, 1994). Methylation of DNA by the diazonium ions occurs mainly in guanine rich sequences of DNA; at guanine-N7 **17**, (70%), occasionally at adenine-N3 **19**, (9%), and at guanine-*O6* **16**, (6%), (Figure 1.5) (Zhang *et al.*, 2012).

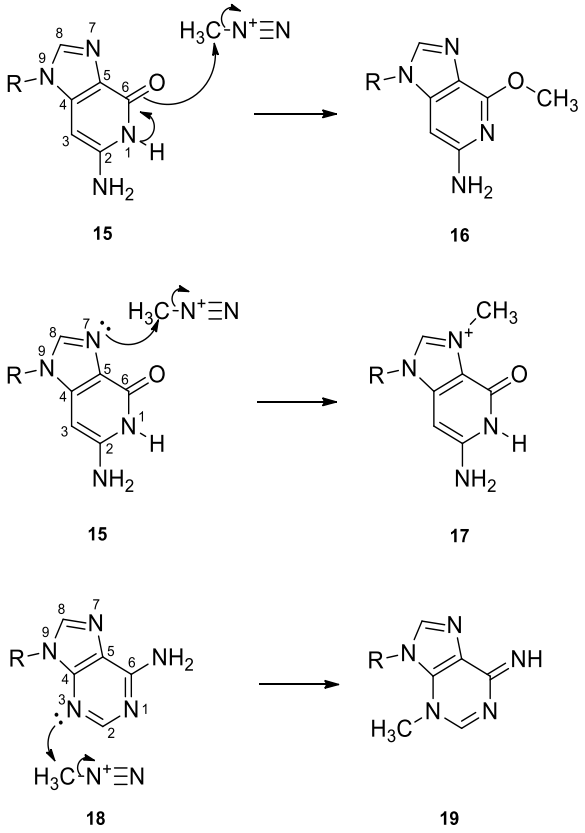

*Figure 1.5: Mechanism of methylation of guanine **15** and adenine **18** producing O6-methyl guanine **16,** N7-methyl guanine **17** and N3-methyl adenine **19**.*

Newlands *et al.,* 1997, describes how methylation tends to occur in the centre of the sequences of three or more consecutive guanines. These results were replicated when other alkylating agents of low molecular weight were used. This phenomenon was attributed to the steric and electronic environment of the DNA. It was found that three consecutive guanine nucleotides give rise to an electron rich environment, and that a run of 3 or more consecutive guanines works to disrupt the double helix shape of the DNA (B-form), leading to an increase in the size of the major groove (Denny *et al.*, 1994). The increase in the size of the major groove results in a better steric access for the methyl diazonium ion which explains the preference of the sites being methylated (Denny *et al.*, 1994).

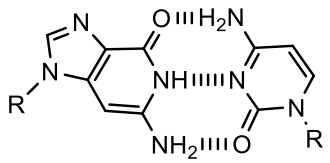

15 **20**

Figure 1.6: Normal base pairing between guanine and cytosine.

The mechanism by which the electrophilic methyl diazonium ion methylates nucleophilic sites on adenine and guanine bases is shown in Figure 1.5 (Wyatt and Pittman, 2006). Methylation at guanine-N7 **17** and adenine-N3 **19** are readily recognised and repaired by base excision repair (BER) pathways, so do not readily contribute to cytotoxicity (Monti *et al.*, 2004). However, methylation at guanine-*O6* **16** is not as readily repaired by BER and so has greater potential to generate cytotoxicity (Fahrer and Kaina, 2013). Normal base pairing between guanine **15** and cytosine **20**, is shown in Figure 1.6 (Watson and Crick, 1953). Hydrogen bonds that dictate base pairing usually exist between positions 1, 2 and 6 on guanine **15** and positions 2, 3 and 4 on cytosine **20**, respectively, (Figure 1.6). Methylation at *O6* on guanine, producing *O6*-methyl

guanine **16** (*O6*-MeG), disrupt hydrogen bonding with cytosine **20** resulting in a preference for bonding with thymine **21**, (Figure 1.7) (Williams and Shaw, 1987).

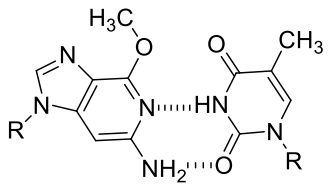

16 **21**

Figure 1.7: Base pairing between methyl guanine and thymine.

The pathway of TMZ-triggered apoptosis in cells, as a result of methylation of guanine, is summarised in Figure 1.8. Mismatch between thymine and *O6*-MeG is recognised by mismatch repair proteins (MMR), prompting the removal of thymine from the replication fork (Roos *et al.*, 2007). In the absence of *O6*-methylguanine-DNA methyltransferase (MGMT) the guanine methylation is not repaired, resulting in reinsertion of thymine into the replication fork. This futile cycle of insertion and deletion persists until the replication fork collapses, inducing a double stranded break (Karran and Bignami, 1994; Hampson *et al.*, 1997). Once a sufficient number of double stranded breaks have occurred, the Ataxia telangiectasia mutated (ATM) and ATM and RAD3-related (ATR) - Chk1 pathways are activated leading to stabilisation of p53, generating an apoptotic response (O'Connell and Cimprich, 2005).

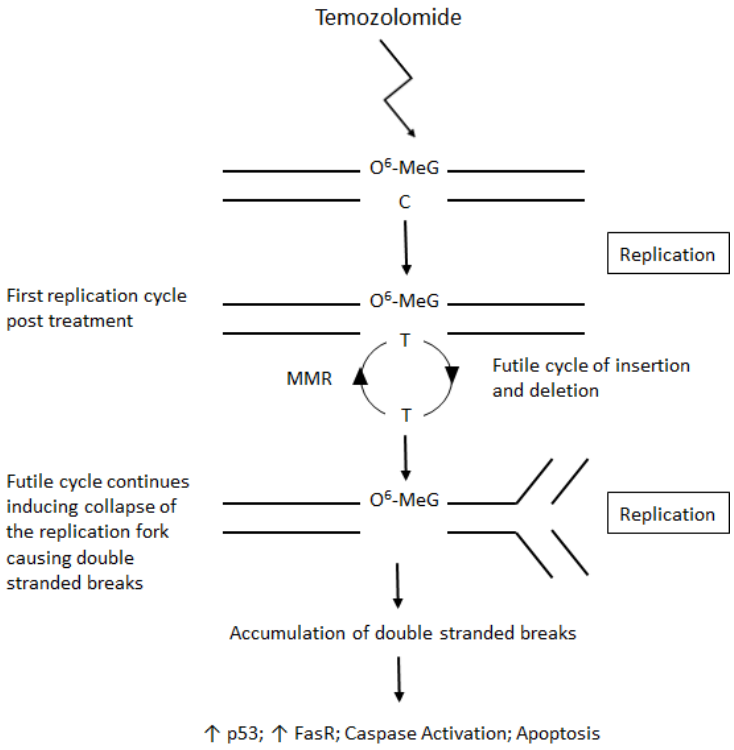

Figure 1.8: A Pathway of temozolomide-triggered apoptosis in glioma cells. (Adapted from: Roos et al., 2007).

1.5. Therapeutic Limitations

The average improvement in the survival of patients with high-grade GBM treated with TMZ and radiotherapy is 2.5 months, when compared with treatment using radiotherapy alone (14.6 months vs 12.1 months, respectively) (Stupp *et al.*, 2005). The improvement of 2.5 months can be, at best, described as modest. Hegi *et al.* (2008) found that 60% of all newly treated patients with GBM receive no benefit from treatment with TMZ (Hegi *et al.*, 2005). Moreover, the study conducted by Stupp *et al.* (2005) did not include patients over the age of 70 or patients who were not capable of independent living, patient cohorts accounting for 20% and 10% of newly diagnosed GBM cases, respectively. Patients within these cohorts are likely to be those with the poorest survival rates and were not included in these studies. It is evident from the literature published that although TMZ does provide a modest improvement for some patients this is not the case for all patients, highlighting the need for an effective alternate therapy (Chamberlain, 2010).

TMZ resistance is one of the principle reasons the majority of patients derive little or no clinical benefit from TMZ treatment. MGMT expression is a major indicator of TMZ resistance and is known to be the sole enzyme responsible for the repair of *O6*-methyl adducts on methyl guanine (Silber *et al.*, 2012). Structure-functionality studies reveal that the enzyme repairs DNA lesions by binding to the minor groove of DNA detecting *O6*-MeG (Tubbs *et al.*, 2007). The methylated base is transferred to the active site of MGMT via a base-flipping mechanism. Once in the active site, MGMT is a reagent in a stoichiometric reaction where the methyl adduct is covalently transferred to a cysteine residue in the active site (Figure 1.9) (Tubbs *et al.*, 2007). MGMT is unique to all other human DNA-repair proteins since once the methyl adducts are transferred to the active site, the enzyme spontaneously degrades. The suicide-repair mechanism of MGMT means resistance is dependent on the rate of methylation of TMZ compared with rate of MGMT synthesis by the cell (Romani *et al.*, 2018). Consequently, the use of MGMT competitive inhibitors such as *O6*-benzylguanine, has been used to increase susceptibility to TMZ treatment,

however to date these efforts have been unsuccessful (Mrugala and Chamberlain, 2008; Kaina *et al.*, 2010).

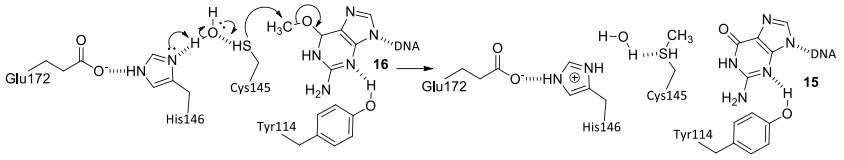

Figure 1.9: O6-Methyl guanine repair by MGMT. During repair the potentially cytotoxic methyl adduct is transferred to a cysteine 145 in the active site of MGMT. (Adapted from: Tubbs et al. (2007)).

Multiple studies have linked the high expression of MGMT in GBM to TMZ resistance. MGMT expression has been shown to relate to levels of methylation in the MGMT promoter (van Nifterik *et al.*, 2010). High levels of methylation within the MGMT promoter region usually result in low levels of protein expression and consequently result in TMZ sensitivity. Consequently, it is generally accepted that TMZ resistance can be best predicted by the methylation status of the MGMT promoter as well as MGMT protein expression levels in the cell/tumour (van Nifterik *et al.*, 2010; Uno *et al.*, 2011). However, some cells, such as cells of the T98G cell line, are MGMT methylated but express high levels of MGMT and confer TMZ resistance. It has been suggested that the resistance observed in the T98G cell line is due to the expression of alkylpurine-DNA-N-glycolase (APNG) as well as MGMT expression (Agnihotri *et al.*, 2012). The APNG protein is a member of the BER machinery and is responsible for the repair of N^3-methyl adenine and N^7-methyl guanine. It has also been shown in patients presenting GBMs that express APNG, have a significantly poorer prognosis than those without (Agnihotri *et al.*, 2012). Similarly, studies investigating patient MGMT promoter methylation status and TMZ sensitivity, found a correlation between methylation and TMZ sensitivity. However, a significant number of patients were found to have a MGMT hypomethylated promoter yet be sensitive to TMZ (Stupp *et al.*, 2005; Hegi *et al.*, 2008). Bocangel et al., failed to find a link between MGMT expression and TMZ

susceptibility in 7 human glial primary cultures. In this case the authors attributed TMZ resistance to non-functional p53 response to DNA damage and not to MGMT expression (Bocangel *et al.*, 2002). Although MGMT promoter methylation status and MGMT protein expression is a useful predictor of TMZ sensitivity for patients, it is clear that multiple proteins play a role.

Known toxicities of TMZ include thrombocytopenia, lymphopenia, neutropenia and the development of myelodysplastic syndrome. Gerber *et al.,* 2007 showed that of 52 newly diagnosed GBM patients, approximately 15-20% went on to develop thrombocytopenia when treated with TMZ and radiotherapy. The development of thrombocytopenia can prevent the safe administration of further chemotherapy, ultimately reducing patient survival. Similarly, Stupp *et al.,* 2007 found that 15% of patients discontinued chemotherapy due to the development of neutropenia or thrombocytopenia. Interestingly, evidence suggests that the development of TMZ toxicity is subject to a significant gender bias. It was found that the development of lymphopenia occurred in 45% of women treated with TMZ, compared to 6% of men (Armstrong *et al.,* 2008). A study conducted by Grossman *et al.,* 2011, found 57% of patients treated with TMZ and radiotherapy went on to develop lymphopenia. Development of lymphopenia bears clinical significance as it is thought to increase a patients' susceptibility to opportunistic infections. *Pneumocystis* pneumonia represents the most clinically-significant of these infections, often leading to co-administration of antipneumoncystis antiparasitic drugs (Grossman *et al.*, 2011).

Additionally, the guidelines on assessing cost effectiveness of drugs was established by The National Institute of Health of Care Excellence (NICE). Cost effectiveness of drugs is expressed as the cost per Quality Adjusted Life-Year (QALY) gained. A QALY takes into account the quantity of life gained as well as the quality of that life through the following: Quality of life (0-1 scale where 1 is equal to perfect health and 0 is equal to death) multiplied by the quantity of life. The cost effectiveness threshold for drugs in the U.K. is between £20,000 and £30,000 per QALY

gained, (Garside *et al.*, 2007). Cost effectiveness analysis of TMZ has shown incremental costs to be £35,861 per QALY. However, a lack of an effective alternative therapy for GBM results in TMZ remaining as the first line treatment, despite the relative costs outweighing patient benefits, (Messali *et al.*, 2013).

As a direct consequence of both the poor clinical performance of TMZ and its subsequent poor cost effectiveness, there is a need for an alternative chemotherapeutic that is more effective and safe for patients diagnosed with GBM, (Chamberlain, 2010). The remainder of this chapter will focus on the efforts that have been made so far to optimise the activity of TMZ in the hope of producing a superior chemotherapeutic for the treatment of GBM.

1.6. Structural Modifications to Optimise Cytotoxicity of Temozolomide

There have been several attempts to optimise the anti-tumour activity of TMZ by modifying its chemical structure. In a study conducted by Lunt *et al.*, 1987, modifications at position 3 of the tetrazine ring were made (Lunt *et al.*, 1987) (figure 1.3). This is a particularly important position on the molecule as it is the site that ultimately bonds to DNA. All ethyl and large alkyl modifications at this position resulted in a significant loss of antitumor activity against TXL5 lymphoma implanted mice. The study found that significant antitumor activity was restricted to TMZ **1** and mitozolomide **2**. It is evident from the results of this study that modifications at position 3 result in compounds that are either too potent for clinical use, as is the case with mitozolomide, or do not exhibit significant antitumor activity, such as the 3-ethyl, 3-alkyl and 3-benzyl modifications (Lunt *et al.*, 1987). Modifications at position 3 may also disrupt the mechanism of imidazotetrazines which could result in undesirable DNA crosslinking leading to potentially fatal side effects, as is the case with mitozolomide (Neijt *et al.*, 1989; Smyth *et al.*, 1989).

One such novel modification made at position 3 was described by Garelnabi *et al.,* 2012. The monofunctional **22** and bifunctional analogues **23** of TMZ from this study are displayed in Figure 1.10. These analogues where tested against colon, non-small-cell lung carcinoma, pancreatic and TMZ resistant cell lines. Both analogues exhibit significantly greater cytotoxic effects when compared with TMZ, regardless of MGMT status. The increased cytotoxicity and success of bifunctional analogues **23** in MGMT positive cells is a result of crosslinking of DNA. As a result, these analogues have presented promising potential and present an intriguing application of imidazotetrazine prodrugs.

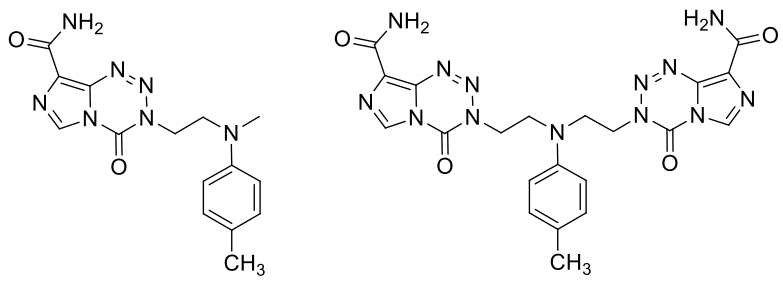

22 **23**

*Figure 1.10: Structure of monofunctional temozolomide analogue, **22**; and bifunctional temozolomide analogue, **23**. (Garelnabi et al., 2012).*

Changes to the imidazotetrazine structure have also included modifications to the core of the molecule. Due to the way in which TMZ and other imidazotetrazines exhibit their mechanism of action, the conformation of the tetrazine ring is vital for ring opening and conversion to MTIC. However, much less detail is known about the role of the imidazole ring during the mechanism of action (Moody and Wheelhouse, 2014). A study conducted by Cheng *et al.,* 1986 analysed the effects of modifying the imidazole ring of mitozolomide and TMZ that involved synthesising a pyrazolo analogue **24** of the two drugs, (Figure 1.11). However, during testing on P388 leukaemia cell lines it was found that the pyrazolo analogue of TMZ was completely inactive. The mitozolomide pyrazolo analogue however, retained some potency and showed good toxicity against the P388 cells (Cheng *et al.*, 1986).

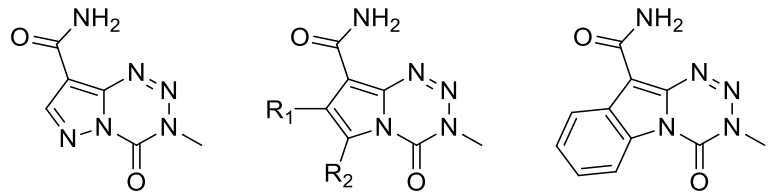

*Figure 1.11: Structures of pyrazolo **24**; pyrrolo **25** and indolo **26** analogues of temozolomide. (Cheng et al., 1986; Diana et al., 2002; Barraja et al., 2004)*

Other modifications to the core of the molecule have been investigated including pyrrole **25** and indolo **26** analogues (Figure 1.11). However, these modifications resulted in very limited efficacy against a small number of cell lines. Drugs that did exhibit growth inhibitory activity were found to work by a different mechanism of action when compared with TMZ, i.e. not methylation. However, the exact mechanism by which these analogues elicit a mechanism of action was not reported (Diana *et al.*, 2002; Barraja *et al.*, 2004). These studies indicate the importance of the imidazole and the tetrazine ring to the activity of the imidazotetrazines.

Modifications of imidazotetrazines at positions 6 and 8 on the imidazole ring have also been investigated (Figure 1.12). Lunt *et al.*, 1987 was the first to characterise modifications to these positions during structure activity relationship (SAR) analysis of imidazotetrazines. Modifications at position 6 included a broad range of alkyl groups. Of these analogues it was found that larger alkyl groups were significantly less cytotoxic, compared to smaller alkyl groups. This effect was attributed to the large alkyl group preventing ring-opening at position 5 due to steric hindrance, thus thwarting nucleophilic attack by water required for the conversion of TMZ to MTIC, which subsequently accounted for the loss of activity of the large 6-alkyl modification (Lunt *et al.*, 1987). Therefore, for optimal cytotoxicity, it is important that position 6 contains only hydrogen in order to allow position 5 to be readily available for nucleophilic attack by water, inducing prodrug activation.

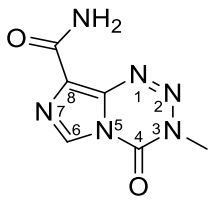

Figure 1.12: Structure of temozolomide showing imidazotetrazine positions.

Modifications at position 8 of the imidazole ring, however, have shown encouraging results. It should be noted that early analogues, synthesised by Lunt *et al.* (1987), were derived from mitozolomide, not TMZ. The presence of a 2-chloroethyl group at position 3 on the tetrazinone ring (mitozolomide) produced acute myelosuppression, and was therefore not approved (Neijt *et al.*, 1989; Smyth *et al.*, 1989). The same study by Lunt *et al.* (1987) found that increasing the size of the amide at position 8, decreased the cytotoxicity of the drug. However, functional groups such as sulfonyl compounds increased cytotoxicity, prompting further research regarding modifications at position 8 of the imidazole ring of TMZ. To date, the role of position 8 of the imidazole ring is much less understood. It has been hypothesised that this position could possibly play a role in a number of different mechanisms that contribute to the activity of imidazotetrazines, these include: exerting a level of control of the conversion to MTIC via ring opening at position 5; increasing the stability of MTIC and the AIC intermediates; adjusting transport and uptake properties of the drug into tumour cells or modifying the non-covalent interactions between the imidazotetrazine intermediates and DNA (Langnel *et al.*, 2000).

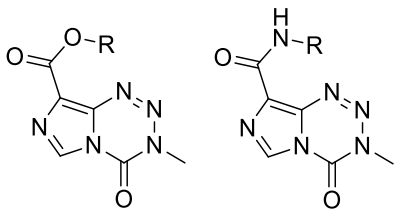

27 **28**

Figure 1.13: General structures of ester and amide analogues synthesised by Liu et al. (2010).

Building on the initial work carried out by Lunt *et al.,* 1987; Liu *et al.,* 2010 synthesised a number of ester **27** and amide **28** analogues at position 8 of the imidazole ring of TMZ. These analogues exhibited a wide range of antitumor activity, which made definitive structural activity relationships difficult to conclude. Ester modifications resulted in analogues that had increased water solubility ranging from 80-110-fold, compared with TMZ. Ester analogues exhibited comparable cytotoxicity to TMZ against PC-3, LNCaP, T47D, MDA-MB-231, DU145, HT29 and HCT-15 cell lines and significantly greater cytotoxicity against HL-60 cells (Liu *et al.,* 2010). Interestingly, the esters that were chosen for analysis in this study all contained amine groups, however, this strategy was not justified. Other modifications at position 8 were carried out by Langnel *et al.,* 2000. These modifications involved the substitution of the amide group at position 8 of the imidazole ring with various 8-cyano-imiazotetrazines using a novel synthetic route. However, the activity of these modified imidazotetrazines was not reported, which may indicate a lack of cytotoxicity displayed by these drugs, similar to what was deduced by Lunt *et al.*, 1987. Suppasansatorn *et al.,* 2006 synthesised a number of TMZ analogues with simple chain ester groups at position 8 with a view to produce analogues that could be suitable for topical administration for melanoma treatment. The hexyl ester analogue was the most promising analogue from this study (Suppasansatorn *et al.*, 2006). Studies conducted by Arrowsmith *et al.,* 1999 and 2002 explored the addition of small linear peptide motifs at position 8 of the imidazole ring, designed to bind to both the major and minor grooves of DNA, however, both studies

concluded limited success, with no significant increase in *in vitro* antitumor activity (Arrowsmith *et al.*, 1999; Arrowsmith *et al.*, 2002).

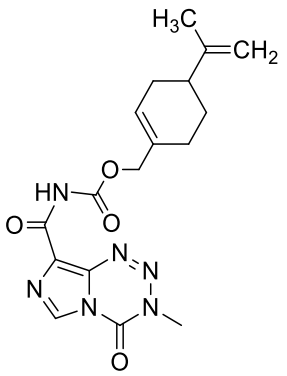

29

Figure 1.14: Structure of NEO212 ***27.*** *(Chen et al., 2015).*

More recently, the conjugation of perillyl alcohol at position 8 has yielded some success. Perillyl alcohol is a naturally occurring alcohol that exhibits anticancer activity against a number of cell lines including TMZ resistant GBM cultures (Chen *et al.*, 2015). Despite encouraging activity of the perillyl alcohol, it did not enter clinical practice due to dose-limiting intestinal toxicity. The structure of the perillyl alcohol conjugate of TMZ (NEO212) **29** is shown in Figure 1.14. NEO212 **29** holds particular promise due to its cytotoxicity against GBM cell lines that are resistant to TMZ and is more potent than the alcohol (Cho *et al.*, 2014). The effectiveness of NEO212 *in vitro* could be attributed to increased cell membrane permeability due to the lipophilic nature of the resulting conjugates allowing improved access to the site of action (Chen *et al.*, 2015). It should be noted that the increase in cytotoxicity of the drug suggests a different mechanism of action from that of TMZ, and could be attributed to the generation of a cytotoxic AIC-perillyl alcohol

degradant, rather than the methylation of DNA via the methyl diazonium ion, currently, this has not been confirmed.

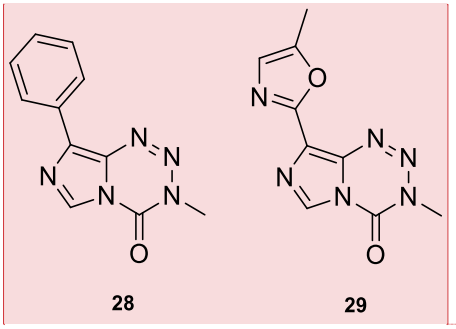

Commented [OI3]: 30 and 31

*Figure 1.15: Structure of 8-phenyl TMZ **28** and 8-(5-methyloxazole) TMZ **29.** (Svec et al., 2018).*

Recently the hydrolytic stability of 3-methylimidazotetrazines, in response to position 8 modifications, has been investigated (Svec *et al.*, 2018). This area of research is of particular interest since currently it is unknown if the rate of prodrug activation of TMZ is optimal to maximise therapeutic efficacy (Wesolowski *et al.*, 2010). Although TMZ has a half-life 1.8 hours in physiological conditions, position-8-modified analogues exhibit half-lives that range from 20 mins for compound **30** to 3 h for compound **31** (Figure 1.15) (Tisdale, 1987; Svec *et al.*, 2018). TMZ analogues that undergo rapid degradation, such as analogue **30**, were shown to exhibit limited efficacy *in-vivo*. The lack of efficacy was attributed to the analogue activating too early, preventing the accumulation of the methyldiazonium ion within the tumour microenvironment. Interestingly, analogue **31** exhibited a half-life of 3 h and enhanced brain distribution (Svec *et al.*, 2018). These results indicate that modifications at position 8 have the potential to affect the electronic properties of the bicyclic ring, in addition to enhanced bio-distribution of the drug, which may lead to analogues with improved therapeutic properties. Similarly, the Nottingham University research group, headed by Malcolm Stevens, reported C8-imidazolyl **32** and C8-methylimidazole **33** TMZ analogues that elicit activity independent of MGMT status (Figure 1.16). Interestingly, these analogues were found to initiate G2/M arrest in cells independent of

both MGMT and MMR status. The research group established that analogues **32** and **33** undergo hydrolytic degradation similar to that of TMZ and were able to methylate similar DNA adducts (Yang *et al.*, 2019). This suggests the increased activity was due to either sheer volume DNA alkylation overcoming the respective repair mechanisms or an additional mechanism of action playing a part. The coupling of TMZ to γ-carboline through amide and amino ethyl linkers has been found to improve brain permeation (Rai *et al.*, 2016). This is supported by the findings of Wollowitz and Kataisto (2009) and Sweetlove (2012) who found TMZ analogues containing γ-carboline are known to have favourable brain penetration properties and thus, exhibit improved therapeutic properties.

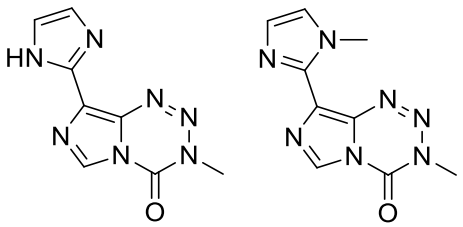

32 **33**

*Figure 1.16: Structure of C8-imidazolyl **32** and C8-methylimidazole **33** TMZ analogues. (Yang et al., 2019).*

1.7. Summary and Aims

1.7.1. Summary

TMZ is the standard of care chemotherapeutic agent used to treat patients with GBM. However, despite this, TMZ provides little benefit to these patients due to systemic toxicity generated through myelosuppression and MGMT mediated resistance. Although NICE guidelines deem TMZ to be a non-cost-effective drug, it is still provided to patients on the NHS as there is no effective alternative. Due to the limited patient benefit and poor cost-effectiveness of TMZ, there is a substantial need for an alternative chemotherapeutic agent for the treatment of GBM. Efforts to increase the efficacy of TMZ through co-administration with MGMT inhibitors have to-date been unsuccessful. Attempts to optimise the activity of TMZ through structural modifications have provided mixed success. Modifications at position 3 on the tetrazine ring have produced analogues that are either too toxic for clinical use or analogues that are inactive. SARs have established that a single hydrogen is optimal for activity at position 6 and that modifications to the imidazotetrazine core disrupts hydrolytic degradation by inhibiting prodrug activation through imidazotetrazine ring opening. It is well established that the amide group present on the imidazole ring is not essential for activity and remains purely as an artefact from its initial synthesis. Therefore, modifications to position 8 modifications holds the most promise for optimising the activity of TMZ. Recent research suggests the substitution of the amide group at position 8 by specific esters appears to increase activity of the molecule. However, as yet no definitive SARs have been deduced. Modifications to TMZ at position 8 can also increase brain permeation as well as effecting the rate of prodrug activation, which has the potential to improve the efficacy of the drug.

1.7.2. Aims

The aim of the following work is to further explore the possibilities of optimising the activity of TMZ by further modifying position 8 of the imidazole tetrazine ring. Evidence to date shows that position 8 plays an important role in the activity of TMZ and by modifying this position, the activity of the drug can be altered. It is speculated that analogues with increased cytotoxic activity could have the potential to become superior cost-effective alternatives to TMZ for patients suffering from GBM.

This study aims:

- To successfully synthesise and characterise novel ester and amide analogues of TMZ using high resolution mass spectrometry, nuclear magnetic resonance spectroscopy, infrared spectroscopy and melting point analysis.
- To evaluate the antiproliferative activity of novel analogues against U87-MG, 1321-N1, GOS-3 and SVG-p12 cell lines.
- To evaluate antiproliferative effects of the most promising novel analogues against MGMT negative and MGMT positive patient-derived primary cells.
- To evaluate the stability of the most promising novel analogues. This will include stability at physiological pH as well as the integrity of ester and amide bonds when subjected to porcine liver esterase.

This thesis will be presented in specialised individual chapters. Chapter 2 will cover the design and synthesis of TMZ analogues. Chapter 3 will investigate the antiproliferative effects of TMZ analogues and identify any potential lead analogues. Chapter 4 will investigate the stability of lead analogues after exposure to an esterase enzyme, monitored by HPLC. Chapter 5 will discuss the findings from chapters 2, 3 and 4; and outline the scope for potential future work.

CHAPTER 2:

CHEMISTRY

2.1. Introduction

It was initially postulated that a H bond donor at position 8 of the imidazole ring of TMZ was central to activity (Figure 2.1) (Lowe *et al.*, 1992; Denny *et al.*, 1994). However, since the understanding of the relationship between imidazotetrazine structural modifications and activity has grown, it has become increasingly apparent that modifications at position 8 on the imidazole ring may be tolerated and have the potential to yield analogues with increased antiproliferative activity (Suppasansatorn *et al.*, 2006; Liu *et al.*, 2010; Garelnabi *et al.*, 2012; Ramirez *et al.*, 2015; Yang *et al.*, 2019). As a result, it is now generally accepted position 8 has potential in terms of improving the efficacy of imidazotetrazines, however, the amide remains solely as an artefact derived from the initial synthesis of imidazotetrazines from DTIC (Svec *et al.*, 2018).

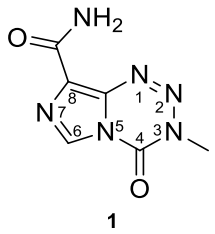

1

Figure 2.1: Structure of temozolomide showing positions.

Structural modifications of TMZ provide a number of challenges to the synthetic chemist. The imidazotetrazine ring opening occurs at physiological pH through base catalysed addition of water to C4=O (Scheme 2.1) (Denny *et al.*, 1994). However, degradation may also occur in acidic conditions, albeit at a much slower rate or as a result of exposure to protic solvents (Stevens *et al.*, 1984; Mirzaei *et al.*, 2015).

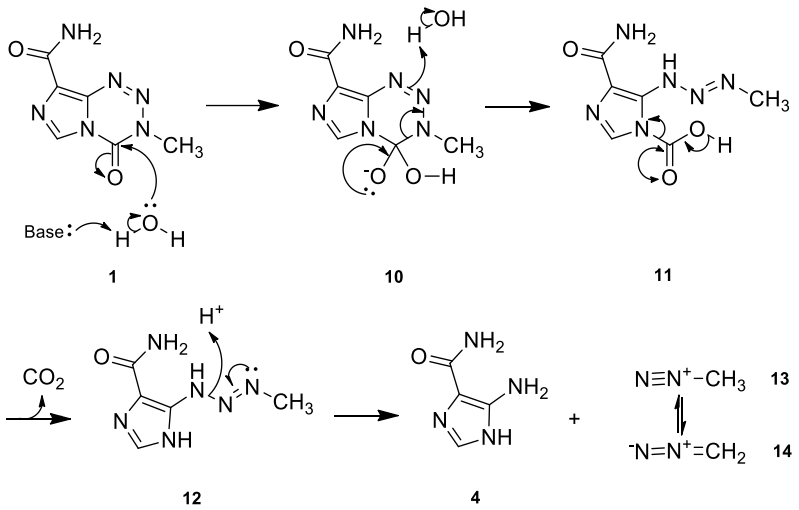

Scheme 2.1: Degradation of temozolomide under physiological conditions.

TMZ is reported to have a half-life of around 1.8 hours at pH 7.4 (Denny *et al.*, 1994). However, in acidic conditions (<pH 4) stability is markedly improved to around 24 hours (Kim *et al.*, 2001). Although the stability of TMZ is greatly improved under acidic conditions degradation persists albeit at a much slower rate.

TMZ also degrades as a result of exposure to protic solvents such as ethanol and methanol. The mechanism of degradation is hypothesised to be due to nucleophilic attack of the hydroxyl group on the protic solvent on the carbonyl at C4, eliciting ring opening similar to that depicted in Scheme 2.1. (Stevens *et al.*, 1984). Due to the relative instability of the imidazotetrazine core, schemes of synthesis must be designed to avoid neutral/basic conditions and protic solvents in order to maximise yields. The remainder of this chapter will focus on the design, synthesis and characterisation of novel temozolomide analogues.

2.2. Rational Design of Temozolomide Analogues

2.2.1. Literature Review of Previous Modifications and Identifying a Suitable Position to Modify

Structure-based drug design is currently the most common method of identifying lead compounds which elicit desired activity. Traditionally, the development of lead compounds is centred around identifying a target macromolecule implicated with the disease in question, such macromolecules may include enzymes, receptors or nucleic acids. Once a suitable target is identified, drugs may be designed with a structure that suitably interacts with the target macromolecule to produce the desired outcome. The desired outcome of chemotherapeutics is to elicit antiproliferative and cytotoxic effects in cancerous cells.

In the case of TMZ **1**, methyl diazonium ions **13** released through prodrug activation, methylate DNA bases preventing replication and initiating antiproliferative effects. Although it is well documented that the methyl diazonium ion **13** bonds to the target (DNA) eliciting the desired antiproliferative effects, the efficiency of TMZ's ability to activate and achieve this aim is questionable due to negligible patient benefit. Therefore an aim of this study was to optimise the activity of TMZ by modifying its chemical structure.

Modifications that perturb or change the mechanism by which TMZ elicits its effects can be a successful approach. Modifications at position 3 determine the group that is ultimately transferred to DNA. Lunt et al., 1987 found chloroethyl and methyl moieties elicited cytotoxicity exclusively. More recently, studies investigating bi-functional TMZ analogues have displayed some success *in vitro* (Ramirez *et al.*, 2015). These analogues give rise to diazonium ions with DNA cross-linking potential.

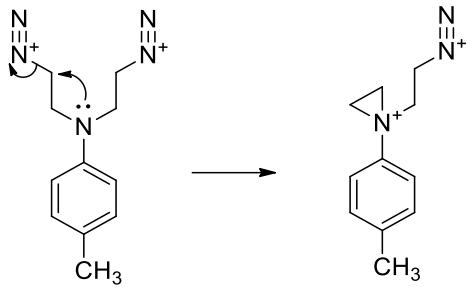

*Figure 2.2: Depicting the intramolecular trapping reaction of (2-[N-(2-diazonioethyl)-4-methyl-anilino]ethanediazonium) **34** to form the corresponding azridinium ion **35**. (Garelnabi et al., 2012)*

Bifunctional analogues **23**, as discussed in the Chapter 1, have been shown to initiate inter-strand cross links thus activating ATM/ATR pathways (Garelnabi *et al.*, 2012; Ramirez *et al.*, 2015). Upon hydrolytic ring opening, producing compound **34**, these analogues undergo an intramolecular trapping reaction, depicted in Figure 2.2, producing aziridinium species **35** that are responsible for alkylating nucleic acids and eliciting a cytotoxic effect. However, it is suggested that imidazotetrazines with the ability to cross-link DNA are unsuitable as chemotherapeutic agents due to the life-threatening myelosuppression they elicit in patients (Lunt *et al.*, 1987; Neijt *et al.*, 1989; Smyth *et al.*, 1989). As a result, it is deemed that the methyl group at position 3 is useful to retain a mechanism of action that elicits cytotoxicity with tolerable side effects. Furthermore, as described in Chapter 1, the addition of alkyl groups at position 6 perturbs prodrug activation, reducing cytotoxic potency (Lunt *et al.*, 1987). Similarly, structural modifications to the core of TMZ also prevent prodrug activation resulting in reduced activity (Cheng *et al.*, 1986; Diana *et al.*, 2002). The amide at position 8 however, holds more promise as a possible site that could increase activity. Multiple studies have described position 8 modified analogues with increased cytotoxic potencies against numerous cell lines (Suppasansatorn *et al.*, 2006; Liu *et al.*, 2010; Svec *et al.*, 2018; Marin-Ramos *et al.*, 2018). In fact it is now widely recognised that the amide at position 8 on TMZ is not central to activity and can

tolerate modifications (Lowe *et al.*, 1992; Svec *et al.*, 2018). Consequently, position 8 was targeted as a site of modification with the view to yield analogues with increased anticancer effects.

2.1.2. Rational Design of Analogues

Since there are no definitive SARs proposed at position 8 on TMZ, the strategic design of compounds which may yield increased anticancer activity holds its own challenges. Although the exact role of this position is unknown, a number of hypothetical roles have been described in the literature. It is hypothesised that the position could play a role in exerting kinetic control over prodrug activation (Langnel *et al.*, 2000; Svec *et al.*, 2018); influencing transport properties of compounds by modifying their subsequent internalisation within cells; or influencing the non-covalent interactions between intact prodrug and DNA (Langnel *et al.*, 2000). Rational drug design was centred around these hypotheses with the aim of both synthesising superior analogues of TMZ alongside extending SAR at the position of modification.

Since it is hypothesised that position 8 plays a role in non-covalent interactions with DNA, influencing the potency of the molecule (Langnel *et al.*, 2000), it appears logical that a series of ester and amide analogues of TMZ would give a useful insight into SARs at this position. Esters and amide groups provide sites for hydrogen bond accepting (HBA) and hydrogen bond donating sites (HBD), respectively (Figure 2.3). Consequently, the effect of changing the hydrogen bonding character at position 8 will be investigated by synthesising analogues with respective ester and amide groups at this position. There have been a number of reviews that help support the strategy behind the use of esters and amides that tend to retain cytotoxic potency (Suppasansatorn *et al.*, 2006; Liu *et al.*, 2010; Marin-Ramos *et al.*, 2018). Whereas, other position 8 modifications such as cyano and nitro moieties resulted in analogues devoid of significant anti-tumour activity (Lunt *et al.*, 1987). Consequently, the synthesis of a series of ester and amide analogues of TMZ would increase the probability of yielding analogues with significant activity, (figure 2.3).

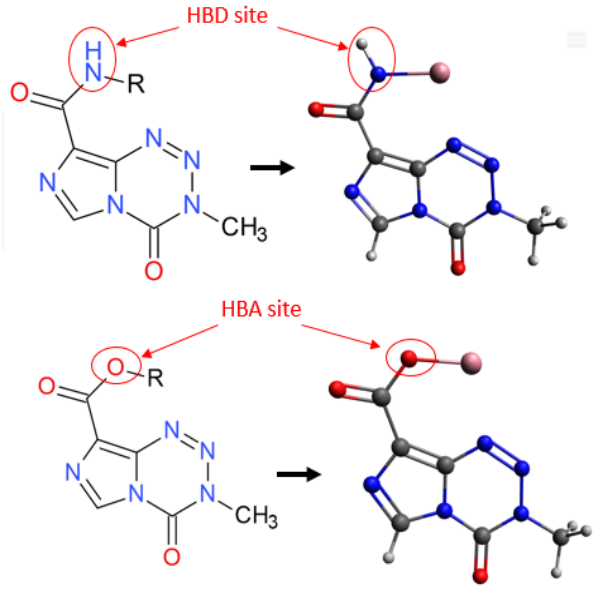

Figure 2.3: Chemical structures and molecular models of ester and amide analogues of temozolomide.

An earlier report regarding ester TMZ analogues at position 8, reviewed in section 1.6.3, failed to assess the antiproliferative effects of phenyl ester and amide groups. Systematic design of 8-phenyl ester and amide TMZ analogues, with various aromatic substituents, should provide an insight into the implications of mesomeric and inductive effects of the molecule, (Figure 2.4). It is hypothesised that mesomeric effects of these groups could influence electron distribution within the molecule, subsequently impacting the kinetics of prodrug activation. Interestingly, post-design of analogues in the present study, Svec et al., 2018 confirmed the hypothesis that position 8 could exert kinetic control over pro-drug activation before the current work was published. However, the design of the analogues described in the present study could provide a greater insight into these effects due to the small systematic changes made at position 8.

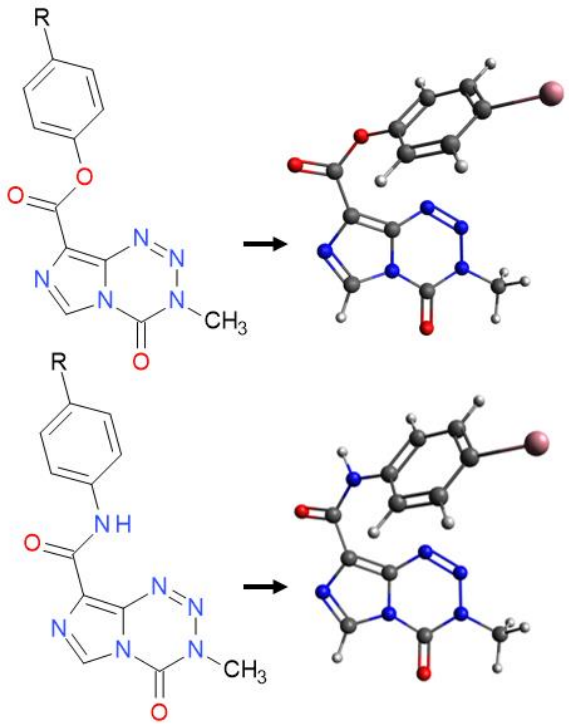

Figure 2.4: Chemical structures and molecular models of phenyl ester and amide analogues of temozolomide.

The addition of various ester and amide derivatives at position 8 will ultimately affect the lipophilicity of the molecule. As previously mentioned, it is hypothesised that position 8 could play a role in the bio-distribution and cellular internalisation of TMZ analogues into cells. The addition of short alkyl chains to esters and amides would serve to increase the lipophilicity of analogues, improving BBB penetration and cellular internalisation, (Figure 2.5). A similar effect is observed when comparing BBB penetration of morphine and heroin (Di and Kerns, 2016). The addition two acetyl groups on morphine, yielding heroin, causes 100-fold increase in BBB penetration (Clark, 2003). It is hypothesised that by adding moieties at position 8 on TMZ could have similar effects.

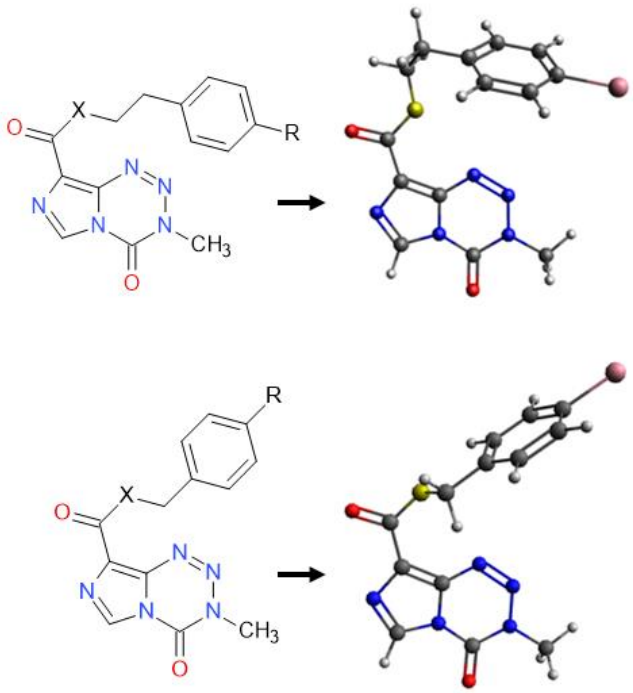

Figure 2.5: Chemical structures and molecular models of benzyl and phenethyl ester and amide analogues of temozolomide. X = O or NH.

The series of TMZ analogues will include the most promising analogues from Liu et al., 2010 and Suppasansatorn et al., 2006. The inclusion of TMZ hexyl ester (Suppasansatorn *et al.*, 2006) and TMZ 3-(dimethylamino)propyl ester (Liu *et al.*, 2010) will provide a basis for comparing the novel analogues synthesised in this study, (Figure 2.6). Furthermore, in both these studies, antiproliferative evaluation was not carried out on glioma cell lines. During this study, the inclusion of TMZ hexyl ester and TMZ 3-(dimethylamino)propyl ester should provide a useful comparison since these analogues will be tested for the first time against glioma cell lines.

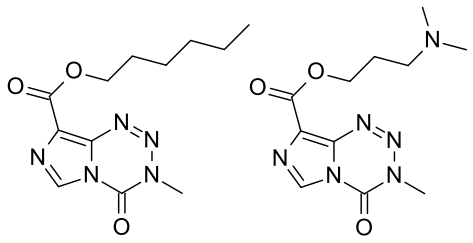

ES2 **ES7**

Figure 2.6: Structures of TMZ hexyl ester (ES2) TMZ 3-(dimethylamino)propyl ester (ES7), first described in Suppasansatorn et al. (2006) and Liu et al. (2010), respectively.

2.1.3. Summary of the Rational Design

- Position 8 on the imidazole ring has been identified as the most promising position that yields analogues with superior antiproliferative activity compared to TMZ.
- The precise role of position 8 of TMZ has still not been elucidated. However, it is hypothesised to be involved in the following:
    - Exerting kinetic control over prodrug activation.
    - Influencing transport properties of the drug.
    - Influencing non-covalent interactions between intact prodrug and DNA.

Table 2.1: A summary of the considerations in the design of novel TMZ analogues.

Modifications to be made at position 8	**Rationale**
Modifications will utilise ester and amide linkages.	Previous literature suggests increased activity in ester and amide TMZ analogues. Additionally provides HBA and HBD sites.
Utilising phenyl ester and amide groups.	Phenyl ester moieties are yet to be investigated at position 8 of TMZ. The inclusion of phenyl ester and amides, with various aromatic substituents, should provide an insight into the mesomeric and inductive effects.
Utilising various alkyl chains within the ester / amide moiety.	The use of alkyl chains in the design of the molecule will increase lipophilicity, potentially improving cellular internalisation of analogues and the ability to penetrate the BBB.

The aim of Chapter 2 will be to successfully synthesise and characterise a series of ester and amide analogues of TMZ that address the rationale covered previously.

2.3. Experimental

2.3.1. Chemicals and Reagents

Temozolomide was purchased from Carbosynth. Deuterated solvents, dimethyl sulfoxide-*d6* and chloroform-*d*, for NMR analysis were purchased from GOSS Scientific. Ethyl acetate, ethanol, anhydrous tetrahyrofuran, anhydrous toluene, petroleum ether 40-60^{o}C and dichloromethane were purchased from Fisher Scientific. Concentrated sulphuric acid, HPLC grade water, 1-(3-dimethylaminopropyl)-3-ethylcarbodiimide hydrochloride and anhydrous magnesium sulphate were purchased from Fisher Scientific. Sodium nitrite, thionyl chloride, anhydrous dimethylformamide, silica gel for column chromatography, 4-methoxyphenylethyl alcohol, phenol, aniline and 4-dimethylaminopyridine were purchased from Sigma Aldrich (now Merk). N,N'-dicyclohexylcarbodiimide was purchased from Alfa Aesar. p-Cresol, 2-phenylethanol, 4-nitrophenylethyl alcohol, 4-methoxybenzyl alcohol, 4-methoxyphenol, 4-nitrophenol, 4-chlorophenol, 4-hydroxybenzonitrile, 2-methoxyphenol, 3-dimethylamino-1-propanol, 2-phenylethyl amine, p-anisidine, 4-methylbenzylamine and 4-chlorobenzylamine were purchased from Alfa Aesar. were purchased from Sigma Aldrich. p-Toluidine, 4-chloroaniline, 4-aminobenzonitrile, hexylamine, o-anisidine and 4-methoxybenzylamine were purchased from Acros Organics. All reagents were commercially sourced and used without any further purification.

2.3.2. Overview of Methods

All solvents and reagents were used without any further purification. Reactions were monitored using silica gel coated TLC plates with fluorescent indicator (254 nm). Flash column chromatography, used for purification, was carried out using silica gel purchased from Sigma Aldrich. Specifications of the silica gel were; 60 Å pore size, 230-400 mesh particle size and 40-63 µm particle size. ^{1}H and ^{13}C NMR spectra were recorded on either Bruker Fourier 300 (300 MHz) or a Bruker Advance III 400 (400 MHz). All chemical shifts are relative to residual solvent

peaks (chloroform-*d* $CDCl_3$, δ_H-7.26; δ_c-77.16); (DMSO-d_6, δ_H-2.50; δ_c-39.52). J Values are calculated in Hz. IR spectra were recorded on Nicolet iS10 Spectrophotometer. Melting points were recorded on a Stuart SMP10 melting point apparatus and were uncorrected. High resolution mass spectrometry (HMRS) was obtained by Pharmidex by means of UHPLC-ToF-MS using electrospray ionisation on a Agilent 1290 UHPLC and Agilent 6550 QToF-MS. In the cases where more than one synthetic route was used, the most efficient route, in terms of yield, was reported. The assignment of carbon environments of ^{13}C NMR spectra was aided by ^{13}C dept-135.

2.3.3. Synthesis

2.3.3.1. Preparation of Ester and Amide Analogues of Temozolomide Utilising Acyl Chlorides (Scheme 2.2)

*Synthesis of 3-Methyl-4-oxo-imidazo[5,1-d][1,2,3,5]tetrazine-8-carboxylic acid (Temozolomide Acid **36**)*

TMZ **1** (2.00 g, 10.3 mmol) was dissolved in conc. sulphuric acid (16 mL). Sodium nitrite (2.65 g, 38.4 mmol) in water (10.4 mL) was added dropwise to the solution, keeping the temperature of the reaction mixture below 15 °C. The resulting mixture was left for 16 h. Ice-water (40 mL) was added to the mixture, precipitating out the desired product. The precipitate **36** was collected via filtration before being dried over phosphorus pentoxide for 48 h. Producing a white solid, 1.36 g (68 % yield).

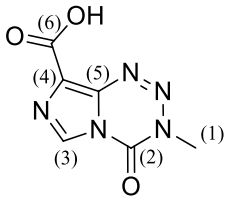

M.p. = 181 °C (decomposition) (lit. = >180 °C); IR (cm^{-1}) 3499 (O-H stretch), 3080 (C-H stretch), 1764 (C=O stretch, COOH), 1686 (C=O stretch, CONH). ^1H NMR (300 MHz, DMSO-d_6), δ_H: 13.40

(bs, 1H, OH), 8.82 (s, 1H, N-CH), 3.87 (s, 3H, N-CH_3). ^{13}C NMR (75 MHz, DMSO-d_6), δ_C: 162.28 (6), 139.52 (2), 136.91 (5), 129.52 (3), 128.17 (4), 36.76 (1). HRMS calc'd for $C_6H_5N_5O_3$ $[M+Na]^+$: 218.0284. Found *m/z*: 218.0293.

*Synthesis of 3-Methyl-4-oxo-imidazo[5,1-d][1,2,3,5]tetrazine-8-carbonyl chloride (Temozolomide Acyl Chloride **37**)*

A mixture of temozolomide acid **36** (200 mg, 1.03 mmol), thionyl chloride (5 mL, 69 mmol) and dimethylformamide (1 drop) was heated under reflux for 3 h. The resulting mixture was evaporated under reduced pressure. Toluene (3 x 10 mL) was added and evaporated to dryness to yield, 3-methyl-4-oxo-imidazo[5,1-d][1,2,3,5]tetrazine-8-carbonyl chloride (**37**, TMZ acyl chloride), as a brown/orange solid 218 mg, (99 % yield). M.p. = 142 °C (lit. = 142 – 143 °C).

General synthesis of target compounds ES1-ES7; AM1-AM11

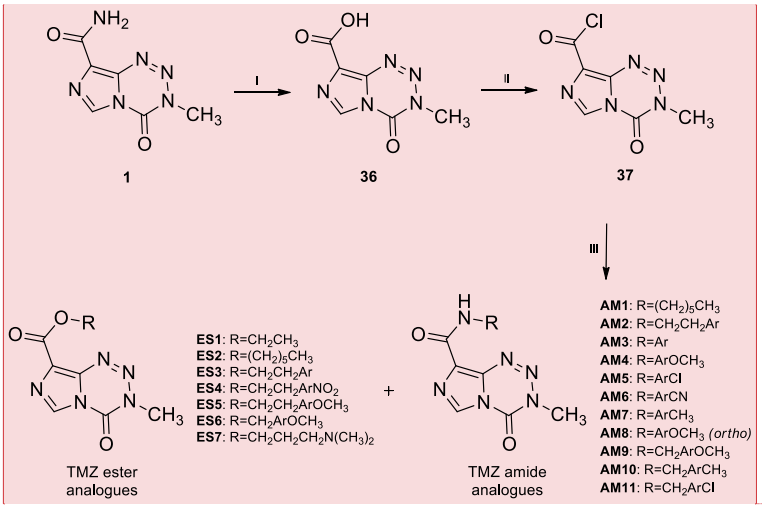

*Scheme 2.2: (I) Sodium nitrite, conc. Sulphuric acid <15 °C; (II) thionyl chloride, dimethylformamide reflux; (III) appropriate alcohol / amine, THF, r.t. Ester and amide analogues are referred to as **ES** and **AM**, respectively.*

Note: All aromatic substituents are in the para- position unless otherwise stated.

Commented [OI4]: These are incorrect

Commented [OI5]: Change CH3

Temozolomide acyl chloride (**37**, 218 mg, 1.02 mmol) was dissolved in tetrahydrofuran (10 mL). A solution of tetrahydrofuran (2 mL) and the appropriate alcohol or amine (≈1.05 mmol) was added dropwise and stirred for 3 h. The crude reaction mixture was absorbed onto silica, and purified by column chromatography using a solvent system of an appropriate ratio of light petroleum ether to ethyl acetate, to afford the desired title compounds.

Ethyl 3-methyl-4-oxo-3,4-dihydroimidazo[5,1-d][1,2,3,5]tetrazine-8-carboxylate - ES1

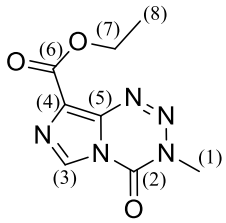

General procedure for synthesis outlined in Section 2.3.3.1., Scheme 2.2. Ethanol (76 µL, 1 mmol, equiv. 1.2) was added dropwise to a solution of temozolomide acyl chloride (0.177 g, 0.83 mmol, equiv. 1.0) in THF (10 mL). EtOAc was used for flash column chromatography to afford compound **ES1**, light orange solid 145 mg, (79 % yield). M.p. 130 °C; IR (cm^{-1}) 1716 (C=O stretch, COO), 1623 (C=O stretch, CONH). ^{1}H NMR (300 MHz, DMSO-d_6), δ_H: 8.85 (s, 1H, N-CH), 4.38 (q, J = 7.1 Hz, 2H, O-CH_2), 3.88 (s, 3H, N-CH_3), 1.33 (t, J = 7.1 Hz, 3H, CH_3). ^{13}C NMR (75 MHz, DMSO-d_6), δ_C: 160.9 (6), 139.4 (2), 137.1 (5), 129.8 (3), 127.1 (4), 61.3 (7), 36.9 (1), 14.7 (8). HRMS calc'd for $C_8H_9N_5O_3$ $[M+Na]^+$: 246.0598. Found *m/z*: 246.0629.

Hexyl 3-methyl-4-oxo-3,4-dihydroimidazo[5,1-d][1,2,3,5]tetrazine-8-carboxylate - ES2

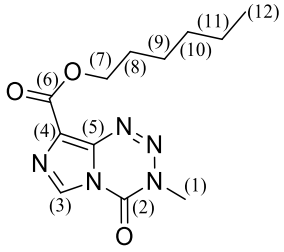

Procedure for synthesis outlined in Section 2.3.3.1., Scheme 2.2. Hexanol (110 µL, 0.88 mmol, equiv. 0.88) was added dropwise to a solution of temozolomide acyl chloride (213 mg, 0.10 mmol, equiv. 1.0) in THF (10 mL). EtOAc : petroleum ether (1:1, v/v) was used for flash column chromatography to afford compound **ES2**, yellow solid 105 mg (29 % yield); m.p. 76 °C; IR (cm^{-1}) 3114 (C-H stretch), 2956 (C-H stretch), 2921 (C-H stretch), 2854 (C-H stretch), 1755 (C=O stretch, COO), 1722 (C=O stretch, CONH). ^{1}H NMR (300 MHz DMSO-d_6), δ_H: 8.85 (s, 1H, N-CH), 4.34 (t, J = 7.1 Hz, O-CH_2), 3.88 (s, 3H, N-CH_3), 1.71 (quint, J = 7.1 Hz, 2H, CH_2), 1.53 – 1.16 (m, 8H, $(CH_2)_4$), 0.87 (t, J = 7.1 Hz, 3H, CH_3). ^{13}C NMR (75 MHz DMSO-d_6), δ_C: 160.96 (6), 139.43 (2), 137.13 (5), 129.80 (3), 127.12 (4), 65.16 (7), 36.84 (1), 31.30 (8), 28.63 (9), 25.51 (10), 22.50 (11), 14.36 (12). HRMS calc'd for $C_{12}H_{17}N_5O_3$ $[M+Na]^+$: 302.1224. Found *m/z*: 302.1239.

Phenethyl 3-methyl-4-oxo-3,4-dihydroimidazo[5,1-d][1,2,3,5]tetrazine-8-carboxylate - ES3

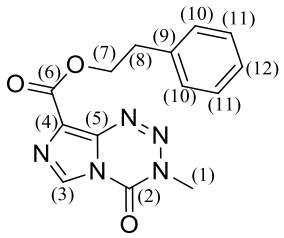

Procedure for synthesis outlined in Section 2.3.3.1., Scheme 2.2. 2-Phenylethanol (110 µL, 0.92 mmol, equiv. 0.89) was added dropwise to a solution of temozolomide acyl chloride (222 mg, 1.03 mmol, equiv. 1.0) in THF (10 mL). EtOAc : petroleum ether (1:1, v/v) was used for flash

column chromatography to afford compound **ES3**, off-white solid 137.4 mg. (44% yield); m.p. 124 °C; IR (cm^{-1}) 3067 (C-H stretch), 1740 (C=O stretch, COO), 1712 (C=O stretch, CONH), ^{1}H NMR (300 MHz DMSO-d_6), δ_H: 8.85 (s, 1H, N-CH), 7.38-7.19, (m, 5H, Ar), 4.55 (t, J = 7.5 Hz, 2H, O-CH_2), 3.89 (s, 3H, N-CH_3), 3.05 (t, J = 7.5 Hz, 2H, CH_2-Ar). ^{13}C NMR (75 MHz DMSO-d_6), δ_C: 160.9 (6), 139.4 (2), 138.4 (9), 137.2 (5), 129.8 (3), 129.5 (11), 128.8 (10), 126.9 (4), 126.9 (12), 65.8 (7), 36.9 (1), 34.9 (8). HRMS calc'd for $C_{14}H_{13}N_5O_3$ $[M+Na]^+$: 322.0911. Found *m/z*: 322.0925.

4-Nitrophenethyl 3-methyl-4-oxo-3,4-dihydroimidazo[5,1-d][1,2,3,5]tetrazine-8-carboxylate - ES4

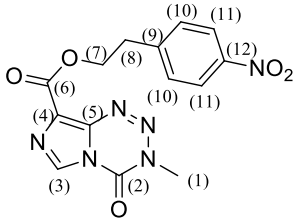

Procedure for synthesis outlined in Section 2.3.3.1., Scheme 2.2. 2-(4-Nitrophenyl)ethanol (150.4 mg, 0.90 mmol, equiv. 0.96), in THF (2 mL), was added dropwise to a solution of temozolomide acyl chloride (201 mg, 0.94 mmol, equiv. 1.0) in THF (10 mL). EtOAc was used for flash column chromatography to afford compound **ES4**, white solid 102.6 mg (27 % yield); m.p. 187 °C; IR (cm^{-1}) 3105 (C-H stretch), 1743 (C=O stretch, COO), 1708 (C=O stretch, CONH). ^{1}H NMR (300 MHz, DMSO-d_6), δ_H: 8.86 (s, 1H, N-CH), 8.15 (d, *J* = 8.3 Hz, 2H, Ar), 7.67 (d, *J* = 8.3 Hz, 2H, Ar), 4.63 (t, *J* = 6.4 Hz, 2H, O-CH_2), 3.90 (s, 3H, N-CH_3), 3.22 (t, *J* = 6.4 Hz, 2H, CH_2-Ar). ^{13}C NMR (75 MHz DMSO-d_6), δ_C: 160.7 (6), 147.0 (12), 146.7 (9), 139.4 (2), 137.2 (5), 130.9 (10), 129.9 (3), 126.7 (4), 123.8 (11), 65.0 (7), 36.9 (1), 34.6 (8). HRMS calc'd for $C_{14}H_{12}N_6O_3$ $[M+Na]^+$: 367.0761. Found *m/z*: 367.0772.

4-Methoxyphenethyl 3-methyl-4-oxo-3,4-dihydroimidazo[5,1-d][1,2,3,5]tetrazine-8-carboxylate - ES5

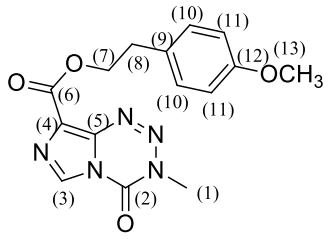

Procedure for synthesis outlined in Section 2.3.3.1., Scheme 2.2. 2-(4-Methoxyphenyl)ethanol (157.0 mg, 1.03 mmol, equiv. 1.0), in THF (2 mL), was added dropwise to a solution of temozolomide acyl chloride (220.8 mg, 1.03 mmol, equiv. 1.0) in THF (10 mL). EtOAc : petroleum ether (1:1, v/v) was used for flash column chromatography. The crude product was subjected twice, to flash column chromatography to afford compound **ES5**, off-white solid 79.2 mg (22 % yield); m.p. 164 °C; IR (cm^{-1}) 3126 (C-H stretch), 1745 (C=O stretch, COO), 1725 (C=O stretch, CONH). ^{1}H NMR (300 MHz, DMSO-d_6), δ_H: 8.85 (s, 1H, N-CH), 7.27 (d, J = 8.4 Hz, 2H, Ar), 6.85 (d, J = 8.4 Hz, 2H, Ar), 4.48 (t, J = 6.8 Hz, 2H, O-CH_2), 3.89 (s, 3H, O-CH_3), 3.71 (s, 3H, N-CH_3), 2.98 (t, J = 6.8 Hz, 2H, CH_2-Ar). ^{13}C NMR (75 MHz DMSO-d_6), δ_C: 160.9 (6), 158.3 (12), 139.4 (2), 137.2 (5), 130.5 (9), 130.1 (3), 129.8 (10), 127.0 (4), 114.2 (11), 66.1 (7), 55.4 (13), 36.9 (1), 34.0 (8). HRMS calc'd for $C_{15}H_{15}N_5O_4$ $[M+Na]^+$: 352.1016. Found *m/z*: 352.1029.

4-Methoxybenzyl 3-methyl-4-oxo-3,4-dihydroimidazo[5,1-d][1,2,3,5]tetrazine-8-carboxylate - ES6

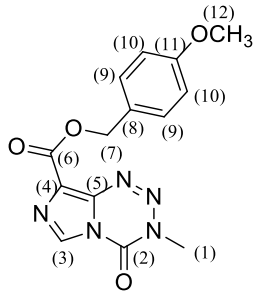

Procedure for synthesis outlined in Section 2.3.3.1., Scheme 2.2. 4-Methoxybenzyl alcohol (122.5 mg, 0.89 mmol, equiv. 0.92), in THF (2 mL), was added dropwise to a solution of temozolomide acyl chloride (209.3 mg, 0.98 mmol, equiv. 1.0) in THF (10 mL). EtOAc : petroleum ether (3:2, v/v) was used for flash column chromatography to afford compound **ES6**, yellow solid 111.4 mg (37 % yield); m.p. 170 ^{o}C, IR (cm^{-1}) 3122 (C-H stretch), 2961 (C-H stretch), 2928 (C-H stretch), 1752 (C=O stretch, COO), 1719 (C=O stretch, CONH), 1615-692. ^{1}H NMR (300 MHz, DMSO-d_6), δ_H: 8.85 (s, 1H, N-CH), 7.44 (d, J = 8.4 Hz, 2H, Ar), 6.96 (d, J = 8.4 Hz, 2H, Ar), 5.36 (s, 2H, O-CH_2), 3.88 (s, 3H, O-CH_3), 3.76 (s, 3H, N-CH_3). ^{13}C NMR (75 MHz DMSO-d_6), δ_C: 160.8 (6), 159.7 (11), 139.4 (2), 137.3 (5), 130.5 (3), 129.9 (9), 128.3 (8), 123.0 (4), 114.3 (10), 66.4 (7), 55.6 (12), 36.9 (1). HRMS calc'd for $C_{14}H_{13}N_5O_4$ $[M+Na]^+$: 338.0860. Found *m/z*: 338.8075.

3-(Dimethylamino)propyl 3-methyl-4-oxo-3,4-dihydroimidazo[5,1-d][1,2,3,5]tetrazine-8-carboxylate – ES7

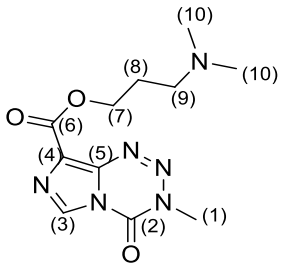

Procedure for synthesis outlined in Section 2.3.3.1., Scheme 2.2. 3-Dimethylamino-1-propanol (103.6 µL, 1.03 mmol, equiv. 1), solubilised in THF (2 mL), was added dropwise to a solution of temozolomide acyl chloride (219.9 mg, 1.03 mmol, equiv. 1.0) in THF (10 mL). EtOAc was used for flash column chromatography to afford compound **ES7**, white solid 132.4 mg (46 % yield); m.p. 204 °C, IR (cm^{-1}) 3074 (C-H), 2595-2483 (C-H), 1747 (C=O stretch, COO), 1719 (C=O stretch, CONH). ^{1}H NMR (300 MHz, DMSO-d_6) δ_H: 8.89 (s, 1H, N-CH), 4.43 (t, J = 6.2 Hz, 2H, O-CH_2), 3.89 (s, 3H, N-CH_3), 3.20 (t, J = 6.2 Hz, 2H, CH_2-N), 2.75 (s, 6H, N-CH_3), 2.18 (quint, *J* = 6.2 Hz, 2H, CH_2). ^{13}C NMR (100 MHz, DMSO) δ 160.2 (6), 138.9 (2), 136.8 (5), 129.4 (3), 126.3 (4), 62.1 (7), 53.8 (9), 42.1 (10), 36.4 (1), 23.3 (8). HRMS calc'd for $C_{14}H_{13}N_5O_4$ $[M+H]^+$: 281.1357. Found *m/z*: 281.1372.

N-hexyl-3-methyl-4-oxo-3,4-dihydroimidazo[5,1-d][1,2,3,5]tetrazine-8-carboxamide - AM1

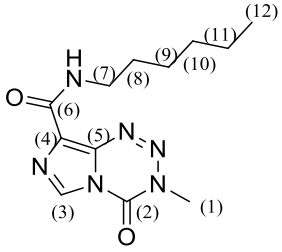

Procedure for synthesis outlined in Section 2.3.3.1., Scheme 2.2. Hexan-1-amine (135.8 µL, 1.03 mmol, equiv. 1.0) was added dropwise to a solution of temozolomide acyl chloride (219.9 mg, 1.03 mmol, equiv. 1.0) in THF (10 mL). EtOAc was used for flash column chromatography to afford **AM1**, off-white solid 156.5 mg (55 % yield); m.p. 138 °C; IR (cm^{-1}) 3295 (N-H stretch), 3118 (C-H stretch), 2921 (C-H stretch), 2856 (C-H stretch), 1726 (C=O stretch, CONH), 1652 (C=O stretch, CONH). ^{1}H NMR (400 MHz, Chloroform-*d*), δ_H: 8.40 (s, 1H, N-CH), 7.35 (t, J = 6.5 Hz, 1H, NH), 4.04 (s, 3H N-CH_3), 3.51 (q, J = 6.5 Hz, 2H, CH_2), 1.63 (quint, J = 4.5 Hz, 2H, CH_2), 1.46-1.27 (m, 6H, $(CH_2)_3$), 0.89 (t, J = 7.2 Hz, 3H, CH_3). ^{13}C NMR (100 MHz Chloroform-*d*), δ_C: 159.3 (6), 138.8 (2), 133.7 (5), 132.1 (4), 127.7 (3), 39.4 (7), 36.5 (8), 31.5 (9), 29.5 (10), 22.5 (11), 14.0 (12). HRMS calc'd for $C_{12}H_{18}N_6O_2$ $[M+Na]^+$: 301.1384. Found *m/z*: 301.1409.

3-Methyl-4-oxo-N-phenethyl-3,4-dihydroimidazo[5,1-d][1,2,3,5]tetrazine-8-carboxamide - AM2

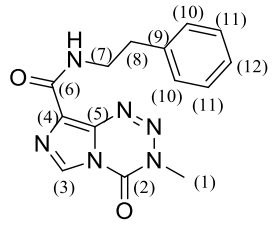

Procedure for synthesis outlined in Section 2.3.3.1, Scheme 2.2. 2-Phenylethanamine (123 µL, 0.98 mmol, equiv. 1.0) was added dropwise to a solution of temozolomide acyl chloride (209.4 mg, 0.98 mmol, equiv. 1.0) in THF (10 mL). EtOAc was used for flash column chromatography to afford **AM2**, off-white solid 169.2 mg (58 % yield); m.p. 158 °C; IR (cm^{-1}) 3312 (N-H stretch), 3082 (C-H stretch), 1745 (C=O stretch, CONH), 1646 (C=O stretch, CONH). ^{1}H NMR (400 MHz, DMSO-d_6), δ_H: 8.84 (s, 1H, N-CH), 8.54 (t, J = 5.9 Hz, 1H, NH), 7.36 – 7.16 (m, 5H, Ar), 3.87 (s, 3H, N-CH_3), 3.54 (q, J = 7.4 Hz, 2H, NH-CH_2), 2.87 (t, J = 7.4 Hz, 2H, CH_2-Ar). ^{13}C NMR (100 MHz DMSO-d_6), δ: 160.0 (6), 139.8 (9), 139.7 (2), 134.9 (5), 130.8 (4), 129.1 (11), 128.9 (3), 128.8 (10), 126.6 (12), 40.6 (7), 36.6 (1), 35.6 (8). HRMS calc'd for $C_{14}H_{14}N_6O_2$ $[M+Na]^+$: 321.1071. Found *m/z*: 321.1088.

-Methyl-4-oxo-N-phenyl-3,4-dihydroimidazo[5,1-d][1,2,3,5]tetrazine-8-carboxamide - AM3

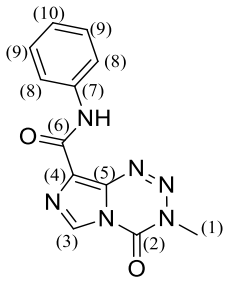

Procedure for synthesis outlined in Section 2.3.3.1, Scheme 2.2. Aniline (93 µL, 1.03 mmol, equiv. 1.0) was added dropwise to a solution of temozolomide acyl chloride (219.9 mg, 1.03 mmol, equiv. 1.0) in THF (10 mL). EtOAc: petroleum ether (2:1, v/v) was used for flash column chromatography to afford **AM3**, light orange solid 110.3 mg (40 % yield); m.p. 189 °C; IR (cm^{-1}) 3356 (N-H stretch), 3118 (C-H stretch), 1734 (C=O stretch, CONH), 1684 (C=O stretch, CONH). ^{1}H NMR (300 MHz, DMSO-d_6), δ_H: 10.40 (s, 1H, NH), 8.96 (s, 1H, N-CH), 7.88 (d, J = 9.0Hz, 2H, Ar), 7.36 (t, J = 6.0 Hz, 2H, Ar), 7.20 – 7.05 (t, J = 6.0 Hz, 1H, Ar), 3.89 (s, 3H, N-CH_3). ^{13}C NMR (75 MHz, DMSO-d_6), δ_C: 158.8 (6), 139.6 (2), 138.9 (7), 135.6 (5), 130.6 (4), 129.1 (9), 129.0 (3), 124.4 (10), 120.7 (8), 36.7 (1). HRMS calc'd for $C_{12}H_{10}N_6O_2$ $[M+Na]^+$: 293.0757. Found *m/z*: 293.0772.

N-(4-Methoxyphenyl)-3-methyl-4-oxo-3,4-dihydroimidazo[5,1-d][1,2,3,5]tetrazine-8-carboxamide - AM4

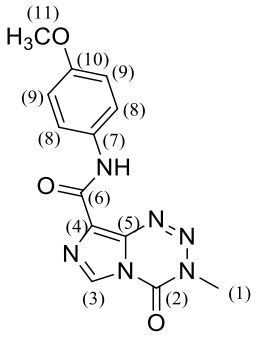

Procedure for synthesis outlined in section 2.3.3.1, scheme 2.2. 4-Methoxyaniline (132.9 mg, 1.09 mmol, equiv. 1.1), in THF (2 mL) was added dropwise to a solution of temozolomide acyl chloride (216.5 mg, 1.01 mmol, equiv. 1.0) in THF (10 mL). EtOAc : petroleum ether (2:1, v/v) was used for flash column chromatography to afford **AM4**, yellow solid (25 % yield); m.p. 192 ^{o}C; IR (cm^{-1}) 3376 (N-H stretch), 3119 (C-H stretch), 2937 (C-H stretch), 1746 (C=O stretch, CONH), 1684 (C=O stretch, CONH). ^{1}H NMR (300 MHz, DMSO-d_6), δ_H: 10.30 (s, 1H, NH), 8.95 (s, 1H, N-CH), 7.79 (d, J = 9.1 Hz, 2H, Ar), 6.94 (d, J = 9.1 Hz, 2H, Ar), 3.89 (s, 3H, O-CH_3), 3.75 (s, 3H, N-CH_3). ^{13}C NMR (75 MHz, DMSO-d_6), δ_C: 158.4 (6), 156.1 (10), 139.7 (2), 135.5 (5), 132.0 (7), 130.8 (4), 128.9 (3), 122.3 (8), 114.2 (9), 55.6 (11), 36.7 (1). HRMS calc'd for $C_{13}H_{12}N_6O_3$ $[M+Na]^+$: 323.0863. Found *m/z*: 323.0877.

N-(4-Chlorophenyl)-3-methyl-4-oxo-3,4-dihydroimidazo[5,1-d][1,2,3,5]tetrazine-8-carboxamide - AM5

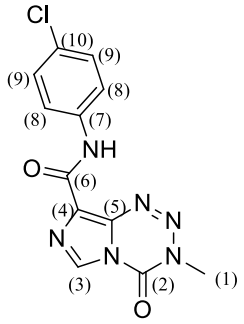

Procedure for synthesis outlined in Section 2.3.3.1, Scheme 2.2. 4-Chloroaniline (145.8 mg, 1.14 mmol, equiv. 1.1), solubilised in THF (2 mL) was added dropwise to a solution of temozolomide acyl chloride (217.0 mg, 1.02 mmol, equiv. 1.0) in THF (10 mL). EtOAc was used for flash column chromatography to afford **AM5**, brown solid 140.7 mg (45 % yield); m.p. 200 ^{o}C; IR (cm^{-1}) 3359 (N-H stretch), 3117 (C-H stretch), 1737 (C=O stretch, CONH), 1689 (C=O stretch, CONH). ^{1}H NMR (400 MHz, DMSO-d_6), δ_H: 10.59 (s, 1H, NH), 8.97 (s, 1H, N-CH), 7.93 (d, J = 8.8 Hz, 2H, Ar), 7.42 (d, J = 8.8 Hz, 2H, Ar), 3.90 (s, 3H, N-CH_3).^{13}C NMR (100 MHz, DMSO-d_6), δ_C: 158.4 (6), 139.1 (2), 137.4 (7), 135.3 (5), 129.8 (3), 128.5 (9), 127.5 (4), 121.8 (8), 36.2 (1). HRMS calc'd for $C_{12}H_9N_6O_2Cl$ $[M+Na]^+$: 327.0368. Found *m/z*: 327.0382.

3-Methyl-4-oxo-N-(p-tolyl)-3,4-dihydroimidazo[5,1-d][1,2,3,5]tetrazine-8-carboxamide - AM7

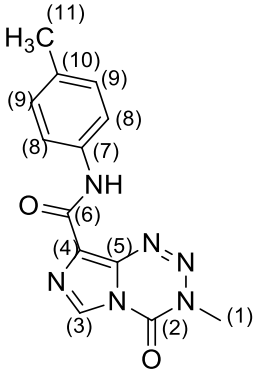

Procedure for synthesis outlined in Section 2.3.3.1, Scheme 2.2. *p*-Toluidine (102.2 mg, 0.95 mmol, equiv. 0.96), solubilised in THF (2 mL) was added dropwise to a solution of temozolomide acyl chloride (212.1 mg, 0.99 mmol, equiv. 1.0) in THF (10 mL). EtOAc was used for flash column chromatography to afford **AM7**, yellow solid 164.7 mg (58 % yield); m.p. 209 ^{o}C; IR (cm^{-1}) 3301 (N-H stretch), 3114 (C-H stretch), 1735 (C=O stretch, CONH), 1672 (C=O stretch, CONH). ^{1}H NMR (400 MHz, DMSO-d_6) δ_H: 10.30 (s, 1H, NH), 8.94 (s, 1H, N-CH), 7.75 (d, J = 8.8 Hz, 2H, Ar), 7.16 (d, J = 8.8 Hz, 2H, Ar), 3.89 (s, 3H, N-CH_3), 2.28 (s, 3H, Ar-CH_3). ^{13}C NMR (100 MHz, DMSO) δ_C: 158.6 (6), 139.6 (2), 136.4 (10), 135.5 (5 or 7), 133.4 (5 or 7), 130.7 (4), 129.5 (9), 128.9 (3), 120.7 (8), 36.7 (1), 21.0 (11). HRMS calc'd for $C_{13}H_{12}N_6O_2$ $[M+Na]^+$: 307.0914. Found *m/z*: 307.0929.

N-(2-Methoxyphenyl)-3-methyl-4-oxo-3,4-dihydroimidazo[5,1-d][1,2,3,5]tetrazine-8-carboxamide – AM8

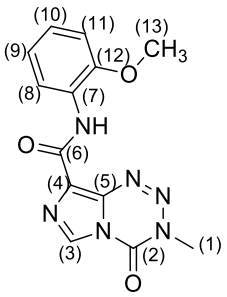

Procedure for synthesis outlined in Section 2.3.3.1, Scheme 2.2. *o*-Anisidine (115.3 µL, 1.01 mmol, equiv. 0.99), solubilised in THF (2 mL) was added dropwise to a solution of temozolomide acyl chloride (220.8 mg, 1.03 mmol, equiv. 1.0) in THF (10 mL). EtOAc was used for flash column chromatography to afford **AM8**, yellow solid 268.7 mg (87 % yield); m.p. 193 ^{o}C; IR (cm^{-1}) 3370 (N-H stretch), 1741 (C=O stretch, CONH), 1677 (C=O stretch, CONH). ^{1}H NMR (400 MHz, DMSO-d_6) δ_H: 9.78 (s, 1H, NH), 8.95 (s, 1H, N-CH), 8.40 (d, *J* = 8.8 Hz, 1H, Ar), 7.14 (d, *J* = 8.8 Hz, 2H, Ar), 7.01 (m, 1H, Ar), 3.94 (s, 3H, OCH_3), 3.90 (s, 3H, OCH_3). ^{13}C NMR (100 MHz, DMSO) δ_C: 157.6 (6), 148.8 (12), 139.5 (2), 135.4 (5), 130.0 (4), 129.2 (3), 127.5 (7), 124.7 (10), 121.2 (9), 119.6 (8), 111.6 (11), 56.6 (13), 36.8 (1). HRMS calc'd for $C_{13}H_{12}N_6O_3$ $[M+Na]^+$: 323.0863. Found *m/z*: 323.0878.

N-(4-Methoxybenzyl)-3-methyl-4-oxo-3,4-dihydroimidazo[5,1-d][1,2,3,5]tetrazine-8-carboxamide – AM9

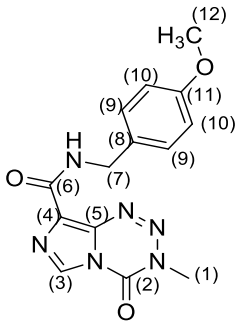

Procedure for synthesis outlined in Section 2.3.3.1, Scheme 2.2. 4-Methoxybenzylamine (136.0 µL, 1.04 mmol, equiv. 1.00), solubilised in THF (2 mL) was added dropwise to a solution of temozolomide acyl chloride (223.1 mg, 1.04 mmol, equiv. 1.0) in THF (10 mL). EtOAc was used for flash column chromatography to afford **AM9**, off-white solid 199.7 mg (61 % yield); m.p. 193 ^{o}C. IR (cm^{-1}) 3371 (N-H stretch), 3126 (C-H stretch), 1735 (C=O stretch, CONH), 1696 (C=O stretch, CONH). ^{1}H NMR (400 MHz, DMSO-d_6) δ: 8.99 (t, *J* = 6.3 Hz, 1H, NH), 8.85 (s, 1H, N-CH), 7.27 (d, *J* = 8.8 Hz, 2H, Ar), 6.88 (d, *J* = 8.8 Hz, 2H, Ar), 4.42 (d, *J* = 6.3 Hz, 2H, NH-CH_2), 3.86 (s, 3H, O-CH_3), 3.72 (s, 3H, N-CH_3). ^{13}C NMR (100 MHz, DMSO) δ_C: 159.5 (6), 158.1 (11), 139.1 (2), 134.5 (5), 131.5 (4), 130.3 (3), 128.7 (9), 128.4 (8), 113.6 (10), 55.0 (7), 41.5 (12), 36.1 (1). HRMS calc'd for $C_{14}H_{14}N_6O_3$ [M+Na]$^{+}$: 337.1020. Found *m/z*: 337.1038.

3-Methyl-N-(4-methylbenzyl)-4-oxo-3,4-dihydroimidazo[5,1-d][1,2,3,5]tetrazine-8-carboxamide - AM10

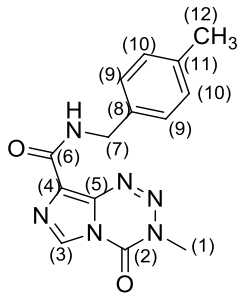

Procedure for synthesis outlined in Section 2.3.3.1, Scheme 2.2. 4-Methylbenzylamine (130.0 µL, 1.02 mmol, equiv. 0.98), solubilised in THF (2 mL) was added dropwise to a solution of temozolomide acyl chloride (220.8 mg, 1.03 mmol, equiv. 1.0) in THF (10 mL). Ethyl acetate solvent system was used for flash column chromatography to afford **AM10**, off-white solid 168.5 mg (54 % yield); m.p. 152 °C. IR (cm^{-1}) 3397 (N-H stretch), 3102 (C-H stretch), 1736 (C=O stretch, CONH), 1665 (C=O stretch, CONH). ^{1}H NMR (400 MHz, DMSO-d_6) δ_H: 9.01 (t, *J* = 6.4 Hz, 1H, NH), 8.86 (s, 1H, N-CH), 7.22 (d, *J* = 4.0 Hz, 2H, Ar), 7.12 (d, *J* = 4.0 Hz, 2H, Ar), 4.44 (d, *J* = 6.4 Hz, 2H, NH-CH_2), 3.86 (s, 3H, N-CH_3), 2.27 (s, 3H, Ar-CH_3). ^{13}C NMR (100 MHz, DMSO) δ_C: 159.6 (6), 139.1 (2), 136.5 (11), 135.7 (5 or 8), 134.5 (5 or 8), 130.3 (4), 128.7 (10), 128.4 (3), 127.3 (9), 41.8 (7), 36.1 (1), 20.6 (12). HRMS calc'd for $C_{14}H_{14}N_6O_2$ $[M+Na]^+$: 321.1071. Found *m/z*: 321.1090.

N-(4-Chlorobenzyl)-3-methyl-4-oxo-3,4-dihydroimidazo[5,1-d][1,2,3,5]tetrazine-8-carboxamide – AM11

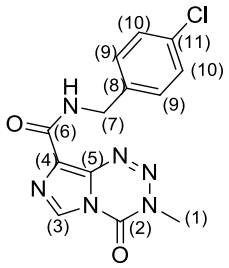

Procedure for synthesis outlined in Section 2.3.3.1, Scheme 2.2. 4-Chlorobenzylamine (122.0 µL, 1.00 mmol, equiv. 0.97), solubilised in THF (2 mL) was added dropwise to a solution of temozolomide acyl chloride (220.1 mg, 1.03 mmol, equiv. 1.0) in THF (10 mL). EtOAc : petroleum ether (2:1, v/v) was used for flash column chromatography to afford **AM11**, off-white solid 154.3 mg (47 % yield); m.p. 148 °C. IR (cm^{-1}) 3288 (N-H stretch), 1735 (C=O stretch, CONH), 1651 (C=O stretch, CONH). ^{1}H NMR (400 MHz, DMSO-d_6) δ_H: 9.15 (t, *J* = 6.3 Hz, 1H, NH), 8.87 (s, 1H, N-CH), 7.41 – 7.33 (m, 4H, Ar), 4.47 (d, *J* = 6.3 Hz, 2H, NH-CH_2), 3.87 (s, 3H, N-CH_3). ^{13}C NMR (100 MHz, DMSO) δ_C: 159.7 (6), 139.1 (2), 138.6 (8), 134.6 (5), 131.3 (4 or 11), 130.1 (4 or 11), 129.2 (9), 128.5 (3), 128.1 (10), 41.4 (7), 36.1 (1). HRMS calc'd for $C_{13}H_{11}N_6O_2Cl$ $[M+Na]^+$: 341.0524. Found *m/z*: 341.0542.

Synthesis of the target compound AM6

Temozolomide acyl chloride **32** (218 mg, 1.02 mmol) was dissolved in tetrahydrofuran (10 mL). A solution of tetrahydrofuran (2 mL) and the appropriate amine (≈1.05 mmol) was added dropwise and stirred for 3 h. The precipitate formed was filtered and washed with tetrahydrofuran to afford the desired title compound AM6. Residual tetrahydrofuran was evaporated under reduced pressure.

N-(4-cyanophenyl)-3-methyl-4-oxo-3,4-dihydroimidazo[5,1-d][1,2,3,5]tetrazine-8-carboxamide - AM6

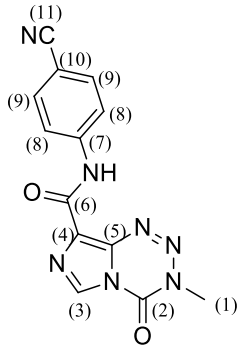

Procedure for synthesis outlined in Section 2.3.3.1, Scheme 2.2. 4-Aminobenzonitrile (124.2 mg, 1.07 mmol, equiv. 1.1), solubilised in THF (2 mL) was added dropwise to a solution of temozolomide acyl chloride (216.3 mg, 1.01 mmol, equiv. 1.0) in THF (10 mL). Precipitate was filtered and wash THF to afford **AM6**, off-white solid 216.0 mg (73 % yield); m.p. 234°C; IR (cm^{-1}) – 3339 (N-H stretch), 3117 (C-H stretch), 2222 (C≡N stretch), 1740 (C=O stretch, CONH), 1689 (C=O stretch, CONH). ^{1}H NMR (400 MHz, DMSO-d_6), δ_H: 10.75 (s, 1H, NH), 8.93 (s, 1H, N-CH), 8.10 (d, J = 8.8 Hz, 2H, Ar), 7.81 (d, J = 8.8 Hz 2H, Ar), 3.90 (s, 3H, N-CH_3). ^{13}C NMR (100 MHz, DMSO-d_6), δ_C: 158.8 (6), 142.7 (7), 139.0 (2), 135.6 (5), 133.0 (9), 129.5 (4), 128.6 (3), 120.3 (8), 118.9 (11), 105.7 (10), 36.2 (1). HRMS calcd for $C_{13}H_9N_7O_2$ $[M+Na]^+$: 318.0710. Found *m/z*: 318.0720.

2.3.3.2. Initial Preparation of Ester Analogues of Temozolomide Utilizing Dicyclohexylcarbodiimide (DCC) / Dimethylaminopyridine (DMAP) Coupling (Scheme 2.3)

Initial general synthesis of target compounds ES8-ES11

Temozolomide acid **36** (200 mg, 1.03 mmol) was solubilised in a mixture of tetrahydrofuran and dichloromethane (10 mL: 10 mL). The appropriate alcohol (≈1.05 mmol), dissolved in tetrahydrofuran (2 mL), was added dropwise to the solution. The mixture was then stirred for 10 mins. A solution of dicyclohexylcarbodiimide (DCC) (255 mg, 1.24 mmol) in dichloromethane (2 mL) was added along with a catalytic amount of 4-dimethylaminopyridine (DMAP). The reaction was stirred for 3 h. The precipitated urea by-products were filtered, and the resulting filtrate was evaporated under reduced pressure. To the resulting off-white/yellow solid, acetonitrile (5 mL) was added and the mixture subjected to 15 min of sonication. The residual precipitated urea by-product was again filtered, and the filtrate was evaporated under reduced pressure. To the resulting off-white/yellow solid was treated with acetonitrile (5 mL) and the process of sonication and filtering was repeated until a yellow oil was afforded. The yellow oil was subjected to flash column chromatography using a solvent system of an appropriate ratio of light petroleum ether to ethyl acetate, to remove any excess alcohol. The resulting off-white/yellow powder was solubilised in dichloromethane (5 mL) and triturated with petroleum ether and dried to afford the desired title compounds. Although compounds ES8-ES11 were successfully synthesised using this route an alternative was developed to help improve yields.

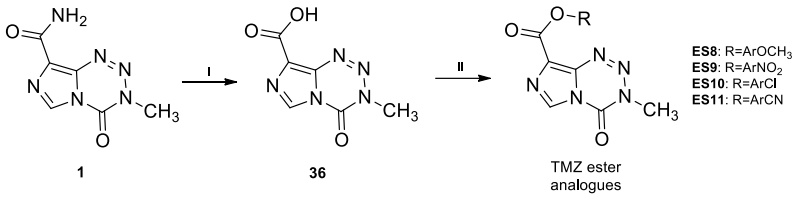

*Scheme 2.3: (I) Sodium nitrite, conc. sulphuric acid <15 °C; (II) dicyclohexylcarbodiimide, 4-dimethylaminopyridine, tetrahydrofuran : dichloromethane (1:1), ArOH, r.t. Ester analogues are referred to as **ES**.*

Note: All aromatic substituents are in the para position unless otherwise stated.

2.3.3.3 Preparation of Ester Analogues of Temozolomide Utilising 1-Ethyl-3-(3-dimethylaminopropyl)carbodiimide (EDC.HCl) / 4-Dimethylaminopyridine (DMAP) Coupling (Scheme 2.4)

General synthesis of target compounds (ES12-ES14)

Temozolomide acid **36** (200 mg, 1.03 mmol) was solubilised in mixture of tetrahydrofuran and dichloromethane (10 mL: 10 mL v/v). The appropriate alcohol was added (≈1.05 mmol) dropwise to the solution. The mixture was then stirred for 10 mins. A solution of 1-ethyl-3-(3-dimethylaminopropyl)carbodiimide (EDC.HCl) (305 mg, 1.60 mmol) in dichloromethane (2 mL) was added along with a 4-dimethylaminopyridine (DMAP) (1 mg). The reaction was stirred for 3 h. The crude reaction mixture was absorbed onto silica, and purified by flash column chromatography using a solvent system of an appropriate ratio of light petroleum ether to ethyl acetate, to remove any excess alcohol. The product was solubilised in dichloromethane (20 mL) and washed with brine (3 x 30 mL) and water (30 mL). The dichloromethane layer was dried over anhydrous sodium sulphate and the solvent was evaporated under reduced pressure to afford the title compounds.

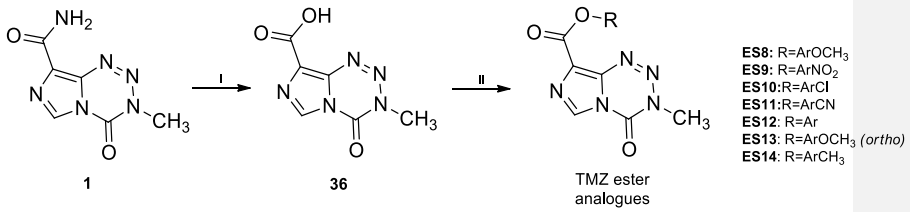

*Scheme 2.4: (I) Sodium nitrite, conc. sulphuric acid <15 °C; (II) 1-ethyl-3-(3-dimethylaminopropyl)carbodiimide, 4-dimethylaminopyridine, tetrahydrofuran : dichloromethane (1:1), ArOH. r.t. Ester analogues are referred to as **ES**.*

Note: All aromatic substituents are in the para position unless otherwise stated.

Optimised synthesis of target compounds (ES8-ES11)

Temozolomide acid **36** (600 mg, 3.07 mmol) was solubilised in mixture of tetrahydrofuran and dichloromethane (30 mL: 30 mL v/v). The appropriate alcohol was added (≈3.10 mmol) dropwise to the solution. The mixture was then stirred for 10 min. A solution of 1-ethyl-3-(3-dimethylaminopropyl)carbodiimide (EDC.HCl) (950 mg, 4.97 mmol) in dichloromethane (6 mL) was added along with a catalytic amount of DMAP (1 mg). The reaction was stirred for 3 h. The crude reaction mixture was absorbed onto silica, and purified by flash column chromatography using a solvent system of an appropriate ratio of light petroleum ether to ethyl acetate, to any remove excess alcohol. The product was solubilised in dichloromethane (40 mL) and washed with brine (3 x 40 mL) and water (40 mL). The dichloromethane layer was dried over sodium sulphate and the solvent was evaporated under reduced pressure to afford the title compounds.

4-Methoxyphenyl 3-methyl-4-oxo-3,4-dihydroimidazo[5,1-d][1,2,3,5]tetrazine-8-carboxylate - ES8

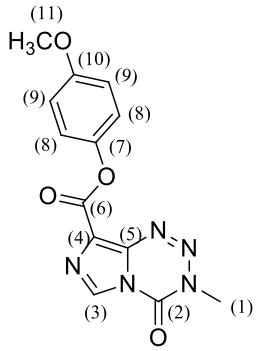

Procedure for synthesis outlined in Section 2.3.3.3., Scheme 2.4. 4-Methoxyphenol (427.8 mg, 3.45 mmol, equiv. 1.11), in THF (6 mL), was added dropwise to a solution of temozolomide acid (607.4 mg, 3.101mmol, equiv. 1.0) in DCM and THF (30 mL: 30 mL, v/v). EDC.HCl (955.9 mg, 5.00 mmol, equiv. 1.61) was added along with a catalytic amount of DMAP (approx. 1 mg). EtOAc : petroleum ether (2:1, v/v) was used for flash column chromatography. The resulting solid solubilised in DCM (20 mL) and washed with brine (3x30 mL) and water (30 mL). The DCM layer was dried over sodium sulphate and the solvent was removed under reduced pressure to afford **ES8**, off-white solid 489.8 mg (50 % yield); m.p. 172°C; IR (cm^{-1}) 3117 (C-H stretch), 1739 (C=O stretch)*. ^{1}H NMR (300 MHz, DMSO-d_6), δ_H: 8.96, (s, 1H, N-CH), 7.22 (d, J = 9.0 Hz, 2H, Ar), 7.03 (d, J = 9.0 Hz, 2H, Ar), 3.92 (s, 3H, Ar-OCH_3), 3.79 (s, 3H, N-CH_3). ^{13}C NMR (75 MHz DMSO-d_6), δ_C: 159.0 (6), 157.5 (10), 143.8 (7), 138.5 (2), 136.3 (5), 128.8 (3), 128.6 (4), 122.3 (8), 114.5 (9), 55.6 (11), 36.8 (1). HRMS calc'd for $C_{13}H_{11}N_5O_4$ $[M+Na]^+$: 324.0703. Found *m/z*: 324.0713.

*Overlap of COO ester carbonyl and CO urea carbonyl.

4-Nitrophenyl 3-methyl-4-oxo-3,4-dihydroimidazo[5,1-d][1,2,3,5]tetrazine-8-carboxylate - ES9

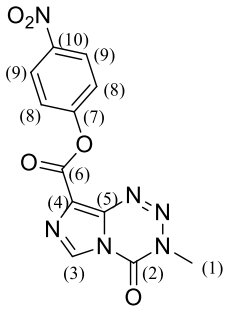

Procedure for synthesis outlined in Section 2.3.3.3, Scheme 2.4. 4-Nitrophenol (453.0 mg, 3.26 mmol, equiv. 1.03), in THF (6 mL), was added dropwise to a solution of temozolomide acid (615.2 mg, 3.15 mmol, equiv. 1.0) in DCM and THF (30 mL: 30 mL, v/v). EDC.HCl (962.1 mg, 5.03 mmol, equiv. 1.59) was added along with a catalytic amount of DMAP (approx. 1 mg). EtOAc : petroleum ether (3:2, v/v) was used for flash column chromatography. The resulting solid solubilised in DCM (20 mL) and washed with brine (3x30 mL) and water (30 mL). The DCM layer was dried over sodium sulphate and the solvent was removed under reduced pressure to afford **ES9**, white solid 488.1 mg (49 % yield); m.p. 190 °C, IR (cm^{-1}) 3154 (C-H stretch), 3114 (C-H stretch), 1754 (C=O stretch, COO), 1727 (C=O stretch, CONH). ^{1}H NMR (300 MHz, DMSO-d_6), δ_H: 8.98 (s, 1H, N-CH), 8.38 (d, J = 9.0 Hz, 2H, Ar), 7.66 (d, J = 9.0 Hz, 2H, Ar), 3.94 (s, 3H, N-CH_3). ^{13}C NMR (75 MHz DMSO-d_6), δ_C: 158.6 (6), 155.3 (7), 145.8 (10), 139.3 (2), 138.3 (5), 130.4 (3), 126.0 (9), 125.2 (4), 123.7 (8), 37.1 (1). HRMS calc'd for $C_{12}H_8N_6O_5$ $[M+Na]^+$: 339.0448. Found *m/z*: 339.0460.

4-Chlorophenyl 3-methyl-4-oxo-3,4-dihydroimidazo[5,1-d][1,2,3,5]tetrazine-8-carboxylate - ES10

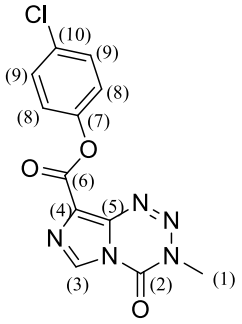

Procedure for synthesis outlined in Section 2.3.3.3. Scheme 2.4. 4-Chlorophenol (409.5 mg, 3.18 mmol, equiv. 1.03), in THF (6 mL), was added dropwise to a solution of temozolomide acid (605.1 mg, 3.10 mmol, equiv. 1.0) in DCM and THF (30 mL: 30 mL, v/v). EDC.HCl (950.0 mg, 4.97 mmol, equiv. 1.60) was added along with a catalytic amount of DMAP (approx. 1 mg). EtOAc : petroleum ether (4:3, v/v) was used for flash column chromatography. The resulting solid solubilised in DCM (20 mL) and washed with brine (3x30 mL) and water (30 mL). The DCM layer was dried over sodium sulphate and the solvent was removed under reduced pressure to afford **ES10**, white solid 442.3 mg (44 % yield); m.p. 164 °C; IR (cm^{-1}) 3089 (C-H stretch), 1733 (C=O stretch). ^{1}H NMR (400 MHz, DMSO-d_6), δ_H: 8.97 (s, 1H N-CH), 7.56 (d, J = 9.0 Hz, 2H, Ar), 7.38 (d, J = 9.0 Hz, 2H, Ar), 3.93 (s, 3H, N-CH_3). ^{13}C NMR (100 MHz DMSO-d_6), δ: 158.7 (6), 148.8 (7), 138.8 (2), 137.5 (5), 130.3 (4), 129.8 (3), 129.6 (9), 125.2 (10), 123.7 (8), 36.6 (1). HRMS calc'd for $C_{12}H_8N_5O_3Cl$ $[M+Na]^+$: 328.0208. Found *m/z*: 328.0219.

*Overlap of COO ester carbonyl and CO urea carbonyl.

4-Cyanophenyl 3-methyl-4-oxo-3,4-dihydroimidazo[5,1-d][1,2,3,5]tetrazine-8-carboxylate - ES11

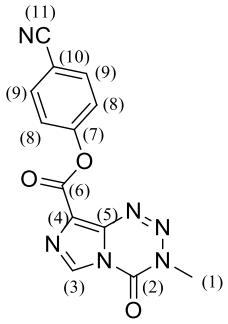

Procedure for synthesis outlined in Section 2.3.3.3., Scheme 2.4. 4-Hydroxybenzonitrile (392.1 mg, 3.29 mmol, equiv. 1.06), in THF (6 mL), was added dropwise to a solution of temozolomide acid (602.8 mg, 3.09 mmol, equiv. 1.0) in DCM and THF (30 mL: 30 mL, v/v). EDC.HCl (962.1 mg, 5.03 mmol, equiv. 1.63) was added along with a catalytic amount of DMAP (approx. 1 mg). EtOAc : petroleum ether (7:5, v/v) was used for flash column chromatography. The resulting solid solubilised in DCM (20 mL) and washed with brine (3x30 mL) and water (30 mL). The DCM layer was dried over sodium sulphate and the solvent was removed under reduced pressure to afford **ES11**, white solid 287.8 mg (30 % yield); m.p. 192 ^{o}C; IR (cm^{-1}) 3146 (C-H stretch), 3110 (C-H stretch), 2224 (C≡N stretch), 1759 (C=O stretch, COO), 1730 (C=O stretch, CONH). ^{1}H NMR (300 MHz, DMSO-d_6), δ_H: 9.00 (s, 1H, N-CH), 8.01 (d, J = 8.8 Hz, 2H, Ar), 7.58 (d, J = 8.8 Hz, 2H, Ar), 3.93 (s, 3H N-CH_3). ^{13}C NMR (75 MHz DMSO-d_6), δ_C: 158.2 (6), 153.4 (7), 138.8 (2), 137.7 (5), 134.2 (9), 129.9 (6), 124.8 (4), 123.3 (8), 118.3 (11), 109.1 (10), 36.6 (1). HRMS calc'd for $C_{13}H_8N_6O_3$ $[M+Na]^+$: 319.0550. Found *m/z*: 319.0550.

Phenyl 3-methyl-4-oxo-3,4-dihydroimidazo[5,1-d][1,2,3,5]tetrazine-8-carboxylate - ES12

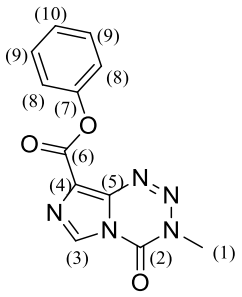

Procedure for synthesis outlined in Section 2.3.3.3., Scheme 2.4. Phenol (117.0 mg, 1.24 mmol, equiv. 1.23), in THF (2 mL), was added dropwise to a solution of temozolomide acid (201.0 mg, 1.03 mmol, equiv. 1.0) in DCM and THF (10 mL: 10 mL, v/v). EDC.HCl (305.4 mg, 1.59 mmol, equiv. 1.55) was added along with a catalytic amount of DMAP (approx. 1 mg). EtOAc : petroleum ether (4:3, v/v) was used for flash column chromatography. The resulting solid was solubilised in DCM (20 mL) and washed with brine (3 x 30 mL) and water (30 mL). The DCM layer was dried over anhydrous sodium sulphate and the solvent was removed under reduced pressure to afford **ES12**, off white solid 75.3 mg (27.0 % yield); m.p. 149 °C; IR (cm^{-1}) 3143 (C-H stretch), 1737 (C=O stretch)*. ^{1}H NMR (400 MHz, Chloroform-*d*), δ_H: 8.53 (s, 1H, N-CH), 7.51 – 7.37 (m, 2H, Ar), 7.35 – 7.23 (m, 3H, Ar), 4.06 (s, 3H, N-CH_3). ^{13}C NMR (100 Chloroform-*d*), δ_C: 158.7 (6), 150.2 (7), 138.4 (2), 136.3 (5), 129.5 (9), 128.8 (3), 128.4 (4), 126.3 (10), 121.5 (8), 36.8 (1). HRMS calc'd for $C_{12}H_9N_5O_3$ $[M+Na]^+$: 294.0597. Found *m/z*: 294.0606.

*Overlap of COO ester carbonyl and CO urea carbonyl.

2-Methoxyphenyl 3-methyl-4-oxo-3,4-dihydroimidazo[5,1-d][1,2,3,5]tetrazine-8-carboxylate - ES13

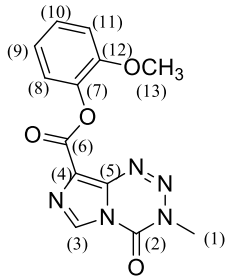

Procedure for synthesis outlined in Section 2.3.3.3., Scheme 2.4. 2-Methoxyphenol (121.0 µL, 1.10 mmol, equiv. 1.07), in THF (2 mL), was added dropwise to a solution of temozolomide acid (200.4 mg, 1.03 mmol, equiv. 1.0) in DCM and THF (10 mL: 10 mL, v/v). EDC.HCl (301.1 mg, 1.58 mmol, equiv. 1.53) was added along with a catalytic amount of DMAP (approx. 1 mg). EtOAc : petroleum ether (4:3, v/v) for flash column chromatography. The resulting solid solubilised in DCM (20 mL) and washed with brine (3x30 mL) and water (30 mL). The DCM layer was dried over sodium sulphate and the solvent was removed under reduced pressure to afford **ES13**, orange solid 150.7 mg (49 % yield); m.p. 165 °C; IR (cm^{-1}) 3153 (C-H stretch), 1737 (C=O stretch)*. ^{1}H NMR (400 MHz, DMSO-d_6), δ_H: 8.95 (s, 1H, N-CH), 7.32 (t, J = 7.7, 1H, Ar), 7.23 (ddd, J = 7.7, 8.2, 1.6 Hz, 2H, Ar), 7.04 (t, J = 7.7 Hz, 1H, Ar), 3.92 (s, 3H, N-CH_3). ^{13}C NMR (100 MHz DMSO-d_6), δ_C: 158.3 (6), 150.8 (12), 138.9 (2), 137.4 (7), 129.7 (3), 127.3 (10), 125.3 (5), 122.8 (9), 120.7 (8), 112.9 (11), 56.0 (13), 36.5 (1). HRMS calc'd for $C_{13}H_{11}N_5O_4$ $[M+Na]^+$: 324.0703. Found *m/z*: 324.0715.

*Overlap of COO ester carbonyl and CO urea carbonyl

***p*-Tolyl 3-methyl-4-oxo-3,4-dihydroimidazo[5,1-d][1,2,3,5]tetrazine-8-carboxylate - ES14**

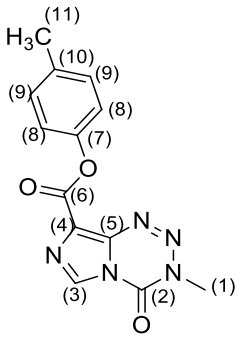

Procedure for synthesis outlined in Section 2.3.3.3., scheme 2.4. *p*-Cresol (107.0 µL, 1.03 mmol, equiv. 1.0), in THF (2 mL), was added dropwise to a solution of temozolomide acid (204.2 mg, 1.03 mmol, equiv. 1.0) in DCM and THF (10 mL: 10 mL, v/v). EDC.HCl (303.4 mg, 1.59 mmol, equiv. 1.51) was added along with a catalytic amount of DMAP (approx. 1 mg). EtOAc : petroleum ether (2:1, v/v) was used for flash column chromatography. The resulting solid solubilised in DCM (20 mL) and washed with brine (3x30 mL) and water (30 mL). The DCM layer was dried over sodium sulphate and the solvent was removed under reduced pressure to afford **ES14**, off-white solid 81.5 mg (28 % yield); m.p. 164 ^{o}C; IR (cm^{-1}) 3122 (C-H stretch), 1734 (C=O stretch)*. ^{1}H NMR (400 MHz, Chloroform-*d*) δ_H: 8.51 (s, 1H, N-CH), 7.22 (d, J = 8.0 Hz, 2H, Ar), 7.17 (d, J = 8.0 Hz, 2H, Ar), 4.05 (s, 3H, N-CH_3), 2.37 (s, 3H, Ar-CH_3). ^{13}C NMR (100 MHz, $CDCl_3$) δ_C 158.8 (6), 148.0 (7), 138.4 (2), 136.3 (10), 136.0 (5), 130.0 (9 or 3), 128.8 (9 or 3), 128.5 (4), 121.2 (8), 36.7 (1), 21.0 (11). HRMS calc'd for $C_{13}H_{11}N_5O_3$ $[M+Na]_+$: 308.0754. Found *m/z*: 308.0764.

*Overlap of COO ester carbonyl and CO urea carbonyl.

2.4. Results and Discussion

The aim of the present chapter was to synthesise a series of position-8-modified ester and amide analogues of TMZ. As previously stated, TMZ is highly unstable in neutral and basic solutions. The imidazotetrazine core undergoes ring opening due to nucleophilic attack by water at position C4 on the tetrazine ring (Scheme 2.1) (Denny *et al.*, 1994). Also, ring opening is known to occur due to exposure to protic solvents (Stevens *et al.*, 1984). As a result, where possible, synthesis of novel analogues utilised acidic conditions and aprotic solvents in order to prevent ring opening and to maximise yields.

2.4.1. Preparation of Ester and Amide Analogues of Temozolomide Utilising Acyl Chloride Generation (Scheme 2.2)

Historically, due to the relative instability of the tetrazine ring, modifications at position 8 were achieved through the reaction of various esters and amides containing 8-substituted diazoazoles **38** with isocyanates (Scheme 2.5) (Lunt *et al.*, 1987). However, a more efficient method for modifying position 8 on imidazotetrazines was described by Horspool et al. (1990), without disrupting the core of the molecule.

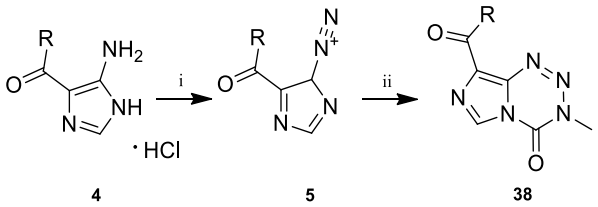

Scheme 2.5: Reaction between 8-substituted diazoazoles and isocyanates to form 8-substituted imidazotetrazines. Reagents: (i) Sodium nitrite, aq. hydrochloric acid; (ii) Methyl isocyanate, dichloromethane, 25 °C, 20 days.

Initial attempts at synthesising the target ester and amide analogues of TMZ followed the route described by Horspool *et al.* (1990) (Scheme 2.2). This first involved the conversion of the amide at position 8 on the imidazole ring to a carboxylic acid **36**. The carboxylic acid group on TMZ acid is converted to the activated TMZ acyl chloride, thus allowing preferential nucleophilic attack of the imidazo carbonyl group on TMZ acyl chloride **37**, by specific alcohols and amines, yielding the target analogues. Horspool *et al.* (1990) reported multiple methods of achieving the conversion of TMZ to TMZ acid, however the most successful route utilised nitrous acid to achieve hydrolysis of the carbamoyl group forming TMZ acid **36**. A mechanism for the reaction is shown in Scheme 2.6.

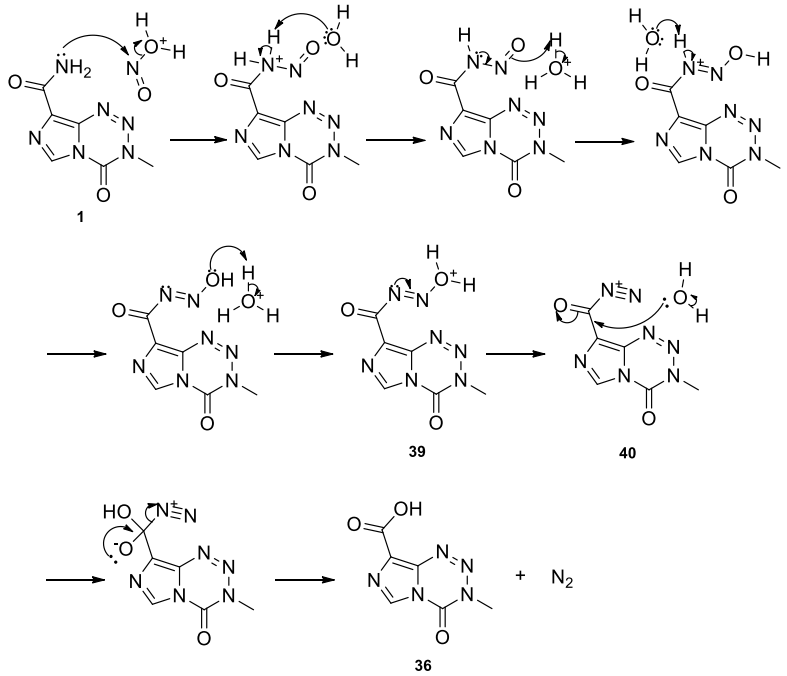

*Scheme 2.6: Mechanism for the reaction between temozolomide and sodium nitrite / concentrated sulphuric acid to produce temozolomide acid (**36**).*

During the reaction outlined in Scheme 2.6, nitrous acid is formed upon the addition of sodium nitrite to concentrated sulphuric acid. The electron deficient nitrogen on nitrous acid is subject to nucleophilic attack by the amide nitrogen of TMZ. The subsequent loss of water from the intermediate **33** leads to the formation of a diazonium leaving group, allowing preferential nucleophilic attack of water to the carbonyl carbon **40**, yielding the carboxylic acid **36**. In practice, the reaction also produces nitrogen dioxide, from the reaction of sodium nitrite and concentrated sulphuric acid. Characterisation of the product using ^{1}H and ^{13}C NMR and IR spectroscopy of the reaction confirmed successful synthesis, (68% yield).

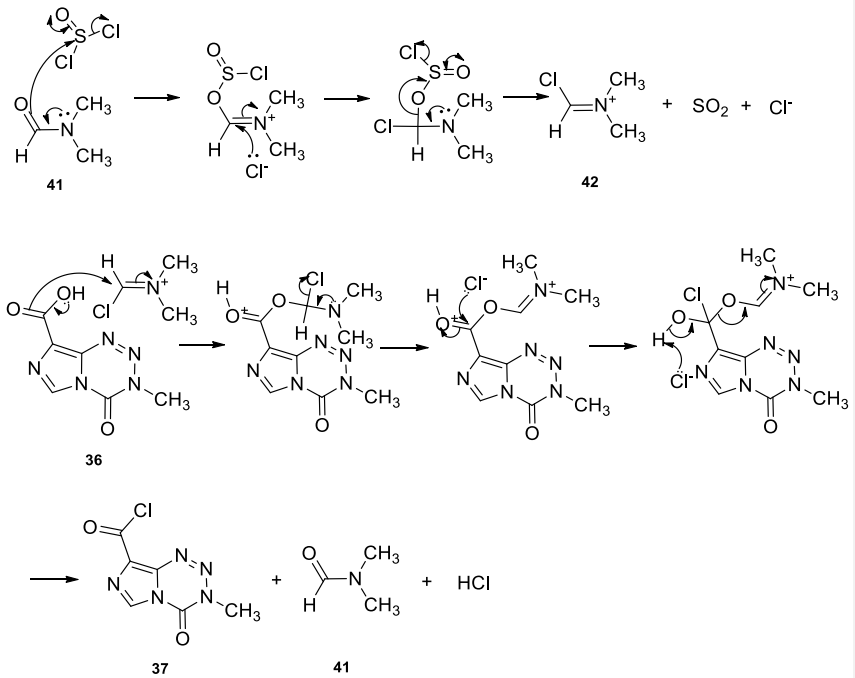

*Scheme 2.7: A Mechanism for the reaction between thionyl chloride and temozolomide acid **36** catalysed by dimethylformamide.*

The second reaction utilised in Scheme 2.2 was the conversion of TMZ acid **36** to the corresponding acyl chloride **37**, using thionyl chloride and DMF **35**. Here, DMF is utilised to catalyse the reaction. A mechanistic view of the DMF catalysed thionyl chloride reaction is shown in Scheme 2.7. Thionyl chloride reacts with DMF to form the Vilsmeier iminium salt **42**, which subsequently reacts with TMZ acid **36** to produce the desired acyl chloride and reforming DMF **41**, Scheme 2.8. However, it should be noted that the desired compound is also formed through a direct reaction of thionyl chloride and TMZ acid **36**, shown in Scheme 2.8. To maximise the yield of the subsequent alcohol/amine quench, characterisation of TMZ acyl chloride **37** was limited to melting point analysis, which was cross-referenced with melting points quoted by Horspool *et al.* (1990) confirming synthesis.

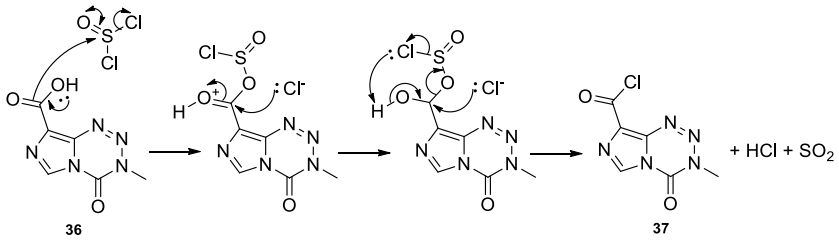

*Scheme 2.8: A mechanism for the direct reaction of thionyl chloride and temozolomide acid **36**, in the absence of dimethylformamide.*

TMZ acyl chloride **37** was subsequently quenched with various alcohols and amines to afford a variety of the desired analogues. A summary of the alcohols and amines used in the reaction are shown in Table 2.2. Reactions of amines with temozolomide acyl chloride **37** tended to afford a better yield compared to equivalent alcohols. The higher yields may be attributed to the lesser electronegativity of nitrogen compared to oxygen, meaning amines are much more effective nucleophiles than the equivalent alcohols. Table 2.2 also shows that phenols did not readily

react with TMZ acyl chloride **37**. This effect was attributed to steric hindrance of the tetrazine ring on TMZ acyl chloride **37** and the aromatic ring of the alcohols. In addition, the lone pairs on oxygen in phenyl alcohols is less available for nucleophilic attack due to partial delocalisation into the aromatic ring. In an attempt to overcome the steric effects the reactions were also carried out under mild reflux 70 °C, with negligible success. As a result, a new approach was needed in order to synthesise the problematic target compounds.

*Table 2.2: Summary of the reactions between temozolomide acyl chloride **32** and various alcohols and amines using acyl chlorides. N/A refers to unsuccessful reactions.*

Target Analogue	Alcohol/Amine	Yield (Using acyl chlorides)
ES1	$HOCH_2CH_3$	78.5%
ES2	$HO(CH_2)_5CH_3$	29.2%
ES3	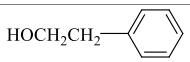	44.3%
ES4	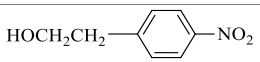	26.9%
ES5	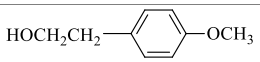	21.8%
ES6	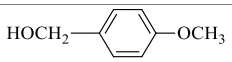	36.5%
ES7	$HOCH_2CH_2CH_2N(CH_3)_2$	45.9%
ES8	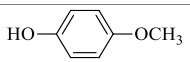	N/A
ES9	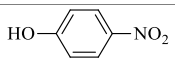	N/A
ES10	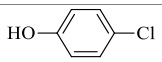	N/A

ES11	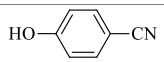	N/A
ES12	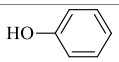	N/A
ES13	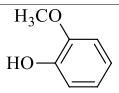	N/A
ES14	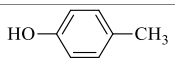	N/A
AM1	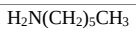	54.6%
AM2	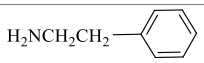	57.8%
AM3	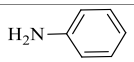	39.6%
AM4	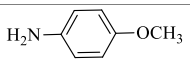	24.8%
AM5	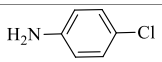	45.3%
AM6	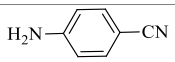	72.9%
AM7	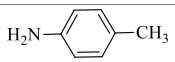	58.3%
AM8	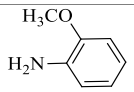	86.8%
AM9	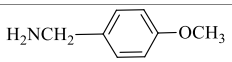	60.8%
AM10	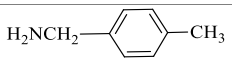	54.3%
AM11	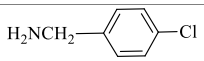	47.0%

2.4.2. Preparation of Ester Analogues of Temozolomide Utilizing Dicyclohexylcarbodiimide (DCC) / Dimethylaminopyridine (DMAP) Coupling (Scheme 2.3)

In order to synthesise the sterically hindered target compounds an adaptation of the Steglich esterification reaction was utilised (Shervington *et al.*, 2009). Scheme 2.10 depicts a mechanism for the reaction between dicyclohexylcarbodiimide (DCC) / 4-dimethylaminopyridine (DMAP, **45**) and temozolomide acid **36**. DCC acts as a base and deprotonates the acid group of temozolomide acid **36**. The lone pair on the oxygen of the acid group simultaneously attacks the imine carbon on DCC intermediate **43**. DMAP then attacks the carbonyl carbon of the temozolomide acid forming a tetrahedral intermediate **44** in which DCC leaves as dicyclohexyl urea (DCU). The desired alcohol then attacks the carbonyl carbon forming another tetrahedral intermediate, in which DMAP **45** leaves affording the desired ester (Scheme 2.9).

The DCU formed in the reaction between DCC / DMAP proved problematic during the initial attempts at purifying the target compounds using Scheme 2.3. DCU is relatively insoluble in most organic solvents allowing most of the impurity to be filtered off (Tsakos *et al.*, 2015). However, trace amounts of DCU persist even after filtration. Initial attempts at separating the DCU via flash column chromatography were unsuccessful due to poor resolution of the impurity, resulting in its elution in numerous fractions including those with the desired product regardless of solvent system. Although DCU is relatively insoluble in most organic solvents it is partially soluble in DCM. The partial solubility of DCU and the high polarity of the target molecules, allowed high purity products to be achieved via trituration with DCM and light petroleum ether. Table 2.3 summarises the alcohols used in this reaction. The yields were relatively low due to a significant proportion of the product being sacrificed during the work up. However, reactions using phenol, p-cresol and 2-methoxyphenol could not be purified due to the products of these reactions exhibiting similar solubility properties to DCU in DCM, resulting in a large quantity of product being lost during the work up.

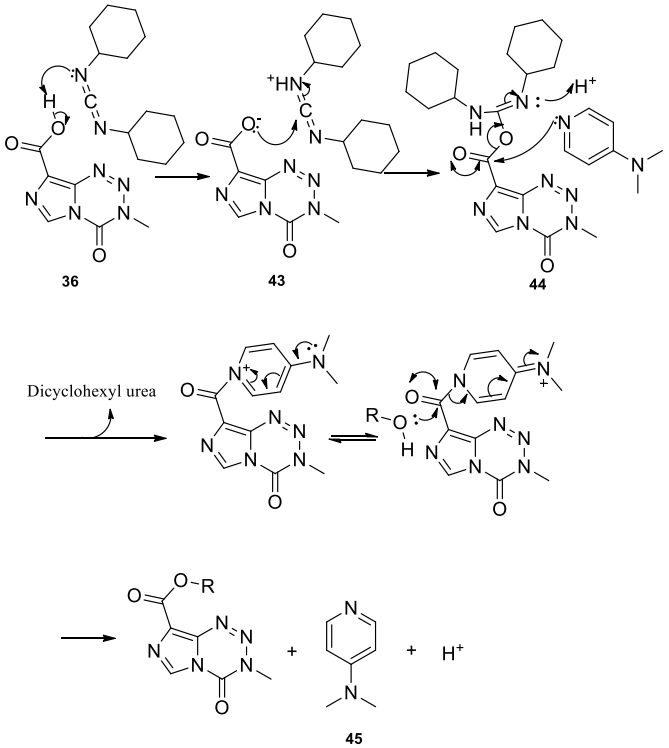

*Scheme 2.9: A mechanism for the reaction between dicyclohexylcarbodiimide / dimethylaminopyridine and temozolomide acid **36**.*

*Table 2.3: Summary of the reactions between temozolomide acid **36** and various alcohols and amines using DCC/DMAP. N/A refers to unsuccessful reactions.*

Target Analogue	Alcohol	Yield (Using DCC/DMAP)
ES8	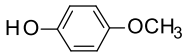	31.9%
ES9	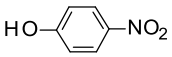	22.8%
ES10	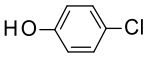	20.1%
ES11	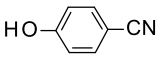	27.9%
ES12	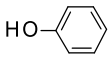	N/A
ES13	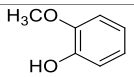	N/A
ES14	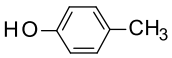	N/A

2.4.3. Preparation of Ester Analogues of Temozolomide Utilising 1-Ethyl-3-(3-dimethylaminopropyl)carbodiimide (EDC.HCl) / 4-Dimethylaminopyridine (DMAP) Coupling (Scheme 2.4)

The variation of the Steglich esterification adapted from Shervington *et al.* (2009) and outlined in Scheme 2.4, produced the desired sterically hindered esters, but due to difficulties in removing the DCU it was not a viable route when using phenol, 2-methoxyphenol or p-cresol. To resolve this problem, 1-ethyl-3-(3-dimethylaminopropyl)carbodiimide (EDC.HCl) was used as a direct replacement for DCC. The mechanism for the reaction of EDC.HCl / DMAP and TMZ acid **36** is shown in Scheme 2.10. In this reaction 1-ethyl-3-(3-dimethylaminopropyl) urea (EDU) is formed as the by-product instead of DCU. Water-soluble EDU is easily removed by a simple aqueous work up. The yields for this reaction were an improvement on those obtained from Scheme 2.3, suggesting this approach to be a more viable option attempting to optimise yields or scaling up the reaction, Table 2.4. Consequently, Scheme 2.4 was investigated for the synthesis of ES8-ES11 analogues with the aim of improving yields.

*Table 2.4: Summary of the reactions between temozolomide acid **36** and various alcohols and amines using EDC.HCl/DMAP.*

Target Analogue	Alcohol	Yield (Using EDC.HCl/DMAP)
ES12	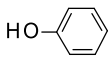	27.0%
ES13	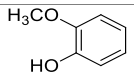	48.6%
ES14	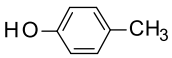	27.8%

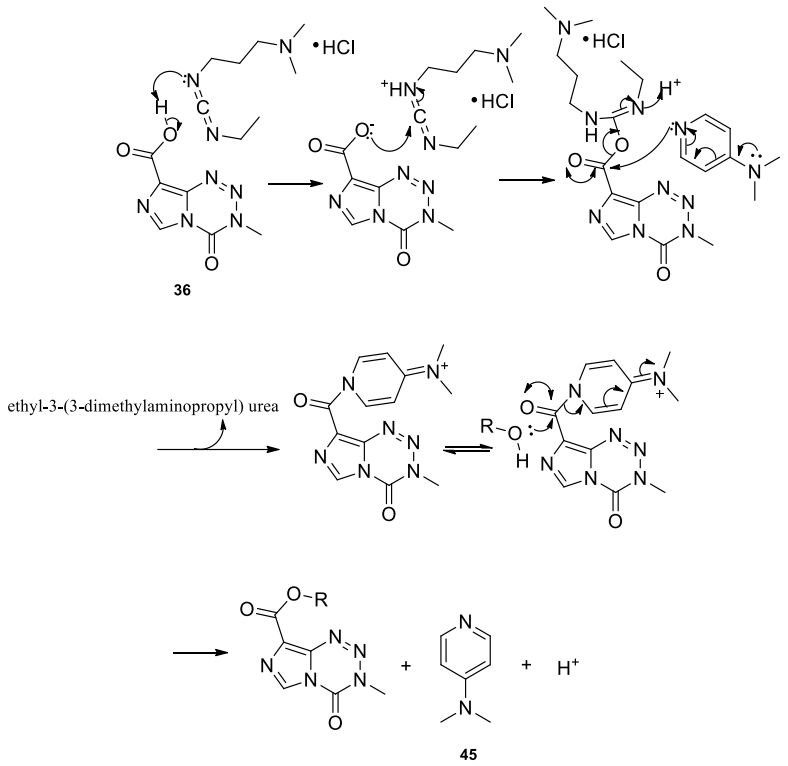

*Scheme 2.10: A mechanism for the reaction between 1-ethyl-3-(3-dimethylaminopropyl)carbodiimide / 4-dimethylaminopyridine and temozolomide acid **36**.*

Due to the success of synthesising ester TMZ analogues using EDC.HCl / DMAP (Scheme 2.4), analogues ES8-ES11 were resynthesized using this route, with the aim of improving yields. Due to the straightforward aqueous work up, yields of ES8-ES11 were dramatically improved (Table 2.5). This phenomenon was attributed to the loss of product, during scheme 2.3's work up, when removing DCU.

Table 2.5: A comparison of yields for the synthesis of ES8-ES11

Target Analogue	Alcohol	Yield (DCC/DMAP)	Yield (EDC.HCl/DMAP)
ES8	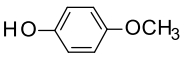	31.9%	49.7%
ES9	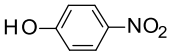	22.8%	44.4%
ES10	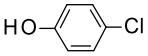	20.1%	29.8%
ES11	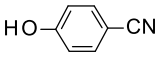	27.9%	48.8%

2.5. Conclusion

The current chapter discussed the synthesis and characterisation of a series of ester and amide analogues of TMZ. Ester and amide TMZ analogues were readily synthesised in acceptable yields, utilising TMZ acyl chloride generation (scheme 2.2) and EDC.HCl / DMAP coupling, (Scheme 2.4). A summary of the structures of the synthesised analogues is shown in Figure 2.7. The next stage of the work involved determining the antiproliferative properties of this series of TMZ analogues in the hope of identifying compounds with promising activity.

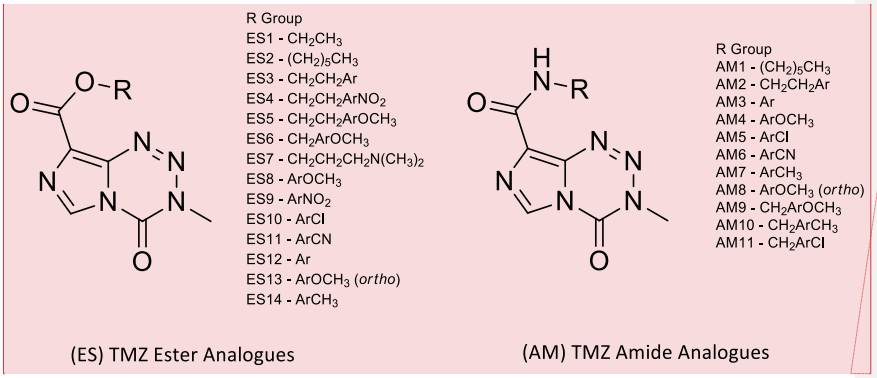

Figure 2.7: Successfully synthesised ester and amide analogues of temozolomide.

Note: All aromatic substituents are in the para position unless otherwise stated.

Commented [OI6]: Review this on phenols

CHAPTER 3:

ANTIPROLIFERATIVE

DETERMINATION OF SYNTHESISED

ANALOGUES

3.1. Introduction

The following chapter will focus on the antiproliferative evaluation of the compounds described in Chapter 2. Glial and glioma cell lines are the logical starting point for the antiproliferative evaluation of novel TMZ analogues. These cell lines have undergone specific mutations that de-regulate the cell cycle leading to indefinite replication, while retaining some similar characteristics present in primary cells found in human glioma and in healthy glial tissue. Consequently, they provided the basis of an acceptable, cost-effective non-animal model for initially comparing the antiproliferative effects of the TMZ analogues described in Chapter 2. Although cell lines provide a model that simulates a primary human tumour, there are limitations that must be recognised when attempting to draw conclusions from results obtained using these cells. Glioma cell lines, including U87-MG, have been shown to exhibit different biological phenotypes compared with primary tumours. Differences in heterogenicity; epidermal growth factor receptor (EGFR) expression and cell replication rates between cell lines and primary tumours, all contribute to the limitations of glioma cell line investigations and limit the conclusions that can be made from the results, (Li *et al.*, 2008). In order to provide a more accurate insight into the antiproliferative effects of TMZ analogues, patient-derived primary cultures can be used in place of cell lines. These cells exhibit cell phenotypes more reminiscent of cells found in primary human tumours, thus, providing the basis of a much more clinically-relevant model compared with the use of cell lines (Ledur *et al.*, 2017). Therefore, primary cells derived from patients suffering from GBM, can be used to more accurately determine the effectiveness of the most promising TMZ analogues, compared with the use of cell lines. Although *in vitro* models provide a cost effective, efficient means of assessing compounds they possess inherent disadvantages compared with animal models, (Aslantürk, 2018). Therefore, once lead TMZ analogues have been identified through *in-vitro* analysis, the next stage of investigation should centre around investigations using animal models.

The characteristics of each cell line used to assess the antiproliferative effects of the analogues is summarised in Table 3.1. Uppsala 87 Malignant Glioma (U87-MG), a cell line originally developed at The University of Uppsala from a male stage IV GBM patient, was initially used to evaluate the TMZ analogues (Allen *et al.*, 2016). Analogues identified as possessing preferential antiproliferative activity, with regards to IC_{50}, were then investigated further against 1321-N1, GOS-3 and SVGp12 cell lines. The 1321-N1 cell line was originally derived as a sub-clone of the 1181-N1 cell line in 1972, which in turn was isolated from the parent line U-118 MG (Arnoldussen *et al.*, 2018). These immortalised cells are representative of a grade II human astrocytoma. The GOS-3 line is a derivative of U-343-MG and represents a grade II/III human astro-oligodendroglioma (Bady *et al.*, 2012). The SVGp12 cell line was originally derived by transfecting primary foetal glial cells with simian virus 40 to achieve immortalisation (Henriksen *et al.*, 2014). SVGp12 serves as a control cell line in the proceeding investigations described in the present chapter, allowing an assessment of the effect of the analogues on healthy cells. The sequential method of evaluation described above allowed for less active analogues to be eliminated earlier in the investigation, leading to a more efficient process.

Table 3.1: A summary of cell lines used to assess the relative antiproliferative effects of TMZ analogues.

Cell Line	**U87-MG**	**GOS-3**	**1321-N1**	**SVGp12**
Grade	Grade IV human glioblastoma	Grade II/III human astro-oligodendroglioma	Grade II human astrocytoma	Human foetal astroglial

Once the most promising analogues were identified using cell lines, the next stage of analysis was to assess the antiproliferative effects of these analogues against primary cells. Primary cultures were obtained from the Brain Tumour North West (BTNW) Tissue Bank in collaboration with The Royal Preston Hospital. The two primary cultures were BTNW914 and BTNW374 (Table 3.2). The BTNW914 primary culture was derived from a 65 year old female GBM patient who exhibited 10 months survival after surgery. The BTNW374 culture was derived from a 33 year old female GBM patient who exhibited 8 months survival after surgery.

Table 3.2: Characteristics and patient information of primary GBM cultures obtained from The Royal Preston Hospital.

Primary Culture	**BTNW914**	**BTNW374**
Gender	Female	Female
Age	65	33
Disease State	GBM (Grade IV)	GBM (Grade IV)
Survival Post Resection	10 Months	8 Months
Allred Score MGMT (Grade)	(PS: 0) + (IS: 0) = TS: 0 (Negative)	(PS: 5) + (IS: 3) = TS: 8 (Positive)

Immunohistochemical (ICH) staining to assess MGMT expression was carried out by the Pathology Department at The Royal Preston Hospital. Allred scores from this assessment are shown in Table 3.2. Allred scores are expressed using both the proportional score (PS), (the proportion of MGMT expressing cells); and the intensity score (IS), (the average intensity of staining). The PS and the IS are then added together to give a total score (TS), the threshold for a sample to be deemed positive is >2, Table 3.3 (Harvey *et al.*, 1999; Fitzgibbons *et al.*, 2014). BTNW914 was found to be devoid of MGMT while BTNW374 was found to express high levels of MGMT. Consequently, analysis using these primary cultures allowed the analogues to be

tested with regards to the MGMT mediated resistance associated with methylating agents such as TMZ.

Table 3.3: Allred score grading system. Proportional score (PS) and Intensity score (IS) are combined to give the total score (TS). TS scores between 0-2 are deemed to be negative, TS scores between 3-8 are deemed to be positive. (Harvey et al., 1999).

Proportion of Positive Cells, %	Proportion Score (PS)	Average Intensity of Staining	Intensity Score (IS)
0	0	None	0
<1	1	Weak	1
1-10	2	Intermediate	2
11-33	3	Strong	3
34-66	4		
>67	5		

In the following study, the CellTiter-Glo® viability assay was used to assess the number of viable cells at the end of the experiments. CellTiter-Glo® allows adenosine triphosphate (ATP) levels to be measured using the enzyme luciferase and luciferin **46** (Niles *et al.*, 2008). ATP is a known biomarker of viable cells (Crouch *et al.*, 1993). Diminished cellular membrane integrity results in an abated ability to synthesise fresh ATP, while endogenous ATPases breakdown cellular ATP reserves. A reaction between luciferin **46** and ATP catalysed by luciferase and magnesium ions producing the luminescent product, oxyluciferin **47** (Scheme 3.1) (Riss *et al.*, 2013).

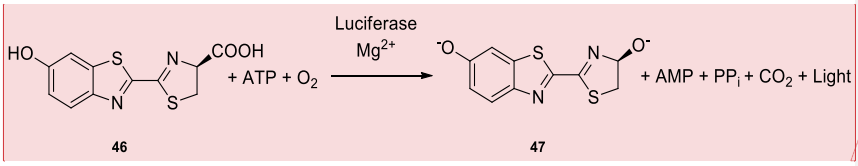

Commented [OI7]: Change numbers

*Scheme 3.1: The reaction between luciferin **46** and ATP, catalysed by luciferase and magnesium ions producing the luminescent product oxyluciferin **47.** Adenosine monophosphate (AMP), pyrophosphate (PPi) and CO_2 are also produced as by-products.*

Upon addition of CellTiter-Glo®, the detergent present in the reagent lyses the cells, causing the release of intracellular ATP. ATPase inhibitors also present within the reaction mixture prevent breakdown of ATP and allow the reaction described as part of Scheme 3.1 to take place. The strength of the luminescent signal from the reaction can then be used to estimate the concentration of ATP, which in turn is directly proportional to the number of viable cells (Crouch *et al.*, 1993; Riss *et al.*, 2013). The luminometric CellTiter-Glo® viability assay is a much faster and sensitive assay than its tetrazolium based counter parts, 3-(4,5-dimethylthiazol-2-yl)-2,5-diphenyltetrazoliumbromide (MTT) and 3-(4,5-dimethylthiazol-2-yl)-5-(3-carboxymethoxyphenyl)-2-(4-sulfophenyl)-2H-tetrazolium (MTS) (Aslantürk, 2018). Additionally, ATP-based luminometric assays are less prone to artefacts, thus generating results that are more consistent. Consequently, CellTiter-Glo® was the preferred assay for the assessment of cell viability in this study.

It is well documented that TMZ generates antiproliferative effects in both glioma cell lines and primary glioma cultures (Sankar *et al.*, 1999; Perazzoli *et al.*, 2015; Moiseeva *et al.*, 2016; William *et al.*, 2018). However, the mechanism of action and the pharmacokinetic profile of the drug must be carefully considered when designing *in vitro* investigations, to ensure results remain clinically significant. When designing a suitable *in vitro* model for the assessment of known or suspected methylating agents, such as the analogues described in the present work, a number of factors must be carefully considered. As discussed in Chapter 2, the ester and amide analogues of TMZ, synthesised as part of this study, were designed so as to not perturb the mechanism of prodrug activation and methylation. Therefore, upon exposure to an aqueous environment at physiological pH, it is reasonable to assume that the analogues degrade into modified MTIC degradants **48** and a methyldiazonium ion **13** (Scheme 3.2) (Denny *et al.*, 1994)**.** Thymine mismatch occurs through electrophilic addition of methyl groups to the *O6*-guanine adducts, producing *O6*-MeG. MMR machinery recognises the incorrect thymine inducing a futile cycle of insertion and deletion, initiating a double stranded break in the DNA. Once a sufficient number of double stranded breaks have occurred the ATM/ATR-Chk1 pathway is activated

leading to stabilisation of p53, generating an apoptotic response. Apoptosis in glioma cells, induced by temozolomide, occurs at least 120 h after treatment (Roos *et al.*, 2007). Consequently, it is important that *in vitro* assays include an appropriate incubation time to allow time for apoptosis to occur. As a result, the antiproliferative determination of TMZ analogues was conducted over a period of 144 h (6 days).

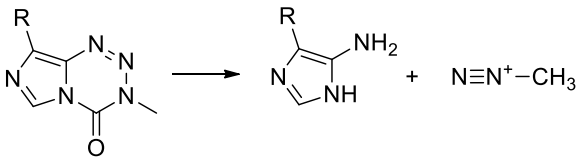

48 **13**

Scheme 3.2: Hypothesised degradation of 8-subsituted TMZ analogues

The aim of the current work will be to assess the antiproliferative effects of the TMZ analogues against a range of glioma cell lines and patient-derived primary cultures. From this information, analogues that show preferential activity will be identified and taken forward for further studies.

3.2. Material and Methods

3.2.1. Cell Lines and Primary Cultures.

The human glioma cell lines, U87-MG and 1321-N1 were purchased from The European Collection of Cell Cultures (ECCAC, UK). The GOS-3 glioma cell line was purchased from Deutsche Sammlung von Mikroorganismen und Zellkulturen (DMSZ, Germany). The SVGp12 cell line was purchased from the American Type Culture Collection (ATCC). Full characterisation of cell lines is included in Table 3.4. Patient-derived primary GBM cultures, BTNW 374 and BTNW 914, were obtained from the BTNW tissue bank in collaboration with The Royal Preston Hospital. Characterisation and culture conditions of these cells is included in Table 3.5. The first phase of antiproliferative determination testing on all TMZ analogues was conducted against the U87-MG cell line, due to it being the most malignant. The most promising analogues identified during the first phase of testing were then assessed against GOS-3 and 1321-N1 cell lines; with SVGp12 serving as the control cell line, as part of the second phase of testing. The most promising analogues identified during the first and second phase of testing were then assessed against MGMT-positive and MGMT-negative patient-derived primary GBM cultures as part of the third phase of testing. All cells were received as frozen samples containing cells in appropriate freezing medium with DMSO as the cryopreservative.

Table 3.4: Characteristics of cell lines used to assess the antiproliferative effects of TMZ analogues. Note: Foetal Bovine Serum Albumin (FBS); Dulbecco's modified Eagle's medium (DMEM); Eagle's minimum essential medium (EMEM); Non-essential amino acids (NEAA).

Cell Line	**U87-MG**	**GOS-3**	**1321-N1**	**SVGp12**
Tissue	Brain	Brain	Brain	Brain
Disease State	Grade IV human glioblastoma	Grade II/III human astro-oligodendroglioma	Grade II human astrocytoma	Healthy human foetal astroglial
Culture Conditions	DMEM supplemented with 10% FBS and 2 mM L-glutamine	DMEM supplemented with 10% FBS and 4 mM L-glutamine	EMEM supplemented with 10% FBS, 2 mM L-glutamine, 1% NEAA, 1 mM sodium pyruvate	EMEM supplemented with 10% FBS, 2 mM L-glutamine, 1% NEAA, 1 mM sodium pyruvate
Supplier	ECACC, UK	DSMZ, Germany	ECACC, UK	ATCC, UK

Table 3.5: Characteristics of patient-derived primary cultures used to assess the antiproliferative effects of TMZ analogues. Note: 4-(2-hydroxyethyl)-1-piperazineethanesulfonic acid (HEPES). ICH staining to assess MGMT status was carried out by pathology staff from The Royal Preston Hospital using the Allred scoring system as described in Section 3.1.

Patient-derived primary culture	**BTNW914**	**BTNW374**
Tissue	Brain	Brain
Disease State	Grade IV human glioblastoma	Grade IV human glioblastoma
Culture Conditions	Nutrient Mixture F-10 Ham supplemented with 20 mM HEPES, 10% FBS and 2 mM L-glutamine	Nutrient Mixture F-10 Ham supplemented with 20 mM HEPES, 10% FBS and 2 mM L-glutamine
MGMT Status	Negative	Positive

3.2.1.1. Media and Reagents Used for Cell Culture

All medium and reagent preparation was completed under sterile conditions in a laminar flow hood. The medium was supplemented as recommended by the provider of the cell lines, as shown in Table 3.4 and Table 3.5. A full list of reagents used for the maintenance of the cell lines is detailed in Table 3.6.

Table 3.6: A list of reagents and their relevant formulations used in cell culture.

Reagent	Formulation	Supplier
Nutrient Mixture F-10 Ham	1.1 g/L glucose; 20 mM HEPES; Containing phenol red; Containing sodium pyruvate.	Sigma Aldrich
DMEM	4.5 g/L glucose; Containing phenol red; 1.0 mM sodium bicarbonate.	Lonza
EMEM	Earle's salt solution; Containing phenol red; 2.2 mM sodium bicarbonate.	Lonza
NEAA	Contains a 10 mM concentration of each non-essential amino acid (100X).	Lonza
Hanks Balanced Salt Solution (HBSS)	1.0 g/L glucose; Containing phenol red; 4.2 mM sodium bicarbonate; Without magnesium; Without calcium.	Gibco
L-glutamine	L-Glutamine, supplied as 29.3 mg/mL (200 mM) in 0.85% NaCl.	Lonza
Sodium Pyruvate	Pyruvic Acid Sodium Salt 100 mM.	Lonza
Trypan Blue	Trypan Blue Solution, 0.4% Phosphate Buffered Saline.	Hyclone
FBS	EU Grade. Origin: Brazil – Standard FBS.	Life Science Production

3.2.1.2. Thawing frozen cells

U87-MG, 1321-N1, GOS-3 and SVGp12 cell lines were stored under liquid nitrogen in The University of Central Lancashire's Tissue Bank. Cells were thawed following protocols recommended by the providers ECACC, ATCC and DSMZ.

1. The frozen cryovial was placed immediately into a 37 ^{o}C water bath for 1-2 min to thaw.
2. Cells were then pipetted aseptically into a 10 mL centrifuge tube with 5 mL of the appropriate supplemented medium at 37 ^{o}C.
3. The cell suspension was centrifuged at 1000 rpm for 5 min.
4. The supernatant was removed and 1 mL of fresh medium was added to resuspend the cell pellet.
5. The cell suspension was then added to a 75 cm^2 vented tissue culture-treated flask along with 10 mL of medium.
6. The cells were then incubated at 37 ^{o}C and 5 % CO_2 in a humidified incubator.
7. The medium was changed every 48 h to replenish nutrients.

Primary cultures obtained from The Royal Preston Hospital were thawed following protocols recommended by the Pathology Directorate. Cryostored vials of cells were collected from The Royal Preston Hospital and transported to The University of Central Lancashire on dry ice before being thawed.

1. The frozen cryovial was placed immediately into a 37 ^{o}C water bath for 1-2 min to thaw.
2. The 1 mL cell suspension was then transferred aseptically to a 25 cm^2 unvented tissue culture-treated flask along with 9 mL of medium.
3. The cells were then incubated at 37 ^{o}C in a humidified incubator for 24 h.
4. The medium was then changed to remove cell debris and unadhered cells.

5. Half the medium was changed every 48 h to ensure nutrients were replenished whilst retaining essential growth factors.

3.2.1.3. Subculture and Working Cell Stock Maintenance

Cells were observed daily and subcultured upon reaching 70-80% confluence. Cells were periodically frozen in order to maintain working stocks of consistent passage number. All cell lines and primary cultures were subcultured using the following protocol:

1. The cell culture medium was removed from the flask and replaced with 5 mL of HBSS (37 ^{o}C). The flask was gently agitated and the HBSS removed, so as to wash the cells, removing cell debris.
2. 5 mL of the appropriate medium was added to the flask (Table 3.4).
3. A sterile cell scraper was then used to detach the cells from the bottom of the flask.
4. The resulting cell suspension was then transferred to a 10 mL centrifuge tube and was centrifuged at 1000 rpm for 5 min.
5. The supernatant was removed and 1 mL of fresh medium was added to resuspend the cell pellet.
6. A 10 µL aliquot of the cell suspension was then transferred to an Eppendorf tube for counting. Cells were counted and subcultured into a fresh 75 cm^2 flask with 10 mL of fresh medium.

In order to ensure working stocks of consistent passage number, cells were periodically frozen. Cells were frozen using the following protocol.

1. A 900 µL cell suspension was obtained using the protocol described above.
2. The 900 µL cell suspension was added dropwise to a cryovial containing 100 µL of DMSO.
3. Cryovials containing cells were stored at -80 ^{o}C overnight in an isopropanol freezing container.

4. Cryovials were then stored under liquid nitrogen.

3.2.1.4. Cell Counting

A 10 µL aliquot of a 1 mL cell suspension was transferred to an Eppendorf, as described in Section 3.2.4. The aliquot of cells was diluted with 20 µL of Trypan Blue. The cell solution was then added to a haemocytometer. Cells were counted using 4 outside squares and averaged, as shown in Figure 3.1.

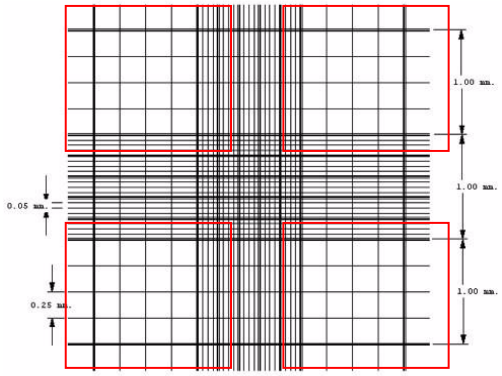

Figure 3.1: A haemocytometer showing the 4 outside squares that were used to count the cells, highlighted in red.

3.2.2. *In-Vitro* Antiproliferative Determination of the Compounds

3.2.2.1. Drug Solution Preparation

TMZ (98%) was purchased from Carbosynth. TMZ acid, along with ester and amide TMZ analogues were synthesised and characterised as part of Chapter 2. Each analogue was found to be >95% pure following ^{1}H NMR analysis. Drugs were dissolved in DMSO to afford 200 mM stock solutions. Appropriate cell culture medium was then used in a series of dilutions to afford the working concentrations. Maximum working concentration used in experiments was 1 mM, ensuring the final DMSO concentrations did not exceed 0.5 % (v/v). The effect of DMSO at a

concentration of 0.5% (v/v) over 6 days on each cell line and primary culture is shown in Appendix 1. The effect of DMSO at 0.5% (v/v) on the cell lines and primary cultures is negligible and indicates no decrease in viability. Consequently, any decreases in viability through exposure to analogues are attributed solely to the effect of the drug.

3.2.2.2. Solubility Evaluation of TMZ Analogues

The conversion of TMZ to ester and amide analogues affects the lipophilicity and subsequently the solubility of the analogues. Therefore it was essential to evaluate the solubility of TMZ analogues in medium prior to assessing their anticancer activity to ensure these analogues were in solution during incubation. All 25 analogues were prepared at concentrations ranging between 200 – 1000 µM in medium. Solutions were then visually inspected under a microscope. Analogues were then tested on cells at concentrations at which they were soluble. The results from solubility evaluation are shown in Appendix 3b.

3.2.2.3. Protocol for *In-Vitro* Antiproliferation Assays

Protocols outlined in Sections 3.2.2.3 and 3.2.2.4. were used to obtain a 1 mL cell pellet and calculate the concentrations of cells. Appropriate cell suspensions were then prepared. Cells were seeded in the appropriate media, in each well of a Costar 96-well plate at a density of 5 x 10^2 immortalised cells; and 2 x 10^3 primary cells. The plates were incubated at 37 ^oC and 5% CO_2 in a humidified incubator for 24 h to allow cells to adhere. Each of the drugs was tested following the protocol outlined in Section 3.2.3.1., ensuring DMSO concentration was no greater than 0.5% (v/v). Drug was added to the cells and incubated for 144 h. After incubation, the drug concentrations were removed and replaced with 100 µL of CellTiter-Glo® and 100 µL of media. The luminescence of each well was measured on GENios Pro plate reader. The results for each of the drug concentrations were expressed as a percentage of the control wells. For cell lines, the regression equation for a polynomial line of best fit of the order 2, was used to calculate the IC_{50}. In the case of the *in-vitro* model used in the present study, the IC_{50} was defined as the concentration of drug that results in a 50% reduction in oxyluciferin production. For primary

cultures, cells were incubated with clinically relevant concentrations for 144 h. Viability was then expressed as a percentage of the control. Each experiment involving cell lines was carried out as a triplicate of triplicates. Experiments using patient derived-primary cultures were carried out in triplicate.

3.2.2.4. Growth Curves

Growth curves of the 4 cell lines used to assess the antiproliferative effects of TMZ analogues in the current study are shown in Figure 3.2. Cells were seeded each day for 8 days at 2000 cells per well using the protocol outlined in Section 3.2.6.3. On the 9th day of incubation cells were assessed using CellTiter-Glo®. Growth curves indicate that cells remain in the log phase of growth throughout the duration of the experiment.

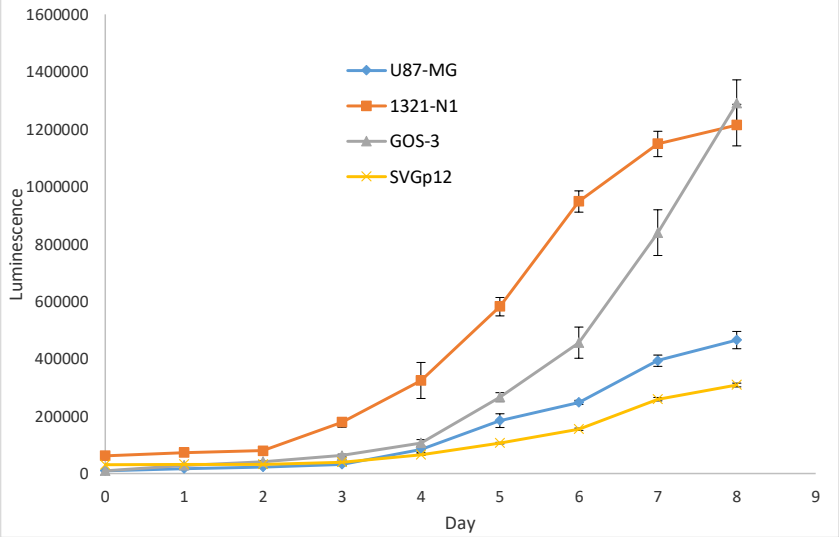

Figure 3.2: Growth curves of U87-MG, 1321-N1, GOS-3 and SVGp12 cell lines. The values shown are mean ±SD, n = 3.

3.3. Results and Discussion

Prior to conducting antiproliferative determination of the TMZ analogues, summarised in Figure 3.3, the solubility of each analogue in aqueous medium was evaluated. TMZ acid, ES1, ES2, ES3, ES7, ES12, ES13 and ES14 were found to be soluble in medium between 0-1000 µM. AM2 was found to be soluble up to 600 µM. ES8, ES9, ES10, ES11, AM1, AM3 and AM10 were found to be soluble between 0-200 µM. ES4, ES5, ES6, AM4, AM5, AM6, AM7, AM8, AM9 and AM11 were found to be insoluble at concentrations of 200 µM or above. Analogues that were found to be insoluble at 200 µM were eliminated from the investigation to allow focus on analogues with preferential solubility. The results of solubility evaluation of each analogue in aqueous medium are illustrated in Appendix 3B. The reduction in aqueous solubility of TMZ analogues, compared with TMZ, as expected due to the addition of lipophilic side chains. Amides were much less soluble than the corresponding esters, an effect attributed to additional hydrogen bond donating sites resulting in stronger intermolecular forces. *In-vitro* antiproliferation assays for each analogue were then conducted at concentrations at which the drugs were soluble. This approach ensured that the true activities of analogues were observed, preventing the viability of cells being compromised due to the mechanical stresses of percipitated drug.

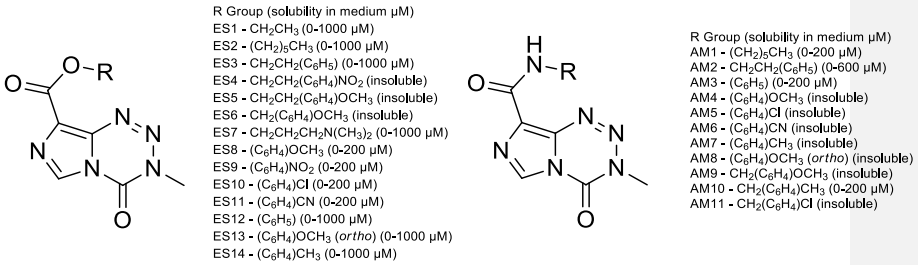

Figure 3.3: Summary of ester and amide analogues of temozolomide under investigation.

It is well acknowledged that TMZ elicits its mechanism of action through methylation of guanine forming *O6*-MeG, causing subsequent mismatch with thymine (Denny *et al.*, 1994). Mismatch between thymine and *O6*-MeG is recognised by MMR, and is subsequently removed from the replication fork. In the absence of MGMT the guanine methylation is not repaired, resulting in a futile cycle of insertion and deletion, eventually triggering apoptosis. Apoptosis in glioma cells, induced by TMZ, occurs at least 120 h after treatment (Roos *et al.*, 2007). Consequently, treated cells in *in-vitro* investigations were incubated for 144 h with the analogues in order to gain a more reliable IC_{50} value. The graph and polynomial regression equation used to calculate IC_{50} values for analogues against each cell line are shown in Appendix 3C.

To assess the antiproliferative potential of TMZ analogues depicted in Figure 3.3, initial screening was conducted against the U87-MG cell line, Table 3.7. For TMZ and TMZ acid the IC_{50} was 696±79 and 662±42 μM, respectively. The equipotency observed between TMZ and TMZ acid against U87-MG is consistent with previous literature published using lymphoma cells (TLX9) (Tsang *et al.*, 1990) and glioma cells (TJ899; TJ905 and SHG-44) (Suppasansatorn *et al.*, 2006). TMZ analogues ES1, ES3, ES7, ES13 and AM2, similar to TMZ acid, exhibited activity comparable to, or less than TMZ. ES7, an analogue originally described by Liu et al., 2010, was reported to exhibit very promising cytotoxic potential; however, testing was not inclusive tof glioblastoma cell lines providing the rationale of its inclusion in the present study (Liu *et al.*, 2010). Unfortunately, the compound was found to be less active than TMZ against U87-MG cells and so it was eliminated from further investigation.

Table 3.7: IC_{50} evaluation (µM) of TMZ analogues against U87-MG cells. Values reported are IC_{50} ± SD, n=3.

Analogue	IC_{50} (µM)	Analogue	IC_{50} (µM)
TMZ	696 ± 79	**ES12**	331 ± 47
TMZ acid	662 ± 42	**ES13**	576 ± 91
ES1	700 ± 109	**ES14**	376 ± 62
ES2	409 ± 45	**AM1**	>200
ES3	615 ± 96	**AM2**	548 ± 48
ES4	-	**AM3**	>200
ES5	-	**AM4**	-
ES6	-	**AM5**	-
ES7	856 ± 20	**AM6**	-
ES8	134 ± 7	**AM7**	-
ES9	142 ± 3	**AM8**	-
ES10	96 ± 3	**AM9**	-
ES11	138 ± 7	**AM10**	139 ± 28
		AM11	-

A significant proportion of amide containing analogues and methyl/ethyl phenyl analogues, (ES4, ES5, ES6, AM1, AM3, AM4, AM5, AM6, AM7, AM8, AM9 and AM11) were insoluble in medium at concentrations greater than 200 µM. The maximum concentration that could be achieved in medium for analogues AM1 and AM3 was approximately 200 µM, at which IC_{50} values could not be generated and so were eliminated from further studies. Interestingly, ester analogues (ES2, ES8, ES9, ES10, ES11, ES12 and ES14) exhibited 2 to 5-fold greater activity against the U87-MG cell lines compared to TMZ, and were subsequently taken forward to test against additional cell lines. The phenyl containing ester analogues ES8, ES9, ES10, ES11, ES12 and ES14 (IC_{50} = 96 - 376 µM) were found to be the most potent, tested against the U87-MG cell line, compared with TMZ (IC_{50} = 696 µM). TMZ hexyl ester ES2 was originally described by Suppasansatorn et al., 2006 as a topical treatment for melanoma (Suppasansatorn *et al.*, 2006). In the present work the potency of this analogue was assessed against glioblastoma cell lines, as

a result of its promising cytotoxic potency against melanoma cells. In the present study TMZ hexyl ester ES2 (IC_{50} = 409 µM), exhibited significantly increased potency against U87-MG cells compared to TMZ.

Analogues ES2, ES8, ES9, ES10, ES11, ES12, ES14 and AM10 were selected to be taken forward due to promising activity shown against U87-MG cells. Additional testing involved antiproliferative determination of these analogues against 1321-N1, GOS-3 and SVGp12 cell, in order to gain a deeper understanding of their activity against the various grades of glioma and healthy glial cells. The results depicted in Table 3.8, show very similar trends and support the results obtained using U87-MG. The effectiveness of the analogues against human glial cells (SVGp12), suggest that these analogues did not have specificity for malignant cells.

Table 3.8: IC_{50} evaluation (µM) of TMZ analogues against 1321-N1, GOS-3 and SVGp12 cells. Values reported are IC_{50} ± SD, n=3.

	IC_{50} (µM)			
Analogue	**U87-MG**	**1321-N1**	**GOS-3**	**SVGp12**
TMZ	696 ± 79	783 ± 40	696 ± 16	239 ± 6
TMZ acid	662 ± 42	596 ± 26	504 ± 30	316 ± 2
ES2	409 ± 45	269 ± 20	269 ± 6	182 ± 11
ES8	134 ± 7	183 ± 1	183 ± 5	44 ± 2
ES9	142 ± 3	104 ± 4	91 ± 1	39 ± 2
ES10	96 ± 3	118 ± 11	54 ± 4	33 ± 1
ES11	138 ± 7	103 ± 7	151 ± 4	36 ± 3
ES12	331 ± 47	511 ± 10	691 ± 35	238 ± 6
ES14	376 ± 62	238 ± 8	314 ± 38	215 ± 26
AM10	139 ± 28	>200	>200	79 ± 6

Commented [OI8]: Add comparison between grades of glioblastoma

The most noteworthy compounds found during the initial antiproliferative determination were ester analogues containing *para*-substituted aromatic moieties, containing methoxy, nitro, chloro and nitrile groups (ES8, ES9, ES10, ES11), which exhibited activity 4 to 5-fold greater than

TMZ, across each of the cell lines. The introduction of an ortho-substituted methoxy moiety (ES13) in place of corresponding *para*-substituted methoxy moiety (ES8) resulted in significantly reduced activity. Additionally, the unsubstituted phenyl analogue ES12 showed less activity than its substituted counter-parts (ES8, ES9, ES10, ES11). Interestingly, although analogue ES14, containing a methyl moiety in the *para*- position, displayed greater activity than the phenyl analogue ES12; it was still found to be significantly less active than analogues containing highly polarising aromatic groups. Consequently, the SAR of ester analogues containing *para*-substituted aromatic moieties was probed further, through the analysis of Hammett constants (Figure 3.4). Compound AM10 was eliminated from the study due to poor efficacy against 1321-N1 and GOS-3 cell lines, where IC_{50} values could not be obtained.

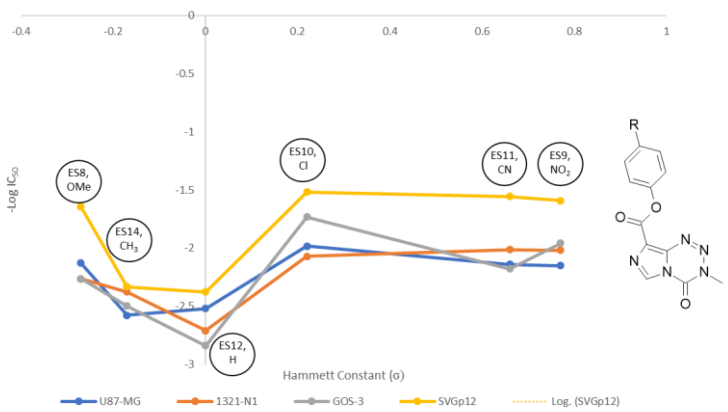

Figure 3.4: Hammett plot showing the relationship between -logIC_{50} vs Hammett Constant.

Analysing the relationship between the Hammett constants and IC_{50} values revealed analogues containing highly polarising groups tended to confer increased activity. However, the lack of a linear relationship between the Hammett constants and log $IC_{50,}$ for *para*-substituted phenyl ester TMZ analogues, suggests that changing the substituent at the *para*- position of the phenyl

ester moiety effects more than one physiochemical property that contributes to potency. It has been recently established that modifications at position 8 of the imidazole ring can influence the rate of prodrug activation, it would be reasonable to suggest that modifying the substituent on the phenyl ester moiety could possibly affect the rate at which these prodrugs produce methyl diazonium ions (Svec *et al.*, 2018; Yang *et al.*, 2019). Svec *et al.* (2018) reported that the addition of electron donating groups, such as methyl and phenyl moieties, increased aqueous stability and potency. However, it is still unknown what the optimum half-life of a methylating imidazotetrazine prodrug should be to maximize efficiency. Consequently, the determination of stability in an aqueous environment of the phenyl ester analogues would be an intriguing aspect of future work (see Chapter 5). Another physiochemical property that may contribute to potency is the lipophilicity of the compounds. Analogues with increased lipophilicity could internalise into cells more efficiently, increasing their activity. Figure 3.5 summarises the relationship between LogP, calculated using Crippen's Fragmentation (CS ChemDraw Ultra 8.0 software) (Ghose and Crippen, 1987), and IC_{50} against U87-MG cells. It is clear from Figure 3.5 that a moderate correlation between LogP and potency exists ($R^2 = 0.2665$). However, the variation in IC_{50}s within analogues that share similar LogP values again suggests more than one physiochemical property is being affected that contributes to activity.

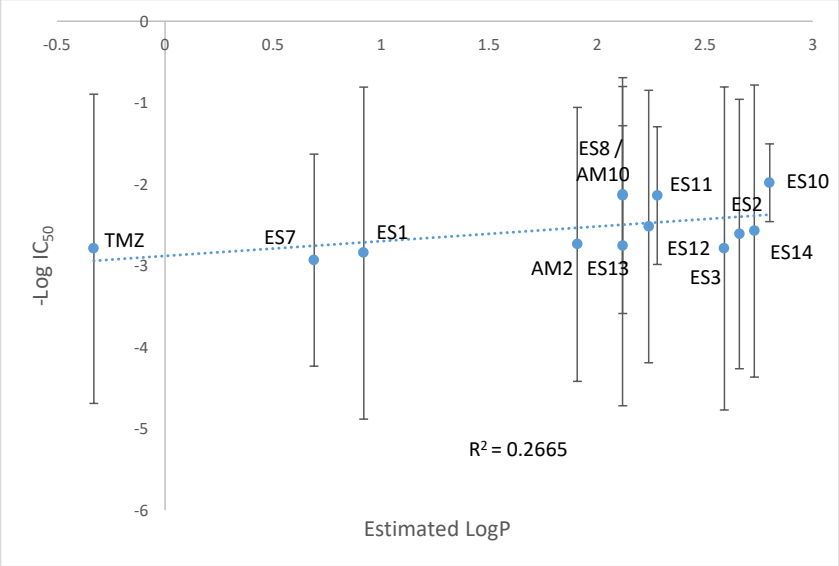

Figure 3.5: A graph showing moderate correlation between -logIC_{50} against U87-MG cells and estimated LogP.

When considering the addition of alkyl chains to esters, it was observed than in the instance of the ethyl containing analogue ES1 and the hexyl containing analogue ES2, a longer alkyl chain increased potency against U87-MG cells, 700 ± 109 µM versus 409 ± 45 µM (Figure 3.6). The increase in potency observed was attributed an increase in lipophilicity, allowing for greater accumulation of ES2 in the cells. However, when considering analogues ES12 and ES3, containing phenyl and phenylethyl moieties respectively, it was found that the addition of an alkyl chain reduced potency against U87-MG cells, 331 ± 47 µM versus 615 ± 96 µM. These results were in direct contradiction with the comparison between ES1 and ES2, where the addition of an alkyl chain increased potency, again suggesting modifications affect more than one physiochemical property that contributes to activity.

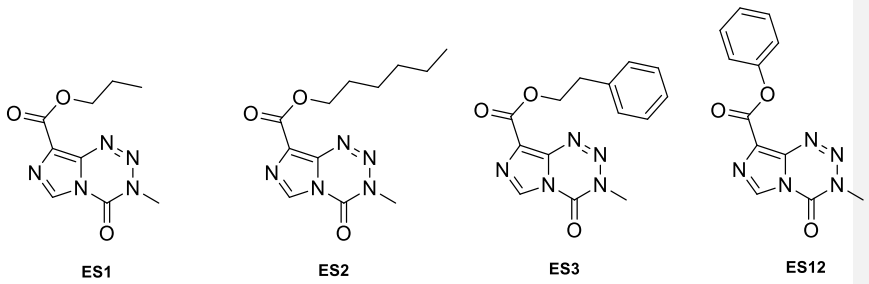

Figure 3.6: Structures of ES1, ES2, ES3 and ES12, containing various lengths of alkyl chains.

Due to the significantly increased potency of phenyl ester TMZ analogues, it was important to assess the effectiveness of the most promising analogues in the presence and absence of MGMT. Patient-derived primary GBM cultures, BTNW914 (MGMT -) and BTNW374 (MGMT +), obtained from The Brain Tumour North West Tissue Bank, were used to assess analogues (ES8, ES9, ES10, ES11, ES12, and ES14) at clinically obtainable concentrations. The results from these investigations are shown in figure 3.7 and 3.8.

In order to maximise the relevance of the results in this study, the analogues were assessed at concentrations that were clinically obtainable. For TMZ, peak plasma levels were found to be 60-75 µM following a 200 mg/m^2 oral dose (Ostermann *et al.*, 2004; Aoki *et al.*, 2007). Brain-tumour concentrations of TMZ are estimated to be around 20% of the plasma concentration, equivalent to approximately 15 µM, (Ostermann *et al.*, 2004; Portnow *et al.*, 2009). However, since TMZ is a prodrug and is not biologically active until it has degraded into AIC and the methyldiazonium ion, these concentrations may not accurately reflect active drug levels within the tumour. In fact, the levels are likely to be higher than what is observed in these studies and as a mixture of TMZ, MTIC and methyl diazonium ions could be present in the tumour, all of which have cytotoxic properties or cytotoxic potential, (Ostermann *et al.*, 2004). It must be noted that the authors acknowledge that modified TMZ analogues may not share the same biodistribution as TMZ. However, as there is no known data on the biodistribution of these novel analogues, the use of clinically-relevant concentrations of TMZ as a means to compare novel analogues, was felt to be the optimum approach.

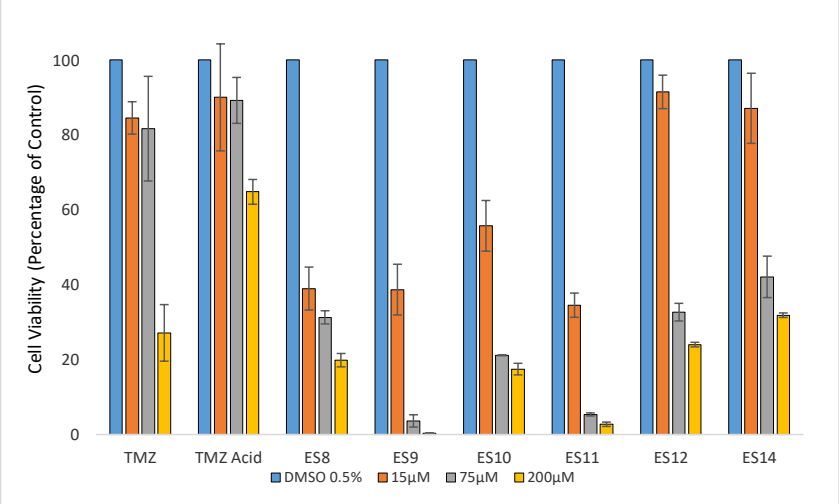

Figure 3.7: Cell Viability of BTNW914 (MGMT -) after treatment by TMZ and phenyl TMZ ester analogues at various clinically relevant concentrations. Values reported are cell viability (%) ± SD, n=3.

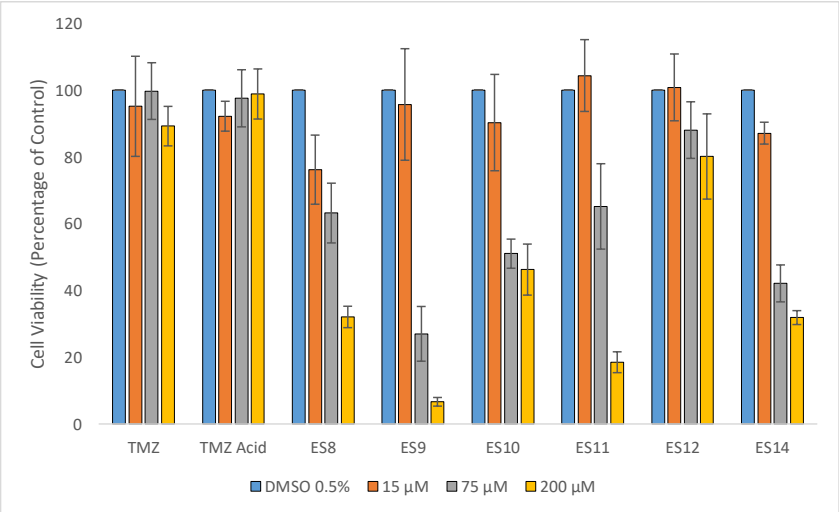

Figure 3.8: Cell Viability of BTNW374 (MGMT +) after treatment by TMZ and phenyl TMZ ester analogues at various clinically relevant concentrations. Values reported are cell viability ± SD, n=3.

At clinically relevant concentrations of 15 and 75 µM, TMZ was found to reduce the viability of MGMT devoid cells by around 20% (Figure 3.7). The relatively modest reduction in viability supports the findings that patients treated with TMZ gain a modest therapeutic benefit (Stupp *et al.*, 2005; Chamberlain, 2010). Results clearly indicate that TMZ is only effective against MGMT-devoid GBM cells at concentrations that are not clinically achievable, following a 200 mg/m^2 oral dose. Interestingly, analogues containing the methoxy, nitro, choro and nitrile phenyl esters (ES8, ES9, ES10 and ES11) generate IC_{50}'s at concentrations that are clinically relevant in the tumour (<15 µM), thus suggesting these analogues could have the potential to generate a significant clinical effect in patients suffering from GBM devoid of MGMT, compared to TMZ. The phenyl esters containing *para*-substituted nitro and nitrile moieties (ES9 and ES11), were observed to be the most potent phenyl ester analogues tested, resulting in a reduction in viability of >90% after treatment at 75 µM. Phenyl ester analogues ES12 and ES14 were also found to be significantly more effective than TMZ, inducing a significant reduction in viability of greater than 50% at 75 µM against MGMT devoid GBM cells. However, these two analogues were found to be less potent than the analogues ES8, ES9, ES10 and ES11 that contain highly polarising groups.

Figure 3.8 shows the activity of the most promising analogues against BTNW374 cells, a MGMT+ expressed patient-derived primary culture. As expected, the repair of cytotoxic *O6*-methylations by MGMT appeared to show TMZ resistance. The MGMT expressing cells demonstrated similar resistance to TMZ acid and phenyl ester ES12, suggesting that these analogues possibly generate activity via a similar mechanism to that of TMZ. Interestingly, the 4-methoxy, 4-nitro, 4-chloro, 4-nitrile and p-cresol phenyl esters (ES8, ES9, ES10, ES11 and ES12, respectively), generated significant activity at 75 µM, independent of the MGMT status. Since the imidazotetrazine ring has remained unchanged in these analogues, it is plausible to assume that methylation still contributes to activity in TMZ sensitive cells. However, as these analogues retain activity against TMZ resistant cells that express MGMT, it is plausible to conclude that an additional mechanism

of action is involved, distinct from methylation (Ferluga *et al.*, 1972; Selassie *et al.*, 2005; Kadoma *et al.*, 2010).

3.4. Conclusion

In the current chapter, the antiproliferative effects of the synthesised ester and amide analogues of TMZ have been evaluated against specified glioma cell lines and patient derived primary cultures. Phenolic ester analogues of TMZ (ES8, ES9, ES10 and ES11) were found to possess upto 5-fold increased potency compared with TMZ, against the specified GBM cell lines. Additionally, lead phenolic esters were found to induce significant antiproliferative effects against TMZ-resistant MGMT-positive primary cells. These results indicate that phenolic TMZ esters could provide an exciting alternative treatment for patients diagnosed with GBM, and could possibly have the potential to induce a greater therapeutic benefit to patients, compared with TMZ. However, further work must be completed in order to ascertain how the lead TMZ esters would behave in an *in-vivo* environment.

CHAPTER 4:

ESTERASE MEDIATED STABILITY OF ANALOGUES USING HPLC

4.1. Introduction

In light of the *in-vitro* activity of phenolic TMZ esters, (ES8, ES9, ES10, ES11, ES12 and ES14), it was important to establish the stability of these analogues in an environment mimicking that of the physiological system. The presence of ester moieties in the lead analogues poses the question of analogue stability when subjected to esterase enzymes. Hydrolysis of the ester would yield TMZ acid and the corresponding alcohol (Scheme 4.1). From the results presented in the previous chapter it is now known that TMZ acid is less active than the intact esters. The esters therefore needed to be examined as rapid hydrolysis of the ester bond may result in a loss of activity.

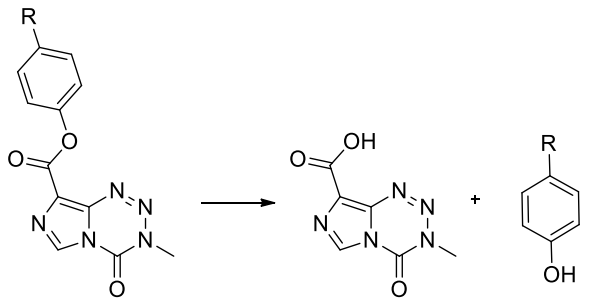

Scheme 4.1: Suspected scheme of esterase mediated degradation of phenolic TMZ esters.

Esterases are found primarily in the liver and gastrointestinal (GI) tract in mammalian systems, consequently playing a pivotal role in drug metabolism, although they are found throughout the body (Timoumi *et al.*, 2019). These enzymes are responsible for the hydrolytic metabolism of numerous drug substrates, including esters, carbamates, thioesters and amides (Laizure *et al.*, 2013). Traditionally, ester prodrugs serve as vehicles for the active portion of the drug which offers increased lipophilicity to enhance oral absorption and cellular penetration (Montella *et al.*, 2012). As previously mentioned one of our hypothesises for the increased activity of the lead compounds in the present study is the increased cellular uptake as a result of increased

lipophilicity. Since the analogues described in the present study act on cancerous brain tissue, it is important to ascertain the stability of our lead ester analogues when subjected to esterases, to have an idea regarding the behaviour of these analogues on their journey towards the site of action.

The most common carboxylesterases found in humans are human carboxylesterase 1 and human carboxylesterase 2 (hCE1 and hCE2, respectively) (Laizure *et al.*, 2013). Mammalian carboxylesterase enzymes are found primarily in cells of the liver and GI tract but are found in other tissues throughout the body (Taketani *et al.*, 2007). The enzymes reside in the cytoplasm and endoplasmic reticulum of cells, contributing to the hydrolysis of various endogenous and exogenous substrates (Imai *et al.*, 2006). hCE1 is primarily found within the liver while hCE2 is found predominantly in the small intestine (Hatfield *et al.*, 2011). Although both hCE1 and hCE2 are promiscuous towards a wide range of ester substrates, one predominates over the other depending on the ester substrate (Fukami and Yokoi, 2012; Laizure *et al.*, 2013). Esters containing large acyl groups and small alcohol groups are the preferred substrates of hCE1, while hCE2 has a preference for esters with small acyl groups and bulkier alcohol groups (Taketani *et al.*, 2007; Vistoli *et al.*, 2010).

HCEs are a member of the α/β-hydrolase protein family. This family of proteins include a number of functionally diverse enzymes each containing an alpha/beta-hydrolase fold domain responsible for their catalytic action. Enzymes of this family, containing this domain include esterases, lipases, dehalogenases, peroxidases and hydrolases. More specifically hCEs are known as serine hydrolases. The active site of hCEs is a catalytic triad of glutamine, histidine and

serine, found at the intersection of the alpha/beta, regulatory and catalytic domains, which are critical for activity (Figure 4.1) (Fleming *et al.*, 2007; Wang *et al.*, 2018).

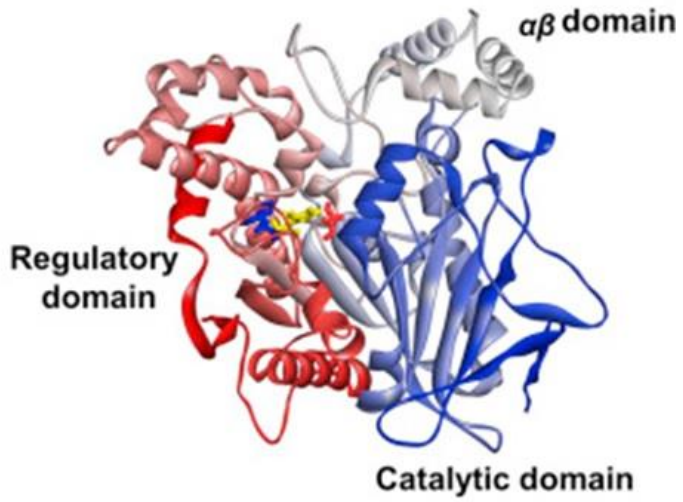

Figure 4.1 General 3D structure of hCEs. The catalytic triad is shown in the centre of the molecule; glutamine (yellow), histidine (blue) and serine (red). Adapted from Wang et al. (2018).

The mechanism by which esterases hydrolyse ester bonds involves a two step base-catalysed reaction which, revolves around a catalytic triad of amino acids (Wang *et al.*, 2018) (Scheme 4.2). The first step of the mechanism involves histidine acting as a base, catalysing the nucleophilic attack of the serine alcohol to the carbonyl of the ester substrate **49** (Imai *et al.*, 2006; Hosokawa, 2008). Pivotal to the reaction is the hydrogen bonds formed between glycine residues within the active site and the ester substrate **50** (Montella *et al.*, 2012). The collapse of the tetrahedral intermediate causes the breaking of the ester forming an acyl-serine intermediate and release of the alcohol **52** (Imai, 2006). The second step of the mechanism

involves the base catalysed attack of water to the acyl-serine intermediate, similar to the first step of the reaction **53**. Again, the tetrahedral intermediate collapses initiating the release of the carboxylic acid **54** and regenerating the hydroxyl group on the serine residue.

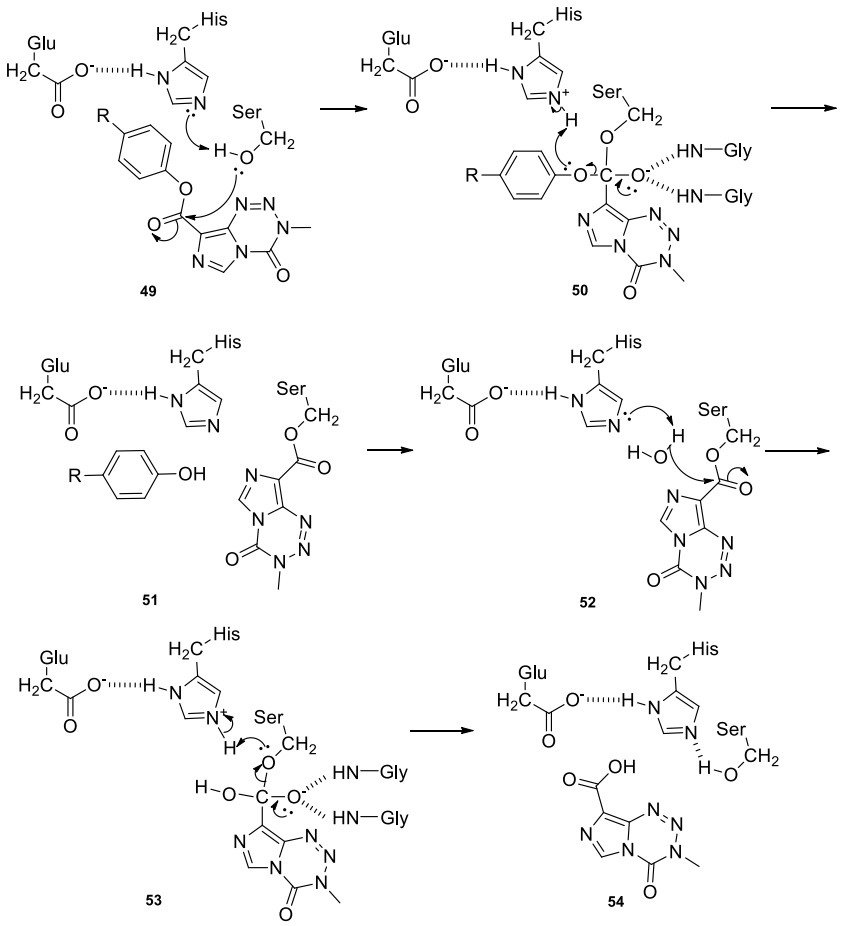

Scheme 4.2: A mechanism showing phenolic TMZ ester hydrolysis by the catalytic triad, glutamine, histidine and serine found in esterase enzymes.

In the present work porcine liver esterase (PLE) was used to assess stability of the ester bond in the phenolic esters. As discussed previously, specific isoenzymes such as hCE1 and hCE2 have different substrate preferences and therefore hydroylse different esters at different rates (Fukami and Yokoi, 2012; Laizure *et al.*, 2013). Therefore, the use of individual specific isoenzymes, such as hCE1 or hCE2 may not give a truly accurate representation of ester hydrolysis *in-vivo*. Additionally, at this preliminary stage of investigation the cost of purchasing hCE isoenzymes to evaluate lead TMZ analogues was deemed not appropriate. As a result, PLE was used in favour of hCE1 or hCE2, as it contains numerous isoenzymes providing an acceptable cost-effective representation of an *in-vivo* environment, instead of focusing on individual hCE isoenzymes (Brüsehaber *et al.*, 2009). This chapter will focus on esterase mediated hydrolysis of TMZ analogues, ES8, ES9, ES10, ES11, ES12 and ES14, that were highlighted as the lead compounds from antiproliferative determination studies, described Chapter 3. It was hoped that the results of esterase mediated degradation would give an indication of the metabolic stability of the ester bonds within each of the analogues, thus detailing their suitability as potential chemotherapeutic agents for the treatment of GBM.

Commented [OI9]: Methylphenidate is the active compound and is brioken down into the inactive COOH

4.2. Methods

4.2.1. Chemicals

Acetonitrile (HPLC grade ≥99.9%), water (HPLC grade ≥99.9%), acetic acid (HPLC grade ≥99.7%), citric acid monohydrate (HPLC grade), dimethyl sulfoxide (reagent grade) were purchased from Fisher Scientific. Sodium phosphate dibasic (HPLC grade ≥99.0%), sodium acetate (HPLC grade ≥99.0%) and porcine liver esterase were purchased from Sigma Aldrich. 4-Nitrophenol (reagent grade >97%), 4-chlorophenol (reagent grade >98%), 3-hydroxybenzonitrile (reagent grade >97%) and 4-methoxyphenol (reagent grade >99%) were purchased from Alfa Aesar. Phenol (reagent grade >99%) and *p*-cresol (reagent grade >98%) were purchased from Sigma Aldrich. All reagents that were purchased from external suppliers were used without further purification.

4.2.2. Instrumentation and HPLC Method

4.2.2.1. Instrumentation

A HPLC system that consisted of a Jasco PI-2089 plus quaternary gradient pump, Jasco AS-1555 intelligent autosampler and a Jasco MD-1510 diode array multiwavelength detector was used for analysis. These three components were linked to a Dell Optiplex 790 computer system using a Jasco LC-Net II/ADC. Chromatograms were acquired and processed using Chromnav software.

4.2.2.2. HPLC Method

HPLC was carried out on an isocratic reverse phase system. The esters were separated from their esterase mediated degradation products, namely TMZ acid and the corresponding phenolic alcohol. Samples were injected using an autosampler from crimp-top sample vials using a Rheodyne injector with a 100 μL loop. Separation was achieved using a Waters Symmetry Shield RP C_{18} column (4.6 x 250 mm), containing particles equivalent to 5 micron. Detection of TMZ acid and TMZ esters (ES8, ES9, ES10, ES11, ES12 and ES14) was carried out at 325 nm. Detection of

4-methoxyphenol and 4-chlorophenol was carried out at 225 nm. Detection of 4-nitrophenol, 4-hydroxybenzonitrile, phenol and p-cresol was carried out at 325 nm, 250 nm, 270 nm and 225 nm, respectively. The mobile phase consisted of a sodium acetate buffer (20 mM) and acetonitrile (60:40, v/v). The pH of the resulting mixture was then adjusted to pH 4.5 using acetic acid. The analysis of the samples was performed over a period of <20 min at 1 mL / min at ambient temperature.

4.2.2.3. Preparation of the Mobile Phase and Standards used for Validation

The mobile phase was made up in batches 2000 mL (1200 mL sodium acetate buffer (20 mM): 800 mL acetonitrile). The sodium acetate buffer was prepared by solubilising sodium acetate (3.282 g) in 2000 mL of HPLC grade water to achieve a final concentration of 20 mM. To ensure imidazotetrazines remained stable the pH of the sodium acetate/ MeCN mixture was adjusted to pH 4.5 by the addition of acetic acid.

10 mg of each of the sample was solubilised in mobile phase (100 mL) to afford the concentrations displayed in Table 4.1. Samples were diluted to provide working concentrations used to validate the method as described in Section 4.2.3.

Table 4.1: Concentrations of standard solutions used for the validation of the HPLC method. Standard solutions were obtained by solubilising 10 mg of each analyte in 100 mL of mobile phase.

Analyte	Concentration (mg / 100 mL)	Concentration (μM)
TMZ Acid	10.01	513.2
ES8	9.99	331.8
4-Methoxyphenol	10.04	808.8
ES9	10.03	317.3
4-Nitrophenol	10.03	721.0
ES10	10.07	330.1
4-Chlorophenol	9.97	775.3
ES11	10.01	301.1
4-Hydroxybenzonitrile	10.07	845.3
ES12	10.09	372.2
Phenol	10.18	1081.7
ES14	10.10	354.3
P-Cresol	10.00	924.7

4.2.3. Method Validation

The method was validated using repeatability, reproducibility linearity, lower limit of detection (LLOD) and lower limit of quantification (LLOQ). Protocols set by The International Council for Harmonization of Technical Requirements for Pharmaceuticals for Human Use (ICH) in ICH Q2(R1) Validation of Analytical Procedures: Text and Methodology were used to validate the method (ICH, 2018).

4.2.3.1. Repeatability

Stock solutions were diluted with mobile phase to 20% of the original concentration, yielding approximately 2 mg / 100 mL for each of the compounds listed in Table 4.1. Each of the prepared solutions was injected 6 times and the peak areas (PA) recorded. The relative standard deviation (RSD) for the 6 determinations was calculated.

4.2.3.2. Reproducibility

Five separate solutions of approximately 2 mg / 100 mL were prepared from each of the standards in Table 4.1, as described above. Each of five solution were injected twice and the average PA recorded. The RSD was calculated for the 5 determinations.

4.2.3.3. Linearity

Solutions of each of the standards were diluted from their respective stock solutions to afford concentrations approximately 2, 4, 6, 8, 10 mg / 100 mL. Each sample was injected twice and the mean PA was recorded. Calibration curves were then drawn for each compound. The coefficient of determination (R^2) and regression equations were calculated to assess the relationship between PA and concentration.

4.2.3.3. LLOD and LLOQ

Standards of each compound were diluted in a systematic fashion, injecting each sample twice until the system could no longer detect a peak. Using the information gained from these dilutions the LLOD and LLOQ were determined. The LLOQ is defined as the lowest concentration

that gives rise to a peak that can be quantified with acceptable accuracy and precision. Whereas the LLOD is defined as the lowest detectable concentration.

4.2.4. General Protocol for Monitoring the Stability of Lead Phenolic TMZ Analogues after Exposure to Porcine Liver Esterase

A disodium phosphate, citric acid buffer (pH 6) was prepared by adding 63.15 mL of disodium phosphate ($Na_2HPO_4 \cdot 12H_2O$, 200 mM) to 36.85 mL of citric acid (100 mM). A stock solution of 80 mg of each of the TMZ esters (ES8, ES9, ES10, ES11, ES12, ES14) were prepared by dissolving in 100 mL of DMSO. Before preparing the esterase reactions, all reagents were incubated at 37°C. The control reaction, without enzyme, was prepared by adding 3000 µL of buffer to the reaction vessel along with 56.25 µL of the 80 mg /100 mL stock solution. The test reaction, with enzyme, was prepared by adding 2999 µL of buffer to the reaction vessel along with 56.25 µL of TMZ ester. The final concentration of TMZ esters in the reaction vessels was 1.47 mg / 100 mL. Porcine liver esterase (1 µL) was added to the test reaction at 0 min. Both the control and test reactions were then incubated at 37 °C. Aliquots of 200 µL were transferred from the reaction vessels to 1 mL Eppendorf tubes, at 3 min intervals for 30 min. To terminate the reaction, each Eppendorf contained 200 µL of acetonitrile. Eppendorf tubes were vortexed for 30 s before being subjected to centrifugation at 13,000 rpm for 10 min. The supernatant (200 µL) was transferred to HPLC vials and diluted with mobile phase (200 µL) before analysis.

4.3. Results and Discussion

4.3.1. Method Development

Standard HPLC analytical methods for the analysis of TMZ, use an acidified buffer to aid with the stability of the imidazotetrazine core (Gilant *et al.*, 2012; Khan *et al.*, 2016; Khosa *et al.*, 2018). The composition of the mobile phases used in HPLC methods developed for TMZ analysis, usually comprise of 80-95% aqueous solvent, (Reyderman *et al.*, 2004). Consequently, initial attempts to develop a HPLC method for the analysis of phenolic TMZ esters utilised an 80:20 mixture of sodium acetate buffer and acetonitrile (pH 4.5) (Kapcak and Satana-Kara, 2018). However, as TMZ esters exhibit increased hydrophobicity, elution times of TMZ esters using this method were found to be upwards of 40 min, which was not practical. As a result, the composition of the mobile phase was optimised in order to reduce elution times. By increasing the proportion of organic solvent to 40 %, resulting in elution times that ranged between 6 and 18 min for TMZ esters.

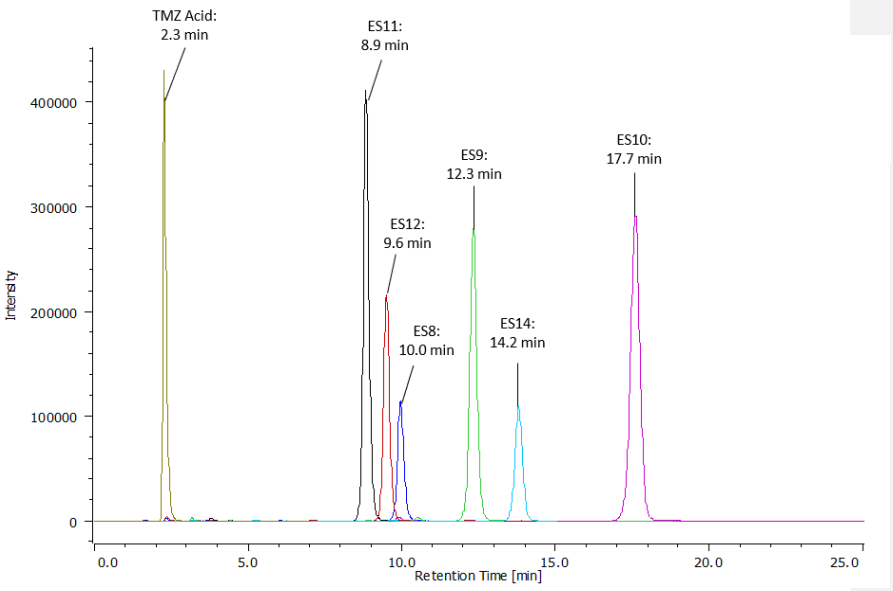

Figure 4.2: TMZ acid and ester analogues of TMZ (ES8, ES9, ES10, ES11, ES12, ES14) analysed using HPLC (sodium acetate buffer: MeCN 60:40, v/v, pH 4.5).

Table 4.2. reports the relative retention times of TMZ esters and their corresponding alcohols using the method outlined in Section 4.2.2. Retention times confirm acceptable resolutions between esters and their corresponding alcohols indicating that esters and corresponding alcohols can be readily quantified.

Table 4.2: Retention times of TMZ esters and their corresponding alcohols using the HPLC method outlined in section 4.2.4.

Analyte	Retention Time (min)
TMZ Acid	2.3
ES8	10.0
4-Methoxyphenol	6.0
ES9	12.3
4-Nitrophenol	10.4
ES10	17.7
4-Chlorophenol	14.8
ES11	8.9
4-Hydroxybenzonitrile	7.1
ES12	9.6
Phenol	7.2
ES14	14.2
***p*-Cresol**	9.8

4.3.2. Method Validation

To assess the precision of the analytical method, each analyte described in Table 4.1 was tested for repeatability at a concentration of approximately 2 mg / 100 mL. Full results are displayed in Appendix 4a. A summary of the RSD over 6 injections for each analyte is shown in Table 4.3. As

stated by the ICH (2018), if the RSD is calculated to be below 2%, the results from replicate analysis (n = 6) is acceptable. Results shown in Table 4.3. indicate that the method achieved suitable precision for each of the analytes in question, with calculated RSD less than 2 %.

Table 4.3: A summary of the repeatability results of TMZ esters and their corresponding alcohols. Each sample was analysed over 6 determinations. Data for each of the solutions was averaged and the standard deviation and RSD calculated.

Analyte (concentration µM)	Average PA ± SD (n = 6)	RSD (%, n = 6)
TMZ Acid (103 µM)	969551 ± 1427	0.15
ES8 (66 µM)	822203 ± 4874	0.59
4-Methoxyphenol (162 µM)	622902 ± 1056	0.17
ES9 (63 µM)	938538 ± 7072	0.75
4-Nitrophenol (144 µM)	1479936 ± 11571	0.78
ES10 (66 µM)	7924253 ± 1785	0.23
4-Chlorophenol (155 µM)	1319539 ± 13022	0.99
ES11 (68 µM)	888369 ± 5353	0.10
4-Hydroxybenzonitrile (196 µM)	2989778 ± 16199	0.54
ES12 (74 µM)	916108 ± 1311	0.14
Phenol (251 µM)	352648 ± 489	0.14
ES14 (71 µM)	713596 ± 9205	1.29
P-Cresol (185 µM)	865262 ± 13405	1.55

To assess the reproducibility of the method, six separate solutions of each of the analytes were prepared at approximately 2 mg / 100 mL. Each solution was injected twice and the average PA recorded. The standard deviation and RSD were calculated between each of the six samples. Complete results are displayed in Appendix 4b. A summary of the results for each analyte is

shown in Table 4.4. The RSD between each of the prepared six solutions was found to be less than 2 %.

Table 4.4: A summary of the reproducibility of TMZ esters and their corresponding alcohols. Six separate solutions, each injected twice and the average PA recorded. Data for each of the solutions was averaged and the standard deviation and RSD calculated.

Analyte (concentration µM)	Average PA ± SD (n = 6)	RSD (%, n = 6)
TMZ Acid (103 µM)	960779 ± 7081	0.74
ES8 (66 µM)	818994 ± 7225	0.88
4-Methoxyphenol (162 µM)	618674 ± 3518	0.57
ES9 (63 µM)	932685 ± 8704	0.93
4-Nitrophenol (144 µM)	1476042 ± 10895	0.74
ES10 (66 µM)	792449 ± 4402	0.56
4-Chlorophenol (155 µM)	1320243 ± 9102	0.69
ES11 (68 µM)	885105 ± 10545	1.19
4-Hydroxybenzonitrile (196 µM)	2990155 ± 16916	0.57
ES12 (74 µM)	957062 ± 15013	1.57
Phenol (251 µM)	369266 ± 5635	1.53
ES14 (71 µM)	715080 ± 11354	1.59
P-Cresol (185 µM)	866773 ± 13556	1.56

In order to confirm that the method gave a response that was directly proportional to the concentration of the analyte in question, linearity determinations were carried out. In Table 4.5, a summary of the regression equations for each analyte is included along with the coefficient of determination (R^2). An R^2 value of 1 indicates perfect positive linear relationship between response and analyte concentration. All analytes assessed exhibited R^2 values above 0.9975, indicating an excellent relationship between response and analyte concentration. Graphical

representations of the relationship between response and analyte concentration are shown in Appendix 4c.

Table 4.5: Summary of regression analysis from linearity investigations of each analyte.

Analyte	Regression Equation	Coefficient of Determination (R^2)
TMZ Acid	Y = 9549x	0.9993
ES8	Y = 12464x	0.9996
4-Methoxyphenol	Y = 3842x	0.9996
ES9	Y = 14840x	0.9999
4-Nitrophenol	Y = 10124x	0.9991
ES10	Y = 12360x	0.9999
4-Chlorophenol	Y = 8282x	0.9990
ES11	Y = 13179x	1.0000
4-Hydroxybenzonitrile	Y = 17653x	1.0000
ES12	Y = 12488x	0.9998
Phenol	Y = 1651x	0.9992
ES14	Y = 5534x	0.9975
P-Cresol	Y = 11115x	0.9989

In order to determine the LLOQ and LLOD of the analytical method, stock solutions of each analyte were diluted and injected sequentially. Figure 4.3 shows an example of this process using ES8 and TMZ acid as examples. Please refer to Table 4.2. for relative retention times of analytes. This process was repeated for each analyte and the chromatograms are reported in Appendix 4d. Using Figure 4.3, injection A, a solution containing TMZ acid (320 nM) and ES8 (207 nM), was determined to be the LLOQ, generating quantifiable peaks. Injection C, a solution containing

TMZ acid and ES8 at concentrations of 80 nM and 52 nM, was determined to be the LLOD. A summary of the LLOQ and LLOD for each analyte is shown in table 4.6.

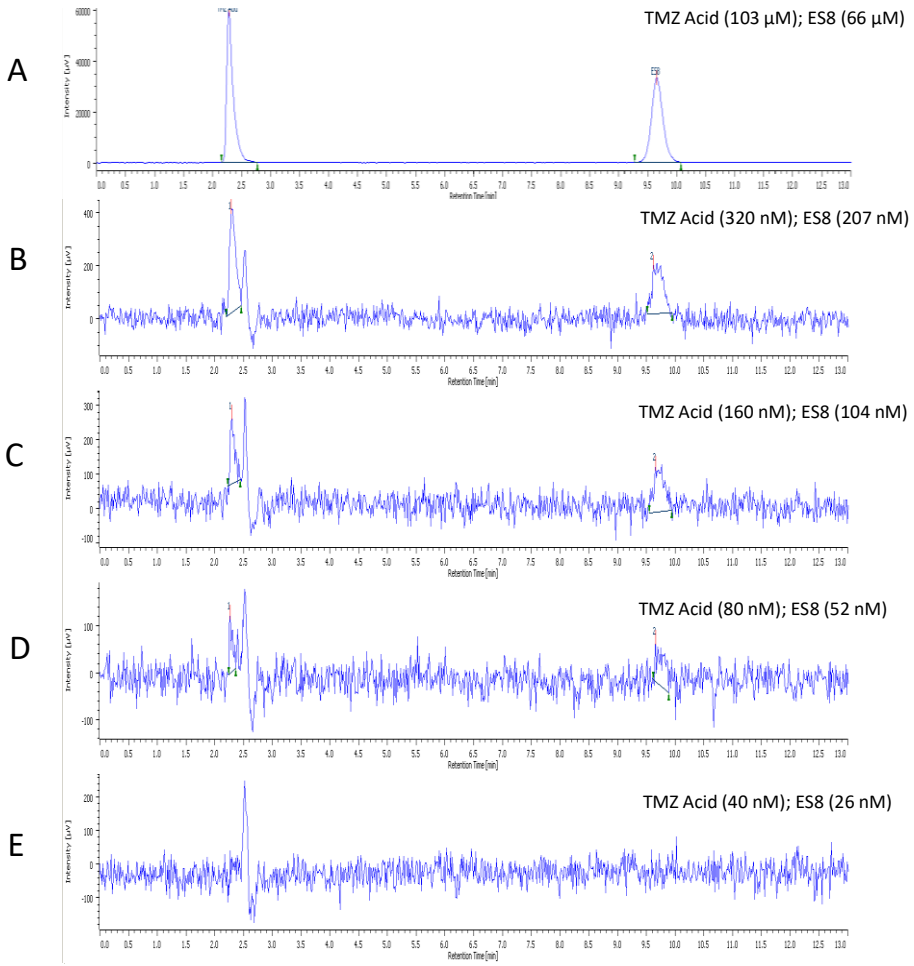

Figure 4.3: An example of how the LLOQ and LLOD were determined. Injection B, (320 nM and 207 nM of TMZ acid (2.25 min) and ES8 (9.75 min), respectively), was estimated to be the LLOQ for both TMZ acid and ES8. Injection D, (80 nM and 52 nM of TMZ acid and ES8, respectively), was judged to be the LLOD. Analysis at 325 nm.

Table 4.6: Summary of the LLOD and LLOQ for each analyte.

Analyte	LLOQ (nM)	LLOD (nM)
TMZ Acid	320	80
ES8	207	52
4-Methoxyphenol	1010	505
ES9	198	99
4-Nitrophenol	451	113
ES10	206	103
4-Chlorophenol	969	485
ES11	133	67
4-Hydroxybenzonitrile	83	21
ES12	145	36
Phenol	490	122
ES14	221	111
P-Cresol	1156	577

The observed acceptable robustness and linear response of the analytical method described in Section 4.2.3 clearly indicated its suitability for monitoring the hydrolysis of the lead TMZ ester by PLE. The sensitivity of the method for imidazotetrazine analytes was acceptable at pH 4.5 with no visible trace of chemical hydrolysis of the imidazotetrazine core. The formation of TMZ acid and the corresponding alcohol; alongside the simultaneous disappearance of the TMZ ester was a logical approach to monitor hydrolytic activity.

4.3.3. Hydrolysis of TMZ esters when subject to porcine liver esterase

The rate of hydrolysis for each of the phenolic TMZ esters, ES8, ES9, ES10, ES11, ES12 and ES14 when treated with PLE, was determined as per the analytical method outlined in Section 4.2.4. As stated in Section 4.2.4, PLE reactions were terminated by quenching with acetonitrile which deactivates the enzyme. In the case of the present investigation, the use of acetonitrile as the quenching reagent, afforded recoveries of the un-hydrolysed TMZ esters in the region of 86 to 98 %. TMZ ester recovery was calculated by expressing the observed concentration of ester in the control reactions as a percentage of the determined ester concentration. In order to ensure degradation of the esters was specific to ester hydrolysis and not hydrolysis of the imidazotetrazine core, reactions were carried out at pH 6. The validation of the analytical method also involved investigating the stability of the imidazotetrazine ring whilst ensuring PLE retained a significant level of activity. These findings were in keeping with work published by Junge and Heymann (1979), who found PLE to have a broad pH optima (pH 6-8).

An example of a typical enzyme reaction profile is shown in Figure 4.4; depicting the gradual hydrolysis of ES11, after exposure to PLE, in addition to the production of TMZ acid and 4-hydroxybenzonitrile. After establishing that the ester was breaking down into its corresponding TMZ acid and alcohol, each analyte was readily quantified. Figure 4.5 shows the quantified hydrolysis of ES11 into an approximately equal concentration of the corresponding acid and alcohol.

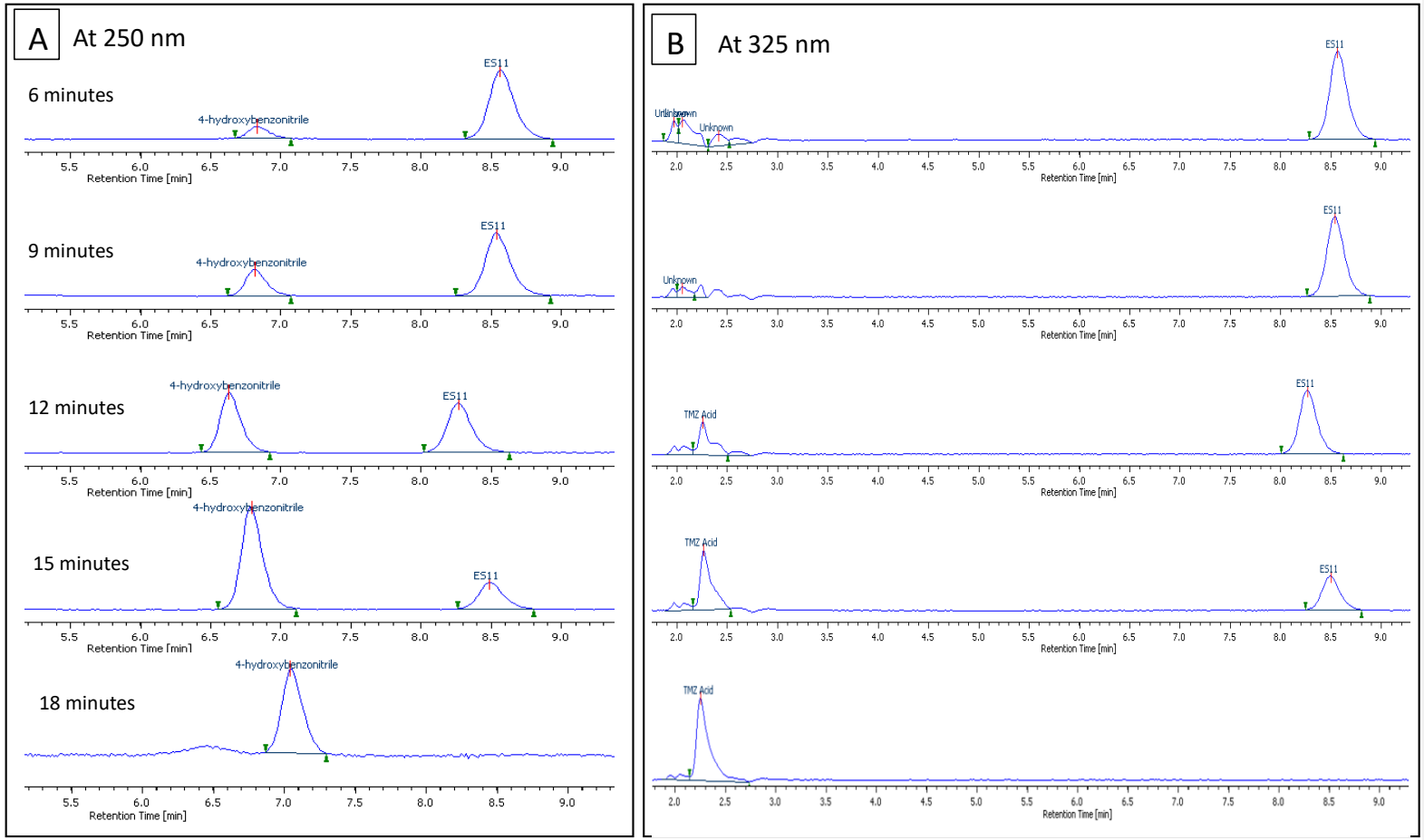

Figure 4.4: A series of chromatograms showing degradation of ES11 into its corresponding TMZ acid and 4-hydroxybenzonitrile. Each series of chromatograms shows a different wavelength, allowing all analytes to be visualised. ***A:*** *Breakdown of ES11 and the formation of 4-hydroxybenzonitrile (250 nm).* ***B****: Breakdown of ES11 and the formation of TMZ acid (325 nm).*

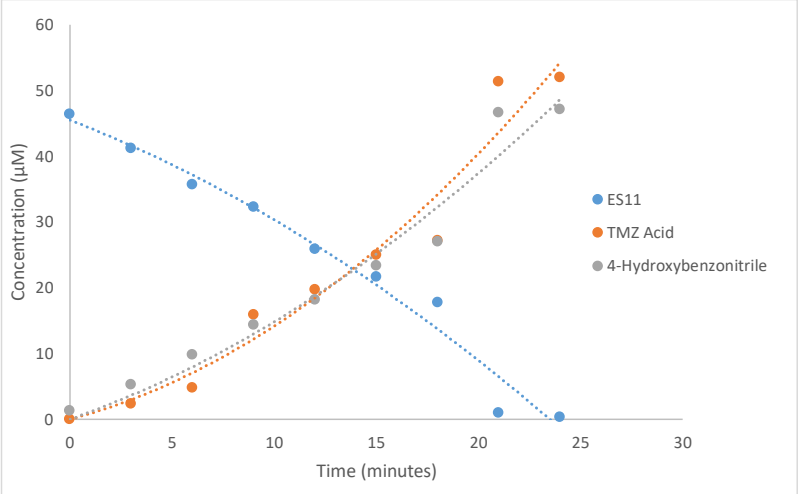

Figure 4.5: Hydrolysis of TMZ ester (ES11) into the corresponding TMZ acid and 4-hydroxybenzonitrile over time. ES11 and TMZ acid (325 nm); 4-hydroxybenzonitrile (250 nm)

It is evident from Figure 4.5. that a slightly higher concentration of the acid and alcohol was produced, compared to the starting concentration of ES11, a phenomenon that was observed consistently across each of the esters tested. This discrepancy is likely accounted for by the recovery rates of the various esters (86-98%), as previously mentioned, or ester hydrolysis occurring during the preparation of the time t = 0 min sample. Another possible explanation is interference from other reaction components with the TMZ acid peak, as evidenced in Figure 4.4. As these smaller peaks cause overlap, the true concentration of TMZ acid cannot be accurately quantified and is likely overestimated (by the software), explaining the discrepancy observed. Graphs similar to Figure 4.5. were constructed for the hydrolysis of each TMZ ester and the time taken to hydrolyse 50% is recorded in Table 4.7.

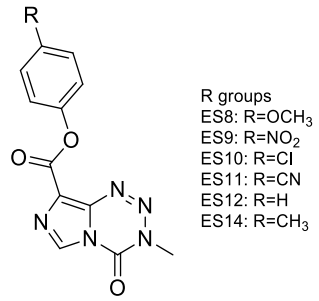

Figure 4.6: Structures of phenolic TMZ esters assessed for esterase mediated stability.

Table 4.7: The time taken for PLE to hydrolyse 50 % of phenolic TMZ esters.

TMZ Ester	**Time taken to hydrolyse 50 % of the ester (min)**
ES8	7.3
ES9	4.2
ES10	4.1
ES11	13.7
ES12	3.4
ES14	3.2

Results depicted in Table 4.7 indicate that 50 % of each of the TMZ esters was hydrolysed by PLE in the first 14 min of exposure. In fact, 50 % of TMZ esters containing *para*- nitro, chloro, phenyl and tolyl groups (ES9, ES10, ES12 and ES14), were hydrolysed within the first 4.2 min of PLE exposure (Table 4.7; Figure 4.6). TMZ esters containing *para*- methoxy and nitrile groups (ES8 and ES11) conferred increased stability, with 50 % hydrolysis being achieved in 7.3 and 13.7 min, respectively. The phenolic TMZ esters analysed displayed rapid hydrolysis upon exposure to PLE.

In the present experiments, a concentration of 7.85 µg / mL of PLE was used. In comparison, work by Höllerer *et al.* (2018), observed 21 % di-(2-ethylhexyl)phthalate hydrolysis after 48 h of exposure to 1.3 µg / mL of PLE. Similarly, (Shervington *et al.*, 2009) reports 24-37 % hydrolysis of various chlorambucil esters over a 24 h period, after exposure to 9.1 µg / mL PLE. Evidence from these two studies suggest a marked fragility of the ester bonds within the phenolic TMZ esters described in the present study. It is thought that this fragility could have a negative impact on the purposed therapeutic potential of these analogues.

When considering the *para*- substituted aromatic substituents of TMZ esters, it would be expected that strong electron withdrawing groups would confer a faster rate of hydrolysis (Figure 4.6). Despite ES9 and ES11 containing nitro and nitrile aromatic substituents, respectively, which share similar electron withdrawing properties, they displayed unexpectedly different rates of hydrolysis. The time taken for 50 % hydrolysis to be achieved for ES11 (*para*-nitrile) was 13.7 min, compared with 4.2 min for ES9 (*para*-nitro). This significant difference in rate brings the results obtained from this study into question. Similarly, ES10, ES12 and ES14 do not fit the expected trend in terms of electron withdrawing and donating effects of substituents. It is well documented that in ester hydrolysis of ethyl benzoates, the rate of hydrolysis is directly proportional to the electronic effects of the substituents on the aromatic ring, an effect that should be mirrored in the present investigation (Clayden, 2012). As a result, the unexpected findings from the present investigations, involving the hydrolysis of the phenolic TMZ esters, needs further work. On evaluation, as the time intervals between samples were relatively short, reaction vessels were removed from the incubator regularly, in order to remove 200 µL aliquots of the reaction mixture. This may have caused reaction temperatures to be inconsistent, which in-turn may have impaired enzyme function. This operation required the operator to carry out the aliquoting, efficiently and consistently, throughout each stage of the analysis. It is therefore conceivable that results may have been skewed as a direct consequence of the varying temperature, which may explain the unexpected findings of the present investigations. Due to time constraints of the present PhD programme, sufficient repeats of the analysis could not be

carried out. This aspect of the work is currently being optimised by representatives of the Shervington research group, with the intention of achieving more conclusive results.

4.4. Conclusion

The present chapter investigated the stability of the most promising analogues, identified in Chapter 3, when exposed to PLE. The phenolic TMZ esters, ES8, ES9, ES10, ES11, ES12 and ES14, were found to be highly susceptible to hydrolysis by PLE, with all esters being 50% hydrolysed within 3-14 min of exposure. As a result, it is hypothesised that the potential therapeutic benefit of these analogues may not translate to an *in-vivo* model without careful consideration of drug delivery strategies. However, it was expected that there would be a strong correlation between the electron withdrawing / donating properties of the aromatic substituents and the hydrolytic rates of reaction. Consequently, these experiments are to be repeated by the research group, applying an optimised procedure, which will involve the use of a number of reaction bottles. A bottle will be removed at given time intervals before being processed and analysed systematically, thus, eliminating possible fluctuations in temperature. This should enable the achievement of more reliable data consistent with knowledge of the electronic effects of the aromatic esters in question.

CHAPTER 5:

GENERAL DISCUSSION AND FUTURE WORK

As described in Chapter 1, TMZ, the standard chemotherapeutic agent prescribed to GBM patients, has a limited therapeutic benefit, increasing median survival by a modest 2.1 months (Stupp *et al.*, 2005; Chamberlain, 2010). *In-vitro* investigations conducted by Sankar *et al.* (1999) found TMZ to be ineffective against a number of primary cells at clinically significant concentrations, perhaps explaining the limited therapeutic benefit gained by GBM patients. Additionally, MGMT-mediated resistance also plays a pivotal role in patient response to TMZ, as discussed in Chapter 1. It was therefore the aim of the present work to synthesise novel analogues of TMZ, with a view to achieving analogues with increased potency.

Following a comprehensive review of the literature, position 8 on the imidazole ring of TMZ was identified as the most promising position to modify in order to yield analogues with increased potency (Suppasansatorn *et al.*, 2006; Liu *et al.*, 2010; Marin-Ramos *et al.*, 2018; Svec *et al.*, 2018; Yang *et al.*, 2019). The rational design of analogues was based on three main concepts. Firstly, a series of ester and amide TMZ analogues were synthesised to assess the impact of HBD and HBA sites at position 8, provided by ester and amide groups. Secondly, the inclusion of phenyl esters and amides, with various aromatic substituents, would provide an insight into the mesomeric and inductive effects of these analogues. Thirdly, the addition of alkyl chains to ester moieties in order to assess the effect of increasing the lipophilicity of TMZ analogues. A rationale for the modification to the TMZ chemical structure is included in Section 2.2.

The target esters and amides were readily synthesised utilising TMZ acyl chloride and EDC.HCl / DMAP coupling. Amide TMZ analogues were readily synthesised in acceptable yields via TMZ acyl chloride intermediate followed by reactions with various amines. This route is also suitable for the synthesis of ES1-ES7 ester analogues, following a reaction between TMZ acyl chloride and appropriate alcohols. However, reactions between phenyl alcohols and TMZ acyl chloride proved problematic due to steric effects. The use of dehydrating coupling agents such as DCC and EDC.HCl, allowed the direct coupling of TMZ acid to appropriate alcohols, yielding ester analogues ES8-ES14. However, the synthesis of analogues using DCC / DMAP coupling, produced

DCU as a by-product, which proved challenging to remove, resulting in a significant loss of the target analogues during purification. The use of EDC.HCl, in place of DCC, improved yields due to the generation of EDU, a water soluble by-product, that was removed by a simple aqueous work up. It was concluded that the use of EDC.HCl / DMAP coupling improved the method of synthesis for analogues ES8-ES14, resulting in improved yields.

Upon the successful synthesis and characterisation of ester and amide TMZ analogues, the activity of each analogue was determined against specified cell lines and primary cultures. The full results are presented in Chapter 3. Unfortunately, many of the amides synthesised as part of the present study were found to be insoluble in medium, prompting their elimination from the study, thus, allowing analogues with preferential solubility to be focused upon. The most prominent finding from antiproliferative determination of TMZ analogues, was the exceptional *in-vitro* potency of phenolic TMZ esters, ES8, ES9, ES10, ES11, ES12 and ES14. During initial determination using various cell lines, the phenolic TMZ esters were found to exhibit activity up to 5-fold greater than TMZ, against specified glioma cell lines. Following this success, the activity of lead phenolic TMZ esters was probed further, using primary GBM cultures. The lead analogues were assessed against MGMT negative and MGMT positive primary cells. In the primary culture devoid of MGMT, TMZ only has a slight effect on the viability of cells at concentrations that may be clinically obtainable (15-75 µM) (Figure 5.1). The observed lack of efficacy could explain why TMZ only has negligible impact on patient survival rates (Stupp *et al.*, 2005; Chamberlain, 2010). In contrast, the phenolic TMZ esters, containing highly polarising aromatic substituents, were found to induce a reduction in viability >50%, at clinically obtainable concentrations of TMZ (15-75 µM) (Figure 5.1). The dramatic improvement in activity as a result of these analogues could translate to improved health care of patients, ultimately resulting in greater survival rates and quality of life. The primary culture, BTNW974, was derived from a female patient whose survival was 10 months, following resection. As TMZ did not elicit a significant reduction in viability at clinically relevant concentrations in these cells, it is unlikely that a therapeutic benefit was gained by this patient as a result of TMZ treatment. However, as phenolic ester analogues of

TMZ appeared to reduce viability at clinically relevant concentrations of TMZ, it is possible that this patient may have gained some benefit if treated with these analogues, providing all other physiological parameters for these TMZ esters is favourable.

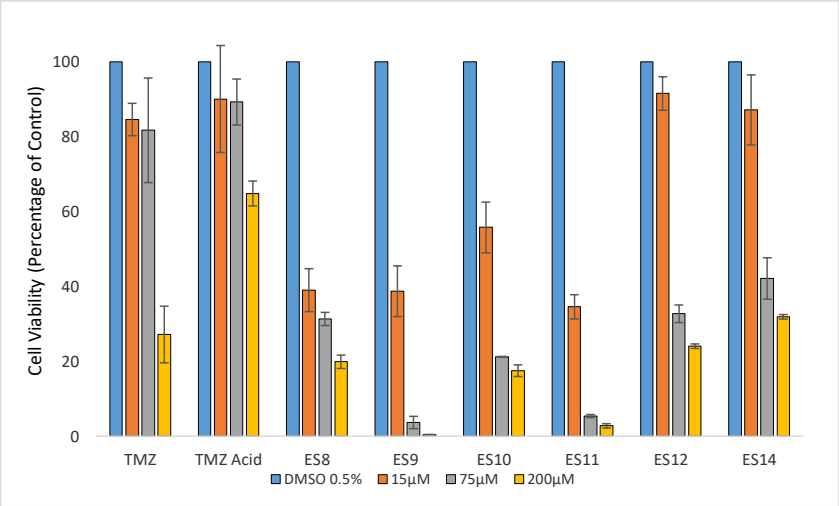

Figure 5.1: Cell Viability of BTNW914 (MGMT -) after treatment by TMZ and phenyl TMZ ester analogues at various clinically relevant concentrations. Values reported are IC_{50} ± SD, n=3.

As expected, primary cultures expressing high levels of MGMT, exhibited resistance to TMZ (Figure 5.2). Interestingly, lead phenolic TMZ esters were able to reduce the viability of MGMT expressing cells. This suggests that either analogues may cause a greater influx of methyldiazonium ions within the cell and subsequent DNA methylation which could overwhelm repair pathways or possibly a mechanism of action distinct from methylation. It should be noted that the phenolic TMZ esters were less potent against MGMT-expressing primary cells, compared to MGMT-devoid primary cells. However, a significant decrease in viability was observed once these cells were treated with 75 µM of the phenolic TMZ esters (Figure 5.2).

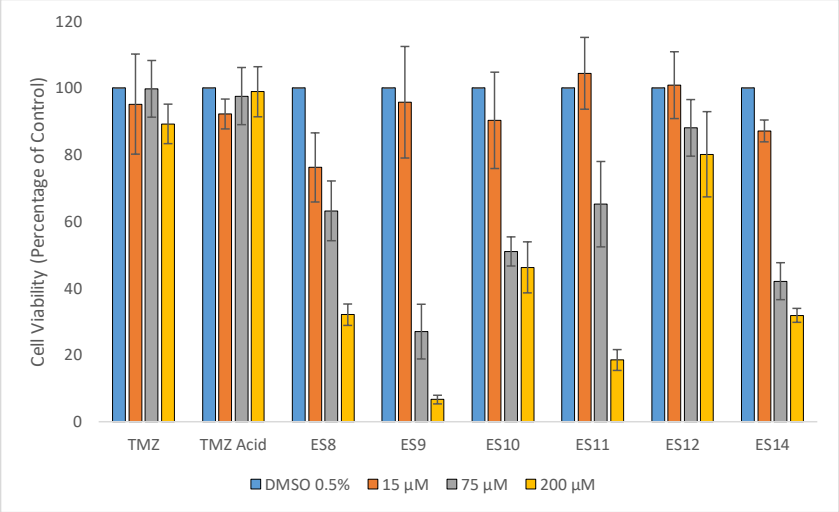

Figure 5.2: Cell Viability of BTNW374 (MGMT +) after treatment by TMZ and phenyl TMZ ester analogues at various clinically relevant concentrations. Values reported are IC_{50} ± SD, n=3.

Interestingly, both Svec *et al.* (2018) and Yang *et al.* (2019) have reported C8-subsituted analogues of TMZ, containing phenyl and imidazole moieties, respectively. These groups were directly attached to position 8 of the imidazole ring of the lead compounds from these studies. Each of these studies reports a marked increase in activity of respective title analogues. Lead analogues of the present study contain phenyl groups similar to that of analogues described by Svec *et al.* (2018). Phenyl groups attached to position 8 on the imidazole ring, directly or via an ester bond, present a marked increased activity irrespective of MGMT expression (Svec *et al.*, 2018). This evidence further supports the notion that the attachment of phenyl groups to this position has the potential to yield analogues of TMZ that elicit a greater therapeutic benefit to GBM patients.

Up until recently, the implications of modifying position 8 of imidazotetrazines was unclear. However, in light of recent findings, reported in studies conducted by Svec *et al.* (2018) and Yang *et al.* (2019), have indicated that modifications at this position have the potential of influencing

the rate of prodrug activation. However, the optimum rate of imidazotetrazine prodrug activation is still unknown. Nevertheless, as part of future work, the rate of prodrug activation should be assessed for the lead phenyl TMZ analogues, in order to assess whether or not the aromatic substituents have the ability to influence the rate at which the analogues degrade to methyl diazonium ions.

The activity of lead phenolic esters ES8, ES9, ES10, ES11, ES12 and ES14, against MGMT positive cells, suggests a mechanism of action distinct from methylation. Each phenol is known to be responsible for a series of complex radical scavenging, antioxidising, and prooxidising effects, all of which can initiate cellular apoptosis (Ferluga *et al.*, 1972; Elia *et al.*, 1994; Chen *et al.*, 2004; Selassie *et al.*, 2005; Kadoma *et al.*, 2010). Providing the phenolic TMZ esters **55**, or one of the imidazole degradation products **56**, retain the characteristics of the corresponding alcohols; it is conceivable that disruptions in the cellular balance between ROS generation and antioxidant generation could contribute to the antiproliferative effects observed in Figure 5.2. In addition to hydrolytic degradation, possibly producing a phenyl ester imidazole **56**; the TMZ phenyl ester **55** could readily degrade to TMZ acid and the corresponding phenyl alcohol **57,** in the presence of esterases. Esterases are known to be present in GBM although they are generally found at lower concentrations in the brain compared with the rest of the body (Fabiani *et al.*, 1970; Sanchez-Diaz *et al.*, 2017). The presence of phenyl ester imidazoles **56** is therefore less likley due to hydrolysis of ester bonds. It is more plausible that phenyl alcohols, degraded from the parent drug, could possibly contribute to the reduction in viability of MGMT expressing cells. However, it should be noted that the literature indicates that phenols do tend to be relatively well tolerated by cell lines *in-vitro*. In primary rat hepatocytes, 4-Nitrophenol has been found not to cause DNA damage at concentrations less than 700 µM (Elia *et al.*, 1994). Similarly, 4-chlorophenol has been shown to initiate apoptosis at relatively high concentrations of approximately 2 mM in mouse fibroblast cells (Chen *et al.*, 2004). Since phenols tend to induce cytotoxic events at relatively high concentrations, it is unlikely that the cleaved alcohols are

responsible for the antiproliferative effects observed in the present study. Consequently, it would be appropriate to investigate the antiproliferative effects of the phenols, used to prepare the six lead TMZ esters, in order to confirm whether or not they contribute to activity.

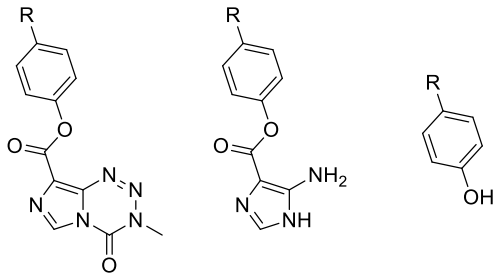

55 **56** **57**

*Figure 5.3: Structures produced by esterase mediated and pH mediated degradation of TMZ phenyl esters that could be responsible for disruptions in the cellular balance between ROS generation and antioxidant generation, resulting in activity. TMZ phenyl ester (**55**); Imidazole phenyl ester produced during pH mediated prodrug activation (**56**); Phenyl alcohols produced during esterase mediated degradation (**57**).*

Similarly, the TMZ acid has been consistently shown throughout antiproliferative determination studies to not be responsible for the increase in cytotoxicity, see data presented in Figure 5.1, 5.2. However, it is unclear whether this is due to poor cellular membrane penetration, due to its polar nature. It is also plausible that the esters could act as vehicles for delivering TMZ acid into the cell. However, this does not explain the activity against MGMT positive cells or the variable activity between various esters. Therefore, it is the authors view that the increased cytotoxicity observed with the phenolic TMZ esters is possibly caused by a synergistic effect involving multiple mechanisms from compounds **55** or **57** (Figure 5.3). However, due to the novelty of the work, there is limited evidence to support this hypothesis, until mechanistic studies are carried out.

Chapter 4 details the stability of lead TMZ analogues when subjected to esterase enzymes. Although these investigations are preliminary and need to be repeated, the results suggest a

marked fragility of the ester bonds in the lead analogues. In fact, 50% of the esters were hydrolysed by esterase enzymes within the first 3-14 min of exposure. The maximum intracranial concentration of TMZ is reported to be approximately 2 ± 0.8 h (Portnow *et al.*, 2009). As a result, it is unlikely that the lead TMZ esters, that are highlighted in Chapter 3, would in fact reach the site of a brain tumour intact. It is therefore probable that TMZ esters would be hydrolysed into TMZ acid and the corresponding alcohol and the increased activity observed *in-vitro* would be lost. Despite the obvious challenges the ester bonds pose, the exceptional *in-vitro* activity displayed, irrespective of MGMT expression, by lead analogues (**ES8**, **ES9**, **ES10**, **ES11**, **ES12** and **ES14**) should be investigated further. Future work involving *in-vivo* models should take into account the fragility of ester bonds, by incorporating a strategic delivery of analogues to the tumour site, in order to ensure the analogues are delivered to the tumour site intact. Such delivery options could possibly involve PEGylated liposomes, which have recently been shown to increase the uptake of TMZ to the brain by 4-fold, compared to a free drug solution (Vanza *et al.*, 2018). Similarly, Kumari *et al.* (2017) reported significant success with lactoferrin nanoparticles, which again could present a viable option for the lead TMZ esters described in the present study.

The evidence collected as part of the present study suggests that lead phenolic TMZ esters have potential to induce greater therapeutic effects in patients, which could contribute to greater survival rates compared to treatment with TMZ. The data collected also suggest that the lead analogues could elicit a therapeutic benefit in patients that present TMZ resistant GBM, as a result of MGMT expression. The results presented in this study are supported by the activity observed in similar phenyl containing TMZ analogues reported by Svec *et al.* (2018). Immediate future work should involve assessing whether the intact phenyl esters of TMZ are the active compounds or whether it is the hydrolysed carboxylate or phenyl alcohol that generate the cytotoxic effect. As stated in Chapter 4, the esterase mediated hydrolysis of the lead phenolic is to be repeated, using the improved method, thus yielding a more conclusive outcome. The

biodistribution of the lead compounds should also be assessed in an *in-vivo* model. This information should help improve our understanding of whether a strategic drug delivery system such as nanoparticles, encapsulating the esters, would be needed to maximise efficacy of lead analogues in an *in-vivo* model. In summary, it is plausible that the lead TMZ analogues, described as part of this chapter, have the potential to replace TMZ as a more effective treatment of GBM. However, as this work is very much in its infancy, a considerable amount of additional work will need to be undertaken in order to confirm the envisaged therapeutic benefit of the phenyl TMZ analogues (Figure 5.4).

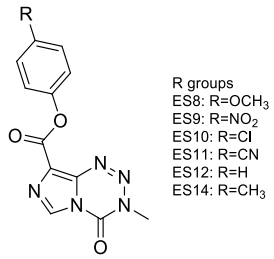

Figure 5.4: Structures of lead phenolic TMZ esters.

REFERENCES

Agarwala, S. S. and Kirkwood, J. M. (2000) 'Temozolomide, a novel alkylating agent with activity in the central nervous system, may improve the treatment of advanced metastatic melanoma', *Oncologist,* 5(2), pp. 144-51.

Agnihotri, S., Gajadhar, A. S., Ternamian, C., Gorlia, T., Diefes, K. L., Mischel, P. S., Kelly, J., McGown, G., Thorncroft, M., Carlson, B. L., Sarkaria, J. N., Margison, G. P., Aldape, K., Hawkins, C., Hegi, M. and Guha, A. (2012) 'Alkylpurine-DNA-N-glycosylase confers resistance to temozolomide in xenograft models of glioblastoma multiforme and is associated with poor survival in patients (vol 122, pg 253, 2012)', *Journal of Clinical Investigation,* 122(2), pp. 782-782.

Allen, M., Bjerke, M., Edlund, H., Nelander, S. and Westermark, B. (2016) 'Origin of the U87MG glioma cell line: Good news and bad news', *Sci Transl Med,* 8(354), pp. 354re3.

Aoki, T., Nishikawa, R., Mizutani, T., Nojima, K., Mishima, K., Adachi, J. and Matsutani, M. (2007) 'Pharmacokinetic study of temozolomide on a daily-for-5-days schedule in Japanese patients with relapsed malignant gliomas: first study in Asians', *Int J Clin Oncol,* 12(5), pp. 341-9.

Argente-Arizon, P., Guerra-Cantera, S., Garcia-Segura, L. M., Argente, J. and Chowen, J. A. (2017) 'Glial cells and energy balance', *J Mol Endocrinol,* 58(1), pp. R59-R71.

Arnoldussen, Y. J., Ervik, T. K., Berlinger, B., Kero, I., Shaposhnikov, S. and Zienolddiny, S. (2018) 'Cellular responses of human astrocytoma cells to dust from the Acheson process: An in vitro study', *NeuroToxicology,* 65, pp. 241-247.

Arora, R. S., Alston, R. D., Eden, T. O., Estlin, E. J., Moran, A. and Birch, J. M. (2009) 'Age-incidence patterns of primary CNS tumors in children, adolescents, and adults in England', *Neuro Oncol,* 11(4), pp. 403-13.

Arrowsmith, J., Jennings, S. A., Clark, A. S. and Stevens, M. F. (2002) 'Antitumor imidazotetrazines. 41. Conjugation of the antitumor agents mitozolomide and temozolomide to peptides and lexitropsins bearing DNA major and minor groove-binding structural motifs', *J Med Chem,* 45(25), pp. 5458-70.

Arrowsmith, J., Missailidis, S. and Stevens, M. F. (1999) 'Antitumour imidazotetrazines. Part 37. Conjugation of the DNA major-groove alkylating imidazotetrazine mitozolomide to peptide motifs recognizing the minor groove', *Anticancer Drug Des,* 14(3), pp. 205-17.

Aslantürk, O. S. (2018) 'In Vitro Cytotoxicity and Cell Viability Assays: Principles, Advantages, and Disadvantages', in Larramendy, M. (ed.) *Genotoxicity: A Predictable Risk to Our Actual World*. London IntechOpen.

Backes, C., Harz, C., Fischer, U., Schmitt, J., Ludwig, N., Petersen, B.-S., Mueller, S. C., Kim, Y.-J., Wolf, N. M., Katus, H. A., Meder, B., Furtwängler, R., Franke, A., Bohle, R., Henn, W., Graf, N., Keller, A. and Meese, E. (2014) 'New insights into the genetics of glioblastoma multiforme by familial exome sequencing', *Oncotarget,* 6(8), pp. 5918-5931.

Bady, P., Diserens, A.-C., Castella, V., Kalt, S., Heinimann, K., Hamou, M.-F., Delorenzi, M. and Hegi, M. E. (2012) 'DNA fingerprinting of glioma cell lines and considerations on similarity measurements', *Neuro-Oncology,* 14(6), pp. 701-711.

Barani, I. J. and Larson, D. A. (2015) 'Radiation therapy of glioblastoma', *Cancer Treat Res,* 163, pp. 49-73.

Barraja, P., Diana, P., Lauria, A., Montalbano, A., Almerico, A. M., Dattolo, G. and Cirrincione, G. (2004) 'Synthesis and antiproliferative activity of [1,2,4]triazino [4,3-a] indoles', *Anticancer Res,* 24(6), pp. 3775-9.

Bocangel, D. B., Finkelstein, S., Schold, S. C., Bhakat, K. K., Mitra, S. and Kokkinakis, D. M. (2002) 'Multifaceted resistance of gliomas to temozolomide', *Clin Cancer Res,* 8(8), pp. 2725-34.

Bondy, M. L., Scheurer, M. E., Malmer, B., Barnholtz-Sloan, J. S., Davis, F. G., Il'yasova, D., Kruchko, C., McCarthy, B. J., Rajaraman, P., Schwartzbaum, J. A., Sadetzki, S., Schlehofer, B., Tihan, T., Wiemels, J. L., Wrensch, M., Buffler, P. A. and Brain Tumor Epidemiology, C. (2008) 'Brain tumor epidemiology: consensus from the Brain Tumor Epidemiology Consortium', *Cancer,* 113(7 Suppl), pp. 1953-1968.

Brüsehaber, E., Böttcher, D. and Bornscheuer, U. T. (2009) 'Insights into the physiological role of pig liver esterase: Isoenzymes show differences in the demethylation of prenylated proteins', *Bioorganic & Medicinal Chemistry,* 17(23), pp. 7878-7883.

Chamberlain, M. C. (2010) 'Temozolomide: therapeutic limitations in the treatment of adult high-grade gliomas', *Expert Rev Neurother,* 10(10), pp. 1537-44.

Chen, J., Jiang, J., Zhang, F., Yu, H. and Zhang, J. (2004) 'Cytotoxic effects of environmentally relevant chlorophenols on L929 cells and their mechanisms', *Cell Biol Toxicol,* 20(3), pp. 183-96.

Chen, T. C., Cho, H. Y., Wang, W., Nguyen, J., Jhaveri, N., Rosenstein-Sisson, R., Hofman, F. M. and Schonthal, A. H. (2015) 'A novel temozolomide analog, NEO212, with enhanced activity against MGMT-positive melanoma in vitro and in vivo', *Cancer Lett,* 358(2), pp. 144-151.

Cheng, C. C., Elslager, E. F., Werbel, L. M., Priebe, S. R. and Leopold, W. R., 3rd (1986) 'Pyrazole derivatives. 5. Synthesis and antineoplastic activity of 3-(2-chloroethyl)-3,4-dihydro-4-oxopyrazolo[5,1-d]-1,2,3, 5-tetrazine-8-carboxamide and related compounds', *J Med Chem,* 29(8), pp. 1544-7.

Cho, H. Y., Wang, W., Jhaveri, N., Lee, D. J., Sharma, N., Dubeau, L., Schonthal, A. H., Hofman, F. M. and Chen, T. C. (2014) 'NEO212, temozolomide conjugated to perillyl alcohol, is a novel drug for effective treatment of a broad range of temozolomide-resistant gliomas', *Mol Cancer Ther,* 13(8), pp. 2004-17.

Choi, B. D. and Curry, W. T. (2017) 'IDH mutational status and the immune system in gliomas: a tale of two tumors?', *Translational cancer research,* 6(Suppl 7), pp. S1253-S1256.

Clark, D. E. (2003) 'In silico prediction of blood–brain barrier permeation', *Drug Discovery Today,* 8(20), pp. 927-933.

Clayden, J. (2012) *Organic chemistry.* 2nd ed. / Jonathan Clayden, Nick Greeves, Stuart Warren. edn. Oxford: Oxford University Press.

Cobbs, C., Khan, S., Matlaf, L., McAllister, S., Zider, A., Yount, G., Rahlin, K., Harkins, L., Bezrookove, V., Singer, E. and Soroceanu, L. (2014) 'HCMV glycoprotein B is expressed in primary glioblastomas and enhances growth and invasiveness via PDGFR-alpha activation', *Oncotarget,* 5(4), pp. 1091-100.

Combs, S. E., Rieken, S., Wick, W., Abdollahi, A., von Deimling, A., Debus, J. and Hartmann, C. (2011) 'Prognostic significance of IDH-1 and MGMT in patients with glioblastoma: one step forward, and one step back?', *Radiation oncology (London, England),* 6, pp. 115-115.

Crouch, S. P., Kozlowski, R., Slater, K. J. and Fletcher, J. (1993) 'The use of ATP bioluminescence as a measure of cell proliferation and cytotoxicity', *J Immunol Methods,* 160(1), pp. 81-8.

Davis, M. E. (2016) 'Glioblastoma: Overview of Disease and Treatment', *Clin J Oncol Nurs,* 20(5 Suppl), pp. S2-8.

Denny, B. J., Wheelhouse, R. T., Stevens, M. F., Tsang, L. L. and Slack, J. A. (1994) 'NMR and molecular modeling investigation of the mechanism of activation of the antitumor drug temozolomide and its interaction with DNA', *Biochemistry,* 33(31), pp. 9045-51.

Di, L. and Kerns, E. H. (2016) 'Chapter 10 - Blood-Brain Barrier', in Di, L. & Kerns, E.H. (eds.) *Drug-Like Properties (Second Edition)*. Boston: Academic Press, pp. 141-159.

Diana, P., Barraja, P., Lauria, A., Montalbano, A., Almerico, A. M., Dattolo, G. and Cirrincione, G. (2002) 'Pyrrolo[2,1-c][1,2,4]triazines from 2-diazopyrroles: synthesis and antiproliferative activity', *Eur J Med Chem,* 37(3), pp. 267-72.

Dobes, M., Khurana, V. G., Shadbolt, B., Jain, S., Smith, S. F., Smee, R., Dexter, M. and Cook, R. (2011) 'Increasing incidence of glioblastoma multiforme and meningioma, and decreasing incidence of Schwannoma (2000-2008): Findings of a multicenter Australian study', *Surg Neurol Int,* 2, pp. 176.

Elia, M. C., Storer, R. D., McKelvey, T. W., Kraynak, A. R., Barnum, J. E., Harmon, L. S., DeLuca, J. G. and Nichols, W. W. (1994) 'Rapid DNA degradation in primary rat hepatocytes treated with diverse cytotoxic chemicals: analysis by pulsed field gel electrophoresis and implications for alkaline elution assays', *Environ Mol Mutagen,* 24(3), pp. 181-91.

Ernest, N. and Sontheimer, H. (2009) 'Glioma', in Ernest, N. (ed.) *Encyclopedia of Neuroscience*, pp. 877-884.

Fabiani, A., Schiffer, D., Paoletti, P. and Grossi-Paoletti, E. (1970) 'Histochemical evaluation of hydrolytic enzymes in tumors induced in the rat by nitrosourea derivatives', *Acta Neuropathol,* 15(3), pp. 272-8.

Fahrer, J. and Kaina, B. (2013) 'O6-methylguanine-DNA methyltransferase in the defense against N-nitroso compounds and colorectal cancer', *Carcinogenesis,* 34(11), pp. 2435-42.

Ferluga, J., Asherson, G. L. and Becker, E. L. (1972) 'The effect of organophosphorus inhibitors, p-nitrophenol and cytochalasin B on cytotoxic killing of tumour cells by immune spleen cells, and the effect of shaking', *Immunology,* 23(4), pp. 577-90.

Fisher, J. L., Schwartzbaum, J. A., Wrensch, M. and Wiemels, J. L. (2007) 'Epidemiology of brain tumors', *Neurol Clin,* 25(4), pp. 867-90, vii.

Fitzgibbons, P. L., Dillon, D. A., Alsabeh, R., Berman, M. A., Hayes, D. F., Hicks, D. G., Hughes, K. S. and Nofech-Mozes, S. (2014) 'Template for reporting results of biomarker testing of specimens from patients with carcinoma of the breast', *Arch Pathol Lab Med,* 138(5), pp. 595-601.

Fleming, C. D., Edwards, C. C., Kirby, S. D., Maxwell, D. M., Potter, P. M., Cerasoli, D. M. and Redinbo, M. R. (2007) 'Crystal structures of human carboxylesterase 1 in covalent complexes with the chemical warfare agents soman and tabun', *Biochemistry,* 46(17), pp. 5063-71.

Fukami, T. and Yokoi, T. (2012) 'The Emerging Role of Human Esterases', *Drug Metabolism and Pharmacokinetics,* 27(5), pp. 466-477.

Garelnabi, E. A., Pletsas, D., Li, L., Kiakos, K., Karodia, N., Hartley, J. A., Phillips, R. M. and Wheelhouse, R. T. (2012) 'Strategy for Imidazotetrazine Prodrugs with Anticancer Activity Independent of MGMT and MMR', *ACS Med Chem Lett,* 3(12), pp. 965-8.

Garside, R., Pitt, M., Anderson, R., Rogers, G., Dyer, M., Mealing, S., Somerville, M., Price, A. and Stein, K. (2007) 'The effectiveness and cost-effectiveness of carmustine implants and temozolomide for the treatment of newly diagnosed high-grade glioma: a systematic review and economic evaluation', *Health Technol Assess,* 11(45), pp. iii-iv, ix-221.

Gausia, S., Markou, M., Voulgaris, S., Bai, M., Polyzoidis, K. and Kyritsis, A. (2009) ' Descriptive epidemiology of cerebral gliomas in northwest Greece and study of potential predisposing factors, 2005–2007', *Neuroepidemiology,* 33(2), pp. 89-95.

Ghose, A. K. and Crippen, G. M. (1987) 'Atomic physicochemical parameters for three-dimensional-structure-directed quantitative structure-activity relationships. 2. Modeling dispersive and hydrophobic interactions', *J Chem Inf Comput Sci,* 27(1), pp. 21-35.

Gilant, E., Kaza, M., Szlagowska, A., Serafin-Byczak, K. and Rudzki, P. J. (2012) 'Validated Hplc Method for Determination of Temozolomide in Human Plasma', *Acta Poloniae Pharmaceutica,* 69(6), pp. 1347-1355.

Grossman, S. A., Ye, X., Lesser, G., Sloan, A., Carraway, H., Desideri, S., Piantadosi, S. and Consortium, N. C. (2011) 'Immunosuppression in patients with high-grade gliomas treated with radiation and temozolomide', *Clinical cancer research : an official journal of the American Association for Cancer Research,* 17(16), pp. 5473-5480.

Hampson, R., Humbert, O., Macpherson, P., Aquilina, G. and Karran, P. (1997) 'Mismatch repair defects and O6-methylguanine-DNA methyltransferase expression in acquired resistance to methylating agents in human cells', *J Biol Chem,* 272(45), pp. 28596-606.

Han, G., Tamaki, M. and Hruby, V. (2001) 'Fast, efficient and selective deprotection of the tert-butoxycarbonyl (Boc) group using HCl/dioxane (4 M)', *Journal of Peptide Research,* 58(4), pp. 338-341.

Hanif, F., Muzaffar, K., Perveen, K., Malhi, S. M. and Simjee, S. U. (2017) 'Glioblastoma Multiforme: A Review of its Epidemiology and Pathogenesis through Clinical Presentation and Treatment', *Asian Pacific journal of cancer prevention : APJCP,* 18(1), pp. 3-9.

Harvey, J. M., Clark, G. M., Osborne, C. K. and Allred, D. C. (1999) 'Estrogen receptor status by immunohistochemistry is superior to the ligand-binding assay for predicting response to adjuvant endocrine therapy in breast cancer', *J Clin Oncol,* 17(5), pp. 1474-81.

Hatfield, M. J., Tsurkan, L., Garrett, M., Shaver, T. M., Hyatt, J. L., Edwards, C. C., Hicks, L. D. and Potter, P. M. (2011) 'Organ-specific carboxylesterase profiling identifies the small intestine and kidney as major contributors of activation of the anticancer prodrug CPT-11', *Biochem Pharmacol,* 81(1), pp. 24-31.

Hegi, M. E., Diserens, A. C., Gorlia, T., Hamou, M. F., de Tribolet, N., Weller, M., Kros, J. M., Hainfellner, J. A., Mason, W., Mariani, L., Bromberg, J. E., Hau, P., Mirimanoff, R. O., Cairncross, J. G., Janzer, R. C. and Stupp, R. (2005) 'MGMT gene silencing and benefit from temozolomide in glioblastoma', *N Engl J Med,* 352(10), pp. 997-1003.

Hegi, M. E., Liu, L., Herman, J. G., Stupp, R., Wick, W., Weller, M., Mehta, M. P. and Gilbert, M. R. (2008) 'Correlation of O6-methylguanine methyltransferase (MGMT) promoter methylation with clinical outcomes in glioblastoma and clinical strategies to modulate MGMT activity', *J Clin Oncol,* 26(25), pp. 4189-99.

Henriksen, S., Tylden, G. D., Dumoulin, A., Sharma, B. N., Hirsch, H. H. and Rinaldo, C. H. (2014) 'The human fetal glial cell line SVG p12 contains infectious BK polyomavirus', *J Virol,* 88(13), pp. 7556-68.

Hochberg, F., Toniolo, P., Cole, P. and Salcman, M. (1990) 'Nonoccupational risk indicators of glioblastoma in adults', *J Neurooncol,* 8(1), pp. 55-60.

Höllerer, C., Becker, G., Göen, T. and Eckert, E. (2018) 'Regioselective ester cleavage of di-(2-ethylhexyl) trimellitates by porcine liver esterase', *Toxicology in Vitro,* 47, pp. 178-185.

Horspool, K. R., Stevens, M. F., Newton, C. G., Lunt, E., Walsh, R. J., Pedgrift, B. L., Baig, G. U., Lavelle, F. and Fizames, C. (1990) 'Antitumor imidazotetrazines. 20. Preparation of the 8-acid derivative of mitozolomide and its utility in the preparation of active antitumor agents', *J Med Chem,* 33(5), pp. 1393-9.

Hosokawa, M. (2008) 'Structure and catalytic properties of carboxylesterase isozymes involved in metabolic activation of prodrugs', *Molecules,* 13(2), pp. 412-31.

ICH (2018) *Validation of Analytical Procedures: Text and Methodology (Q2(R1))*: ICH Secretariat.

Imai, T. (2006) 'Human carboxylesterase isozymes: catalytic properties and rational drug design', *Drug Metab Pharmacokinet,* 21(3), pp. 173-85.

Imai, T., Taketani, M., Shii, M., Hosokawa, M. and Chiba, K. (2006) 'Substrate specificity of carboxylesterase isozymes and their contribution to hydrolase activity in human liver and small intestine', *Drug Metab Dispos,* 34(10), pp. 1734-41.

Junge, W. and Heymann, E. (1979) 'Characterization of the Isoenzymes of Pig-Liver Esterase 2. Kinetic Studies', *European Journal of Biochemistry,* 95(3), pp. 519-525.

Kadoma, Y., Murakami, Y., Ogiwara, T., Machino, M., Yokoe, I. and Fujisawa, S. (2010) 'Radical-scavenging activity and cytotoxicity of p-methoxyphenol and p-cresol dimers', *Molecules,* 15(3), pp. 1103-12.

Kaina, B., Margison, G. P. and Christmann, M. (2010) 'Targeting O(6)-methylguanine-DNA methyltransferase with specific inhibitors as a strategy in cancer therapy', *Cell Mol Life Sci,* 67(21), pp. 3663-81.

Kapcak, E. and Satana-Kara, E. H. (2018) 'Development and Full Validation of a Stability-indicating HPLC Method for the Determination of the Anticancer Drug Temozolomide in Pharmaceutical Form', *Turkish Journal of Pharmaceutical Sciences,* 15(3), pp. 271-277.

Karran, P. and Bignami, M. (1994) 'DNA damage tolerance, mismatch repair and genome instability', *Bioessays,* 16(11), pp. 833-9.

Kettenmann, H. and Ransom, B. (2013) *Neuroglia.* New York: Oxford University Press Inc.

Khan, A., Imam, S. S., Aqil, M., Sultana, Y., Ali, A. and Khan, K. (2016) 'Design of experiment based validated stability indicating RP-HPLC method of temozolomide in bulk and pharmaceutical dosage forms', *Beni-Suef University Journal of Basic and Applied Sciences,* 5(4), pp. 402-408.

Khosa, A., Krishna, K. V., Saha, R. N., Dubey, S. K. and Reddi, S. (2018) 'A simplified and sensitive validated RP-HPLC method for determination of temozolomide in rat plasma and its application to a pharmacokinetic study', *Journal of Liquid Chromatography & Related Technologies,* 41(10), pp. 692-697.

Kim, H., Likhari, P., Parker, D., Statkevich, P., Marco, A., Lin, C.-C. and Nomeir, A. A. (2001) 'High-performance liquid chromatographic analysis and stability of anti-tumor agent temozolomide in human plasma', *Journal of Pharmaceutical and Biomedical Analysis,* 24(3), pp. 461-468.

Kumari, S., Ahsan, S. M., Kumar, J. M., Kondapi, A. K. and Rao, N. M. (2017) 'Overcoming blood brain barrier with a dual purpose Temozolomide loaded Lactoferrin nanoparticles for combating glioma (SERP-17-12433)', *Scientific Reports,* 7(1), pp. 6602.

Kuo, S. (2005) *Synthesis of temozolomide and analogs*. US Patent Patent no. US6844434B2. [Online].

Kuo, S., Mas, J. and Donald, H. (2006) *Synthesis of temozolomide and analogs*. US Patent Patent no. US7087751B2. [Online].

Lacroix, M., Abi-Said, D., Fourney, D. R., Gokaslan, Z. L., Shi, W., DeMonte, F., Lang, F. F., McCutcheon, I. E., Hassenbusch, S. J., Holland, E., Hess, K., Michael, C., Miller, D. and Sawaya, R. (2001) 'A multivariate analysis of 416 patients with glioblastoma multiforme: prognosis, extent of resection, and survival', *J Neurosurg,* 95(2), pp. 190-8.

Laizure, S. C., Herring, V., Hu, Z., Witbrodt, K. and Parker, R. B. (2013) 'The role of human carboxylesterases in drug metabolism: have we overlooked their importance?', *Pharmacotherapy,* 33(2), pp. 210-22.

Langnel, D. A. F., Arrowsmith, J. and Stevens, M. F. G. (2000) 'Antitumor imidazotetrazines. 38. New 8-substituted derivatives of the imidazo[5,1-d]-1,2,3,5-tetrazines temozolomide and mitozolomide', *ARKIVOC,* 3(1), pp. 421-437.

Lanzetta, G. and Minniti, G. (2010) 'Treatment of glioblastoma in elderly patients: an overview of current treatments and future perspective', *Tumori,* 96(5), pp. 650-8.

Ledur, P. F., Onzi, G. R., Zong, H. and Lenz, G. (2017) 'Culture conditions defining glioblastoma cells behavior: what is the impact for novel discoveries?', *Oncotarget,* 8(40), pp. 69185-69197.

Li, A., Walling, J., Kotliarov, Y., Center, A., Steed, M. E., Ahn, S. J., Rosenblum, M., Mikkelsen, T., Zenklusen, J. C. and Fine, H. A. (2008) 'Genomic changes and gene expression profiles reveal that established glioma cell lines are poorly representative of primary human gliomas', *Mol Cancer Res,* 6(1), pp. 21-30.

Linos, E., Raine, T., Alonso, A. and Michaud, D. (2007) 'Atopy and Risk of Brain Tumors: A Meta-analysis', *JNCI: Journal of the National Cancer Institute,* 99(20), pp. 1544-1550.

Liu, D., Yang, J. G., Cheng, J. and Zhao, L. X. (2010) 'Synthesis and antitumor activity of 3-methyl-4-oxo-3,4-dihydroimidazo [5,1-d][1,2,3,5]tetrazine-8-carboxylates and -carboxamides', *Molecules,* 15(12), pp. 9427-37.

Liu, H. L., Yang, H. W., Hua, M. Y. and Wei, K. C. (2012) 'Enhanced therapeutic agent delivery through magnetic resonance imaging-monitored focused ultrasound blood-brain barrier disruption for brain tumor treatment: an overview of the current preclinical status', *Neurosurg Focus,* 32(1), pp. E4.

Liu, M., Thakkar, J. P., Garcia, C. R., Dolecek, T. A., Wagner, L. M., Dressler, E. V. M. and Villano, J. L. (2018) 'National cancer database analysis of outcomes in pediatric glioblastoma', *Cancer Medicine,* 7(4), pp. 1151-1159.

Louis, D. N., Perry, A., Reifenberger, G., von Deimling, A., Figarella-Branger, D., Cavenee, W. K., Ohgaki, H., Wiestler, O. D., Kleihues, P. and Ellison, D. W. (2016) 'The 2016 World Health Organization Classification of Tumors of the Central Nervous System: a summary', *Acta Neuropathol,* 131(6), pp. 803-20.

Lowe, P. R., Sansom, C. E., Schwalbe, C. H., Stevens, M. F. and Clark, A. S. (1992) 'Antitumor imidazotetrazines. 25. Crystal structure of 8-carbamoyl-3-methylimidazo[5,1-d]-1,2,3,5-tetrazin-4(3H)-one (temozolomide) and structural comparisons with the related drugs mitozolomide and DTIC', *J Med Chem,* 35(18), pp. 3377-82.

Lunt, E., Newton, C. G., Smith, C., Stevens, G. P., Stevens, M. F., Straw, C. G., Walsh, R. J., Warren, P. J., Fizames, C., Lavelle, F. and et al. (1987) 'Antitumor imidazotetrazines. 14. Synthesis and antitumor activity of 6- and 8-substituted imidazo[5,1-d]-1,2,3,5-tetrazinones and 8-substituted pyrazolo[5,1-d]-1,2,3,5-tetrazinones', *J Med Chem,* 30(2), pp. 357-66.

Manrique-Guzman, S., Herrada-Pineda, T. and Revilla-Pacheco, F. (2017) 'Surgical Management of Glioblastoma', in De Vleeschouwer, S. (ed.) *Glioblastoma*. Brisbane (AU).

Marin-Ramos, N. I., Thein, T. Z., Cho, H. Y., Swenson, S. D., Wang, W. J., Schonthal, A. H., Chen, T. C. and Hofman, F. M. (2018) 'NEO212 Inhibits Migration and Invasion of Glioma Stem Cells', *Molecular Cancer Therapeutics,* 17(3), pp. 625-637.

McKeage, M., Dady, P., Clear, M. and MacDonald, A. (1992) 'A clinical and pharmacological study of high-dose mitozolomide given in conjunction with autologous bone marrow rescue', *Cancer Chemother Pharmacol,* 29(3), pp. 201-6.

Messali, A., Hay, J. W. and Villacorta, R. (2013) 'The cost-effectiveness of temozolomide in the adjuvant treatment of newly diagnosed glioblastoma in the United States', *Neuro Oncol,* 15(11), pp. 1532-42.

Mirzaei, S., Khalilian, M. H. and Taherpour, A. A. (2015) 'Mechanistic study of the hydrolytic degradation and protonation of temozolomide', *Rsc Advances,* 5(51), pp. 41112-41119.

Mizuno, N. S. and Decker, R. W. (1976) 'Alteration of DNA by 5-(3-methyl-1-triazeno)imidazole-4-carboxamide (NSC-407347)', *Biochem Pharmacol,* 25(23), pp. 2643-7.

Moiseeva, N. I., Susova, O. Y., Mitrofanov, A. A., Panteleev, D. Y., Pavlova, G. V., Pustogarov, N. A., Stavrovskaya, A. A. and Rybalkina, E. Y. (2016) 'Connection between Proliferation Rate and Temozolomide Sensitivity of Primary Glioblastoma Cell Culture and Expression of YB-1 and LRP/MVP', *Biochemistry (Mosc),* 81(6), pp. 628-35.

Montella, I. R., Schama, R. and Valle, D. (2012) 'The classification of esterases: an important gene family involved in insecticide resistance--a review', *Mem Inst Oswaldo Cruz,* 107(4), pp. 437-49.

Monti, P., Iannone, R., Campomenosi, P., Ciribilli, Y., Varadarajan, S., Shah, D., Menichini, P., Gold, B. and Fronza, G. (2004) 'Nucleotide excision repair defect influences lethality and mutagenicity induced by Me-lex, a sequence-selective N3-adenine methylating agent in the absence of base excision repair', *Biochemistry,* 43(19), pp. 5592-5599.

Moody, C. L. and Wheelhouse, R. T. (2014) 'The medicinal chemistry of imidazotetrazine prodrugs', *Pharmaceuticals (Basel),* 7(7), pp. 797-838.

Mrugala, M. M. and Chamberlain, M. C. (2008) 'Mechanisms of disease: temozolomide and glioblastoma--look to the future', *Nat Clin Pract Oncol,* 5(8), pp. 476-86.

Neijt, J. P., van der Burg, M. E., Guastalla, J. P., George, M., Piccart, M., Vermorken, J., Carnino, F. and Rotmensz, N. (1989) 'Phase II trial of mitozolomide in patients with advanced ovarian cancer. A study of the EORTC Gynecological Cancer Cooperative Group', *Acta Oncol,* 28(5), pp. 663-5.

Newlands, E. S., Stevens, M. F., Wedge, S. R., Wheelhouse, R. T. and Brock, C. (1997) 'Temozolomide: a review of its discovery, chemical properties, pre-clinical development and clinical trials', *Cancer Treat Rev,* 23(1), pp. 35-61.

Niles, A. L., Moravec, R. A. and Riss, T. L. (2008) 'Update on in vitro cytotoxicity assays for drug development', *Expert Opin Drug Discov,* 3(6), pp. 655-69.

Nuthalapati, S., Munasinghe, W., Giranda, V. and Xiong, H. (2018) 'Clinical Pharmacokinetics and Mass Balance of Veliparib in Combination with Temozolomide in Subjects with Nonhematologic Malignancies', *Clinical Pharmacokinetics,* 57(1), pp. 51-58.

O'Connell, M. J. and Cimprich, K. A. (2005) 'G2 damage checkpoints: what is the turn-on?', *J Cell Sci,* 118(Pt 1), pp. 1-6.

Ohgaki, H., Dessen, P., Jourde, B., Horstmann, S., Nishikawa, T., Di Patre, P. L., Burkhard, C., Schuler, D., Probst-Hensch, N. M., Maiorka, P. C., Baeza, N., Pisani, P., Yonekawa, Y., Yasargil, M. G., Lutolf, U. M. and Kleihues, P. (2004) 'Genetic pathways to glioblastoma: a population-based study', *Cancer Res,* 64(19), pp. 6892-9.

Ohgaki, H. and Kleihues, P. (2007) 'Genetic pathways to primary and secondary glioblastoma', *Am J Pathol,* 170(5), pp. 1445-53.

Ohgaki, H. and Kleihues, P. (2009) 'Genetic alterations and signaling pathways in the evolution of gliomas', *Cancer Sci,* 100(12), pp. 2235-41.

Ostermann, S., Csajka, C., Buclin, T., Leyvraz, S., Lejeune, F., Decosterd, L. A. and Stupp, R. (2004) 'Plasma and cerebrospinal fluid population pharmacokinetics of temozolomide in malignant glioma patients', *Clin Cancer Res,* 10(11), pp. 3728-36.

Ostrom, Q. T., Gittleman, H., Farah, P., Ondracek, A., Chen, Y., Wolinsky, Y., Stroup, N. E., Kruchko, C. and Barnholtz-Sloan, J. S. (2013) 'CBTRUS statistical report: Primary brain and central nervous system tumors diagnosed in the United States in 2006-2010', *Neuro Oncol,* 15 Suppl 2, pp. ii1-56.

Perazzoli, G., Prados, J., Ortiz, R., Caba, O., Cabeza, L., Berdasco, M., Gonzalez, B. and Melguizo, C. (2015) 'Temozolomide Resistance in Glioblastoma Cell Lines: Implication of MGMT, MMR, P-Glycoprotein and CD133 Expression', *PLoS One,* 10(10), pp. e0140131.

Portnow, J., Badie, B., Chen, M., Liu, A., Blanchard, S. and Synold, T. W. (2009) 'The neuropharmacokinetics of temozolomide in patients with resectable brain tumors: potential implications for the current approach to chemoradiation', *Clin Cancer Res,* 15(22), pp. 7092-8.

Prasad, G. and Haas-Kogan, D. A. (2009) 'Radiation-induced gliomas', *Expert review of neurotherapeutics,* 9(10), pp. 1511-1517.

Purves, D., G;, A. and Fitzpatrick, D. (2001) *Neuroscience.* 2nd edn. Sunderland: Sinauer Associates.

Rai, R., Banerjee, M., Wong, D. H., McCullagh, E., Gupta, A., Tripathi, S., Riquelme, E., Jangir, R., Yadav, S., Raja, M., Melkani, P., Dixit, V., Patil, U., Shrivastava, R., Middya, S., Olivares, F., Guerrero, J., Surya, A., Pham, S. M., Bernales, S., Protter, A. A., Hung, D. T. and Chakravarty, S. (2016) 'Temozolomide analogs with improved brain/plasma ratios - Exploring the possibility of enhancing the therapeutic index of temozolomide', *Bioorg Med Chem Lett,* 26(20), pp. 5103-5109.

Ramirez, Y. P., Mladek, A. C., Phillips, R. M., Gynther, M., Rautio, J., Ross, A. H., Wheelhouse, R. T. and Sakaria, J. N. (2015) 'Evaluation of novel imidazotetrazine analogues designed to overcome temozolomide resistance and glioblastoma regrowth', *Mol Cancer Ther,* 14(1), pp. 111-9.

Reyderman, L., Statkevich, P., Thonoor, C. M., Patrick, J., Batra, V. K. and Wirth, M. (2004) 'Disposition and pharmacokinetics of temozolomide in rat', *Xenobiotica,* 34(5), pp. 487-500.

Riss, T. L., Moravec, R. A. and Niles, A. L. (2013) 'Cell Viability Assays', in Sittampalam, G.S., Coussens, N.P. & Brimacombe, K. (eds.) *Assay Guidance Manual*: Eli Lilly & Company and the National Center for Advancing Translational Sciences.

Romani, M., Pistillo, M. P. and Banelli, B. (2018) 'Epigenetic Targeting of Glioblastoma', *Front Oncol,* 8, pp. 448.

Roos, W. P., Batista, L. F. Z., Naumann, S. C., Wick, W., Weller, M., Menck, C. F. M. and Kaina, B. (2007) 'Apoptosis in malignant glioma cells triggered by the temozolomide-induced DNA lesion O-6-methylguanine', *Oncogene,* 26(2), pp. 186-197.

Salvati, M., Frati, A., Russo, N., Caroli, E., Polli, F. M., Minniti, G. and Delfini, R. (2003) 'Radiation-induced gliomas: report of 10 cases and review of the literature', *Surgical Neurology,* 60(1), pp. 60-67.

Sanai, N. and Berger, M. S. (2009) 'Operative techniques for gliomas and the value of extent of resection', *Neurotherapeutics,* 6(3), pp. 478-86.

Sanchez-Diaz, P. C., Chang, J. C., Moses, E. S., Dao, T., Chen, Y. and Hung, J. Y. (2017) 'Ubiquitin carboxyl-terminal esterase L1 (UCHL1) is associated with stem-like cancer cell functions in pediatric high-grade glioma', *PLoS One,* 12(5), pp. e0176879.

Sankar, A., Thomas, D. G. and Darling, J. L. (1999) 'Sensitivity of short-term cultures derived from human malignant glioma to the anti-cancer drug temozolomide', *Anticancer Drugs,* 10(2), pp. 179-85.

Schering-Plough, N.I.C.E (2005) *Temozolomide for the treatment of newly diagnosed high-grade glioma in England and Wales*: URL: https://www.nice.org.uk/guidance/ta121/history/.

Selassie, C. D., Kapur, S., Verma, R. P. and Rosario, M. (2005) 'Cellular apoptosis and cytotoxicity of phenolic compounds: a quantitative structure-activity relationship study', *J Med Chem,* 48(23), pp. 7234-42.

Shervington, L. A., Smith, N., Norman, E., Ward, T., Phillips, R. and Shervington, A. (2009) 'To determine the cytotoxicity of chlorambucil and one of its nitro-derivatives, conjugated to prasterone and pregnenolone, towards eight human cancer cell-lines', *European Journal of Medicinal Chemistry,* 44(7), pp. 2944-2951.

Shih, H. A., Sherman, J. C., Nachtigall, L. B., Colvin, M. K., Fullerton, B. C., Daartz, J., Winrich, B. K., Batchelor, T. T., Thornton, L. T., Mancuso, S. M., Saums, M. K., Oh, K. S., Curry, W. T., Loeffler, J. S. and Yeap, B. Y. (2015) 'Proton therapy for low-grade gliomas: Results from a prospective trial', *Cancer,* 121(10), pp. 1712-9.

Silber, J. R., Bobola, M. S., Blank, A. and Chamberlain, M. C. (2012) 'O-6-Methylguanine-DNA methyltransferase in glioma therapy: Promise and problems', *Biochimica Et Biophysica Acta-Reviews on Cancer,* 1826(1), pp. 71-82.

Silverstein, R. M. (2015) *Spectrometric identification of organic compounds.* 8th ed. edn.: Wiley.

Smyth, J. F., Gundersen, S., Renard, J. and Pinedo, H. M. (1989) 'Randomized phase II trial of TCNU versus mitozolomide in malignant melanoma. EORTC Early Clinical Trials Group', *Eur J Cancer Clin Oncol,* 25(4), pp. 755-7.

Soroceanu, L., Matlaf, L., Khan, S., Akhavan, A., Singer, E., Bezrookove, V., Decker, S., Ghanny, S., Hadaczek, P., Bengtsson, H., Ohlfest, J., Luciani-Torres, M. G., Harkins, L., Perry, A., Guo, H., Soteropoulos, P. and Cobbs, C. S. (2015) 'Cytomegalovirus Immediate-Early Proteins Promote Stemness Properties in Glioblastoma', *Cancer Res,* 75(15), pp. 3065-76.

Stevens, M. F., Hickman, J. A., Stone, R., Gibson, N. W., Baig, G. U., Lunt, E. and Newton, C. G. (1984) 'Antitumor imidazotetrazines. 1. Synthesis and chemistry of 8-carbamoyl-3-(2-chloroethyl)imidazo[5,1-d]-1,2,3,5-tetrazin-4(3 H)-one , a novel broad-spectrum antitumor agent', *J Med Chem,* 27(2), pp. 196-201.

Stupp, R., Mason, W. P., van den Bent, M. J., Weller, M., Fisher, B., Taphoorn, M. J., Belanger, K., Brandes, A. A., Marosi, C., Bogdahn, U., Curschmann, J., Janzer, R. C., Ludwin, S. K., Gorlia, T., Allgeier, A., Lacombe, D., Cairncross, J. G., Eisenhauer, E., Mirimanoff, R. O., European Organisation for, R., Treatment of Cancer Brain, T., Radiotherapy, G. and National Cancer Institute of Canada Clinical Trials, G. (2005) 'Radiotherapy plus concomitant and adjuvant temozolomide for glioblastoma', *N Engl J Med,* 352(10), pp. 987-96.

Sturm, D., Bender, S., Jones, D. T., Lichter, P., Grill, J., Becher, O., Hawkins, C., Majewski, J., Jones, C., Costello, J. F., Iavarone, A., Aldape, K., Brennan, C. W., Jabado, N. and Pfister, S. M. (2014) 'Paediatric and adult glioblastoma: multiform (epi)genomic culprits emerge', *Nat Rev Cancer,* 14(2), pp. 92-107.

Suppasansatorn, P., Wang, G., Conway, B. R., Wang, W. and Wang, Y. (2006) 'Skin delivery potency and antitumor activities of temozolomide ester prodrugs', *Cancer Lett,* 244(1), pp. 42-52.

Svec, R. L., Furiassi, L., Skibinski, C. G., Fan, T. M., Riggins, G. J. and Hergenrother, P. J. (2018) 'Tunable Stability of Imidazotetrazines Leads to a Potent Compound for Glioblastoma', *ACS Chem Biol,* 13(11), pp. 3206-3216.

Sweetlove, M. (2012) 'Phase III CONCERT Trial of Latrepirdine', *Pharmaceutical Medicine,* 26(2), pp. 113-115.

Taketani, M., Shii, M., Ohura, K., Ninomiya, S. and Imai, T. (2007) 'Carboxylesterase in the liver and small intestine of experimental animals and human', *Life Sci,* 81(11), pp. 924-32.

Thakkar, J. P., Dolecek, T. A., Horbinski, C., Ostrom, Q. T., Lightner, D. D., Barnholtz-Sloan, J. S. and Villano, J. L. (2014) 'Epidemiologic and molecular prognostic review of glioblastoma', *Cancer Epidemiol Biomarkers Prev,* 23(10), pp. 1985-96.

Timoumi, R., Buratti, F. M., Abid-Essefi, S., Dorne, J.-L. C. M. and Testai, E. (2019) 'Metabolism of triflumuron in the human liver: Contribution of cytochrome P450 isoforms and esterases', *Toxicology Letters,* 312, pp. 173-180.

Tisdale, M. J. (1987) 'Antitumor imidazotetrazines--XV. Role of guanine O6 alkylation in the mechanism of cytotoxicity of imidazotetrazinones', *Biochem Pharmacol,* 36(4), pp. 457-62.

Tsakos, M., Schaffert, E. S., Clement, L. L., Villadsen, N. L. and Poulsen, T. B. (2015) 'Ester coupling reactions--an enduring challenge in the chemical synthesis of bioactive natural products', *Nat Prod Rep,* 32(4), pp. 605-32.

Tsang, L. L., Farmer, P. B., Gescher, A. and Slack, J. A. (1990) 'Characterisation of urinary metabolites of temozolomide in humans and mice and evaluation of their cytotoxicity', *Cancer Chemother Pharmacol,* 26(6), pp. 429-36.

Tubbs, J. L., Pegg, A. E. and Tainer, J. A. (2007) 'DNA binding, nucleotide flipping, and the helix-turn-helix motif in base repair by O-6-alkylguanine-DNA alkyltransferase and its implications for cancer chemotherapy', *DNA Repair,* 6(8), pp. 1100-1115.

Uno, M., Oba-Shinjo, S. M., Camargo, A. A., Moura, R. P., de Aguiar, P. H., Cabrera, H. N., Begnami, M., Rosemberg, S., Teixeira, M. J. and Marie, S. K. N. (2011) 'Correlation of MGMT promoter methylation status with gene and protein expression levels in glioblastoma', *Clinics,* 66(10), pp. 1747-1755.

van Nifterik, K. A., van den Berg, J., van der Meide, W. F., Ameziane, N., Wedekind, L. E., Steenbergen, R. D. M., Leenstra, S., Lafleur, M. V. M., Slotman, B. J., Stalpers, L. J. A. and Sminia, P. (2010) 'Absence of the MGMT protein as well as methylation of the MGMT promoter predict the sensitivity for temozolomide', *British Journal of Cancer,* 103(1), pp. 29-35.

Vanza, J., Jani, P., Pandya, N. and Tandel, H. (2018) 'Formulation and statistical optimization of intravenous temozolomide-loaded PEGylated liposomes to treat glioblastoma multiforme by three-level factorial design', *Drug Development and Industrial Pharmacy,* 44(6), pp. 923-933.

Varma, D. and Varma, R. (2005) 'The Bhopal Disaster of 1984', *Bulletin of Science, Technology & Society,* 25(1), pp. 37-45.

Vistoli, G., Pedretti, A., Mazzolari, A. and Testa, B. (2010) 'Homology modeling and metabolism prediction of human carboxylesterase-2 using docking analyses by GriDock: a parallelized tool based on AutoDock 4.0', *J Comput Aided Mol Des,* 24(9), pp. 771-87.

Wang, D., Zou, L., Jin, Q., Hou, J., Ge, G. and Yang, L. (2018) 'Human carboxylesterases: a comprehensive review', *Acta Pharm Sin B,* 8(5), pp. 699-712.

Wang, Y., Wheelhouse, R., Zhao, L., Langnel, D. and Stevens, M. F. (1998) 'Antitumour imidazotetrazines. Part 36.1 Conversion of 5-aminoimidazole-4-carboxamide to imidazo[5,1-d][1,2,3,5]tetrazin-4(3H)-ones and imidazo[1,5-a][1,3,5]triazin-4(3H)-ones related in structure to the antitumour agents temozolomide and mitozolomide', *Journal of the Chemical Society, Perkin Transactions,* 1(10), pp. 1669-1675.

Watson, J. D. and Crick, F. H. (1953) 'Molecular structure of nucleic acids; a structure for deoxyribose nucleic acid', *Nature,* 171(4356), pp. 737-8.

Wesolowski, J. R., Rajdev, P. and Mukherji, S. K. (2010) 'Temozolomide (Temodar)', *AJNR Am J Neuroradiol,* 31(8), pp. 1383-4.

William, D., Walther, M., Schneider, B., Linnebacher, M. and Classen, C. F. (2018) 'Temozolomide-induced increase of tumorigenicity can be diminished by targeting of mitochondria in in vitro models of patient individual glioblastoma', *PLoS One,* 13(1), pp. e0191511.

Williams, L. D. and Shaw, B. R. (1987) 'Protonated base pairs explain the ambiguous pairing properties of O6-methylguanine', *Proceedings of the National Academy of Sciences of the United States of America,* 84(7), pp. 1779-1783.

Wolburg, H., Wolburg-Buchholz, K., Reichenbach, A. and Mack, A. (2015) 'Ependymal Cells', *Reference Module in Biomedical Sciences*: Elsevier.

Wollowitz, S. and Kataisto, E. (2009) *Methods for preparing pyridylethyl-substituted carbolines*. World Intellectual Property Organization Patent no. PCT/US2009/035992. [Online].

Wyatt, M. D. and Pittman, D. L. (2006) 'Methylating agents and DNA repair responses: Methylated bases and sources of strand breaks', *Chem Res Toxicol,* 19(12), pp. 1580-94.

Yang, Z., Wei, D., Dai, X., Stevens, M. F. G., Bradshaw, T. D., Luo, Y. and Zhang, J. (2019) 'C8-Substituted Imidazotetrazine Analogs Overcome Temozolomide Resistance by Inducing DNA Adducts and DNA Damage', 9(485).

Zelnick, S. D., Mattie, D. R. and Stepaniak, P. C. (2003) 'Occupational exposure to hydrazines: treatment of acute central nervous system toxicity', *Aviat Space Environ Med,* 74(12), pp. 1285-91.

Zhang, J., Stevens, M. F. and Bradshaw, T. D. (2012) 'Temozolomide: mechanisms of action, repair and resistance', *Curr Mol Pharmacol,* 5(1), pp. 102-14.

APPENDIX

Appendix to Chapter 3

Appendix 3a: DMSO Controls for Cell Lines and Primary Cultures

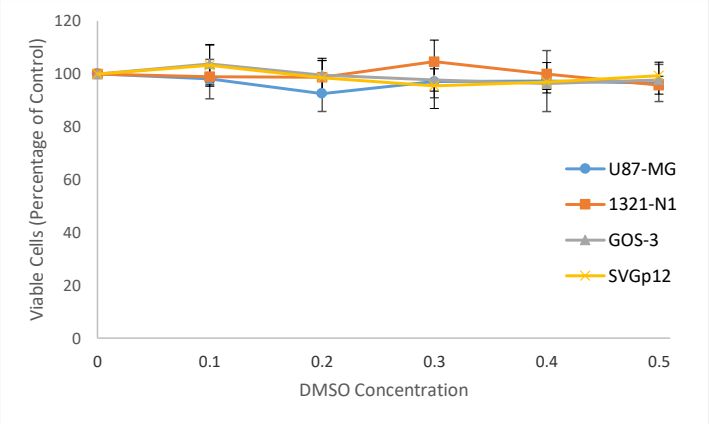

Appendix 1: The effect of DMSO at various concentrations on U87-MG, 1321-N1, GOS-3 and SVGp12 cell lines. The values shown are mean ±SD, n = 3

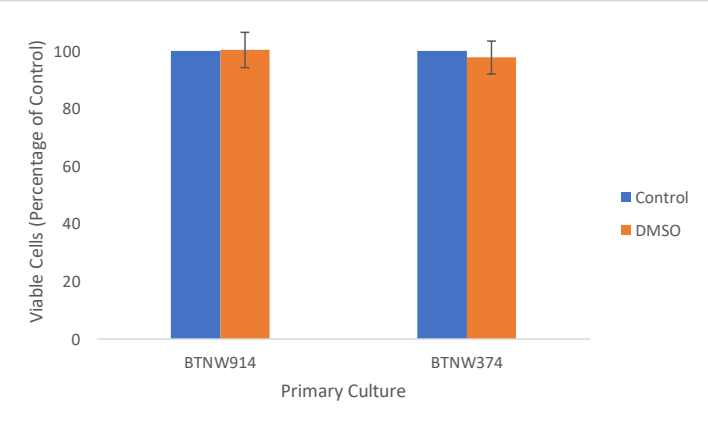

Appendix 2: The effect of DMSO at 0.5% DMSO on primary cultures, BTNW914 and BTNW374. The values shown are mean ±SD, n = 9.

Appendix 3b: Solubility Evaluation of TMZ, TMZ acid and Ester and Amide Analogues of TMZ

3-Methyl-4-oxo-imidazo[5,1-d][1,2,3,5]tetrazine-8-carboxamide – (**TMZ**)

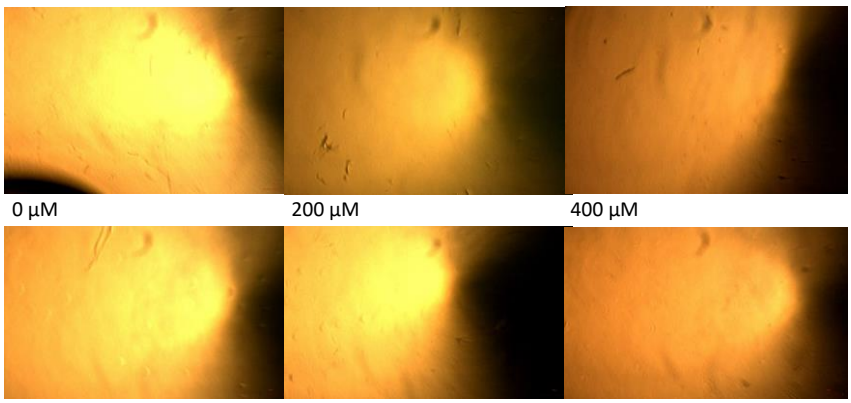

Appendix 3: Solubility evaluation of TMZ. TMZ was found to be soluble in media, ranging from 0-1000 µM. Images shown at x40 magnification.

3-Methyl-4-oxo-imidazo[5,1-d][1,2,3,5]tetrazine-8-carboxylic acid – (**TMZ Acid**)

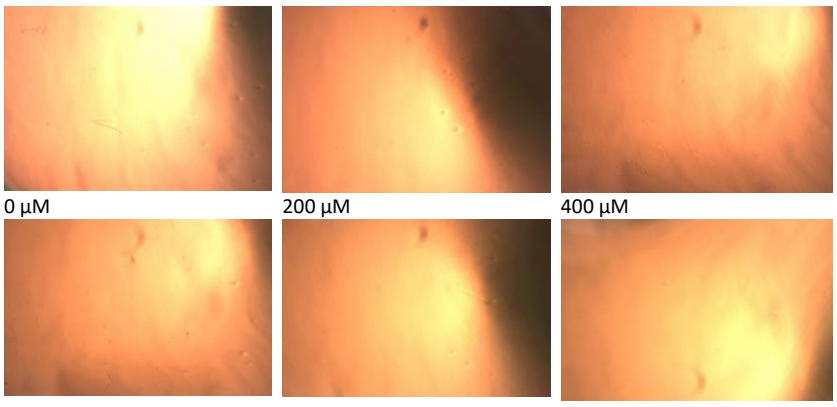

Appendix 4: Solubility evaluation of TMZ Acid. TMZ Acid was found to be soluble in media, ranging from 0-1000 µM. Images shown at x40 magnification.

Ethyl 3-methyl-4-oxo-3,4-dihydroimidazo[5,1-d][1,2,3,5]tetrazine-8-carboxylate - (ES1)

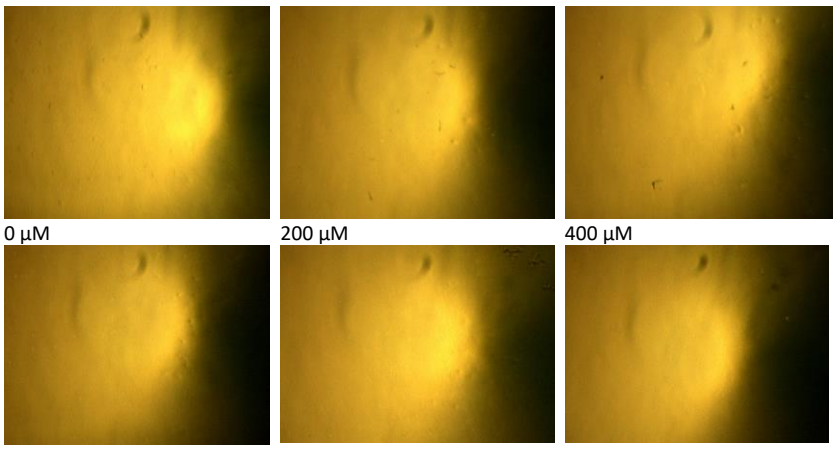

Appendix 5: Solubility evaluation of ES1. ES1 (0-1000 µM) was found to be soluble in media. Images shown at x40 magnification.

Hexyl 3-methyl-4-oxo-imidazo[5,1-d][1,2,3,5]tetrazine-8-carboxylate – (**ES2**)

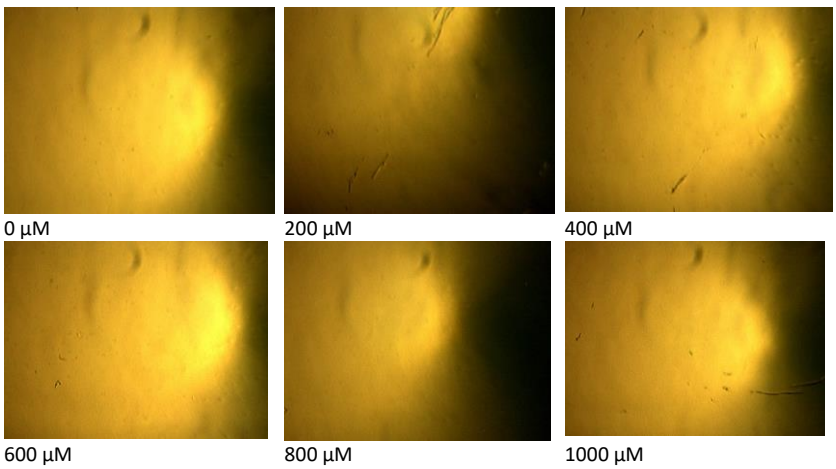

Appendix 6: Solubility evaluation of ES2. ES2 was found to be soluble in media, ranging from 0-1000 µM. Images shown at x40 magnification.

Phenethyl 3-methyl-4-oxo-imidazo[5,1-d][1,2,3,5]tetrazine-8-carboxylate – (**ES3**)

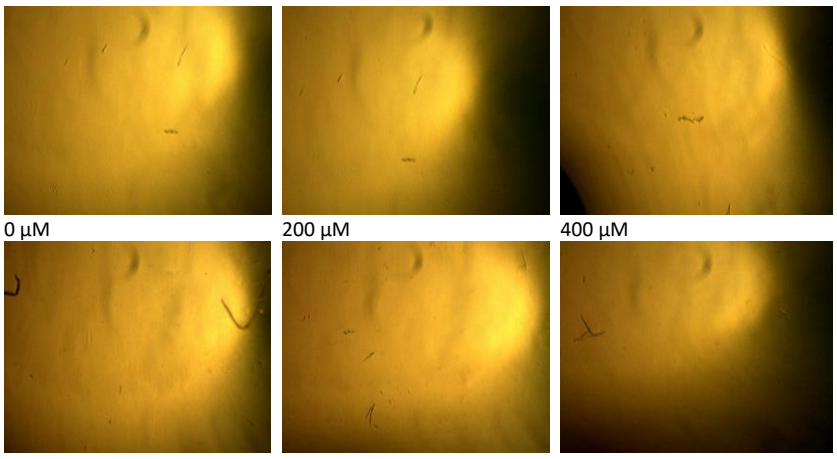

Appendix 7: Solubility evaluation of ES3. ES3 was found to be soluble in media, ranging from 0-1000 µM. Images shown at x40 magnification.

2-(4-Nitrophenyl)ethyl 3-methyl-4-oxo-imidazo[5,1-d][1,2,3,5]tetrazine-8-carboxylate – (**ES4**)

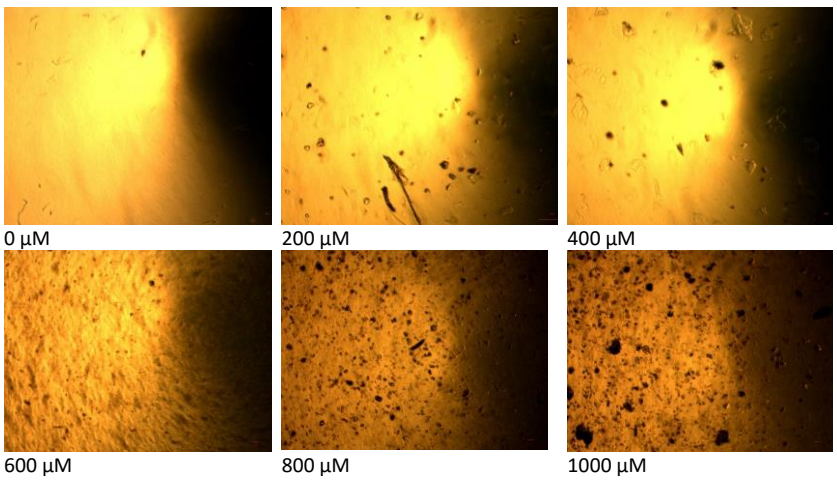

Appendix 8: Solubility evaluation of ES4. ES4 was found to be insoluble in media. Images shown at x40 magnification.

2-(4-Methoxyphenyl)ethyl 3-methyl-4-oxo-imidazo[5,1-d][1,2,3,5]tetrazine-8-carboxylate (**ES5**)

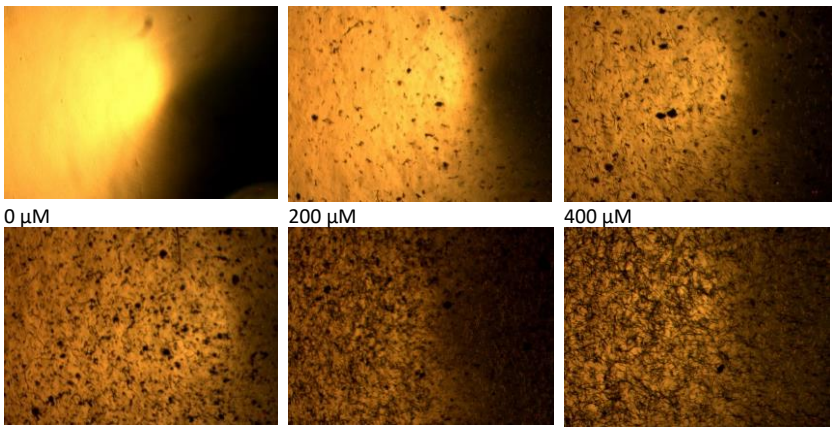

Appendix 9: Solubility evaluation of ES5. ES5 was found to be insoluble in media. Images shown at x40 magnification.

(4-Methoxyphenyl)methyl 3-methyl-4-oxo-imidazo[5,1-d][1,2,3,5]tetrazine-8-carboxylate (**ES6**)

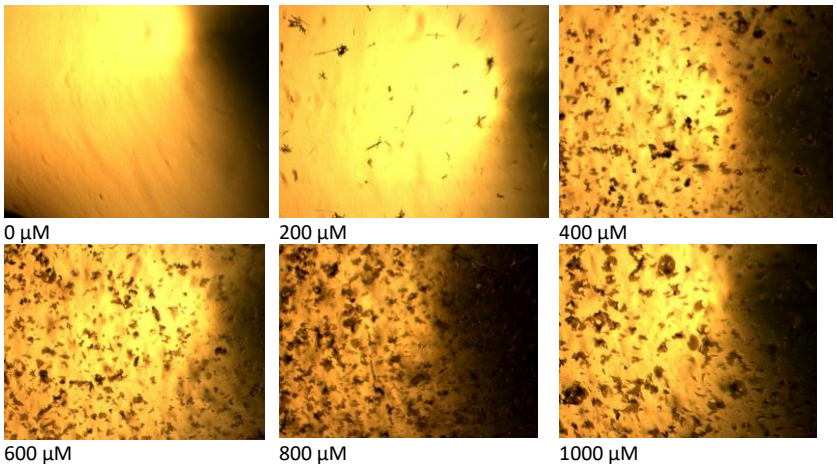

Appendix 10: Solubility evaluation of ES6. ES6 was found to be insoluble in media. Images shown at x40 magnification

3-(Dimethylamino)propyl 3-methyl-4-oxo-imidazo[5,1-d][1,2,3,5]tetrazine-8-carboxylate (**ES7**)

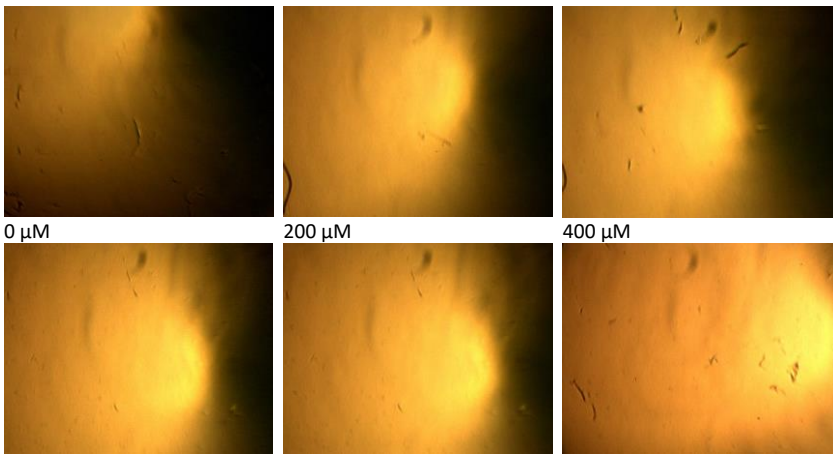

Appendix 11: Solubility evaluation of ES7. ES7 was found to be soluble in media, ranging from 0-1000 µM. Images shown at x40 magnification.

(4-Methoxyphenyl) 3-methyl-4-oxo-imidazo[5,1-d][1,2,3,5]tetrazine-8-carboxylate – (**ES8**)

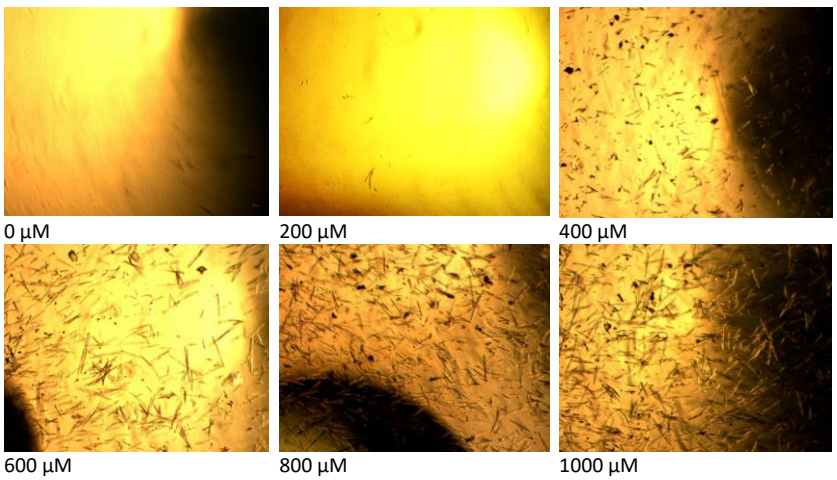

Appendix 12: Solubility evaluation of ES8. ES8 was found to be soluble in media, ranging from 0-200 µM. Images shown at x40 magnification

(4-Nitrophenyl) 3-methyl-4-oxo-imidazo[5,1-d][1,2,3,5]tetrazine-8-carboxylate – (**ES9**)

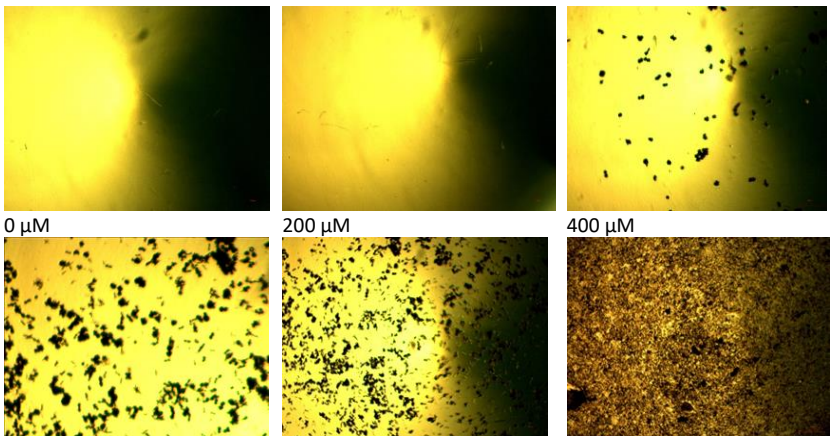

Appendix 13: Solubility evaluation of ES9. ES9 was found to be soluble in media, ranging from 0-200 µM. Images shown at x40 magnification.

(4-Chlorophenyl) 3-methyl-4-oxo-imidazo[5,1-d][1,2,3,5]tetrazine-8-carboxylate – (ES10)

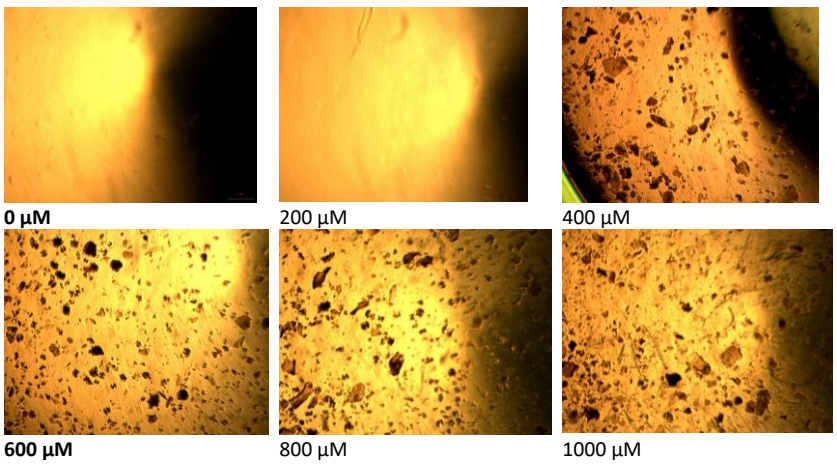

Appendix 14: Solubility evaluation of ES10. ES10 was found to be soluble in media, ranging from 0-200 µM. Images shown at x40 magnification

(4-Cyanophenyl) 3-methyl-4-oxo-imidazo[5,1-d][1,2,3,5]tetrazine-8-carboxylate - (ES11)

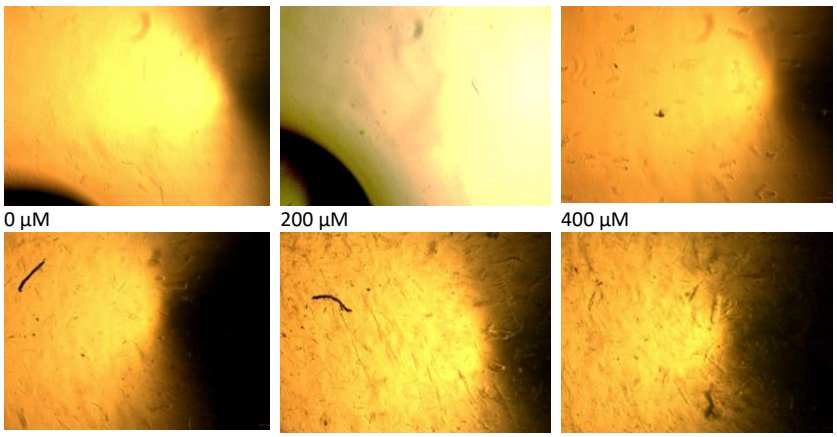

Appendix 15: Solubility evaluation of ES11. ES11 was found to be soluble in media, ranging from 0-200 µM. Images shown at x40 magnification.

Phenyl 3-methyl-4-oxo-imidazo[5,1-d][1,2,3,5]tetrazine-8-carboxylate – (ES12)

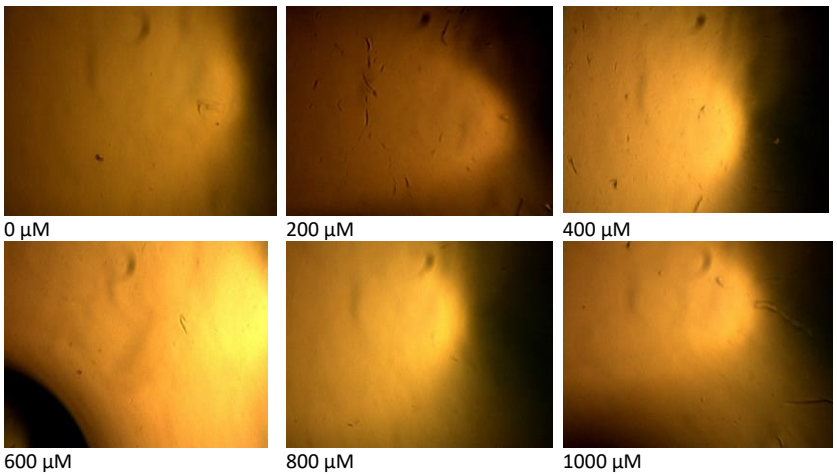

Appendix 16: Solubility evaluation of ES12. ES12 was found to be soluble in media, ranging from 0-1000 µM. Images shown at x40 magnification.

(2-Methoxyphenyl) 3-methyl-4-oxo-imidazo[5,1-d][1,2,3,5]tetrazine-8-carboxylate – (ES13)

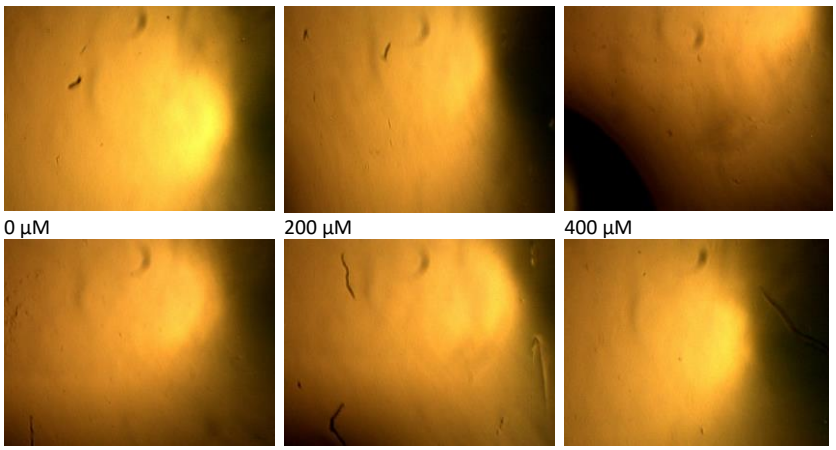

Appendix 17: Solubility evaluation of ES13. ES13 was found to be soluble in media, ranging from 0-1000 µM. Images shown at x40 magnification.

p-Tolyl 3-methyl-4-oxo-imidazo[5,1-d][1,2,3,5]tetrazine-8-carboxylate – (ES14)

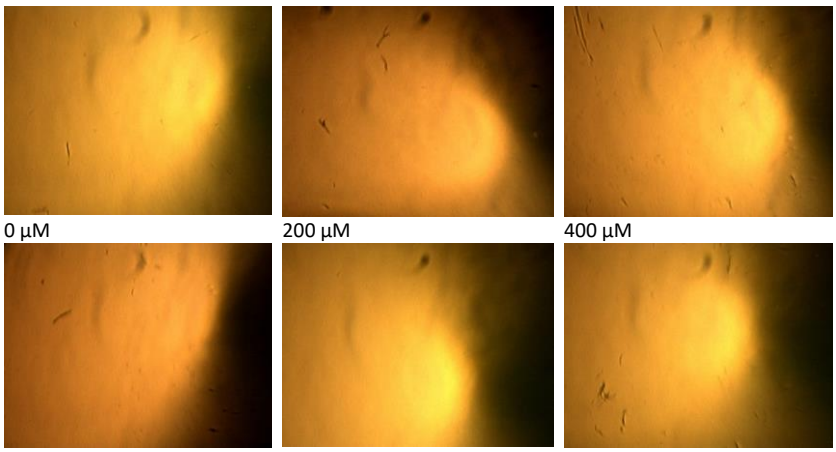

Appendix 18: Solubility evaluation of ES14. was found to be soluble in media, ranging from 0-1000 µM. Images shown at x40 magnification

N-Hexyl-3-methyl-4-oxo-imidazo[5,1-d][1,2,3,5]tetrazine-8-carboxamide – (**AM1**)

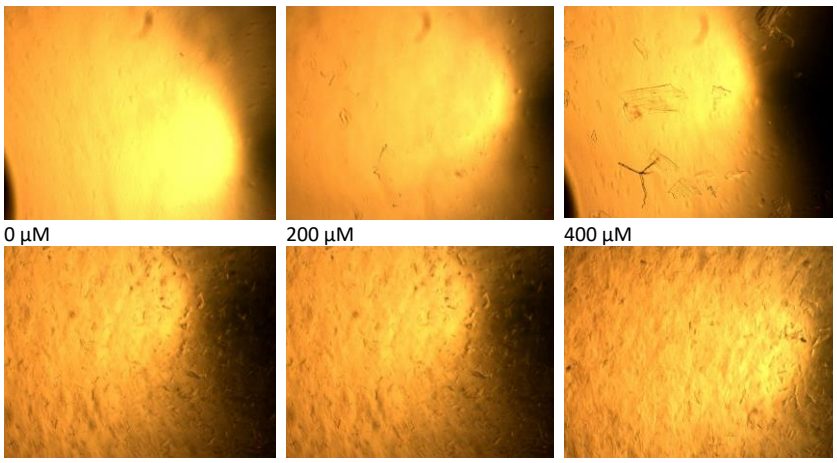

Appendix 19: Solubility evaluation of AM1. AM1 was found to be soluble in media, ranging from 0-200 µM. Images shown at x40 magnification.

3-Methyl-4-oxo-N-phenethyl-imidazo[5,1-d][1,2,3,5]tetrazine-8-carboxamide – (**AM2**)

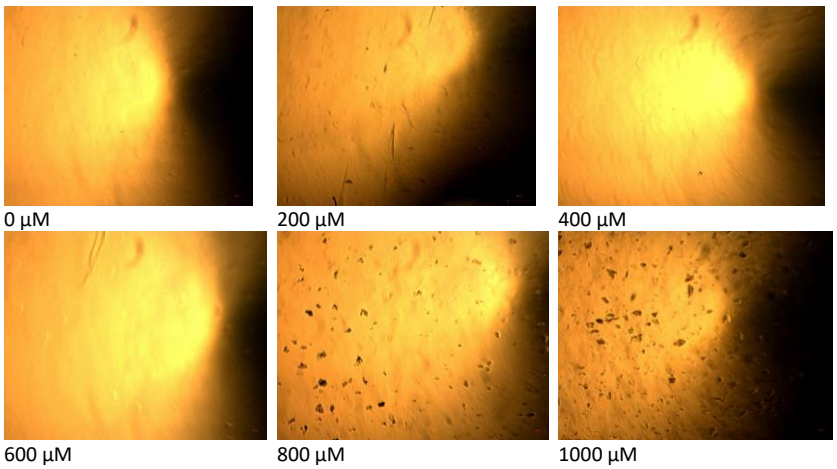

Appendix 20: Solubility evaluation of AM2. AM2 was found to be soluble in media, ranging from 0-600 µM. Images shown at x40 magnification.

3-Methyl-4-oxo-N-phenyl-imidazo[5,1-d][1,2,3,5]tetrazine-8-carboxamide – (**AM3**)

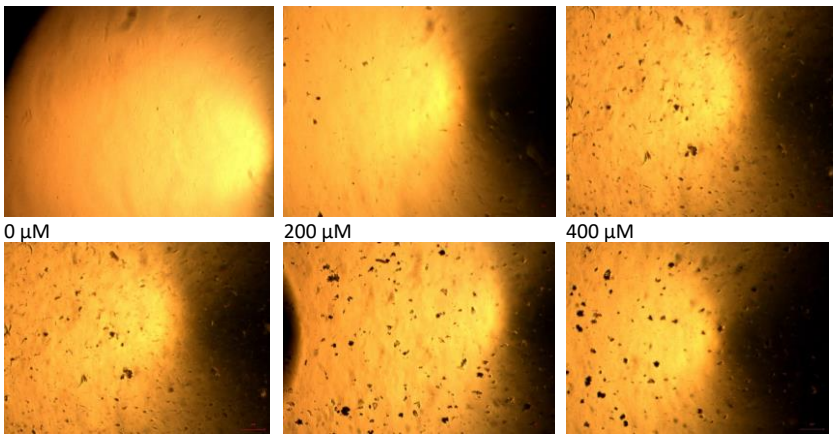

Appendix 21: Solubility evaluation of AM3. AM3 was found to be soluble in media, ranging from 0-200 µM media. Images shown at x40 magnification.

N-(4-Methoxyphenyl)-3-methyl-4-oxo-imidazo[5,1-d][1,2,3,5]tetrazine-8-carboxamide – (**AM4**)

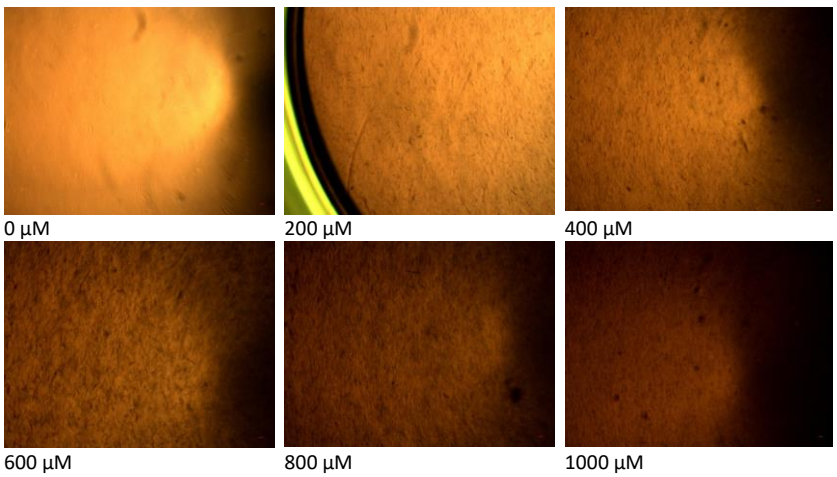

Appendix 22: Solubility evaluation of AM4. AM4 was found to be insoluble in media. Images shown at x40 magnification

N-(4-Chlorophenyl)-3-methyl-4-oxo-imidazo[5,1-d][1,2,3,5]tetrazine-8-carboxamide – (**AM5**)

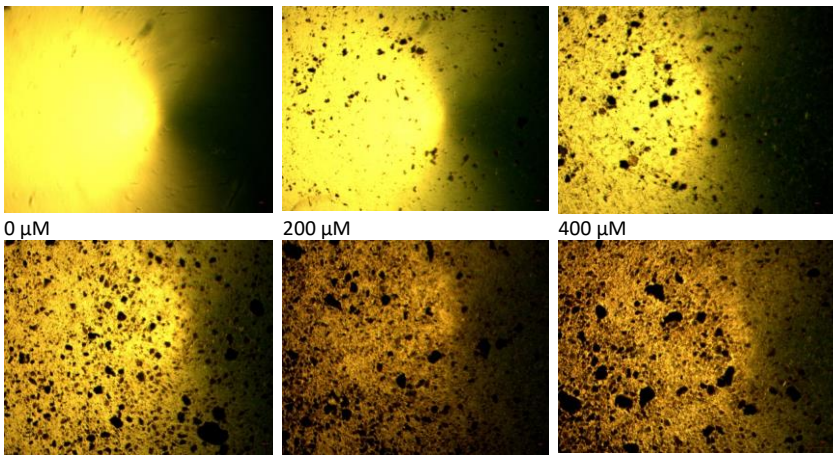

Appendix 23: Solubility evaluation of AM5. AM5 was found to be insoluble in media. Images shown at x40 magnification.

N-(4-Cyanophenyl)-3-methyl-4-oxo-imidazo[5,1-d][1,2,3,5]tetrazine-8-carboxamide – (**AM6**)

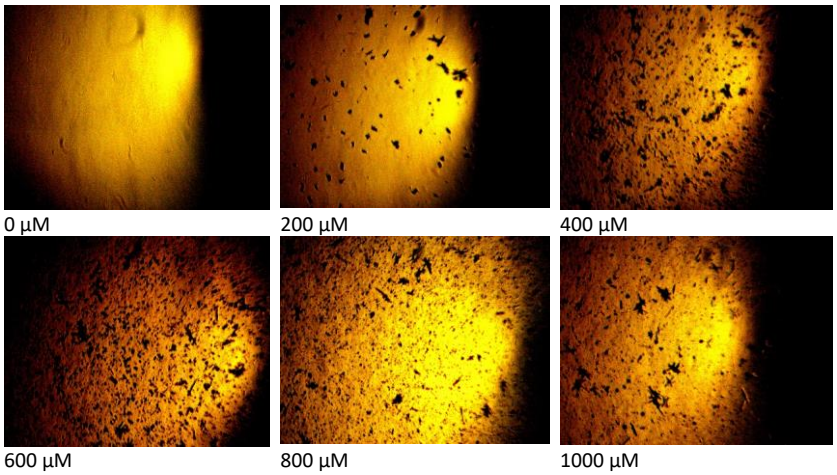

Appendix 24: Solubility evaluation of AM6. AM6 was found to be insoluble in media. Images shown at x40 magnification.

3-Methyl-4-oxo-N-(p-tolyl)imidazo[5,1-d][1,2,3,5]tetrazine-8-carboxamide – (**AM7**)

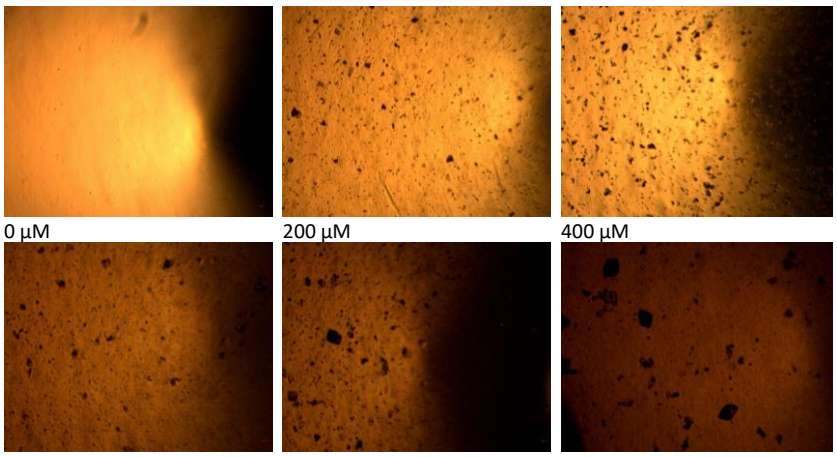

Appendix 25: Solubility evaluation of AM7. AM7 was found to be insoluble in media. Images shown at x40 magnification.

N-(2-Methoxyphenyl)-3-methyl-4-oxo-imidazo[5,1-d][1,2,3,5]tetrazine-8-carboxamide – (**AM8**)

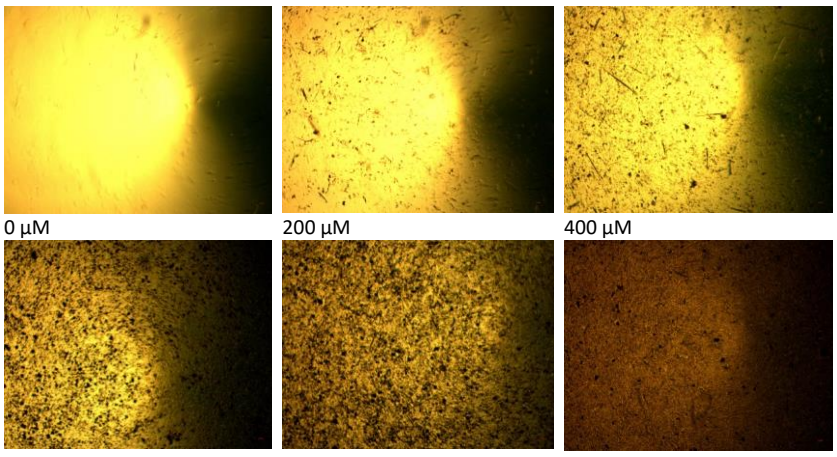

Appendix 26: Solubility evaluation of AM8. AM8 was found to be insoluble in media. Images shown at x40 magnification.

N-[(4-Methoxyphenyl)methyl]-3-methyl-4-oxo-imidazo[5,1-d][1,2,3,5]tetrazine-8-carboxamide - (**AM9**)

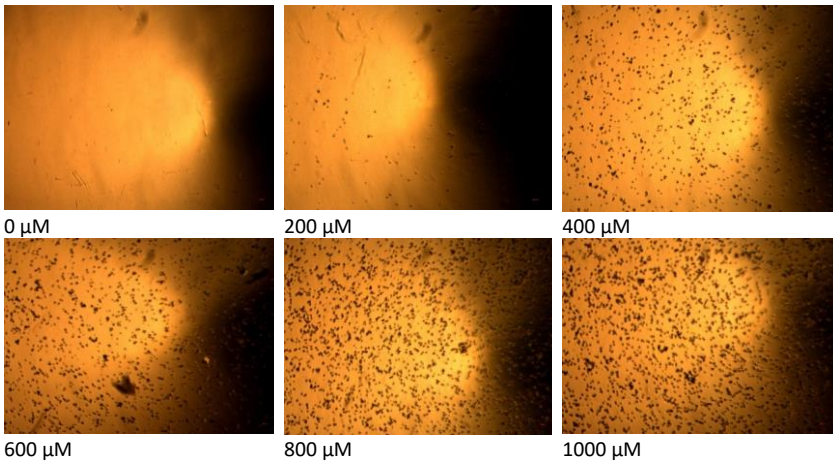

Appendix 27: Solubility evaluation of AM9. AM9 was found to be insoluble in media. Images shown at x40 magnification.

3-Methyl-4-oxo-N-(p-tolylmethyl)imidazo[5,1-d][1,2,3,5]tetrazine-8-carboxamide – (**AM10**)

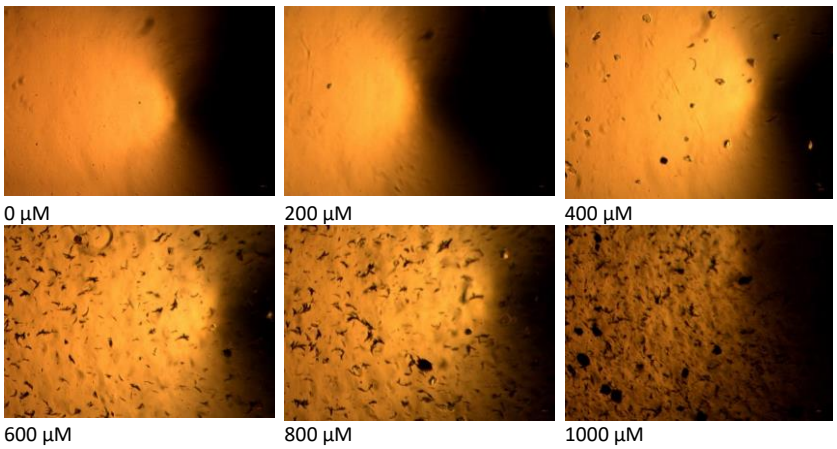

Appendix 28: Solubility evaluation of AM10. AM10 was found to be soluble in media, ranging from 0-200 µM. Images shown at x40 magnification

N-[(4-Chlorophenyl)methyl]-3-methyl-4-oxo-imidazo[5,1-d][1,2,3,5]tetrazine-8-carboxamide – (AM11)

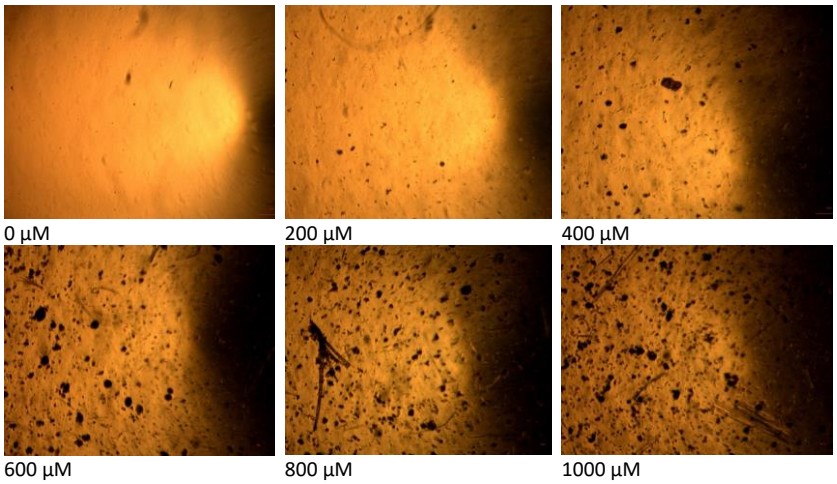

Appendix 29: Solubility evaluation of AM11. AM11 was found to be insoluble in media. Images shown at x40 magnification.

Appendix 3c: Graphs to Show the Antiproliferative Determination of Each Analogue Against Various Cell Lines

The following figures indicate the relationship between concentration of each drug and the viability of cells following 6 days of incubation. Each experiment was carried out in triplicate and the IC_{50} was calculated plus/minus standard deviation.

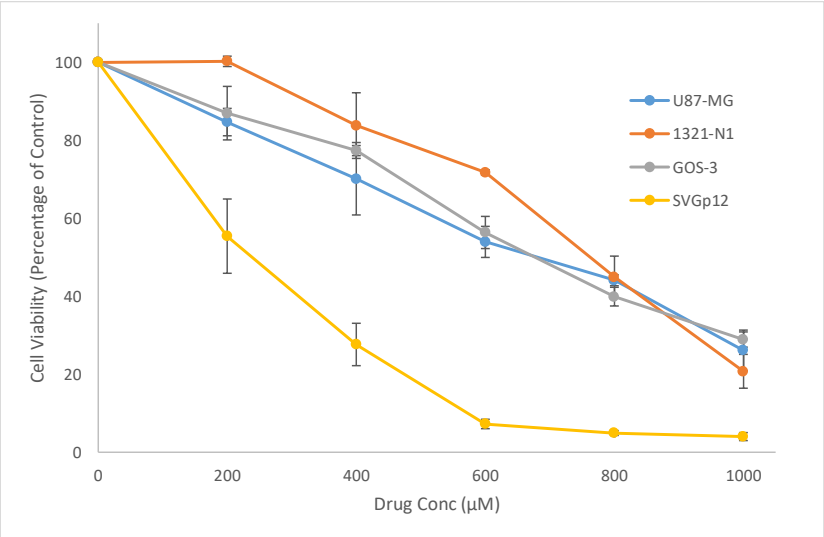

Appendix 30: **IC_{50} evaluation of temozolomide.** Temozolomide (0-1000 µM) inhibits growth of U87-MG, 1321-N1, GOS-3 and SVGp12 cell lines with IC_{50} values of 696±79, 783±40, 698±15, 239±6, respectively. The data values displayed are mean ± SD, (n=3). Polynomial regression equations used to calculate IC_{50} values are as follows: U87-MG - $y = 3E\text{-}06x^2 - 0.075x + 99.73$; 1321-N1 – $y = -7E\text{-}05x^2 – 0.0091x + 101.52$; GOS-3 – $y = -8E\text{-}06x^2 – 0.0663x + 100.86$; SVGp12 – $y = 0.0001x^2 – 0.2361x + 98.819$.

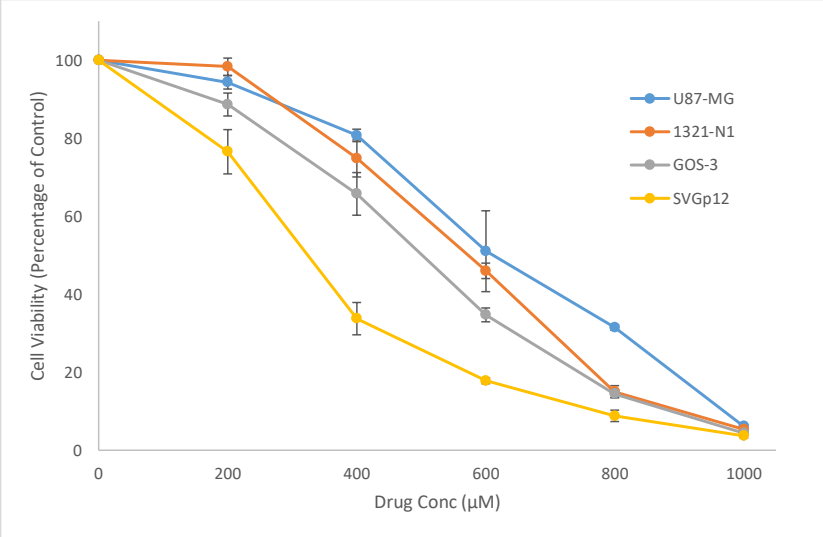

Appendix 31: **IC_{50} evaluation of temozolomide acid**. Temozolomide acid (0-1000 µM) inhibits growth of U87-MG, 1321-N1, GOS-3 and SVGp12 cell lines with IC_{50} values of 662±42, 596±26, 504±30 and 316±2, respectively. The data values displayed are mean ± SD, (n=3). Polynomial regression equations used to calculate IC_{50} values are as follows: U87-MG - $y = 5E\text{-}05x^2 - 0.0437x + 102.45$; 1321-N1 – $y = -3E\text{-}05x^2 – 0.0762x + 106.14$; GOS-3 – $y = 8E\text{-}06x^2 – 0.1121x + 104.6$; SVGp12 – $y = 0.0001x^2 – 0.2014x + 103.65$.

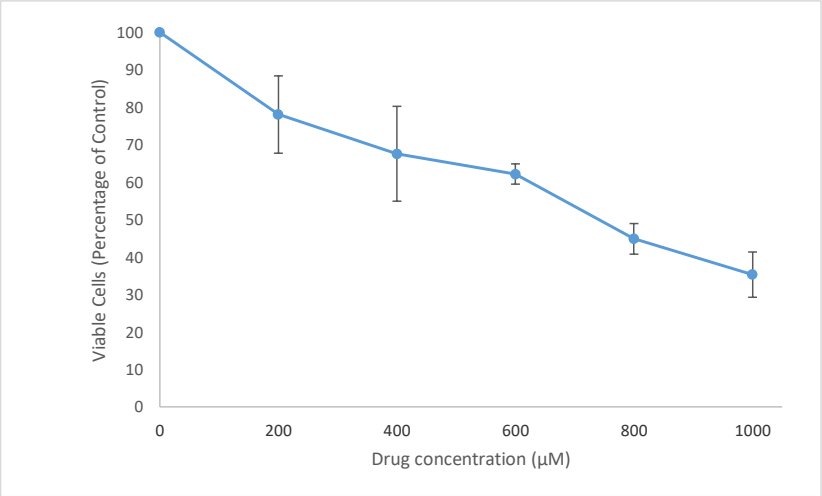

Appendix 32: ***IC_{50} evaluation of ES1.*** *ES1 (0-1000 µM) inhibits growth of U87-MG cell line, with an IC_{50} of 700.55±108.59 µM. The data values displayed are mean ± SD, (n=3). This compound was eliminated from further testing due to poor potency compared to TMZ.* Polynomial regression equations used to calculate IC_{50} values are as follows: U87-MG - $y = 2E\text{-}05x^2 - 0.0767x + 97.325$.

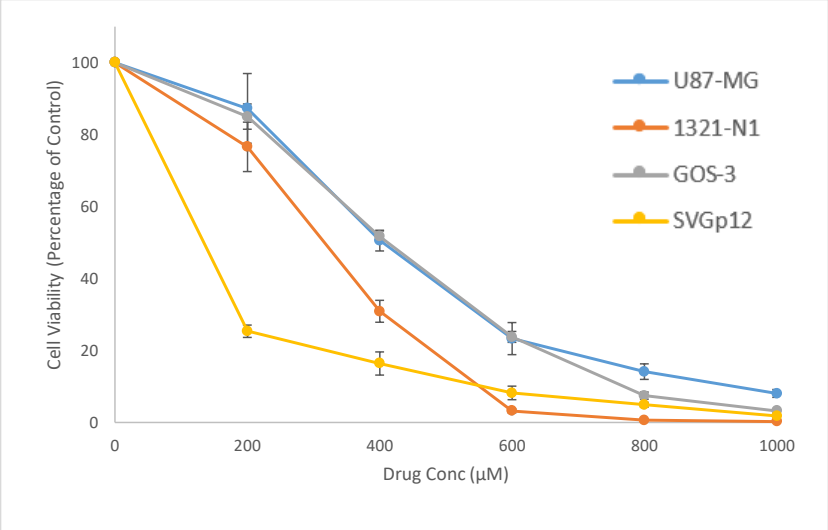

Appendix 33: ***IC_{50} evaluation of ES2****. ES2 (0-1000 µM) inhibits growth of U87-MG, 1321-N1, GOS-3 and SVGp12 cell lines, with IC_{50} values of 409±45, 269±20, 400±4 and 182±11 µM, respectively.* Polynomial regression equations used to calculate IC_{50} values are as follows: U87-MG - $y = 6E\text{-}05x^2 - 0.165x + 106.22$; 1321-N1 – $y = 0.0001x^2 – 0.2361x + 106.26$; GOS-3 – $y = 5E\text{-}05x^2 – 0.1607x + 105.61$; SVGp12 – $y = 0.0002x^2 – 0.2499x + 88.783$.

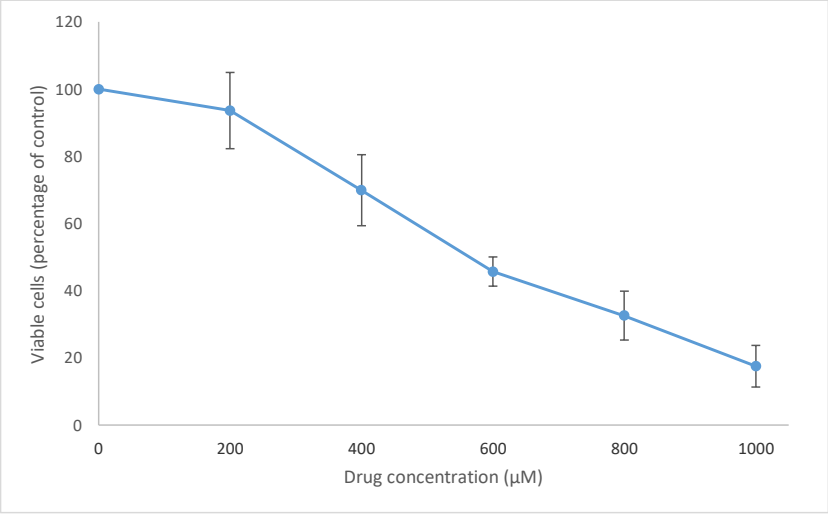

Appendix 34: ***IC_{50} evaluation of ES3.*** *ES3 (0-1000 µM) inhibits growth of U87-MG cell line, with an IC_{50} of 615±96 µM. The data values displayed are mean ± SD, (n=3). This compound was eliminated from further testing due to poor potency compared to TMZ.* Polynomial regression equations used to calculate IC_{50} values are as follows: U87-MG - $y = -4E\text{-}07x^2 - 0.0881x + 104.09$.

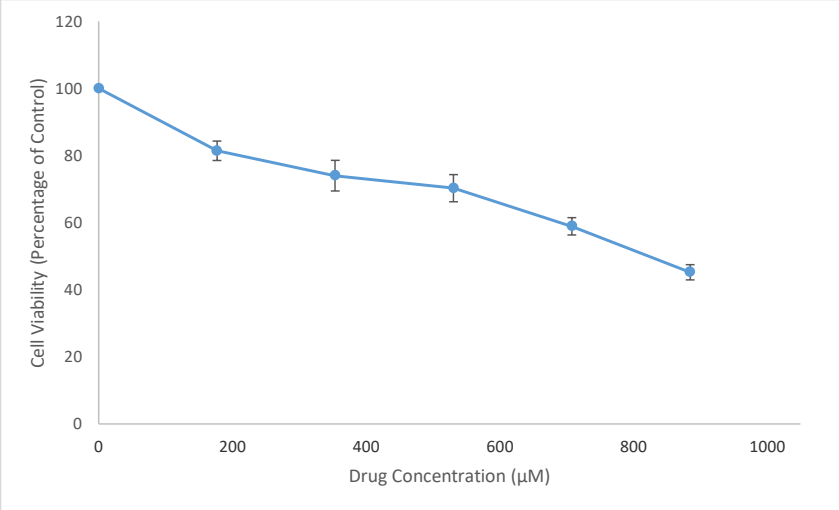

Appendix 35: ***IC_{50} evaluation of ES7.*** *ES7 (0-1000 µM) inhibits growth of U87-MG cell line, with an IC_{50} of 856±20 µM. The data values displayed are mean ± SD, (n=3). This compound was eliminated from further testing due to poor potency compared to TMZ.* Polynomial regression equations used to calculate IC_{50} values are as follows: U87-MG - $y = 5E\text{-}06x^2 - 0.0601x + 96.801$.

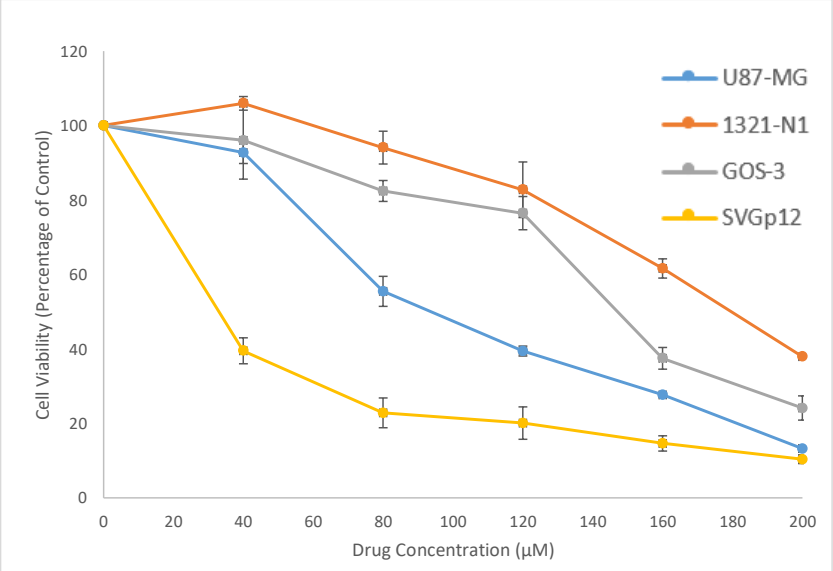

Appendix 36: ***IC_{50} evaluation of ES8.*** *ES8 (0-200 µM) inhibits the growth of U87-MG, 1321-N1 GOS-2 and SVGp12 cell lines, with IC_{50} values of 103±6, 183±0.4, 155±5 and 44±2 µM, respectively. The data values displayed are mean ± SD, (n=3).* Polynomial regression equations used to calculate IC_{50} values are as follows: U87-MG - $y = 0.0005x^2 - 0.4367x + 99.595$; 1321-N1 – $y = 0.0021x^2 – 0.0888x + 101.84$; GOS-3 – $y = 0.0017x^2 – 0.0693x + 100.65$; SVGp12 – $y = 0.0036x^2 – 1.1033x + 91.518$.

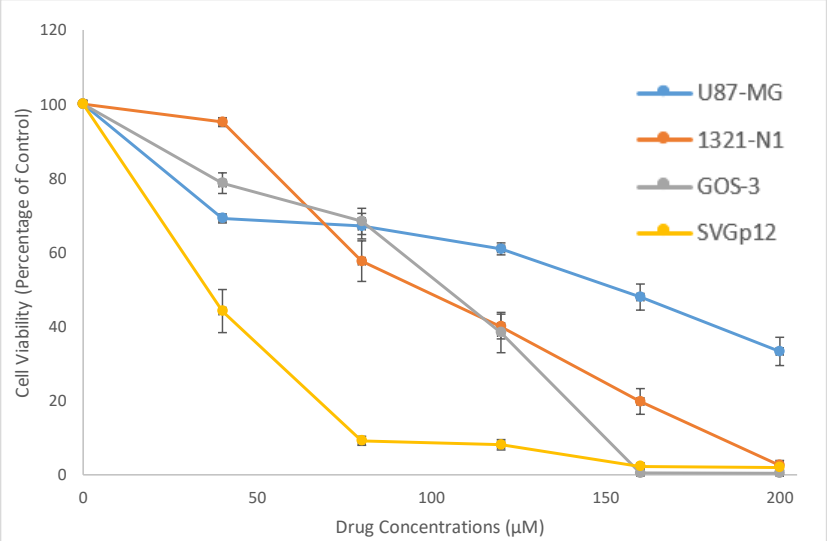

Appendix 37: ***IC_{50} evaluation of ES9.*** *ES9 (0-200 µM) inhibits growth of U87-MG, 1321-N1, GOS-3 and SVGp12 cell lines, with IC_{50} values of 142±3, 106±7, 96±1 and 39±2 µM, respectively. The data values displayed are mean ± SD, (n=3).* Polynomial regression equations used to calculate IC_{50} values are as follows: U87-MG - $y = 0.0004x^2 - 0.3712x + 94.096$; 1321-N1 – $y = 8E\text{-}05x^2 – 0.5382x + 105.16$; GOS-3 – $y = -5E\text{-}05x^2 – 0.5355x + 101.94$; SVGp12 – $y = 0.0044x^2 – 1.3207x + 95.15$.

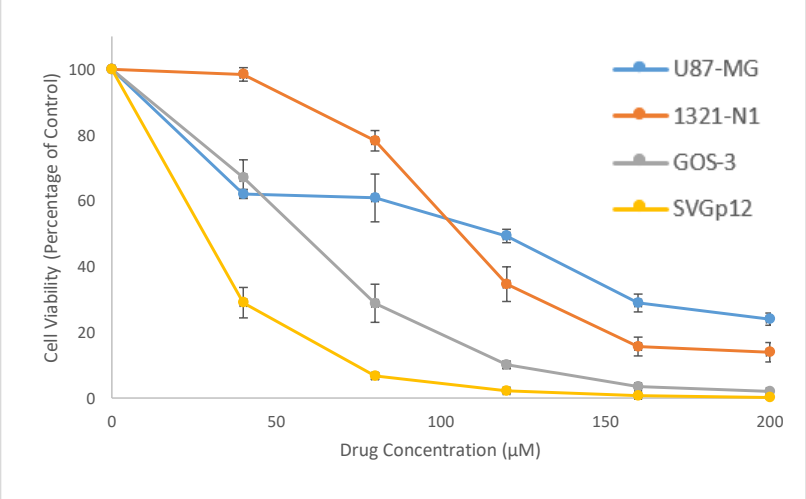

Appendix 38: ***IC_{50} evaluation of ES10.*** *ES10 (0-200 µM) inhibits growth of U87-MG, 1321-N1, GOS-3 and SVGp12 cell lines, with IC_{50} values of 96±3, 118±11, 54±4 and 33±1 µM, respectively. The data values displayed are mean ± SD, (n=3).* Polynomial regression equations used to calculate IC_{50} values are as follows: U87-MG - $y = 0.001x^2 - 0.548x + 94.53$; 1321-N1 – $y = 4E\text{-}05x^2 – 0.5247x + 108.65$; GOS-3 – $y = 0.0032x^2 – 1.1334x + 102.1$; SVGp12 – $y = 0.0049x^2 – 1.3925x + 91.093$.

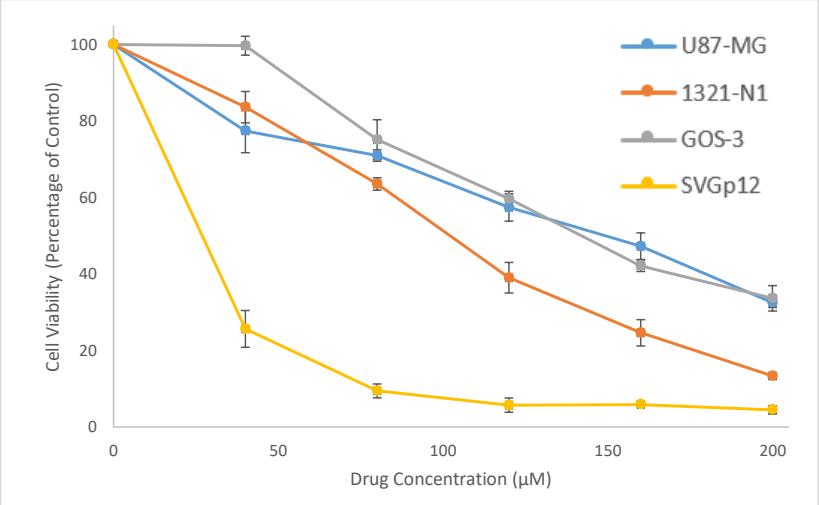

Appendix 39: ***IC_{50} evaluation of ES11.*** *ES11 (0-200 µM) inhibits growth of U87-MG, 1321-N1, GOS-3 and SVGp12 cell lines, with IC_{50} values of 142±5, 103±7, 151±4 and 36±3 µM, respectively. The data values displayed are mean ± SD, (n=3).* Polynomial regression equations used to calculate IC_{50} values are as follows: U87-MG - $y = 0.0003x^2 - 0.3693x + 97.245$; 1321-N1 – $y = 0.0005x^2 – 0.5609x + 102.24$; GOS-3 – $y = 0.0001x^2 – 0.3431x + 104.75$; SVGp12 – $y = 0.0048x^2 – 1.3464x + 89.42$.

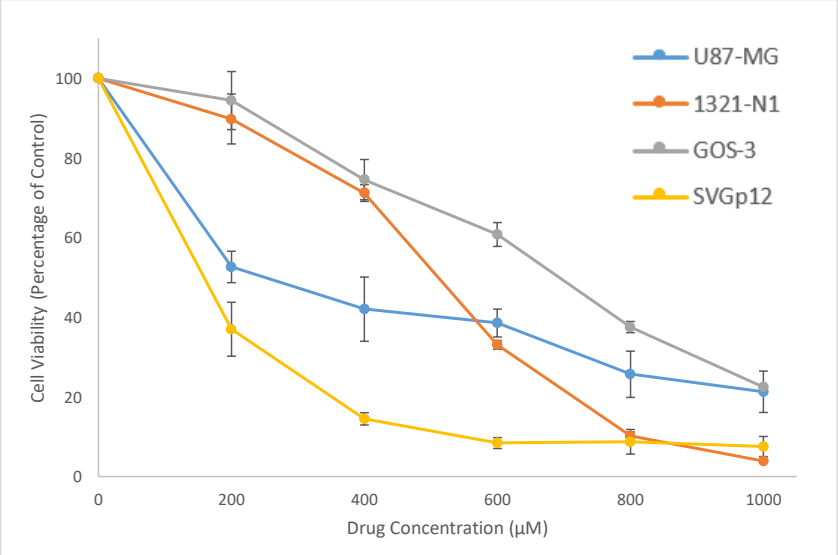

Appendix 40: ***IC_{50} evaluation of ES12.*** *ES12 (0-1000 µM) inhibits growth of U87-MG, 1321-N1, GOS-2 and SVGp12 cell lines, with IC_{50} values of 331±47, 510±10, 691±34 and 238±6 µM, respectively. The data values displayed are mean ± SD, (n=3).* Polynomial regression equations used to calculate IC_{50} values are as follows: U87-MG - $y = 9E\text{-}05x^2 - 0.1601x + 93.085$; 1321-N1 – $y = 1E\text{-}06x^2 – 0.1093x + 105.6$; GOS-3 – $y = -3E\text{-}05x^2 – 0.0545x + 102.19$; SVGp12 – $y = 0.0002x^2 – 0.2578x + 92.704$.

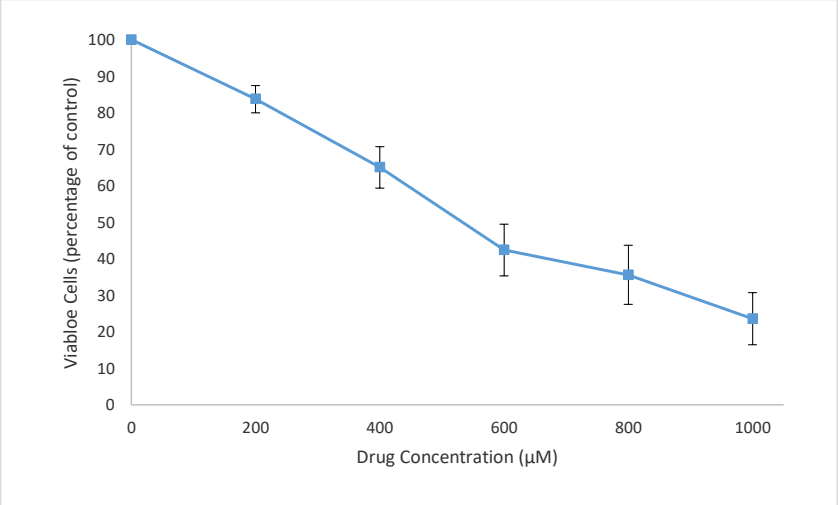

Appendix 41: ***IC_{50} evaluation of ES13.*** *ES13 (0-1000 µM) inhibits growth of U87-MG cell line, with an IC_{50} of 567±92 µM. The data values displayed are mean ± SD, (n=3). This compound was eliminated from further testing due to poor potency compared to TMZ.* Polynomial regression equations used to calculate IC_{50} values are as follows: U87-MG - $y = 7E\text{-}05x^2 - 0.1577x + 99.012$.

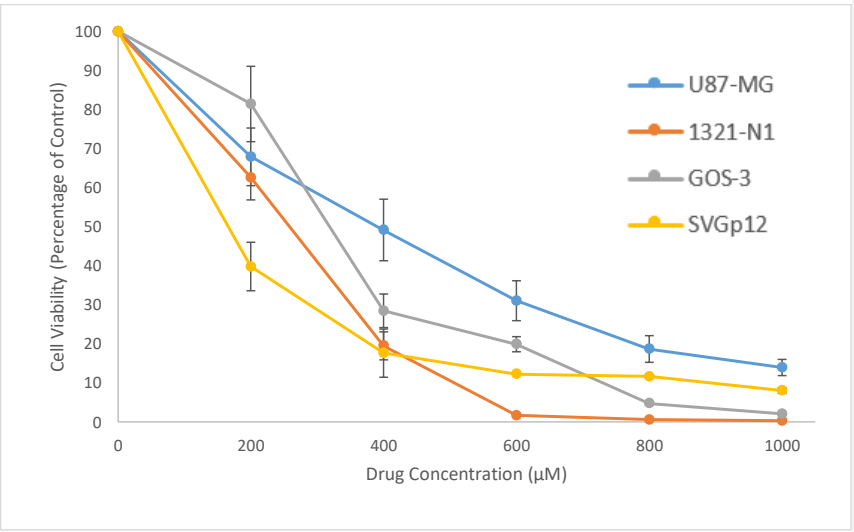

Appendix 42: ***IC_{50} evaluation of ES14.*** *ES14 (0-1000 µM) inhibits growth of U87-MG, 1321-N1, GOS-3, SVGp12 cell lines, with IC_{50} values of 376±62, 238±8, 314±38 and 215±26 µM, respectively. The data values displayed are mean ± SD, (n=3).* Polynomial regression equations used to calculate IC_{50} values are as follows: U87-MG - $y = 7E\text{-}05x^2 - 0.1577x + 99.012$; 1321-N1 – $y = 0.0002x^2 – 0.2584x + 101.99$; GOS-3 – $y = 0.0001x^2 – 0.2071x + 105.17$; SVGp12 – $y = 0.0002x^2 – 0.2434x + 92.792$.

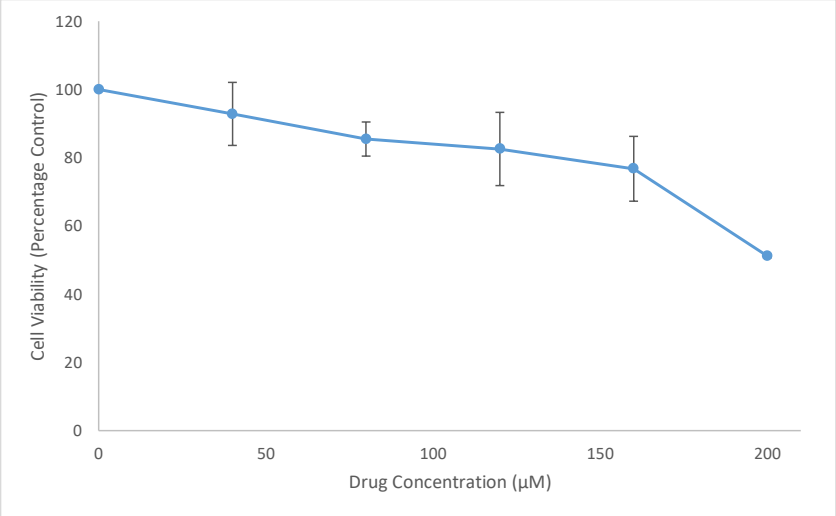

Appendix 43: ***IC_{50} evaluation of AM1.*** *AM1 (0-200 µM) inhibits growth of U87-MG cell line. IC_{50} could not be generated from the data without extrapolating past measured data points. The data values displayed are mean ± SD, (n=3). This compound was eliminated from further testing due to poor potency compared to TMZ.*

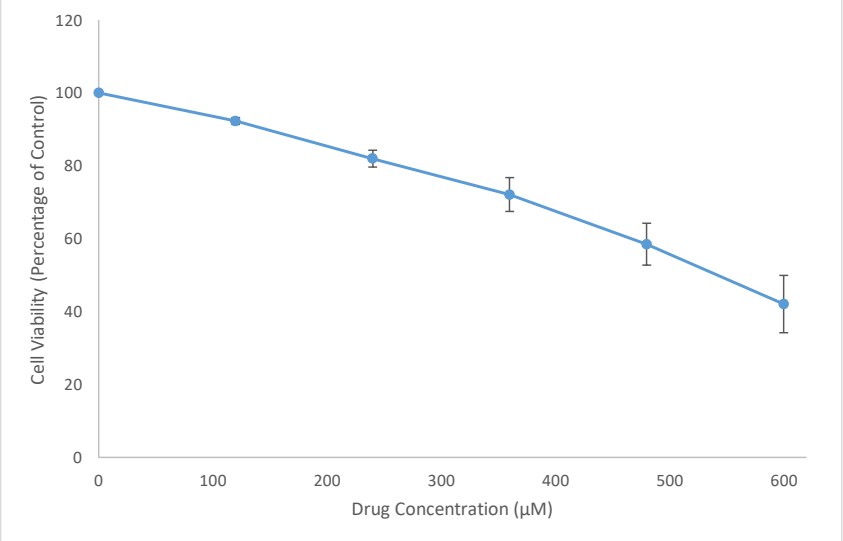

Appendix 44: ***IC_{50} evaluation of AM2.*** *AM2 (0-600 µM) inhibits growth of U87-MG cell line, with an IC_{50} of 548±48. The data values displayed are mean ± SD, (n=3). This compound was eliminated from further testing due to poor potency compared to TMZ.* Polynomial regression equations used to calculate IC_{50} values are as follows: U87-MG - $y = -7E\text{-}05x^2 - 0.0532x + 99.742$.

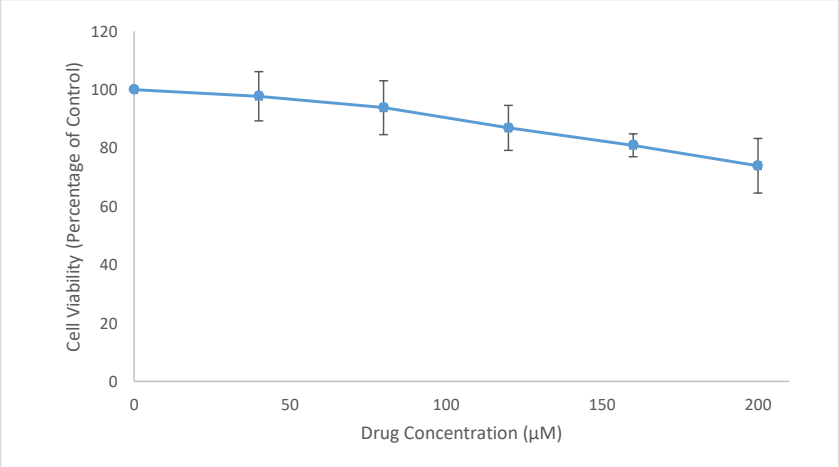

Appendix 45: ***IC_{50} evaluation of AM3.*** *AM3 (0-200 µM) inhibits growth of U87-MG cell line. IC_{50} could not be generated from the data without extrapolating past measured data points. The data values displayed are mean ± SD, (n=3). This compound was eliminated from further testing due to poor potency compared to TMZ.*

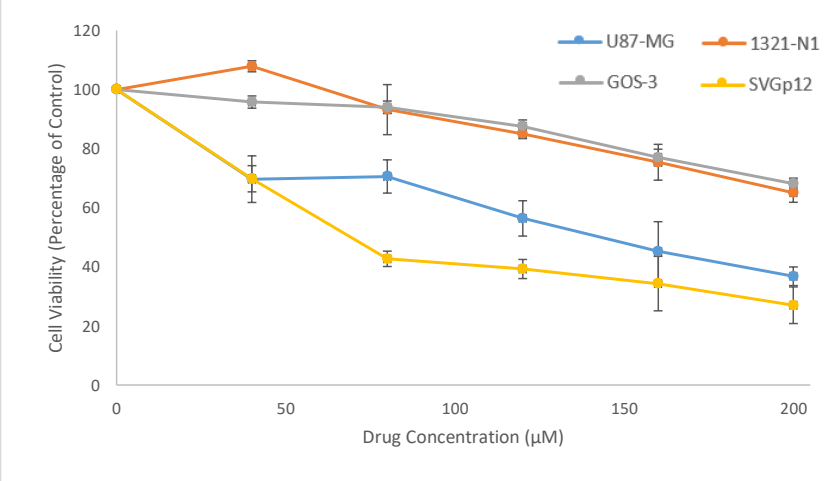

Appendix 46: ***IC_{50} evaluation of AM10.*** *AM10 (0-200 µM) inhibits growth of U87-MG, 1321-N1, GOS-2 and SVGp12 cell lines. The IC_{50} values for U87-MG and SVGp12 are 139±28 and 79±6, respectively. IC_{50} values for 1321-N1 and GOS-3 could not be generated, due to a lack of activity. The data values displayed are mean ± SD, (n=3).* Polynomial regression equations used to calculate IC_{50} values are as follows: U87-MG - $y = 0.0007x^2 - 0.4251x + 95.586$; 1321-N1 – $y = -0.0008x^2 – 0.0422x + 103.57$; GOS-3 – $y = -0.0007x^2 – 0.0282x + 99.481$; SVGp12 – $y = 0.0023x^2 – 0.7925x + 98.188$.

Appendix to Chapter 4

Appendix 4a: Repeatability of TMZ acid, TMZ esters and Corresponding Alcohols Using HPLC

TMZ Acid (103 µM)	
Injection	**PA**
1	970246
2	970389
3	968042
4	971509
5	967882
6	969240
Average	969551.33
SD	1426.77
RSD	0.15%

Appendix 47: Repeatability of TMZ acid (103 µM) over 6 injections.

ES8 (66 µM)	
Injection	**PA**
1	826976
2	820152
3	820481
4	825462
5	825951
6	814193
Average	822202.50
SD	4874.06
RSD	0.59%

Appendix 48: Repeatability of ES8 (66 µM) over 6 injections.

4-Methoxyphenol (162 µM)	
Injection	**PA**
1	623139
2	622380
3	624173
4	623183
5	621095
6	623442
Average	622902.00
SD	1056.40
RSD	0.17%

Appendix 49: Repeatability of 4-methoxyphenol (162 µM) over 6 injections.

ES9 (63 µM)	
Injection	**PA**
1	935362
2	946376
3	936223
4	945668
5	927576
6	940022
Average	938537.83
SD	7072.27
RSD	0.75%

Appendix 50: Repeatability of ES9 (63 µM) over 6 injections.

4-Nitrophenol (144 µM)	
Injection	**PA**
1	1476342
2	1472228
3	1496376
4	1490570
5	1465367
6	1478730
Average	1479935.50
SD	11570.62
RSD	0.78%

Appendix 51: Repeatability of 4-nitrophenol (144 µM) over 6 injections.

ES10 (66 µM)	
Injection	**PA**
1	792054
2	794655
3	794323
4	792464
5	790458
6	790595
Average	792424.83
SD	1785.074
RSD	0.23%

Appendix 52: Repeatability of ES10 (66 µM) over 6 injections.

4-Chlorophenol (155 µM)	
Injection	**PA**
1	1336524
2	1303198
3	1321441
4	1331901
5	1308566
6	1315605
Average	1319539.17
SD	13021.81
RSD	0.99%

Appendix 53: Repeatability of 4-chlorophenol (155 µM) over 6 injections.

ES11 (68 µM)	
Injection	**PA**
1	888821
2	888193
3	892401
4	895825
5	881495
6	883476
Average	888368.50
SD	5353.084
RSD	0.60%

Appendix 54: Repeatability of ES11 (68 µM) over 6 injections.

4-Hydroxybenzonitrile (169 µM)	
Injection	**PA**
1	2983782
2	2990218
3	3001127
4	3015080
5	2970794
6	2977672
Average	2989778.83
SD	16199.28
RSD	0.54%

Appendix 55: Repeatability of 4-hydroxybenzonitrile (169 µM) over 6 injections.

ES12 (74 µM)	
Injection	**PA**
1	915420
2	918514
3	915893
4	914602
5	916190
6	916031
Average	916108.33
SD	1310.66
RSD	0.14%

Appendix 56: Repeatability of ES12 (74 µM) over 6 injections.

Phenol (251 µM)	
Injection	**PA**
1	352732
2	353484
3	352815
4	352359
5	352077
6	352420
Average	352647.83
SD	488.96
RSD	0.14%

Appendix 57: Repeatability of phenol (251 µM) over 6 injections.

ES13 (71 µM)	
Injection	**PA**
1	699869
2	722660
3	709228
4	711617
5	713206
6	724994
Average	713595.70
SD	9204.88
RSD	1.29%

Appendix 58: Repeatability of ES13 (71 µM) over 6 injections.

p-Cresol (185 µM)	
Injection	**PA**
1	844451
2	885658
3	864988
4	862930
5	862337
6	871207
Average	865261.8
SD	13405.27
RSD	1.55%

Appendix 59: Repeatability of ES13 (71 µM) over 6 injections.

Appendix 4b: Reproducibility of TMZ acid, TMZ esters and Corresponding Alcohols Using HPLC

TMZ Acid (103 µM)			
Sample	**PA1**	**PA2**	**AVG PA**
1	970246	970389	970317.50
2	968042	971509	969775.50
3	967882	969240	968561.00
4	954308	954020	954164.00
5	959385	961683	960534.00
6	940118	942527	941322.50
		Average	960779.10
		SD	7081.36
		RSD	0.74%

Appendix 60: Reproducibility of TMZ Acid (103 µM).

ES8 (66 µM)			
Sample	**PA1**	**PA2**	**AVG PA**
1	813894	826976	820435.00
2	820152	820481	820316.50
3	825462	825951	825706.50
4	814193	814975	814584.00
5	826795	825095	825945.00
6	806874	807085	806979.50
		Average	818994.40
		SD	7224.90
		RSD	0.88%

Appendix 61: Reproducibility of ES8 (66 µM).

4-Methoxyphenol (162 µM)			
Sample	**PA 1**	**PA2**	**AVG PA**
1	623139	622380	622759.50
2	624173	623183	623678.00
3	621095	623442	622268.50
4	613151	616580	614865.50
5	618205	623060	620632.50
6	607039	608646	607842.50
		Average	618674.40
		SD	3518.42
		RSD	0.57%

Appendix 62: Reproducibility of 4-methoxyphenol (162 µM).

ES9 (63 µM)			
Sample	**PA1**	**PA2**	**AVG PA**
1	936223	935362	935792.50
2	945668	946376	946022.00
3	927576	940022	933799.00
4	941346	906787	924066.50
5	928203	915913	922058.00
6	934340	934405	934372.50
		Average	932685.10
		SD	8704.40
		RSD	0.93%

Appendix 63: Reproducibility of ES9 (63 µM).

4-Nitrophenol (144 µM)			
Sample	**PA1**	**PA2**	**AVG PA**
1	1476342	1472228	1474285.00
2	1496376	1490570	1493473.00
3	1465367	1478730	1472049.00
4	1491848	1441278	1466563.00
5	1472751	1458248	1465500.00
6	1483128	1485642	1484385.00
		Average	1476042.00
		SD	10894.73
		RSD	0.74%

Appendix 64: Reproducibility of 4-nitrophenol (144 µM).

ES10 (66 µM)			
Sample	**PA1**	**PA2**	**AVG PA**
1	792054	794655	793354.50
2	794323	792464	793393.50
3	790458	790595	790526.50
4	786808	785570	786189.00
5	797483	801775	799629.00
6	791151	792052	791601.50
		Average	792449.00
		SD	4401.51
		RSD	0.56%

Appendix 65: Reproducibility of ES10 (66 µM).

4-Chlorophenol (155 µM)			
Sample	**PA1**	**PA2**	**AVG PA**
1	1336524	1303198	1319861.00
2	1321441	1331901	1326671.00
3	1308566	1315605	1312086.00
4	1313775	1315605	1314690.00
5	1341691	1328644	1335168.00
6	1303942	1322029	1312986.00
		Average	1320243.00
		SD	9102.28
		RSD	0.69%

Appendix 66: Reproducibility of 4-chlorophenol (155 µM).

ES11 (68 µM)			
Sample	**PA1**	**PA2**	**AVG PA**
1	883197	884466	883831.50
2	892625	898000	895312.50
3	888821	888193	888507.00
4	892401	895825	894113.00
5	881495	883476	882485.50
6	865802	866960	866381.00
		Average	885105.10
		SD	10544.97
		RSD	1.19%

Appendix 67: Reproducibility of ES11 (68 µM).

4-Hydroxybenzonitrile (169 µM)			
Sample	**PA1**	**PA2**	**AVG PA**
1	2964287	2971625	2967956.00
2	3001984	3014323	3008154.00
3	2983782	2990218	2987000.00
4	3001127	3015080	3008104.00
5	2970794	2977672	2974233.00
6	2992530	2998438	2995484.00
		Average	2990155.00
		SD	16915.98
		RSD	0.57%

Appendix 68: Reproducibility of 4-hydroxybenzonitrile (169 µM).

ES12 (74 µM)			
Sample	**PA1**	**PA2**	**AVG PA**
1	968115	970613	969364.00
2	972963	973955	973459.00
3	976836	976486	976661.00
4	966892	973323	970107.50
5	938898	940028	939463.00
6	910633	916006	913319.50
		Average	957062.30
		SD	15012.62
		RSD	1.57%

Appendix 69: Reproducibility of ES12 (74 µM).

Phenol (251 µM)			
Sample	**PA1**	**PA2**	**AVG PA**
1	375439	376867	376153.00
2	373240	375059	374149.50
3	375517	376571	376044.00
4	374022	373780	373901.00
5	362477	362882	362679.50
6	352012	353321	352666.50
		Average	369265.60
		SD	5634.58
		RSD	1.53%

Appendix 70: Reproducibility of phenol (251 µM).

ES14 (71 µM)			
Sample	**PA1**	**PA2**	**AVG PA**
1	698166	729880	714023.00
2	715688	720746	718217.00
3	703956	700006	701981.00
4	705671	706018	705844.50
5	728550	740391	734470.50
6	722660	709228	715944.00
		Average	715080.00
		SD	11354.07
		RSD	1.59%

Appendix 71: Reproducibility of ES14 (71 µM).

P-Cresol (185 µM)			
Sample	**PA1**	**PA2**	**AVG PA**
1	864988	862337	863662.50
2	884100	846344	865222.00
3	881069	871643	876356.00
4	844419	855450	849934.50
5	854528	860594	857561.00
6	877607	898202	887904.50
		Average	866773.40
		SD	13556.19
		RSD	1.56%

Appendix 72: Reproducibility of p-cresol (185 µM).

Appendix 4c: Linearity Investigations of TMZ esters and Corresponding Alcohols Using HPLC

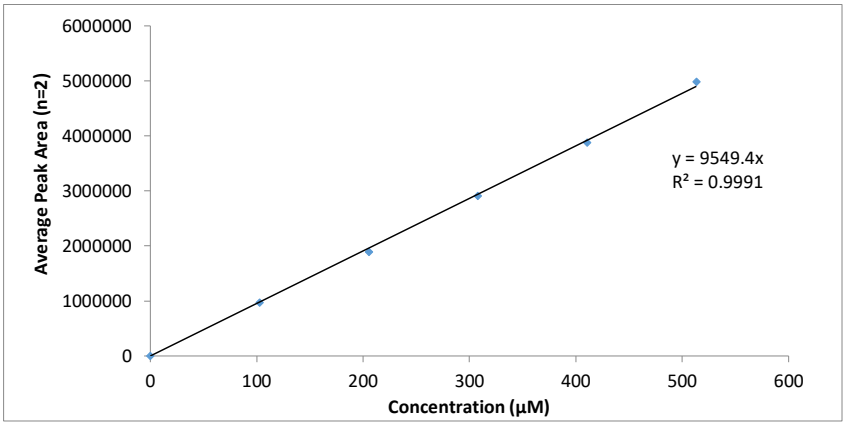

Appendix 73: A calibration curve to assess the relationship between TMZ acid concentration and response (peak area).

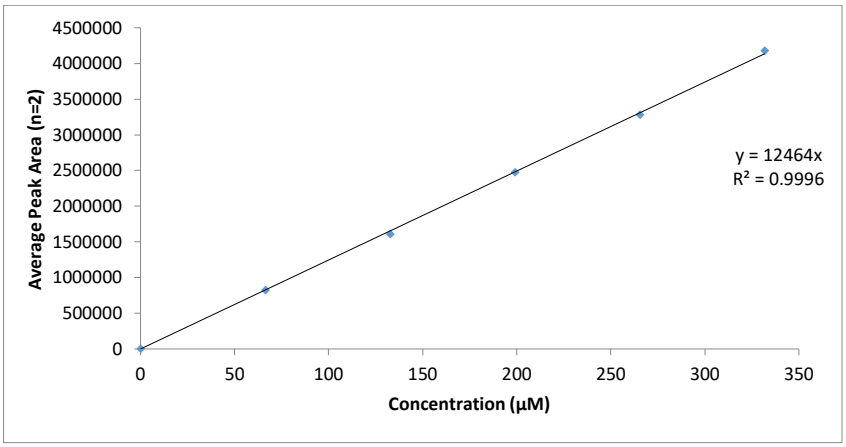

Appendix 74: A calibration curve to assess the relationship between ES8 concentration and response (peak area).

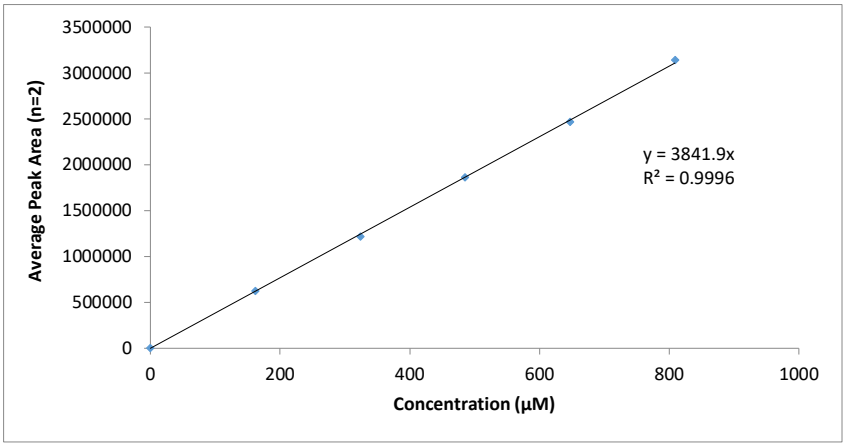

Appendix 75: A calibration curve to assess the relationship between 4-methoxyphenol concentration and response (peak area).

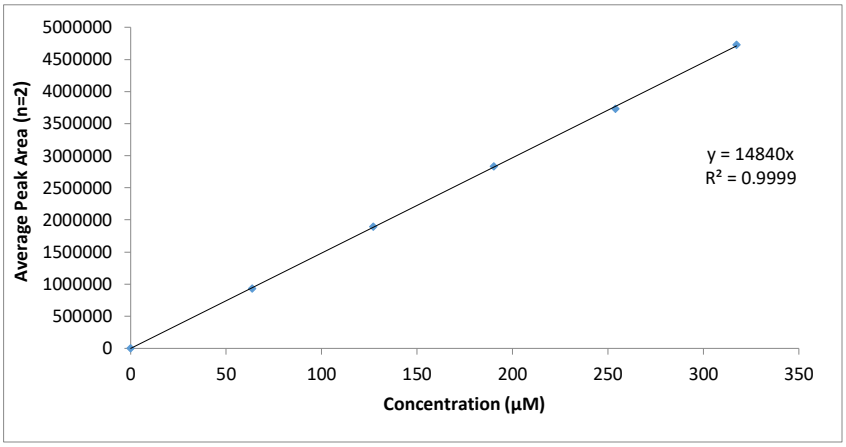

Appendix 76: A calibration curve to assess the relationship between ES9 concentration and response (peak area).

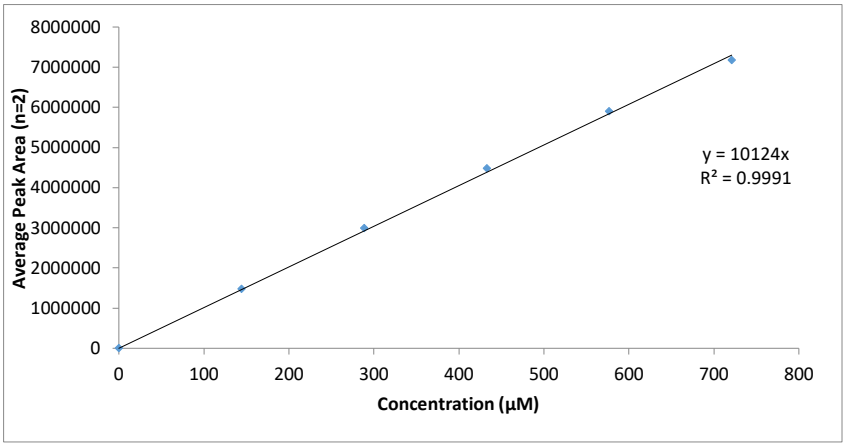

Appendix 77: A calibration curve to assess the relationship between 4-nitrophenol concentration and response (peak area).

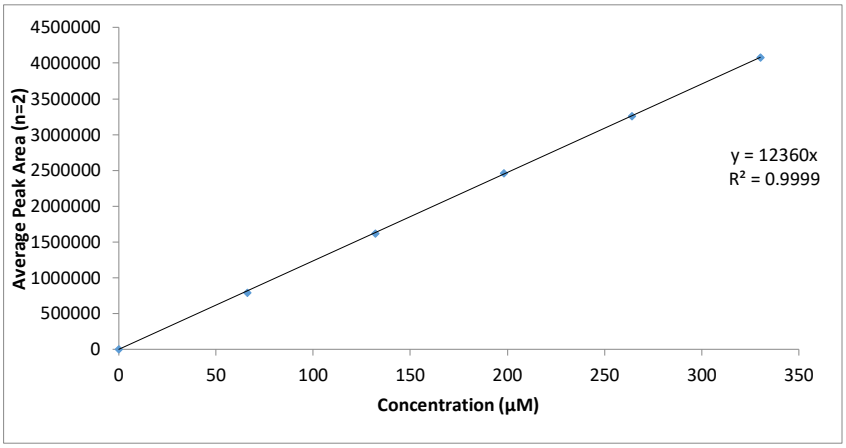

Appendix 78: A calibration curve to assess the relationship between ES10 concentration and response (peak area).

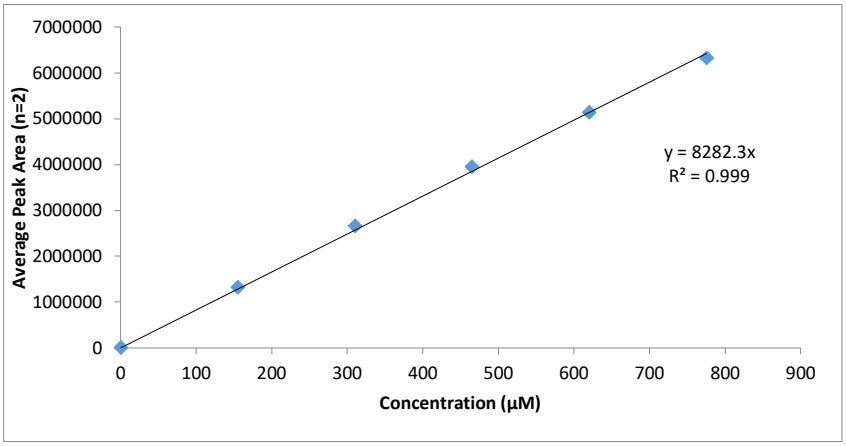

Appendix 79: A calibration curve to assess the relationship between 4-chlorophenol concentration and response (peak area).

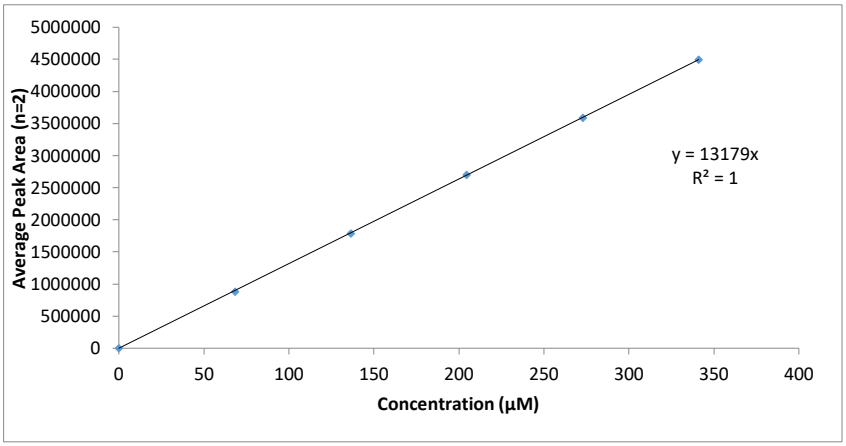

Appendix 80: A calibration curve to assess the relationship between ES11 concentration and response (peak area).

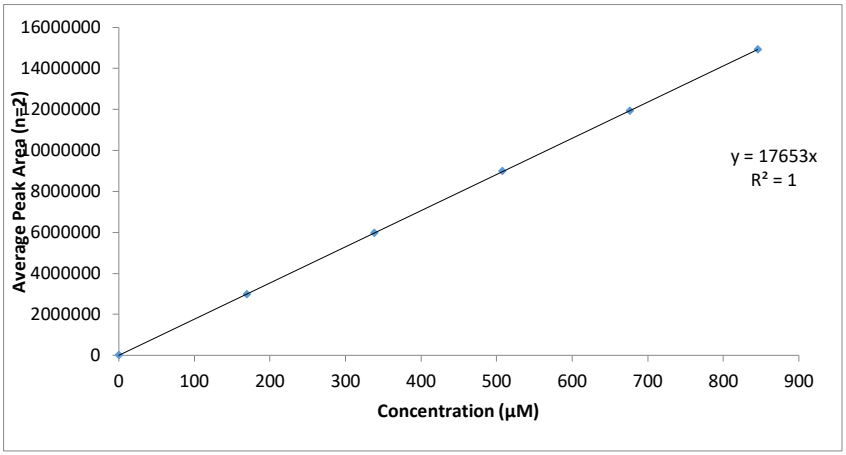

Appendix 81: A calibration curve to assess the relationship between 4-hydroxybenzonitrile concentration and response (peak area).

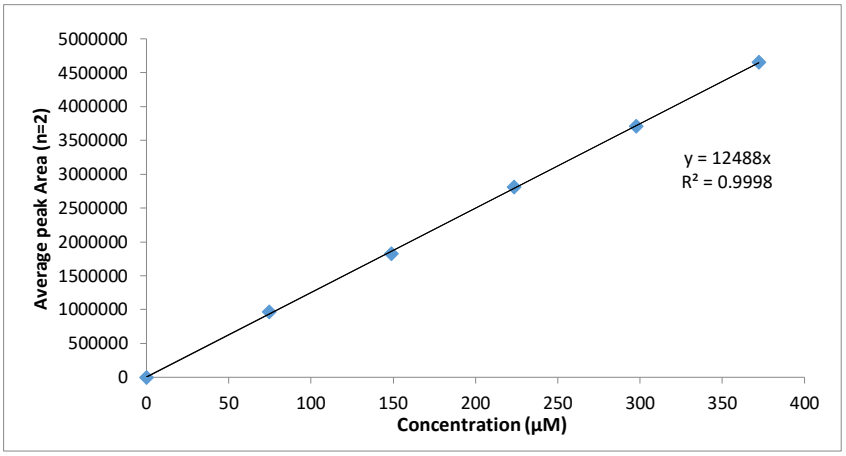

Appendix 82: A calibration curve to assess the relationship between ES12 concentration and response (peak area).

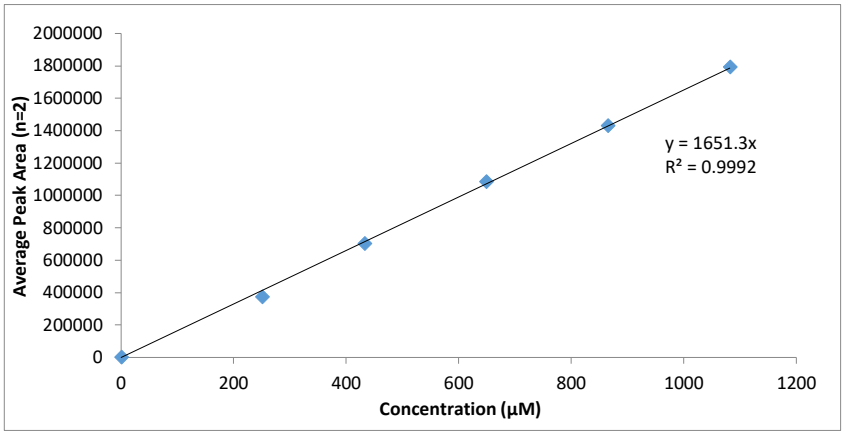

Appendix 83: A calibration curve to assess the relationship between phenol concentration and response (peak area).

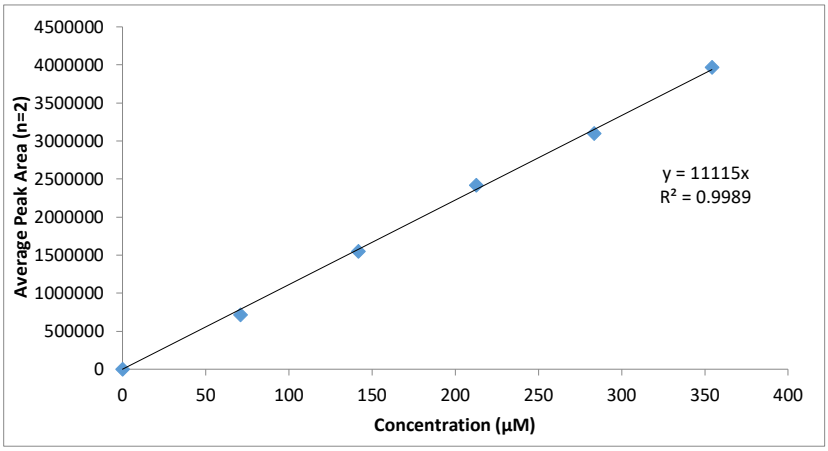

Appendix 84: A calibration curve to assess the relationship between ES14 concentration and response (peak area).

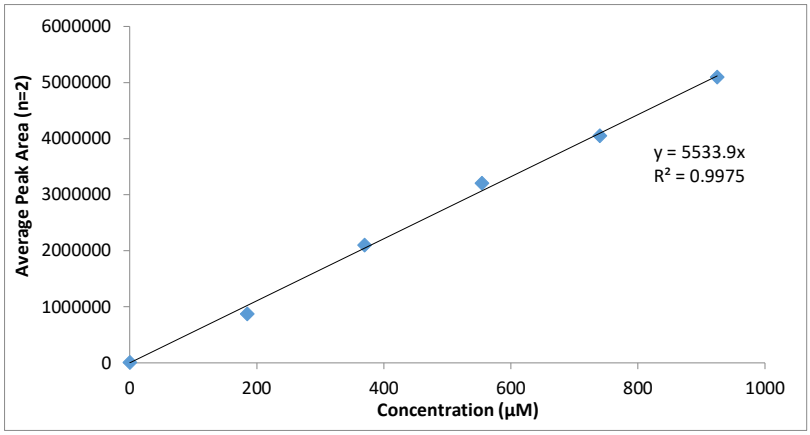

Appendix 85: A calibration curve to assess the relationship between p-cresol concentration and response (peak area).

Appendix 4d: LLOQ and LLOD of TMZ Esters and Corresponding Alcohols

A

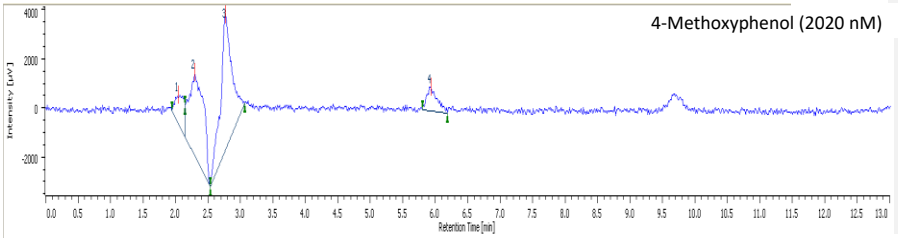

B

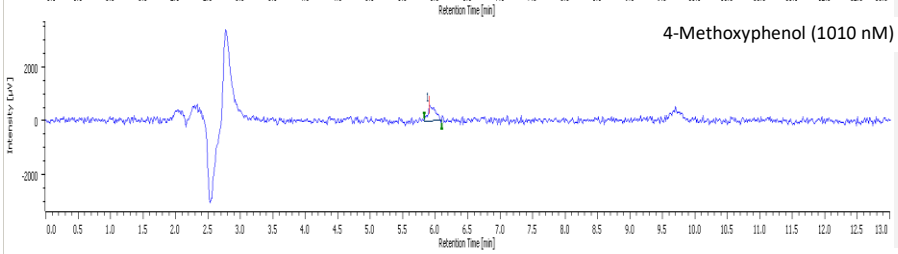

C

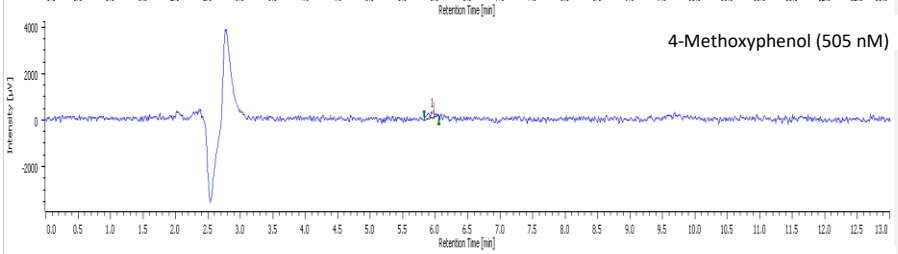

D

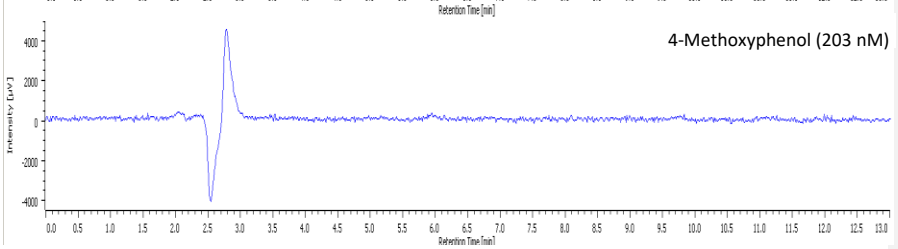

Appendix 86: Determining the LLOQ and LLOD of 4-methoxyphenol. Injection B, 4-methoxyphenol (6.0 mins; 1010 nM), was estimated to be the LLOQ. Injection C, 4-methoxyphenol (6 mins; 505 nM), was estimated to be the LLOD. Analysis at 230 nm.

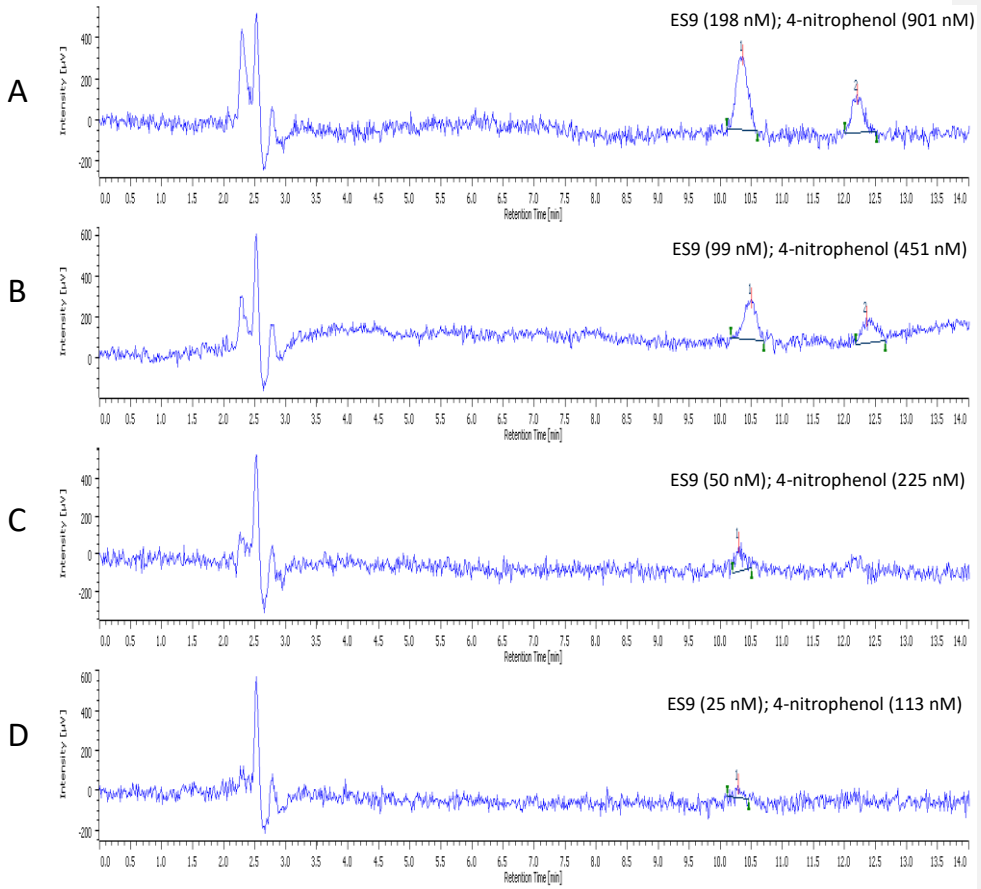

Appendix 87: Determining the LLOQ and LLOD of ES9 and 4-nitrophenol. Injection A, (198 nM and 901 nM of ES9 (12.25 min) and 4-nitrophenol (10.5 min), respectively), was determined to be the LLOQ for ES9. Injection B, (99 nM and 451 nM of ES9 and 4-nitrophenol, respectively), was determined to be the LLOD for ES9 and the LLOQ for 4-nitrophenol. Injection C, (50nM and 225 nM of ES9 and 4-nitrophenol, respectively), was determined to be the LLOD for 4-nitrophenol. Analysis at 325 nm.

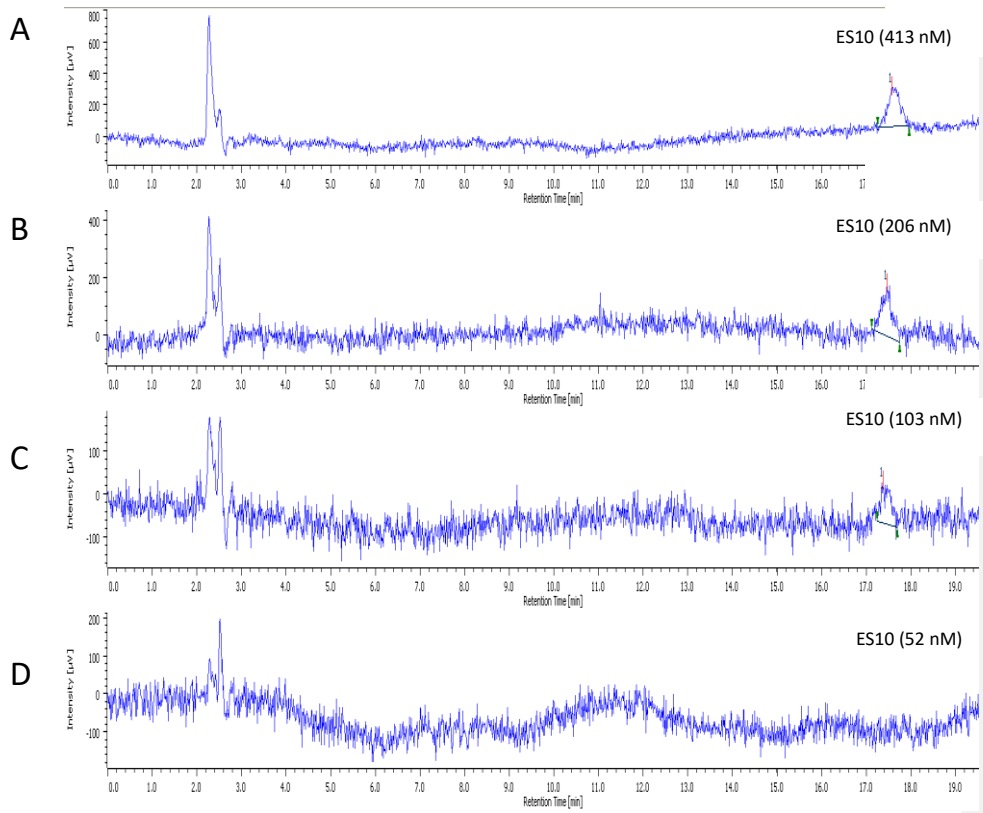

Appendix 88: Determining the LLOQ and LLOD of ES10. Injection B, ES10 (17.5 mins; 206 nM), was estimated to be the LLOQ. Injection C, ES10 (17.5 mins; 103 nM), was estimated to be the LLOD. Analysis at 325 nm.

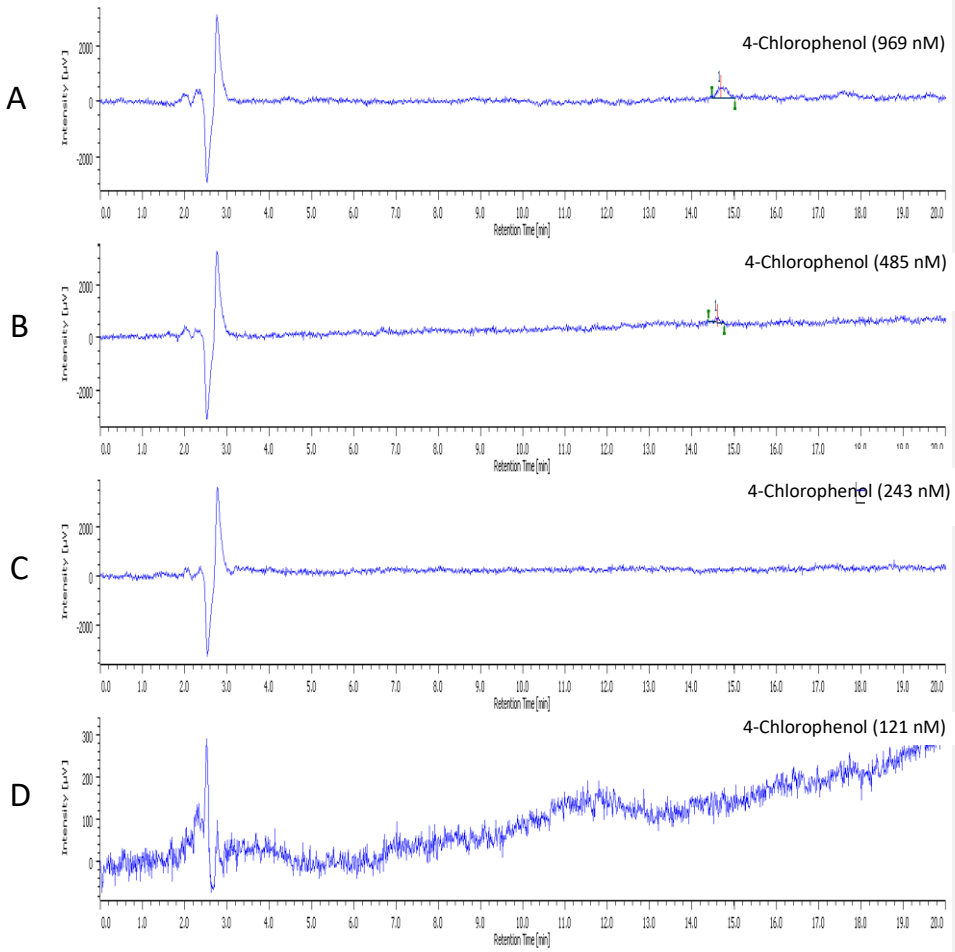

Appendix 89: Determining the LLOQ and LLOD of 4-chlorophenol. Injection A, 4-chlorophenol (14.8 mins; 969 nM), was estimated to be the LLOQ. Injection B, 4-chlorophenol (14.8 mins; 485 nM), was estimated to be the LLOD. Analysis at 225 nm.

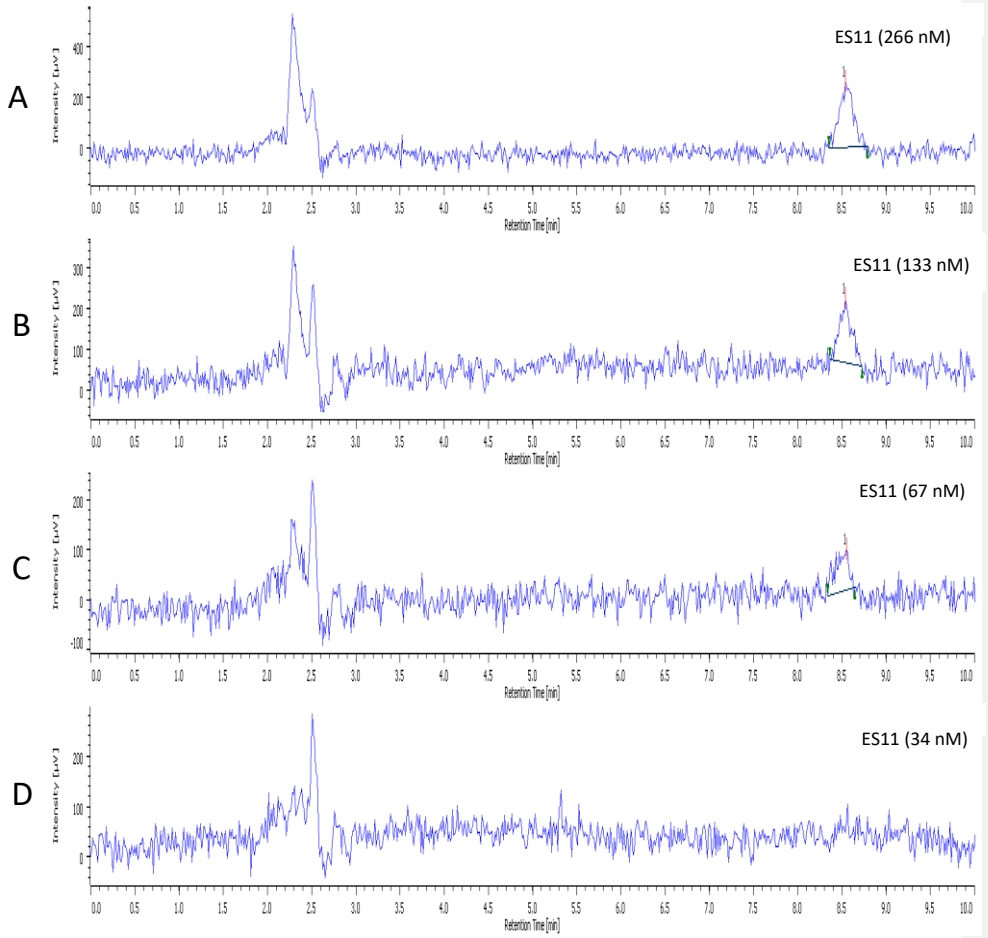

Appendix 90: Determining the LLOQ and LLOD of ES11. Injection B, ES11 (8.5 mins; 133 nM), was estimated to be the LLOQ. Injection C, ES11 (8.5 mins; 67 nM), was estimated to be the LLOD. Analysis at 325 nm.

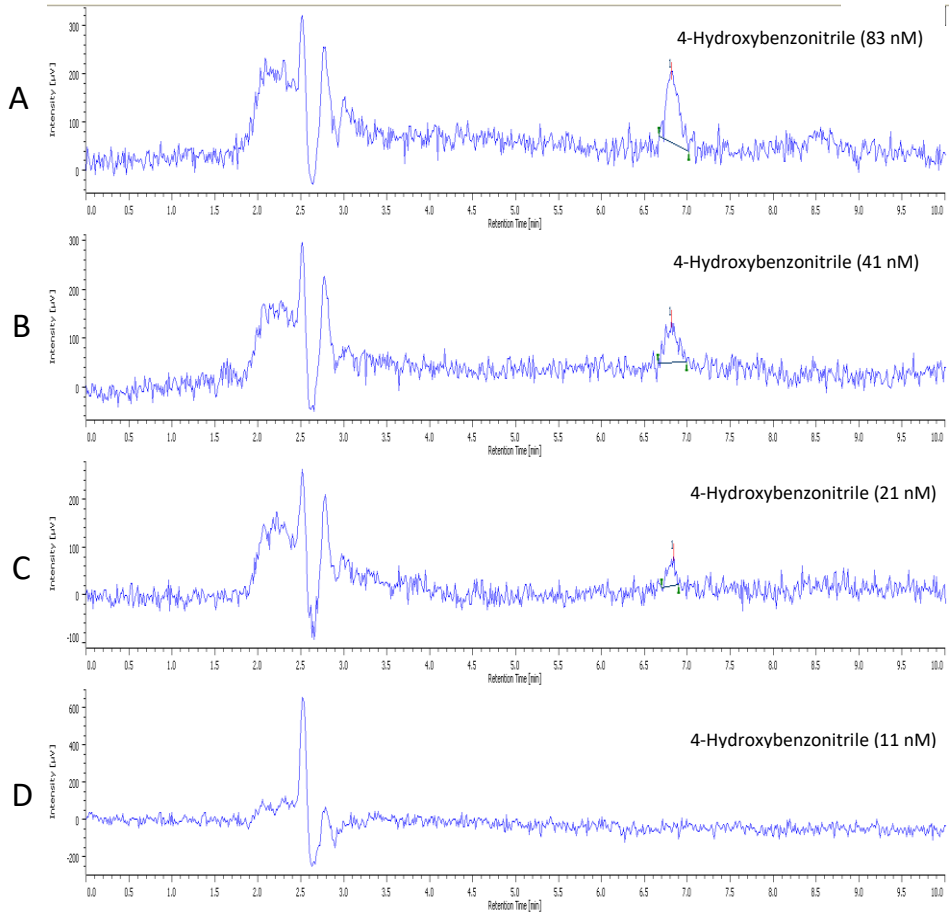

Appendix 91: Determining the LLOQ and LLOD of 4-hydroxybenzonitrile. Injection A, 4-hydroxybenzonitrile (6.8 mins; 133 nM), was estimated to be the LLOQ. Injection C, 4-hydroxybenzonitrile (6.8 mins; 21 nM), was estimated to be the LLOD. Analysis at 250 nm.

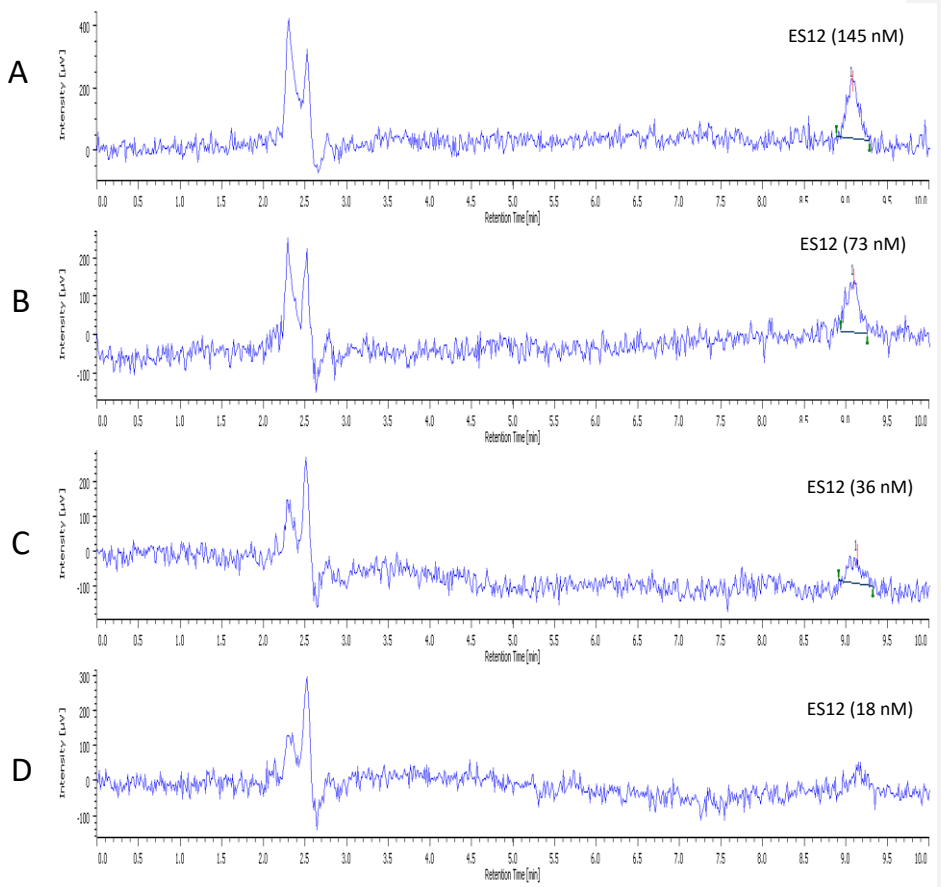

Appendix 92: Determining the LLOQ and LLOD of ES12. Injection A, ES12 (9.1 mins; 145 nM), was estimated to be the LLOQ. Injection C, ES12 (9.1 mins; 36 nM), was estimated to be the LLOD. Analysis at 250 nm.

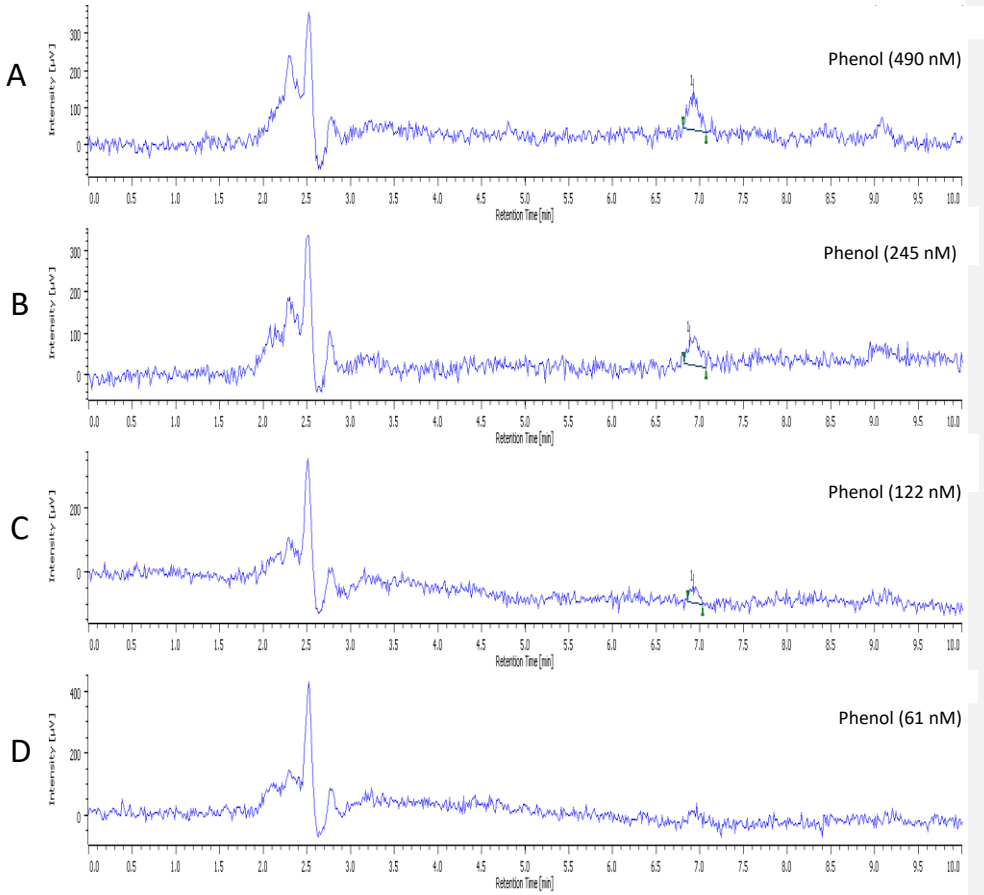

Appendix 93: Determining the LLOQ and LLOD of phenol. Injection A, phenol (7.0 mins; 490 nM), was estimated to be the LLOQ. Injection C, phenol (7.0 mins; 122 nM), was estimated to be the LLOD. Analysis at 325 nm.

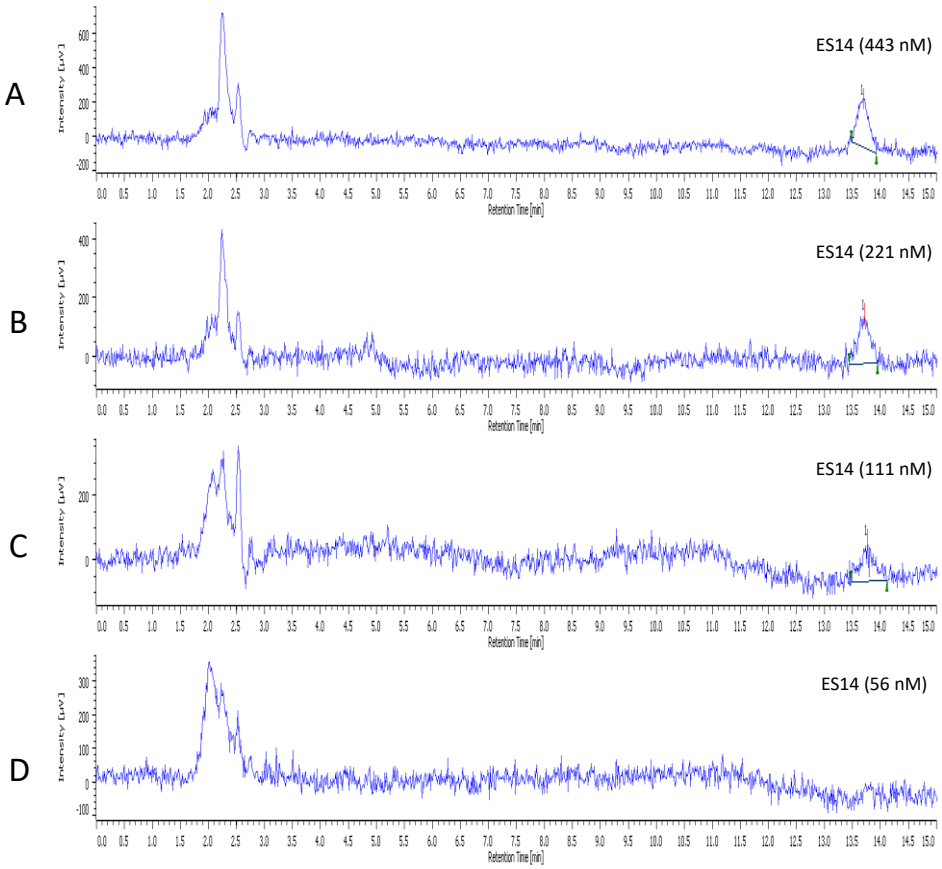

Appendix 94: Determining the LLOQ and LLOD of ES14. Injection B, ES14 (13.75 mins; 221 nM), was estimated to be the LLOQ. Injection C, ES14 (7.0 mins; 111 nM), was estimated to be the LLOD. Analysis at 325 nm.

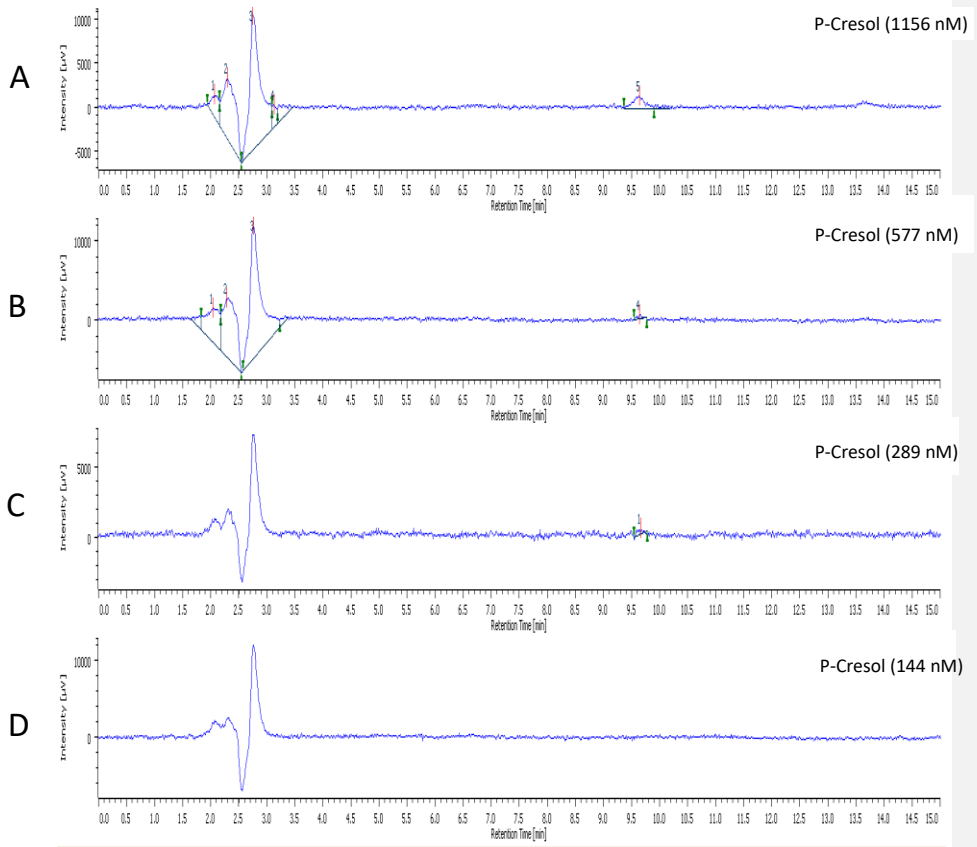

Appendix 95: Determining the LLOQ and LLOD of p-cresol. Injection A, p-cresol (9.6 mins; 1156 nM), was estimated to be the LLOQ. Injection C, p-cresol (9.6 mins; 289 nM), was estimated to be the LLOD. Analysis at 225 nm.